THE UNIVERSITY *of* EDINBURGH

THE SPATIAL, TEMPORAL AND FUNCTIONAL MOLECULAR ARCHITECTURE OF THE MUNC18-SYNTAXIN INTERACTION

ANNYA SMYTH
BSc Hons

University of Edinburgh
2012

THESIS SUBMITTED FOR THE DEGREE OF DOCTOR OF PHILOSOPHY

Declaration

I, Annya Mary Smyth, candidate for a PhD in Biomedical Sciences, declare that this thesis has been composed solely by myself, and that this work herein described is my own, except that mentioned in the acknowledgements, and that this work has not been submitted for any other degree or professional qualification.

Annya M. Smyth
BSc (Hons)

ACKNOWLEDGEMENTS

First and foremost I would like to express my sincere gratitude to my supervisors Rory Duncan, Colin Rickman and Mike Cousin for giving me the continuous guidance, encouragement and enthusiasm to complete my PhD project and thesis. I honestly couldn't have asked for better supervisors, your knowledge, ideas and teaching was invaluable.

I would also like to thank all those members of the Duncan and Cousin labs, particularly Sarah Gordon for her help in teaching me all about FM imaging and the art of cortical cultures and Ali Dun for her continued friendship over the last few years. I'd like to say a special thanks to Karen Bell, Ruth Milne, Clare Puddifoot and Paul Baxter for making the HRB such a sociable and fun place to work. I'd also like to thank the girls in the Duncan lab at Heriot Watt University for making me feel so welcome when I arrived and particular thanks goes out to Deirdre Kavanagh and Kirsty Martin for their help and sound advice with FCS. Also, thank you to David Bruce and Lisa Reynolds for your sense of adventure, humour and for just being there.

I would also like to thank Colin Rickman for generating Figure 5.12, Amy Gray for generating Figure 5.6 and Lei Yang for processing and analysing the tracking results of the live neuroendocrine and neuronal PALM data sets.

Last but not least; I would like to say a heartfelt thank you to my family for all their love and support, I wouldn't have been able to do it without you. A special thank you has to go out to my beloved mum and dad for their unwavering love and guidance over the years and for putting up with me whilst writing my thesis at home, you almost made it easy. Dad, you have always provided me with confidence, advice and direction and were a fantastic help in proof reading my thesis and mum, your encouragement, optimism and never-ending support was an inspiration. To them I dedicate this thesis.

TABLE OF CONTENTS

LIST OF FIGURES

ABSTRACT

Regulation of soluble *N*-ethylmaleimide-sensitive fusion protein attachment protein receptors (SNARE) mediated exocytosis is dependent upon four key proteins; the vesicular SNARE synaptobrevin, target SNAREs SNAP-25 and syntaxin and the Sec1/Munc18 (SM) protein munc18-1. Despite the munc18-1-syntaxin interaction being central to regulated vesicle exocytosis the spatial and temporal pattern of their molecular distribution and interaction in neuroendocrine and neuronal cells remains undefined. Using *in vitro* and molecular approaches this thesis shows that disruption of the munc18-1-syntaxin-N-terminal interaction results in significant changes in syntaxin localisation, membrane-proximal vesicle dynamics and fusion efficiency within neuroendocrine cells. Using the super-resolution techniques Ground State Depletion-Individual molecule return (GSDIM) Microscopy and Photoactivation Localisation Microscopy (PALM) this thesis has demonstrated that the spatial distribution of single munc18-1 molecules is non-random and that few munc18-1 molecules are required for exocytosis to proceed in neuroendocrine cells. Furthermore, targeted disruption of the N-terminal interaction resulted only in a reorganisation of interaction with syntaxin with no change in the molecular spatial pattern of secretory vesicles, syntaxin or munc18-1. Single molecule imaging PALM (sptPALM) enabled the investigation of the complex spatio-temporal behaviours of single munc18-1 molecules in living neuroendocrine cells. Spatially resolved maps of single munc18-1 molecules demonstrated that munc18-1 exhibits a caged motion within areas of the plasma membrane and were found to move between molecular storage depots distinct from vesicle docking sites. To explore the precise spatial and temporal sequence of interactions between syntaxin and munc18-1 in living neurons, super-resolution imaging techniques PALM and sptPALM were employed. Two kinetically and spatially distinct populations of munc18-1 molecules co-exist within a living neuron and munc18-1 requires syntaxin to traffic efficiently in axons but not for its retention in nerve terminals. Moreover, Fluorescence Correlation Spectroscopy (FCS) revealed that the majority of munc18-1 molecules do not interact with syntaxin in nerve terminals and the diffusion rate of syntaxin is significantly slowed down upon neuronal depolarisation.

CHAPTER 1:

INTRODUCTION

1.1 An Introduction to Cellular Communication

The defining feature of all eukaryotic cells is the division of their intracellular space into a series of highly differentiated membrane bound compartments in which specialised and distinct functions occur. The transfer of newly synthesized material between intracellular compartments requires the action of membrane bound transport vesicles which bud from one compartment and fuse with the next (Caro and Palade, 1964; Jamieson and Palade, 1967; Palade, 1975). However, the major disadvantage of compartmentalizing biological membranes results in the isolation of a cell from its immediate external environment. In order to overcome this isolation, extracellular transport involves the timely release of biological substances from the interior of secretory vesicles into the extracellular milieu. The process whereby vesicles fuse with the plasma membrane and release their contents, including proteins, lipids and cellular metabolites, is known as exocytosis (Bellen, 1999; Jahn et al, 2003). Despite the enormous diversity of all intra- and inter-cellular fusion reactions, the underlying steps from membrane contact to aqueous fusion pore formation have been heavily conserved throughout evolution (Jahn et al, 2003).

1.1.2 Constitutive vs Regulated Exocytosis

Exocytosis can occur by either a constitutive or a regulatory pathway, both involving the sorting of proteins or lipids destined for release into secretory vesicles within the trans-Golgi network (Burgess and Kelly, 1987). Constitutive exocytosis is a fundamental pathway in all eukaryotic cells and involves the continual release of proteins and other internalized cargo from the lumen of secretory vesicles upon fusion with the plasma membrane (Burgess and Kelly, 1987; Burgoyne and Morgan, 2003). This pathway is instrumental to both cellular growth and the delivery and insertion of newly synthesised lipids and proteins to the plasma membrane (Burgess and Kelly, 1987; Burgoyne and Morgan, 2003). As inferred in its name, regulated exocytosis involves the fusion of secretory vesicles with the plasma membrane upon the arrival of a physiological stimulus (Burgess and Kelly, 1987; Jahn and Südhof, 1999; Burgoyne and Morgan, 2003; Jahn, 2004). This stimulus often originates from the extracellular milieu, for example through a change in the cellular environment or a signal from an adjacent cell. Specialised

eukaryotic secretory cells, for example, neurons and neuroendocrine cells, have exploited this release mechanism in order to efficiently transfer information between adjacent cells and throughout the whole organism respectively (Bellen, 1999; Cowan and Kandel, 2000; Burgoyne and Morgan, 2003). Regulated secretion in neurons and neuroendocrine cells is both spatially and temporally restricted in order for their enclosed signalling compounds, neurotransmitters and hormones respectively, to be released when and where required. The physiological stimulus involved in catalysing this release mechanism commonly results in an influx of extracellular Ca^{2+} (Dodge and Rahamimoff, 1967; Burgess and Kelly, 1987; Jahn, 2004). In neuronal cells synaptic transmission is initiated when an action potential, which results in an influx of extracellular Ca^{2+}, triggers neurotransmitter release from a presynaptic nerve terminal (Katz and Miledi, 1967). Membrane exocytosis and signal transmission is followed by endocytic retrieval and recycling of the plasma membrane and vesicular proteins, enabling more rounds of membrane fusion to occur (Goldstein et al, 1979; Ceccarelli and Hurlbut, 1980; Betz and Bewick, 1993).

1.1.3 VESICLE COMPARTMENTALISATION

Neurons share many properties with their neuroendocrine counterparts; in part both cell types package their secretory products, from small molecules to multimeric proteins, into cell specific membrane bound organelles (Kelly, 1993). Synaptic vesicles are approximately 50 nm in diameter and compose of low-molecular weight chemical neurotransmitters such as acetylcholine and glutamate (Del Castillo and Katz, 1954; De Robertis and Bennett, 1955). Secretory vesicles of chromaffin cells, similar to large dense core vesicles in neurons, are in the range of 70 to 400 nm in diameter and contain a variety of neuropeptides and soluble proteins, giving them a characteristic dense core in electron micrographs (Kelly, 1993; Voets et al, 2001; de Wit et al, 2006).

Vesicles contained within neuroendocrine and neuronal cells are generally organised into morphologically and functionally distinct pools, the readily releasable pool (RRP) and the reserve pool (RP). In order for specialised secretory cells to respond rapidly to a physiological stimulus they require a number of pre-assembled and fusion competent vesicles positioned in close apposition to the plasma membrane (Harata et al, 2001). This

pool of vesicles is commonly referred to as the 'readily releasable pool' (RRP), a subset of vesicles which have undergone a number of maturation steps in order to enable them to fuse with the membrane on immediate demand (Burgess and Kelly, 1987; Rosenmund and Stevens, 1996; Rizzoli and Betz, 2004). The RRP only represents a small fraction of the total vesicle complement (Greengard et al, 1993; Pieribone et al, 1995; Brodin et al, 1997; Kuromi and Kidokoro, 1998; Rorsman and Renstrom, 2003). However, it is important to note that the structural organisation of the RRP is not similar in all chemical synapses, for example, at the frog neuromuscular junction the readily releasable vesicles are not in close proximity with the presynaptic membrane (Rizzoli and Betz, 2004). It is thought that the extensive subcellular actin network within neuroendocrine secretory cells acts as a barrier to the pool of secretory vesicles in the cell periphery, thereby segregating vesicles into distinct pools and ensuring the release of only fusion competent vesicles (Nakata and Hirokawa, 1992; Doussau and Augustine, 2000; Malacombe et al, 2006). Those vesicles residing in the RRP in both neuronal and neuroendocrine cells are thought to undergo two maturation steps. First vesicles are 'docked', a molecular state where they are considered to be within 'no measurable distance' from the plasma membrane (Verhage and Sorensen, 2008; de Wit, 2010). Second, docked vesicles are subsequently 'primed', an ATP-dependent step rendering secretory vesicles competent for Ca^{2+} triggered fusion (Burgoyne and Morgan, 2003; Südhof, 2004).

The process of vesicle exocytosis within neurons and neuroendocrine cells has been remarkably well conserved but differences still exist within the regulation (Childs et al, 1987; McNeilly et al, 2003) and speed of vesicle release (Barrett and Stevens, 1972; Voets et al, 1999; Braun et al, 2009). Despite these subtle variations, all eukaryotic secretory cells share a common mechanism of vesicular exocytosis (Clary et al, 1990; Bennett and Scheller, 1993a; Ferro-Novick and Jahn, 1994). Regulated exocytosis involves the pairing of highly conserved proteins on the opposing vesicular and plasma membranes, with the soluble *N*-ethylmaleimide-sensitive fusion protein attachment protein receptors (SNARE) proteins and their regulatory partners found at the core of this cascade of protein-protein interactions (Söllner et al, 1993a,b).

1.2 SNARE PROTEINS

The compartmentalisation of intracellular membranes has made it necessary for vesicles to be brought into close proximity with the plasma membrane in order for them to release their enclosed components. A number of studies conducted in the 1970s and 1980s began to probe both the mechanisms and players behind the a) cascade of events involved in intracellular transport, specifically between the ER and the Golgi complex, and the b) intricacies of the membrane fusion reaction. These studies established that individual proteins are involved in a chain of events from initial synthesis in the endoplasmic reticulum to carrying out their desired biological function. Post ER-synthesis, proteins are sorted in the Golgi complex and subsequently transported to their specific cellular destination within vesicles destined for fusion with the plasma membrane (Griffiths and Simons, 1986; Jamieson and Palade, 1967; Palade, 1975). It was not until the late 1970s when Novick and co-workers pioneered the initial study which led to the identification of various components of the cellular machinery involved in driving compartmental transport and membrane fusion. Novick and co-workers generated 188 secretion deficient or *sec* thermosensitive yeast (*Saccharomyces cerevisia*) mutants and screened their individual abilities to secrete invertase, an enzyme that catalyses the hydrolysis of sucrose (Novick and Schekman, 1979; Novick et al, 1980, 1981). This approach resulted in the discovery and isolation of 23 gene products that were principally involved in intracellular membrane trafficking events. *Sec* mutants resulted in defects in a number of stages of the intracellular trafficking pathways; from the ER to the Golgi complex to the trafficking of secretory vesicles to the plasma membrane (Novick et al, 1980). Major components of the yeast secretory pathway identified in this study, and now heavily characterised, included Sec1 (a Sec1/munc18 protein), Sec4 (a Rab/GTPase), Sec9 (a target membrane SNARE protein), and Sec22 (a vesicle membrane SNARE protein) (Novick et al, 1980).

These pioneering studies led by Novick and colleagues in the 1970s coincided with the characterisation of both novel and previously identified proteins involved in the catalysis of ATP dependent intracellular transport (Glick and Rothman, 1987). Only a few years later another study led by Rothman in 1981 identified a number of proteins also essential for intracellular transport reactions through the use of reconstituted Golgi compartments

from wild-type and secretion mutant Chinese hamster ovary (CHO) cells (Rothman and Fries, 1981; Balch et al, 1984). This study led to the identification of both *N*-ethylmaleimide-sensitive fusion protein (NSF; Fries and Rothman, 1980; Rothman and Fries, 1981) and soluble NSF attachment proteins (SNAPs), the latter required at the same step of membrane fusion as NSF (Clary et al, 1990; Clary and Rothman, 1990). NSF, a trimeric ATPase, was shown to be essential for intracellular membrane fusion as its genetic ablation resulted in the accumulation of vesicles in the acceptor membrane (Malhotra et al, 1988). Essential factors in mediating intracellular transport steps initially identified by Novick and co-workers, specifically Sec17 and Sec18, were found to be homologous to α-SNAP (Clary et al, 1990) and NSF (Wilson et al, 1989), respectively. In summary, the fact that the same components, SNAPs and NSF, were identified in two distantly related eukaryotic model systems highlights the conserved nature of intracellular trafficking and membrane fusion reactions.

Despite identifying a number of highly conserved proteins involved in catalysing membrane fusion it was still unclear what determined the specificity of membrane trafficking, in other words, how does a vesicle recognise a membrane it is destined to fuse with? Following the characterisations of NSF and SNAPs, Rothman and colleagues later set out to investigate the identity of the membrane receptors of these proteins. Using highly purified NSF and SNAPs from bovine brain extract they successfully isolated their targets, leading to the identification of SNAP receptors (SNAREs) (Söllner et al, 1993b). SNAREs, syntaxin and Synaptosome-Associated Protein of 25 kDa (SNAP-25), were found to be localised to the plasma membrane and Vesicle Associated Membrane Protein (VAMP) was found to reside on the vesicular membrane (Söllner et al, 1993b). However, it is often overlooked that all three SNARE proteins had already been previously identified in a number of separate studies. VAMP (Trimble et al, 1988) or synaptobrevin (Baumert et al, 1989) was initially labelled as a major constituent of synaptic vesicles and syntaxin was first identified using a monoclonal antibody raised against a synaptosomal membrane preparation (Barnstable et al, 1985; Inoue et al, 1992). Synaptosome-associated protein of 25 kDa (SNAP-25) had been previously isolated (Oyler et al, 1989) and shown to be a major substrate for fatty acid palmitoylation (Hess et al, 1992). Despite their previous identification Rothman and colleagues were the first to demonstrate that SNARE proteins form a core complex upon bilayer fusion (Söllner et al, 1993a,b).

Following the identification of the SNARE proteins the most direct evidence to suggest that they are central to the process of membrane exocytosis originated through the initial characterisation of clostridial neurotoxins (Südhof et al, 1993; Montecucco and Schiavo, 1995; O'Kane et al, 1999). The clostridial neurotoxin family is composed of tetanus neurotoxin (TeNT) and seven different serotypes of botulinum neurotoxins (BoNT) (Minton, 1995), produced respectively by the obligate anaerobic bacteria *Clostridium tetani* and *Clostridium botulinum*. These neurotoxins are comprised of two fragments, termed the heavy (100 kDa) and light (50 kDa) chains which block neurotransmitter release both *in vitro* and *in vivo* (Schiavo and Montecucco, 1997). *C. tetani* produces tetanus neurotoxin (TeNT) which is transported retrogradely to the spinal cord, travelling through the synaptic cleft to block release of neurotransmitter from inhibitory neurons (Schwab and Thoenen, 1976, 1978; Dumas et al, 1979; Schwab et al, 1979). Conversely, the seven serotypes of botulinum neurotoxin (BoNT) termed A-G infect a host by being absorbed into the blood through the gut wall, later taken up at neuromuscular junctions (NMJ) to inhibit neurotransmitter release (Maksymowych and Simpson, 1998; Maksymowych et al, 1999).

Identification and characterisation of the specificity of these toxins was achieved by incubating purified recombinant SNARE proteins with specific toxins and sequencing the N-terminal portion of these protein fragments. This demonstrated that all clostridial neurotoxins specifically target the neuronal SNAREs, syntaxin, SNAP-25 and synaptobrevin by cleaving the different peptide bonds. TeNT and BoNT B, D, F and G target synaptobrevin (Schiavo et al, 1992, 1993a,c, 1994; Yamasaki et al, 1994a,b,c), while BoNT A and E instead cleave SNAP-25 (Schiavo et al, 1993a,b). Only BoNT C has a dual-specificity for SNAP-25 and syntaxin 1 (Blasi et al, 1993a; Schiavo et al, 1995; Foran et al, 1996; Osen Sand et al, 1996; Williamson et al, 1996). Clostridial neurotoxins result in the complete suppression of vesicle exocytosis by detaching the cytoplasmic portion of syntaxin and synaptobrevin from their membrane anchors (Schiavo and Montecucco, 1997), thereby reducing the stability required for the correct formation and assembly of the SNARE complex (Hayashi et al, 1994, 1995).

Clostridial neurotoxins and the associated phenotype of the affected nerve cell have been particularly useful in unravelling the role of SNAREs in exocytosis. Despite the complete

abolition of exocytosis seen in synapses treated with TeNT or BoNT/C, a normal distribution of synaptic vesicles is observed by electron microscopy, with a sub-population of vesicles docked at the plasma membrane (Hunt et al, 1994; O'Connor et al, 1997). This finding suggested that the SNAREs are not involved in the process of docking but fundamental to the fusion process itself. The three SNARE proteins form an extremely stable complex *in vivo* which has been shown to be resistant to cleavage by clostridial neurotoxins *in vitro* (Hayashi et al, 1994; Pellegrini et al, 1994). It is therefore likely that the SNAREs only form a stable SNARE complex at a very late stage in the fusion process, most likely after the triggering of fusion by Ca^{2+} influx into the presynaptic terminal (Xu et al, 1998). Over the subsequent years a vast number of studies have confirmed that SNARE proteins are universally fundamental to all eukaryotic membrane fusion events and essential for membrane exocytosis (Südhof et al, 1989; Bennett and Scheller, 1993a; Söllner et al, 1993a; Ferro-Novick and Jahn, 1994; Hayashi et al, 1994; Jahn and Südhof, 1999). Thus the discovery of the SNARE proteins and the fact that they are targets for clostridial neurotoxins marked the initial understanding of how these proteins regulate the dynamics of donor-acceptor membrane fusion.

1.2.1 SNARE COMPLEX FORMATION

The fusion of membranes is driven by a complex interaction between three SNARE proteins, syntaxin, SNAP-25 and synaptobrevin (Söllner et al, 1993a,b). SNARE proteins belong to a universally conserved superfamily of either vesicle anchored (v-SNARE) or target (t-SNARE) membrane anchored proteins (Söllner et al, 1993a). In neuronal and neuroendocrine cells synaptobrevins (v-SNARE), syntaxins (t-SNARE), and synaptosomal-associated protein of 25 kDa (SNAP-25s) (t-SNARE) make up the minimal SNARE machinery required to drive membrane fusion (Jahn and Südhof, 1999; Chen and Scheller, 2001; Jahn, 2004). SNARE proteins interact via their tightly conserved SNARE motifs, a highly conserved sequence of 60-70 amino acids which have a high propensity to form α-helical coiled coils (Chapman et al, 1994). The t-SNAREs syntaxin and synaptobrevin donate one SNARE motif (Fasshauer, 2003) whereas SNAP-25 contributes two motifs, separated by a linker region (Poirier et al, 1998a; Sutton et al, 1998; Gerst, 1999), to the ternary SNARE complex. It is now well established that this linker region

includes a number of cysteine residues which are palmitoylated in order to anchor SNAP-25 in the plasma membrane (Oyler et al, 1989; Veit et al, 1996; Gonzalo et al, 1999; Loranger and Linder, 2002). Syntaxin, in contrast, is associated with the membrane via its transmembrane domain, allowing its extreme C-terminal α-helical coil to occupy the intracellular space and interact with the N-terminal α-helix of SNAP-25 (Hayashi et al., 1994).

A number of different studies have shown that the formation of the SNARE complex is sequential and initiated by the association of the t-SNAREs, SNAP-25 and syntaxin, most likely in a 1:1 stoichiometry at the plasma membrane (Chen et al, 2001; Fasshauer and Margittai, 2004; Rickman et al, 2004; Weninger et al, 2008). Upon the formation of the t-SNARE heterodimer complex, synaptobrevin binds and results in the formation of a tight four-helical trans-SNARE core complex (Weber et al, 1998). Interaction between cognate v- and t-SNAREs in opposite membranes forms a ternary core complex that contributes significantly to the energy required for membrane fusion (Poirier et al, 1998b) and drives bilayer unification and subsequent exocytosis (Sutton et al, 1998; Weber et al, 1998; Parlati et al, 1999; Hu et al, 2002).

1.2.2 THE SNARE HYPOTHESIS

The SNARE hypothesis was introduced alongside the discovery of the SNARE proteins and their role in catalysing membrane fusion (Söllner et al, 1993a,b; Rothman, 1994a,b). The original hypothesis suggested that secretory vesicles fuse with the plasma membrane by virtue of the specificity of cognate v-SNARE and t-SNARE interactions. The second main postulate of the hypothesis stated that both NSF and SNAP bind to the assembled SNARE complex and through NSF hydrolysis of ATP drive bilayer unification. The SNARE hypothesis therefore addressed the major outstanding questions in the field at the time, 1) what molecular mechanism specified membrane fusion and 2) what made it energetically possible? However, over the last ten years facets of the SNARE hypothesis have either been called into serious question or disproved. It has now been shown that the function of NSF and SNAP is not to drive fusion (Mayer et al, 1996) but to disassemble and recycle SNARE complexes post fusion (Nichols et al, 1997; Ungermann et al, 1998),

specifically through the enzymatic activity of NSF. This fits with other members of the same family of proteins, some of which have been implicated in disentangling protein complexes (Hanson and Whiteheart, 2005). The other main principle of the hypothesis, i.e., SNARE protein interactions account for the specificity reported in membrane fusion reactions, has also been disputed. The sequencing of the yeast *Saccharomyces cerevisiae* genome revealed that SNAREs could not specify all intracellular transport steps as there simply were not enough of them present (The Yeast Genome Directory, 1997). Another line of evidence discrediting the 'SNARE specificity model' of the original hypothesis is that a single SNARE can participate in more than one transport step (Fischer von Mollard and Stevens, 1999) and noncognate mammalian SNARE complexes can form *in vitro* (Fasshauer et al, 1999; Yang et al, 1999). Despite the fact that parts of the SNARE hypothesis have been heavily disputed the core message has survived, i.e. the formation of SNARE complexes confers specificity necessary to drive bilayer unification.

Over the last decade an overwhelming body of evidence has established that SNARE proteins make up the minimal molecular machinery required for membrane fusion. However, it is now generally accepted that additional accessory factors are essential to regulate and maintain cellular compartmentalisation and the kinetics of membrane exocytosis. For example, the single-membrane spanning synaptotgamin protein (Syt) 1 has been labelled as the Ca^{2+} sensor for fast synaptic fusion (Chapman, 2002). Genetic removal of Syt1 in both mice and *Drosophila* results in the loss of the fast, Ca^{2+}-dependent phase of transmitter release (Chapman 2002). In addition, ubiquiteously expressed Rab proteins have been shown to be instrumental in both membrane docking and fusion (reviewed in Jahn, 2000). It has recently been shown that membrane-specific Rab proteins ensure the directionality and specificity of both vesicular docking and fusion (Grosshans et al, 2006). Another protein critical to membrane fusion is complexin (CPX), a small neuronal protein that binds rapidly and with high affinity to the SNARE complex (McMahon et al, 1995; Pabst et al, 2002). In pancreatic β-cells, insulin secretion is reduced by silencing CPX I expression (Abderrahmani et al, 2004) and the genetic knockdown of CPX II in mast cells also leads to suppressed secretion (Tadokoro et al, 2005). Furthermore, Sec1/Munc18 (SM) proteins are required for every step of intracellular membrane fusion and have been recently shown to accelerate SNARE pairing

and complex assembly between bilayers, therefore enhancing fusion specificity and driving the basal fusion reaction (Shen et al, 2007).

1.3 SEC1/MUNC18 (SM) PROTEINS

SNARE proteins are critical to all membrane fusion events but rely heavily on the presence of a number of molecular regulators which provide both the spatial and temporal specificity seen in bilayer unification. One such regulator is the Sec1/Munc18 (SM) proteins, a 65-70 kDa family of proteins composed of seven mammalian and four yeast members. As previously mentioned, SM proteins were initially identified as crucial components of the intracellular trafficking machinery in secretion deficit strains of *S. cerevisia* (Novick and Schekman, 1979; Novick et al, 1980, 1981). Sec1p and its homologue, slp1, have been implicated in a number of intracellular transport pathways, from secretion to ER-Golgi transport, respectively in *S.cerevisiae* (Novick et al, 1980; Wada et al, 1990).

Around the same time Brenner independently identified mutations in 77 genes which resulted in the altered movement and coordination of the roundworm, *Caenorhabditis elegans* (Brenner, 1974). Disrupting the function of SM protein unc-18 (uncoordinated-18) resulted in paralysis and an accumulation of acetylcholine, suggesting impairment in the mechanisms underlying neurosecretion (Brenner, 1974). A similar phenotype for the Sec1 homologue, Rop, was later recorded in *Drosophila melanogaster* (Salzberg et al, 1993). The highly conserved sequence homology between Rop and Sec1p suggests that the Rop protein may also function in vesicle trafficking among membranes of Drosophila cells (Pevsner et al, 1994a). The prevailing phenotype evident in yeast, worm and fly highlights the conserved function of SM proteins throughout eukaryotic evolution and their necessity in both general secretion and synaptic transmission (Harrison et al, 1994).

The mammalian homologue of Sec1p, munc18-1, was identified through its specific interaction with syntaxin1a (Hata et al, 1993). In mammalian cells three munc18 isoforms exist, munc18-1 is primarily expressed in neurons and neuroendocrine cells (Hata et al, 1993; Garcia et al, 1994), munc18-2 is expressed in all non-neuronal tissue and munc18-3

is expressed ubiquitously (Hata and Südhof, 1995; Katagiri et al, 1995; Tellam et al, 1995). The study into the specificity of the interaction between different munc18 and syntaxin isoforms revealed that munc18-1 and munc18-2 can interact with syntaxin-1A, -1B, -2 and -3 whereas munc18-3 can only bind syntaxin-2 and -4 (Hata and Südhof, 1995; Halachmi and Lev, 1996; Tellam et al, 1997). This highly selective interaction highlighted the conserved function of SM proteins in membrane fusion may actually be mediated via syntaxin (Jahn, 2000). Munc18-1 was originally considered an oddity among other SM members as its interaction with its cognate SNARE, syntaxin, inhibited SNARE complex assembly (Pevsner et al, 1994a; Yang et al, 2000). This inhibitory role assigned to munc18-1 was however in stark contrast to the functionality of its homologues. Was this simply due to the divergence of SM protein function along the evolutionary tree or was the function of munc18-1 more complicated than first thought?

Whereas munc18-1 has been shown to have a strong affinity for monomeric syntaxin (Pevsner et al, 1994b) its yeast homologues Sly1p and Sec1p only bind to their cognate syntaxin, Sed5p and Ssolp respectively, when in the ternary SNARE complex (Carr et al, 1999; Bracher and Weissenhorn, 2002). Another yeast SM protein, Vps45p, binds to Tlg2p, its cognate syntaxin, both in the monomeric state and in the ternary SNARE complex (Bryant and James, 2001). This apparent discrepancy in binding modes was initially explained by apparent differences in the structures, binding sites and recognition motifs of the SM proteins and their syntaxin partners. However, another way to interpret the inconsistency between interaction modes was that SM proteins were interacting with their cognate syntaxin in two distinct manners (Misura et al, 2000; Bracher and Weissenhorn, 2002).

The complicated mechanism of SM-syntaxin interaction was finally elucidated upon the completion of the crystal structures of both munc18-1 and Sly1p, in complex with their cognate syntaxins (Misura et al, 2000; Bracher and Weissenhorn, 2002). Munc18-1 exists as a three-domain V-shaped molecule with a central cleft of approximately 15-20 Å which binds to syntaxin (Figure 1.1, based on crystal structure PDB 3C98 (Burkhardt et al, 2008)). The crystal structure of Sly1p revealed, in the presence of a Sed5p peptide, that it also exists in a similar arch like structure to munc18-1 (Bracher and Weissenhorn, 2002). Interestingly, comparison of both crystal structures revealed two separate binding motifs

between syntaxins and their respective SM protein. Sed5p bound only to the N-terminal domain of Slylp on the surface of the protein (Bracher and Weissenhorn, 2002) whereas syntaxin binds to domains 1 and 3 of munc18-1 and occupies most of the space of the arch of munc18-1 (Misura et al, 2000). A recent study comparing the membrane fusion machinery between the choanoflagellate *Monosiga brevicollis* and mammalian cells found that the structure and function of the munc18-1-syntaxin complex was remarkably similar. This finding indicates that this dual mode of interaction must have existed in the last common ancestor of choanoflagellates and animals and is a key step in driving SNARE mediated membrane fusion (Burkhardt et al, 2011). Therefore the conservation of components of the fusion machinery and their mechanisms of interaction from unicellular organisms to man suggests that these proteins were versatile enough to allow its adaptation to all intracellular fusion reactions (Bennett and Scheller, 1993a; Jahn and Südhof, 1999). The fact that SM homologues interact with their cognate syntaxins via two distinct mechanisms has partially explained the controversy regarding the functionality of SM proteins in exocytosis.

1.1

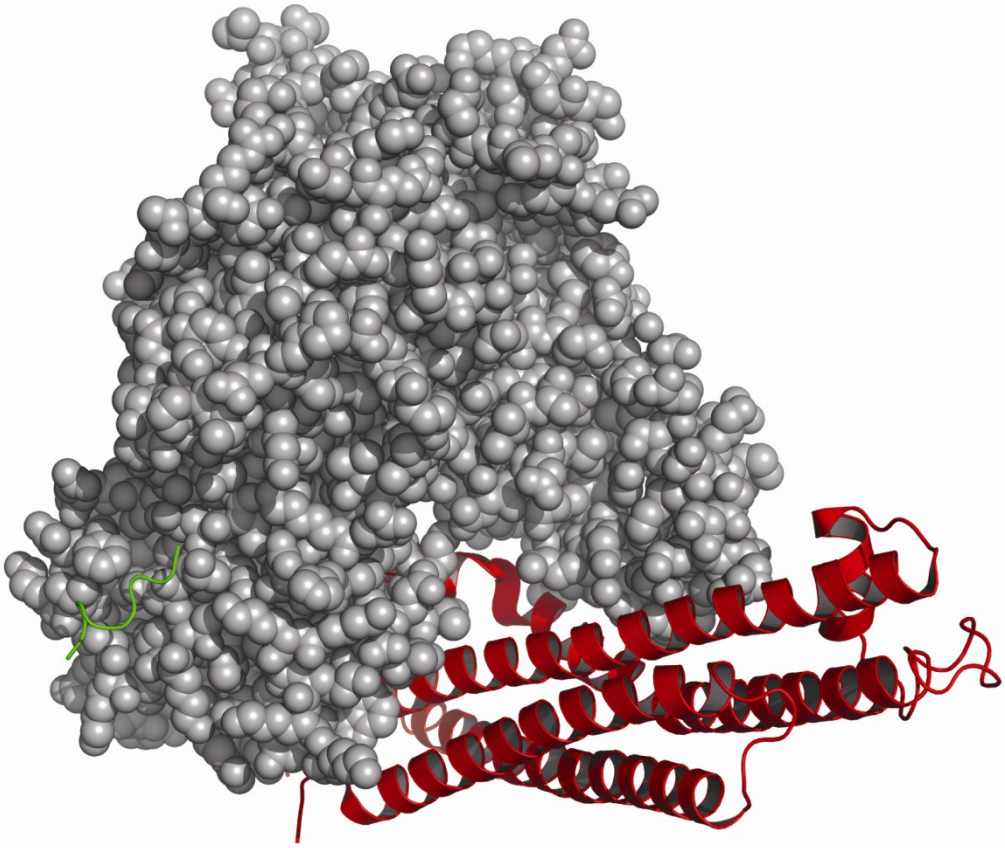

Figure 1.1 *Munc18-1 and syntaxin interact via two distinct binding modes.* Structure of munc18-1 (space fill) bound to syntaxin (red helices, closed form) and via the N-terminus of syntaxin (green helices) (PDB 3C98, Burkhardt et al, 2008). This highlights the dual modes of interaction through distinct binding sites on the surface of munc18-1.

1.3.1 MUNC18-1 AND ITS ROLE IN EXOCYTOSIS

The release of internalized cargo from a membrane bound vesicle involves a highly complex and regulated cascade of protein-protein interactions. The regulators of this process are therefore of vital importance in controlling the rate and extent of vesicle exocytosis. Munc18-1 is now widely accepted as a key player of the exocytotic reaction but for many years its precise function was hard to decipher, owing mostly to its complex interaction with syntaxin.

Preliminary findings found that SM proteins were imparting a negative effect on membrane fusion (Yang et al, 2000; Rickman and Davletov, 2005), for example, overexpressing munc18 orthologs Rop and s-Sec1 resulted in a 50% reduction in spontaneous vesicle fusion and inhibited evoked neurotransmitter release in *Drosophila* and squid respectively (Schulze et al, 1994; Dresbach et al, 1998). However, the interpretation that SM proteins were negative regulators of exocytosis simply did not fit with other findings of SM protein function *in vivo*. For example, yeast sec1 mutants exhibited a temperature-sensitive block in exocytosis (Novick and Schekman, 1979; Novick et al, 1980, 1981) and a single amino acid substitution in another yeast SM protein, Sly1p, demonstrated its fundamental importance in cell viability (Dascher et al, 1991). Perturbing unc-18 function within *C. elegans* affected acetylcholine metabolism (Hosono et al, 1992) and impaired neurotransmission at its neuromuscular junctions (Gengyo-Ando et al, 1993). Furthermore, *Drosophila* rop mutants (Harrison et al, 1994) and munc18-1 knockout mice exhibit a complete loss of spontaneous and evoked neurotransmitter release (Verhage et al, 2000) with the latter leading to postnatal neurodegeneration. Therefore, SM protein function reported in a wide range of organisms is wholly inconsistent with previous findings suggesting a simple inhibitory function.

One way these conflicting *in vitro* versus *in vivo* results have been partially reconciled is through the analysis of the diverging interaction profiles between SM proteins and their cognate syntaxins. Despite the fact that this interaction is evolutionarily conserved, the modality of their binding has diverged, complicating the understanding of their functional significance. Crystallographic analysis revealed that munc18-1 can interact with its

cognate syntaxin via two binding mechanisms, an interaction with 'closed form' syntaxin and via the highly conserved N-terminus of syntaxin (Burgoyne and Morgan, 2007; Dulubova et al, 2007; Rickman et al, 2007; Shen et al, 2007). Re-analysis of this data revealed that both binding modes can occur simultaneously (Burkhardt et al, 2008). Munc18-1 binds to syntaxin in its 'closed' conformation, in which the N-terminal Habc domain of syntaxin folds back onto the C-terminal α-helical SNARE motif (Pevsner et al, 1994b; Dulubova et al, 1999). This 'closed' conformation has a high affinity (2-20 nM) for munc18-1 (Pevsner et al, 1994b; Burkhardt et al, 2008) and prevents the formation of the SNARE complex due to the occlusion of the syntaxin SNARE motif. Closed form binding is utilised at the plasma membrane and within intracellular compartments of specialised secretory cells (Rickman et al, 2007). Syntaxin must travel from the ER to the plasma membrane in order to form SNARE complexes and drive exocytosis. Closed form binding has been shown to prevent syntaxin from forming any ectopic complexes with other intracellular SNAREs (Medine et al, 2007) until it reaches its final destination. Closed form binding thus prevents unregulated vesicular release by preventing indiscriminate SNARE complex formation and also proves to stabilise the SNARE complex immediately prior to fusion (Dulubova et al, 1999; Chen et al, 2008). The second mode of binding involving the extreme N-terminus of syntaxin is far less characterised and its functionality is the subject of intense debate.

1.3.2 The Functionality of Munc18-1-Syntaxin N-terminal Binding

Munc18-1 is able to interact with syntaxin via its highly conserved N-terminal sequence, a mode of interaction recently confirmed in a number of other SM homologues (Misura et al, 2000; Yang et al, 2000; Rickman et al, 2007). In fact, yeast SM proteins, Sly1p and Vps45p, involved in various intracellular trafficking steps only bind to monomeric syntaxin via its highly conserved N-terminal motif (Toonen and Verhage, 2007). This mode of binding involves an interaction between the outer surface of munc18-1 domain 1 and the extreme N-terminal peptide of syntaxin (Hu et al, 2007; Burkhardt et al, 2008). Munc18-1 can also bind to the assembled SNARE complex through 'open' syntaxin (Dulubova et al, 2007; Shen et al, 2007), a mode of interaction which involves the same

N-terminal binding motif and is consistent with the general function of SM proteins (Hu et al, 2007). The fact that the same N-terminal motif is employed in binding 'open' syntaxin is the reason for why this thesis only refers to two binding modes between munc18-1 and syntaxin. Over the last few years a huge amount of research has focussed on elucidating the functionality of N-terminal binding.

To date, N-terminal binding has been shown to stimulate secretory vesicle dynamics at the plasma membrane (Rickman and Duncan, 2010), SNARE assembly *in vitro* (Shen et al, 2007; Schollmeier et al, 2011), synaptic fusion in the calyx of Held (Khvotchev et al, 2007) and synaptic vesicle priming (Deak et al, 2009). Moreover, the interaction between munc18-1 and the N-peptide of syntaxin acts to recruit munc18-1 to the SNARE bundle to initiate the assembly of the SNARE-SM membrane fusion complex (Rathore et al, 2010) and has been shown to constitute the minimal complement for munc18-1 binding and activation (Shen et al, 2010). In *C. elegans*, a mutation in unc18 designed to disrupt N-terminal binding (F113R) with syntaxin did not rescue its locomotion defects, thereby suggesting that this second mode of binding is essential for Unc-18 function *in vivo* (Johnson et al, 2009). Other studies using site-directed mutagenesis in and around this area of munc18-1 reported that N-terminal interaction has little influence on neuroendocrine exocytosis (Arunachalam et al, 2008; Han et al, 2009; Malintan et al, 2009). However, a mutation used in one study was observed to have a low degree of evolutionary conservation and may therefore reflect a poor choice of mutation rather than the functionality behind the N-terminal interaction (Malintan et al, 2009). More recently it was shown using purified vesicles that N-terminal binding is indispensable for SNARE mediated membrane fusion (Diao et al, 2010). Furthermore, this year Verhage and colleagues found that mutations in munc18-1 that disrupted binding to the free syntaxin N-terminus and to assembled SNARE complexes support normal docking, priming and fusion of synaptic vesicles in munc18-1 null neurons (Meijer et al, 2012). This most recent interpretation of the role of the syntaxin N-terminal peptide suggests that it plays a role before and during SNARE-complex assembly but becomes dispensable during the later stages of synaptic transmission (Meijer et al, 2012).

As mentioned before, it is thought that N-terminal binding to free syntaxin and the assembled SNARE complex involves the same N-terminal domain of syntaxin. The exact

mechanism of how N-terminal binding contributes to SNARE complex assembly and downstream membrane fusion is still unknown. It has been demonstrated in multiple studies that N-terminal interaction is crucial for SNARE complex binding (Dulubova et al, 2007; Rickman et al, 2007; Shen et al, 2007). One possibility is that N-terminal binding supports the binary interaction between munc18-1 and syntaxin and acts to prevent indiscriminate and inappropriate SNARE complex assembly until required (Burkhardt et al, 2008). A recent study found that the association of munc18-1 with the assembled ternary SNARE complex affects fusion pore properties via multiple interactions with syntaxin, Rab3A and mints (Jorgacevski et al, 2011). Another study employing FRET-based reconstitution assays showed that the N-terminal peptide of syntaxin is able to recruit munc18-1 to the SNARE complex during the early stages of membrane fusion (Rathore et al, 2010). To date, the precise functionality of the N-peptide and its interaction with munc18-1 remains contradictory and thus requires further work to clarify its exact role in the membrane fusion process.

Another aspect of the munc18-1-syntaxin interaction which has never been elucidated is when munc18-1 and syntaxin enter into a long (or short) lived interaction and whether they ever dissociate from one another. Using intact and exocytosis-competent lawns of plasma membrane one study showed that the SNARE complex containing munc18-1 bound syntaxin can be effectively displaced by adding recombinant synaptobrevin or by endogenous SNAP-25 (Zilly et al, 2006). Therefore munc18-1 allows for the formation of a complex between syntaxin and SNAP-25 which serves as an acceptor for vesicle-bound synaptobrevin, thus acting as a positive regulator in the fusion process. Other evidence suggests that munc18-1 remains bound to syntaxin via its N-terminus throughout SNARE complex formation and subsequent membrane fusion (Dulubova et al, 2007). Therefore, quantification of molecular changes in interaction on a physiological (μs) time scale will elucidate when munc18-1 and syntaxin initially associate and if they ever actually dissociate from one another.

1.3.3 The Action of Munc18-1 as a Molecular Chaperone for Syntaxin

SM proteins play a chaperone-like role for their cognate t-SNARE, in addition to other regulatory functions. In *S. cerevisiae* cells lacking Vps45p, a munc18/Sec1p homologue, the cognate t-SNARE Tlg2p is down-regulated to undetectable levels by rapid proteasomal degradation (Bryant and James, 2001). Re-analysis of null munc18-1 embryonic murine chromaffin cells revealed more than a 50% reduction in syntaxin expression levels (Voets et al, 2001), providing more evidence for a chaperone-like role for munc18-1. In these mice, catecholamine release from embryonic chromaffin cells was reduced 10-fold but could be reversed by the over expression of munc18-1, leading investigators to conclude that munc18-1 was directly impacting on the exocytotic process. However, this phenotype can also be explained by changes in the expression levels of functional syntaxin on the plasma membrane and not only the lack of endogenous munc18-1. The reciprocal study, led by the same group, involved the acute deletion of the t-SNARE syntaxin in mice and resulted in an exact phenocopy of the munc18-1 null phenotype (de Wit et al, 2006). Unsurprisingly the cellular and plasma membrane levels of munc18-1 were reduced indicating that both proteins work in conjunction, making it nearly impossible to resolve their individual and independent functions. Furthermore, the inhibition of neurotransmitter release in *Drosophila* caused by overexpression of ROP can be fully rescued by co-overexpression of syntaxin (Wu et al, 1998).

Experiments carried out in non-neuronal cells revealed that overexpressed syntaxin becomes trapped in intracellular compartments (Medine et al, 2007). Co-expression of munc18-1 restored the correct plasma membrane localisation of syntaxin (Rowe et al, 1999; Rowe et al, 2001; Medine et al, 2007; Rickman et al, 2007). In PC12 cells lacking endogenous munc18-1, secretory events and large dense core vesicle docking was significantly impaired (Arunachalam et al, 2008). This was attributed to the absence of munc18-1 despite a reduction in syntaxin expression by 20% and its mislocalisation. A more recent study, using double munc18-1/-2 knockdown PC12 cells, found that both the expression and distribution of syntaxin determines the extent of vesicle docking and fusion (Han et al, 2009, 2011), not munc18-1. Further support for such a chaperoning role

demonstrated a disturbance in syntaxin homologue unc-64 anterograde trafficking upon a knockdown of endogenous munc18- in *C.elegans* neurons (McEwen and Kaplan, 2008).

Importantly it is now thought that instead of inhibiting SNARE complex formation (Pevsner et al, 1994a; Dulubova et al, 1999; Yang et al, 2000), munc18-1 acts as a molecular chaperone to prevent unregulated SNARE complex assembly until signalled to release syntaxin (Jahn, 2000). All of the above studies clearly indicate that munc18-1 is absolutely required for stabilizing monomeric syntaxin and for its efficient transport to the plasma membrane. All documented phenotypes involving the knockout or knockdown of a SM protein are therefore partly attributed to the subsequent reduction in expression levels of its cognate syntaxin.

1.3.4 Regulators of the Munc18-1-Syntaxin Interaction

Pivotal to understanding the dynamic interaction between munc18-1 and syntaxin is dissecting how their interaction is regulated. Over the last decade a number of kinases, proteins and fatty acids have been proposed to regulate this complex interaction and therefore a number of steps in the exocytotic pathway. It has been shown that munc18-1 is a substrate for protein kinase C (PKC) and can be phosphorylated at sites Ser313 (Craig et al, 2003), Ser306 and Ser307 (Fujita et al, 1996). PKC activation is triggered upon neuronal depolarisation (de Vries et al, 2000) and has been shown to prevent munc18-1 and syntaxin from associating (Fujita et al, 1996). Using munc18-1 phospho-mutants it was demonstrated that the phosphorylation of munc18-1 by PKC leads to vesicle pool replenishment following a physiological stimulus (Nili et al, 2006). PKC phosphorylation is thought to be essential for the regulation of exocytosis (Barclay et al, 2003), probably down to the fact that PKC phosphorylation of munc18-1 reduces its affinity for closed syntaxin (Fujita et al, 1996; Toonen and Verhage, 2007). It has also been shown that munc18-1 can be phosphorylated by cyclin-dependent kinase 5 (Cdk5), resulting in the dissociation of the munc18-1-syntaxin complex (Fletcher et al, 1999). Both PKC and Cdk5 phosphorylation sites are contained deep within the munc18-1-syntaxin complex, suggesting that this type of phosphorylation can only act after munc18-1 and syntaxin disassociation (Barclay et al, 2003).

Moreover, it has also been shown that the phosphorylation of syntaxin can modulate its interaction with munc18-1. Death-associated protein kinase (DAPK) phosphorylates syntaxin at Ser188 and decreases its ability to bind munc18-1 in a Ca^{2+}-dependent manner (Tian et al, 2003). Initial investigation into the function of synaptotagmin, the proposed neuronal calcium sensor, observed that it was phosphorylated *in vivo* by casein kinase II (CKII) (Bennett et al, 1993b). Further work identified residue serine[14] on syntaxin as a target for CKII (Risinger and Bennett, 1999; Foletti et al, 2000). Using a series of phosphomimetic and phospho-null mutations, it was later shown that serine[14] is a key regulator of the N-terminal interaction between syntaxin and munc18-1 (Rickman and Duncan, 2010). The enzymatic activity of these kinases therefore provides a signal transduction pathway by which the function of both munc18-1 and syntaxin could be regulated in response to an external stimulus.

Immediately prior to SNARE mediated vesicle exocytosis, syntaxin transitions from a closed to open conformation which is compatible with SNARE complex assembly (Dulubova et al, 1999; Gerber et al, 2008). Munc13, a comparatively large active zone protein, interacts directly with the extreme N-terminus of syntaxin, a site similar to that used by munc18-1 (Betz et al, 1997), explaining why the unc-13 and unc-18 phenotypes overlap considerably. Unc-13 has been shown to displace unc-18 from a complex with syntaxin, thereby modulating the interaction between unc-18 and syntaxin (Sassa et al, 1999). It is noteworthy to mention that this finding has never been repeated. However, following on from this finding, it has been hypothesised that munc13 is involved in the conversion between binding modes and is able to regulate the SNARE complex through binding directly to syntaxin (Betz et al, 1997). A more recent study has shown, through NMR and fluorescence experiments, that the munc13-1 MUN domain markedly accelerates the transition from the syntaxin-1-Munc18-1 complex to the SNARE complex (Ma et al, 2011).

Another possible regulator of this conformational switch is unsaturated arachidonic acid, shown to both stimulate munc18-regulated SNARE complex assembly and overcome the inhibition of syntaxin when munc18-1 is bound *in vitro* (Rickman and Davletov, 2005). Arachidonic acid has also been shown to act directly on syntaxin in its closed

conformation, permitting the transition of syntaxin from its inhibited state into the ternary SNARE complex where it can interact with SNAP-25 (Connell et al, 2007). These findings point to a role of fatty acids in the regulation of the conformational status of syntaxin and thus SNARE complex formation. Both munc18-1 and syntaxin are key players in the regulation of membrane fusion and it is their interaction with a number of regulatory partners, PKC, munc13-1, or the action of fatty acids that provides the temporal control necessary for their dynamic interaction and function.

1.3.5 MUNC18-1 AND ITS SYNTAXIN-INDEPENDENT MODES OF INTERACTION

Munc18-1 performs multiple functions in membrane exocytosis by acting as (i) a molecular chaperone of syntaxin, (ii) a mediator of vesicle docking, and (iii) a fusogenic component of the membrane fusion machinery. Despite its well characterised interaction with syntaxin, the multiple roles of munc18-1 in exocytosis may not be due to its interaction with syntaxin alone. The idea that SM proteins are not restricted to one role in the vesicle transport and fusion process is supported by a variety of studies in diverse organisms. In yeast cells the genetic interaction between Sly1 and the Rab-like GTPase Ypt1 (Dascher et al, 1991; Ossig et al, 1991) suggests an involvement of SM proteins in the early stages of vesicle recruitment. On the other hand a number of SM homologues have been reported to act at a late stage in membrane fusion, downstream of SNARE complex assembly (Carr et al, 1999; Grote et al, 2000; Fisher et al, 2001). A post-docking role of munc18-1 has been further supported by studies demonstrating that munc18-1 regulates fusion pore expansion, one of the last steps of membrane fusion (Fisher et al, 2001; Barclay et al, 2003). SM proteins have also been extensively linked to 'docking' stages of the vesicle lifecycle, an intermediate stage between vesicle trafficking and plasma membrane fusion. Within *C. elegans* unc-18 mutant synapses there is a reduction in the number of docked vesicles (Weimer et al, 2003), a similar phenotype recorded in the chromaffin cells from munc18-1 knockout mice (Voets et al, 2001). Interestingly, another study using the same munc18-1 knockout mice revealed that there was no synaptic vesicle docking phenotype despite a silencing of neurotransmission (Verhage et al, 2000), again supporting the role of munc18-1 downstream of vesicle docking. The disparity between

docking phenotypes in neuronal and neuroendocrine munc18-1 null cells indicates that additional regulatory mechanisms have evolved in order to support the more specific requirements of neurotransmission.

Recently, attention has been drawn to other proteins implicated in exocytosis that also bind to munc18-1. Granuphilin, a protein identified in pancreatic β cells that associates with dense core granules, has been reported to bind munc18-1, Rab3, and Rab27A (Coppola et al, 2002; Fukuda et al, 2002), providing a potential mechanism for the modulation of munc18-1 function through Rab activity. Using a gain-of-function mutant of munc18-1 (E466K), Graham et al (2008) identified a direct interaction between munc18-1 and Rab3A. Mutant munc18-1 increased exocytosis in both adrenal chromaffin cells and PC12 cells, indicating that Rab3A is involved in bridging Rab- and SNARE-mediated events in exocytosis (Graham et al, 2008). In support of this mechanism a more recent study found that the Rab3A cycle is coupled with the activation of munc13-1 via Rab3-interacting molecules (RIM; Huang et al, 2011). Munc18-1 could therefore act downstream of the macromolecular munc13-1/RIM/Rab3A complex and trigger fusion by promoting the dissociation of Rab3A dissociation from vesicles (Huang et al, 2011). However, despite these recent findings no convincing evidence exists which strongly supports this hypothesis.

Doc2 proteins, specifically doc2a and doc2b, which co-purify with synaptic vesicles, also bind to munc18-1 and have been suggested to act as adaptors in the regulation of the munc18-1-syntaxin interaction during vesicle docking (Verhage et al, 1997). Interestingly, these doc2 proteins contain C2-like domains, therefore linking them to the binding of Ca^{2+}, introducing a possible activity dependent mechanism with munc18-1. Furthermore, Mint proteins have been implicated in the regulation of both synaptic and large dense core vesicle exocytosis (Okamoto and Südhof, 1997; Zhang et al, 2004) by mediating the function of munc18-1. Therefore granuphilin (Coppola et al, 2002; Fukuda et al, 2002), doc2 (Orita et al, 1996; Verhage et al, 1997) and mints (Okamoto and Südhof, 1997; Ho et al, 2003) have all been implicated in the regulation of exocytosis but the exact nature of their function regarding munc18-1 and syntaxin is not well understood.

A study, using mutations in munc18-1 previously modelled on those in *Drosophila* (Harrison et al, 1994; Wu et al, 1998) and *C. elegans* (Sassa et al, 1999), revealed that despite retaining wild-type syntaxin binding affinities both the extent of exocytosis and the kinetics of individual release events in chromaffin cells were altered (Ciufo et al, 2005). Interestingly, a number of these munc18-1 mutants displayed reduced binding to mint1 and mint2 proteins, introducing another potential mechanism for the observed alteration in release kinetics. In support of this, a study rescuing defects in unc18 mutants by expressing constitutively open syntaxin mutants (Weimer et al, 2003) indicated that the function of SM proteins in exocytosis was not solely to regulate the conformational state of syntaxin. These studies therefore highlighted that munc18-1 can control multiple functions within a single membrane trafficking step via both syntaxin-dependent and -independent protein interactions (Ciufo et al, 2005).

The active zone is a structure found beneath the presynaptic plasma membrane and is thought to be the site of spatially regulated neurotransmitter release (Landis et al, 1988). Since the characterisation and identification of the active zone, a number of proteins have been shown to reside in its matrix, including bassoon (tom Dieck et al, 1998), piccolo (Cases-Langhoff et al, 1996), RIM1 (Wang et al, 1997), munc13-1 (Brose et al, 1995) and CAST (Ohtsuka et al, 2002). Most active zone proteins are thought to form elaborate protein-protein interactions resulting in the formation of a macromolecular protein complex (Ohtsuka et al, 2002). The functional interactions between active zone proteins have been shown to mediate synaptic vesicle priming (Betz et al, 2001), vesicle transport (Wang et al, 2002) and the release of neurotransmitters (Mochida et al, 1996; Schoch et al, 2002). Munc18-1 and syntaxin have also been repeatedly implicated in mediating these specific stages of membrane fusion, implying that a cascade of protein-protein interactions orchestrate the fusion of synaptic vesicles with the presynaptic plasma membrane. In summary, this intricate network of proteins has complicated our understanding of whether various munc18-1 binding proteins function by regulating SM-syntaxin interactions or whether their association with SM proteins involves syntaxin-independent pathways that are also linked to fusion.

1.4 THE MOLECULAR MACHINERY DRIVING MEMBRANE FUSION

It is established that the SNARE complex is a central component of the molecular machinery which drives membrane fusion. However, the molecular arrangement of the SNAREs and various accessory proteins required to catalyse membrane fusion is currently unknown. Up until now it has been widely accepted that a number of integral membrane proteins are highly clustered, for example insulin receptors (Uhles et al, 2003), lipid phosphate phosphatases (Kai et al, 2006) and synaptotagmins (Willig et al, 2006) are reported to exist in nonoverlapping, defined clusters. So, what is known about the spatial patterning of munc18-1 and syntaxin? Super-resolution imaging techniques Photoactivatable Localisation Microscopy (PALM) and Stimulated Emission Depletion Microscopy (STED) have shown that single syntaxin molecules adopt a highly clustered, non-random distribution across the plasma membrane (Sieber et al, 2007; Rickman et al, 2010). PALM data generated in this study provided an estimate of approximately 30–40 syntaxin molecules within a syntaxin cluster, a value comparable to a previous estimate using STED microscopy in combination with molecular modelling (Sieber et al, 2007). Munc18-1 has been previously localised on a gross scale in multiple studies (Zilly et al, 2006; Medine et al, 2007; Rickman et al, 2007) but diffraction-limited imaging, with a maximum lateral resolution of 178 nm (Medine et al, 2007), is too low to report subtle changes in the spatial distribution of any protein. Therefore the localisation of all membrane associated proteins to date has been at the limit of the resolution of the microscope or technique used and therefore cannot probe spatial arrangements of individual molecules on a nanometre scale.

Alongside membrane protein nano-patterning, the evidence concerning the composition of the fusion pore and specifically the minimal number of SNARE complexes required to drive single vesicular fusion is currently lacking. The advancement of molecular imaging and biochemical techniques has now made it possible to quantify the number of SNARE proteins needed to execute membrane fusion. In 2004 it was reported that as little as one SNARE interaction was necessary to drive liposome bilayer fusion by recording inter-protein fluorescence resonance energy transfer changes (Bowen et al, 2004). Interestingly this study demonstrated that both syntaxin and synaptobrevin are necessary in opposing

membranes to facilitate liposome docking whereas SNAP-25 had little effect on the efficacy of bilayer fusion (Bowen et al, 2004). However, a more recent study demonstrated that one SNARE complex was indeed sufficient for liposomal-liposome fusion but only at a low speed (van den Bogaart et al, 2010). These studies argue against a synergistic mechanism of membrane fusion between multiple SNARE molecules. However, these studies were conducted in a highly purified *in vitro* system that lacked the presence of other accessory molecules, known to regulate the formation of the SNARE complex, and could therefore potentially modify the number of SNAREs required to execute *in vivo* fusion.

What is perhaps most confusing about such a limited requirement of SNAREs in membrane fusion is the fact that synaptic vesicles express as many as 70 synaptobrevin molecules (Takamori et al, 2006) while PC12 fusion sites can contain on average 75 clustered syntaxin molecules (Sieber et al, 2007). So, if only one SNARE molecule is required for membrane fusion, why do specialised membranes express so many of them? Perhaps only a subset of expressed SNARE molecules exist in the correct orientation and conformation to drive membrane fusion making a large proportion of the molecules redundant? It has been shown that SNARE molecules are highly mobile and can rapidly diffuse through membranes (Wienisch and Klingauf, 2006), thereby increasing the probability of limited subset of fusion competent SNARE molecules to be present at a specific fusion site. It has been shown that SNAREs are highly promiscuous (Bajohrs et al, 2005), therefore making it conceivable to imagine that a large proportion of SNAREs are in fact redundant, with only a small subset performing the functions related to vesicular exocytosis.

It was over a decade ago when Scheller and colleagues demonstrated that three SNARE complexes dynamically cooperate to drive the fusion of a single secretory vesicle (Hua and Scheller, 2001). This was achieved by measuring the fusion kinetics of large dense core vesicles within PC12 cells alongside *in vivo* titration of inhibitors, in this case, a soluble SNARE coil domain derived from synaptobrevin. This is in agreement with a study conducted recently which used another titration approach to quantify the required number of SNARE complexes in intact chromaffin cells. The expression of different ratios of either wild-type SNAP-25 and a SNAP-25 mutant unable to support exocytosis

revealed a third-power relation for the fast phase of exocytosis, indicating that membrane fusion in neurosecretory cells is driven by three SNARE complexes (Mohrmann et al, 2010). Electrophysiological recordings of PC12 cells expressing a number of mutations within the transmembrane segment of syntaxin demonstrated a change in both transmitter flux and pore conductance (Han et al, 2004). This mutagenesis assay and steric hindrance measurements indicated that between five and eight SNARE complexes were positioned in a circular arrangement lining the fusion pore in order to drive membrane fusion (Han et al, 2004).

Clearly, over the last decade there have been a range of divergent estimates on the number of SNARE molecules required to catalyse membrane fusion. The wide range of estimates can be explained in a number of ways. Firstly, each study used different *in vitro* and *in vivo* models. Liposomal membranes used in one study had an average radius of 17 nm (van den Bogaart et al, 2010) whereas large dense core vesicles used in another are on average 10 fold larger (Han et al, 2004). These different membrane models will probably alter both the amount of energy and number of SNAREs required to drive fusion. Secondly, most purified *in vitro* systems neglect to express accessory proteins which have been shown to contribute to exocytotic events. For example, synaptotagmin has been repeatedly implicated in altering the curvature of plasma membranes in order to facilitate membrane fusion (Arac et al, 2006; Martens et al, 2007; Hui et al, 2009). Without accessory molecules the entire process of membrane fusion may exhibit different dynamics and impact on the number of fusogenic molecules required. Lastly, it is plausible that the number of SNARE complexes required to fuse a vesicle may differ depending on when the vesicle is recruited to a fusion site upon the arrival of a physiological stimulus. Those vesicles already resident at the plasma membrane, part of the readily releasable pool (RRP), feasibly have enough time to form multiple SNARE complexes before the arrival of a stimulus. A higher number of recruited SNARE and accessory molecules may well provide those RRP vesicles with a higher probability of undergoing fusion in a faster time scale. On the other hand, vesicles recruited to the plasma membrane under continuous and sustained stimulation may fuse with fewer, and possibly only one, SNARE complex (Bowen et al, 2004; van den Bogaart et al, 2010), due to time and demand constraints. In summary, establishing the correct number of SNAREs and their accessory factors necessary to drive vesicular fusion remains a huge challenge as

the composition of the RRP and how vesicles are spatially organised and prioritized in recruitment is more complex than originally thought (Duncan et al, 2003).

1.5 Summary and Thesis Aims

It is clear that all intracellular trafficking and membrane fusion events absolutely require the presence of the SNAREs and a number of accessory proteins, specifically munc18-1. Major findings, for example, the existence of divergent binding modes between munc18-1 and syntaxin to their temporal and spatial regulation across an intact biological membrane have led to a greater understanding of the regulatory steps involved in membrane fusion. It is now well known that multiple munc18-1-syntaxin binding mechanisms are utilised in distinct cellular locations and perform different regulatory roles (Rickman et al, 2007). Closed form binding is important in facilitating the trafficking of syntaxin to the plasma membrane (Rowe et al, 1999; Medine et al, 2007) whereas N-terminal/SNARE complex binding is involved in vesicle mobilization (Rickman and Duncan, 2010), SNARE complex binding (Dulubova et al, 2007) and regulating the extent and specificity of membrane fusion in *vitro* (Shen et al, 2007). Due to the close interrelationship between both binding modes it has been difficult to dissect the functional outcomes of these spatially organised protein interactions. This thesis will test which specific residues are critical in mediating the munc18-1-syntaxin N-terminal interaction and determine the functionality behind this interaction in live neuroendocrine cells.

Despite a large effort focused on the roles of munc18-1 and syntaxin in the exocytotic pathway it still remains unknown how both proteins are organised on the plasma membrane at a molecular level. The existence of their spatial arrangement and the mechanism behind such a self-organizing process is still unknown due to the limited techniques available to probe the spatial patterning and dynamics of these membrane proteins. Using both ground state depletion followed by individual molecule return microscopy (GSDIM) and photoactivatable localisation microscopy (PALM) this thesis aims to elucidate the molecular arrangement of both munc18-1 and syntaxin on a nanometer scale in both neuronal and neuroendocrine cells. It is still currently unknown, despite a number of estimates, how many SNAREs and accessory proteins are required to

drive membrane fusion. Using PALM this thesis explores the molecular distribution of munc18-1 in relation to membrane associated secretory vesicles to determine the number of munc18-1 molecules required to drive the fusion of a single secretory vesicle. By employing single particle tracking PALM (sptPALM) this thesis also investigates how munc18-1 molecules behave at the plasma membrane in order to provide information at the level of individual molecular motions for the whole population of proteins observed.

It is thought that munc18-1 functions through its direct interaction with syntaxin (Hata et al, 1993; Pevsner et al, 1994a). The universal importance of munc18-1 has been evidenced in a number of studies which genetically manipulated the function of munc18-1, resulting in deficits in intracellular trafficking (Novick and Schekman, 1979), syntaxin trafficking (Rowe et al, 1999; Arunachalam et al, 2008), large dense core vesicle docking (Voets et al, 2001) and neurotransmission (Gengyo-Ando et al, 1993; Verhage et al, 2000). What remains unknown however is the precise molecular kinetics and functionality of the munc18-1-syntaxin on a molecular level in live neuronal cells. This thesis aims to probe the dynamics of the munc18-1-syntaxin interaction at a single molecule resolution and physiological time scale in live neuronal cells. Despite a large body of evidence detailing the modes of interaction between munc18-1 and syntaxin, nothing is currently known about precisely when these proteins interact on a physiologically relevant time scale. Therefore, this thesis also aims to address, using Fluorescence Correlation Spectroscopy (FCS), the interaction profile between munc18-1 and syntaxin on a nanosecond time scale and whether this interaction is dynamically regulated by neuronal activity.

CHAPTER 2:

MATERIALS, METHODS AND OPTICAL TECHNIQUES

2.1 MATERIALS

2.1.1 GROWTH MEDIA AND SOLUTIONS

All chemicals were supplied by Sigma Aldrich, UK, unless otherwise stated and all tissue culture reagents were supplied by Invitrogen, UK, unless otherwise stated.

LB media

1% (w/v) Yeast Extract
1% (w/v) Bacto-tryptone
86 mM NaCl

2 X TY media

1.6% (w/v) Bacto-tryptone
1% Yeast extract
172 mM NaCl

SDS Sample Buffer (4X)

200 mM Tris-HCl, pH 6.8
6.4% (w/v) SDS
5 mM EDTA
16% (v/v) Glycerol
A few grains of Bromophenol blue

SDS PAGE Running Buffer

25 mM Tris
0.2 M Glycine
0.1% (w/v) SDS

Western Transfer Buffer

25 mM Tris
0.2 M Glycine
20% (v/v) Methanol

1 X PBS, pH 7.4

0.01 M Phosphate Buffer (pH 7.0)
0.0027 M Potassium chloride
0.137 M Sodium chloride

PBST

0.01 M Phosphate Buffer (pH 7.0)
0.0027 M Potassium chloride

0.137 M NaCl
0.02% Tween-20

Coomassie stain

10% (v/v) Methanol
20% (v/v) Acetic acid
200 mg/L Coomassie G-250

Orange-G loading dye

50% (v/v) Glycerol
5 mg/ml Orange G

Buffer A – GST tagged proteins

20 mM HEPES, pH 7.4
100 mM NaCl
1 mM EDTA
0.1% (v/v) Triton X-100

Buffer B (His_6-tagged proteins)

20 mM HEPES (pH 7.4)
100 mM NaCl
20 mM Imidazole
0.1% (v/v) Triton X-100

KD43 PC12 cell culture media

Advanced RPMI 1640 supplemented with-
5% (v/v) Fetal bovine serum
10% (v/v) Horse serum
1% Glutamax
50 μg/ml Gentamicin
2.5 μg/ml Puromycin

Primary embryonic cortical neuron culture media

Neurobasal medium supplemented with-
B-27 (50X)
0.5 mM L-glutamine
1% (v/v) penicillin/streptomycin

Primary embryonic dissection media

Dulbecco's Modified Eagle Medium (DMEM (Invitrogen)) supplemented with -

10% FBS
1% (v/v) penicillin/streptomycin

Primary embryonic transfection media

Minimal Essential Media (MEM (Invitrogen))

Primary embryonic cortical neuron stimulation buffer

136 mM NaCl
2.5 mM KCl
10 mM glucose
10 mM HEPES (pH 7.4)
2 mM $CaCl_2$
1.3 mM $MgCl_2$
Final pH – 7.3

Primary embryonic cortical neuron Ca^{2+} free stimulation buffer

136 mM NaCl
2.5 mM KCl
10 mM glucose
10 mM HEPES (pH 7.4)
1.3 mM $MgCl_2$
1 mM EGTA
Final pH – 7.3

GSDIM imaging buffer (in PBS)

0.5 mg/ml glucose oxidase
40 µg/ml catalase
10% (w/v) glucose
50 mM ß-mercaptoethylamine (MEA)

2.1.2 ANTIBODIES

The following antibodies were used for both immunofluorescence (IF) and western immunoblotting (WB).

Table 2.1 Primary and secondary antibodies

Antibody	Host	Clone	Dilution for IF	Dilution for WB	Supplier
anti-munc18-1	Mouse		1:500	1:5000	BD Biosciences
anti-munc18-1	Rabbit			1:5000	Synaptic Systems
anti-syntaxin	Mouse	HPC-1	1:1000	1:5000	Sigma
Syntaxin 1a (phospho S14)	Rabbit		1:1000	1:5000	Abcam
anti-SNAP-25	Mouse	SMI81	1:1000	1:10000	Cambridge Bioscience
anti-synaptobrevin	Mouse	69.1	1:1000	1:5000	Synaptic Systems
anti-β-tubulin	Mouse			1:5000	Abcam
anti-synapsin	Goat		1:500	1:1000	Santa Cruz
anti-synaptotagmin	Rabbit		1:1000		Invitrogen
anti-mouse-Alexa488	Mouse		1:1000		Invitrogen
anti-rabbit-Alexa488	Donkey		1:1000		Invitrogen
anti-mouse Alexa647	Goat		1:1000		Invitrogen

2.1.3 *ESCHERICHIA COLI* (*E.COLI*) STRAINS

A number of different *E.coli* strains were used for both DNA amplification and stable protein expression (Table 2.2). XL10-Gold ultracompetent cells were used for the transformation of DNA. BL21 competent cells were used for the transformation and expression of GST tagged proteins whereas M15 (pREP4) competent cells were used for the transformation and expression of His_6 tagged proteins.

Table 2.2 *E. coli* strains

***E.Coli* strain**	**Usage**	**Supplier**
X10-Gold	DNA amplification	Stratagene
BL21	GST-tagged protein expression	Stratagene
M15 (pREP4)	His_6 tagged protein expression	Qiagen

2.1.4 DNA PLASMIDS

The following table lists those DNA plasmids that were used during this study. A construct map is included in the Appendix.

Table 2.3 DNA plasmids

Plasmid	Protein fragment	Fusion tag	Antibiotic resistance	Promoter	Supplier
pCI	Munc18-1	-	Ampicillin	CMV	Promega, UK
pGEM-T-Easy	-	-	Ampicillin	T7, SP6	Promega, UK
pmCerulean-C1	Syntaxin, Syntaxin[S14E]	pmCerulean	Kanamycin	CMV	*Dr D Piston
pdkEYFP-C1	Syntaxin	pdkEYFP	Kanamycin	CMV	Clontech, UK
pEYFP-C1	Munc18-1 and mutants [D122A, D112K, I127A, I127F, E132A, E132K]	pEYFP	Kanamycin	CMV	Clontech, UK
pEGFP-C1	Munc18-1, Syntaxin, Syntaxin[openΔ6]	pEGFP	Kanamycin	CMV	Clontech, UK
pEGFP-N1	NPY	EGFP	Kanamycin	CMV	Clontech, UK
pmCherry	Munc18-1, Munc18-1[I127A] Syntaxin, Synapsin	mCherry	Kanamycin	CMV	Clontech, UK
PA-Cherry	Munc18-1, Munc18-1[I127A], Syntaxin	PA-Cherry	Kanamycin	CMV	Clontech, UK

*Kind gift of Dr D. Piston, Vanderbilt Kennedy Centre for Research on Human Development, Nashville, USA.

2.1.5 BACTERIAL PROTEIN EXPRESSION PLASMIDS

The following proteins were expressed in *Escherichia coli* BL21 or M15 (pREP4) cells (section 2.1.3) depending on the purification tag (Table 2.4).

Table 2.4 Bacterial protein expression plasmids

Protein + Protein Fragment	Purification Tag	Parent Vector	Source
Syntaxin 1a (1-261)	GST	pGEX-KG	(Medine et al, 2007)
Syntaxin 1a (7-261)	GST	pGEX-KG	(Medine et al., 2007)
Syntaxin 1a (1-225)	GST	pGEX-KG	See Appendix
Syntaxin 1a (1-213)	GST	pGEX-KG	See Appendix
Syntaxin1a (7-225)	GST	pGEX-KG	See Appendix
Syntaxin 1a (7-213)	GST	pGEX-KG	See Appendix
Munc18-1	His_6	pQE-30	(Rickman et al, 2007)
Munc18-1[D112A]	His_6	pQE-30	See Appendix
Munc18-1[D112K]	His_6	pQE-30	See Appendix
Munc18-1[I127A]	His_6	pQE-30	See Appendix
Munc18-1[I127F]	His_6	pQE-30	See Appendix
Munc18-1[E132A]	His_6	pQE-30	See Appendix
Munc18-1[E132K]	His_6	pQE-30	See Appendix

2.1.6 OLIGONUCLEOTIDES

All custom designed oligonucleotides used for cloning were purchased from Sigma-Aldrich, UK.

2.2 MOLECULAR BIOLOGY TECHNIQUES

2.2.1. POLYMERASE CHAIN REACTION (PCR)

Amplification of DNA fragments from template DNA was performed using the Expand High Fidelity PCR System (Roche, UK). Custom oligonucleotides (Sigma Genosys, Sigma-Aldrich, UK) were designed and used in the amplification of the DNA fragment of interest. All PCR reactions were performed using a Gene Amp PCR System 9700 (Applied Biosystems).

The following standard reaction was used:

DNA template (50 ng/ml)	1 µl
Oligonucleotide 1 (10 pmol/µl)	1 µl
Oligonucleotide 2 (10 pmol/µl)	1 µl
Nucleotide mix (10 mM of each dNTP)	1 µl
Expand High Fidelity Buffer (10X conc.)	5 µl
Expand High Fidelity enzyme mix	1 µl
Sterile double distilled water	Final volume of 50 µl

The PCR cycle parameters were as stated in the manufacturer's (Thermo Scientific) instructions. The reaction was prepared and the Expand High Fidelity enzyme mix was added at 95 ºC. The thermostable polymerase enzyme mix (*Taq* DNA polymerase and *Tgo* DNA polymerase) acts by extending the annealed oligonucleotides to synthesise DNA from 3' to 5' end of the oligonucleotide. The process of denaturation, annealing and extension is repeated numerous times, with each newly synthesised DNA acting as a template for the next reaction. The PCR product size was confirmed through agarose gel electrophoresis (section 2.2.3) and subsequently ligated into the plasmid of interest (section 2.2.5) and transformed into XL-10 Gold ultra-competent *E. coli* cells (section 2.2.6).

2.2.2 SITE-DIRECTED MUTAGENESIS

The technique of site-directed mutagenesis was used to introduce defined point mutations *in vitro* into previously cloned DNA. The QuickChange XL Site-Directed Mutagenesis Kit (Stratagene, UK) used parent DNA template and two complementary mismatched oligonucleotide primers (Sigma Genosys, Sigma-Aldrich, UK), both containing the desired base change flanked by unmodified nucleotide sequence.

The standard reaction was as follows:

10X Reaction Buffer	5 µl
DNA template	5 ng/µl of plasmid DNA
Oligonucleotide 1	100 ng/µl
Oligonucleotide 2	100 ng/µl
Nucleotide mix (10 mM of each dNTP)	1 µl
Quiksolution	3 µl
Pfu Ultra DNA polymerase	2.5 U/µl
Sterile double distilled water	Final volume of 50 µl

The PCR cycle parameters were as stated in the manufacturer's instructions, with an extension time of 1 min per kb of plasmid. Agarose gel electrophoresis (section 2.2.3) was used to confirm that a PCR product was present. *Dpn* I (1 µl) restriction enzyme was added directly to each amplification reaction to digest the parental supercoiled dsDNA at 37 °C for 1 hour. The PCR product was subsequently transformed into XL-10 Gold ultra-competent *E. coli* cells (section 2.2.6) and was later amplified depending on the selective survival of the *E. coli* on an antibiotic background.

2.2.3 AGAROSE GEL ELECTROPHORESIS

Agarose gel electrophoresis was used to separate and resolve different DNA fragments based on both their length and size. A 1% (w/v) agarose gel solution was added to 1 x Tris/Borate/EDTA (TBE) buffer and boiled. SYBR Safe (Invitrogen, Paisley, UK) was added at a 1:10,000 dilution and the mixture was poured into the gel rack containing an appropriate gel comb. A volume of loading dye (Orange G) was added to the DNA mixture and the samples were loaded alongside a 1 Kb plus DNA marker (Invitrogen, Paisley, UK). DNA gels were run at 120 V in 1 x TBE buffer until the sample reached the end of the polyacrylamide gel and imaged using a UV light source.

2.2.4 RESTRICTION ENDONUCLEASE DIGESTS

Restriction endonucleases were used to verify that plasmid DNA inserts were in the correct orientation and to switch the fluorescent tag contained within a plasmid. Restriction endonucleases (Promega, UK) are commercially available bacterial enzymes that cleave DNA at specific recognition nucleotide sequences. Double digests were commonly performed if the activity of selected restriction enzymes were compatible with the same buffer. A typical double restriction enzyme digest reaction was as follows:

Plasmid DNA	3 µg plasmid DNA
Restriction enzyme 1	1.5 µl (enzymes 1/10 final volume)
Restriction enzyme 2	1.5 µl
10 X Enzyme Buffer	3 µl
Sterile double distilled H_2O	Final volume of 30 µl

A standard double restriction digest involved incubating the reaction for 1 hour at 37 ºC. DNA digestion was confirmed using agarose gel electrophoresis (section 2.2.3). DNA was subsequently imaged under UV light, cut out of the agarose gel and purified using a QIAquick gel extraction kit (Qiagen, UK).

2.2.5 LIGATION OF INSERT AND VECTOR DNA

To ligate the double-stranded insert and vector DNA T4 DNA ligafast enzymes (Promega, UK) were used. A typical ligation reaction was performed according to the manufacturer's instructions and was set up as follows:

Vector DNA	1 µl
Insert DNA	3 µl
Rapid Ligation Buffer	5 µl
T4 DNA Ligase	1 µl
Sterile double distilled water	Final volume of 10 µl

All ligation mixtures were incubated at room temperature for 30 minutes and confirmed by agarose gel electrophoresis (section 2.2.3). Upon successful ligation DNA was transformed in *E.coli* competent cells (section 2.2.6).

2.2.6 PLASMID TRANSFORMATION

XL-10 Gold ultracompetent cells (Table 2.2) were used for the high efficiency transformation of plasmid DNA. In the case of protein expression, BL21 (DE3) or M15 (pREP4) (Table 2.2) competent cells were used. 1 μg of DNA or 10 μl of ligation product was added to 35 μl of competent cells on ice. The suspension was incubated for 10 minutes on ice, exposed to a 42 °C heat shock for 30 seconds to permeabilise the *E.Coli* cell membrane and returned to ice for 2 minutes. Suspensions were then incubated with 0.5 ml preheated Luria Bertani (LB) media and left in a 37 °C cell shaker (200rpm) for 1 hour. 100 μl of each suspension was plated on LB agar plates containing 0.1 mg/ml of the appropriate antibiotic and incubated at 37 °C overnight.

2.2.7 SMALL AND LARGE SCALE PLASMID DNA PURIFICATION

The isolation and purification of small and large scale plasmid DNA was carried out according to the manufacturer's instructions using a QIAprep Miniprep Kit (Qiagen, UK) and HiPure Maxiprep Kit (Invitrogen, Paisley UK) respectively. DNA that was used to transfect primary embryonic cortical neurons was isolated and purified using a QIAprep Maxiprep kit (Qiagen, UK) according to the manufacturer's protocol.

2.2.8 DNA QUANTIFICATION AND SEQUENCING

The concentration of plasmid DNA was determined using spectrophotometry at 260 nm. DNA was diluted 1:200 with 0.5% DEPC H_2O in balanced Hellma 6040-UV 10 mm Quartz cuvettes and measured using a Thermo Electron Corporation, Biomate 3 UV-Vis spectrophotometer. The sequencing of all constructs used standard or custom designed

oligonucleotides (Cogenics, UK). To verify correct sequencing, DNA sequences were analysed using Invitrogen Vector NTI software.

2.3 Protein Biochemistry Techniques

2.3.1 SDS-Polyacrylamide Gel Electrophoresis (SDS-PAGE)

SDS-Polyacrylamide gel electrophoresis (SDS-PAGE) was used for the separation of proteins based on their molecular weights. 10% protein gels were made using the following recipe –

Resolving gel	
Sterile H_2O	3 ml
50% (v/v) glycerol	3 ml
1.5 M Tris, pH 8.8	3.75 ml
30% (w/v) Acrylamide	5 ml
10% (w/v) SDS	150 µl
10% (w/v) APS	100 µl
TEMED	10 µl
	Final volume 15 ml
Stacking gel	
Sterile H_2O	4.75 ml
0.5 M Tris, pH 6.8	1.875 ml
30% (w/v) Acrylamide	0.75 ml
10% (w/v) SDS	75 µl
10% (w/v) APS	100 µl
TEMED	10 µl
	Final volume 7.5 ml

Resolving gel was poured into pre-assembled gel boxes and left to polymerize for 30 minutes. To provide a smooth surface and interface at the top of the separating gel, sterile H_2O was placed on top of the resolving gel during polymerization. Following resolving gel polymerization the sterile H_2O is removed and the stacking gel is poured to make up 15-20% of the gel height. The appropriate comb was then inserted and the stacking gel was left to polymerize for 15 minutes. The difference in pH and acrylamide concentration of both gels functions to compress the sample at the interface and provides better resolution when the protein bands reach the resolving gel.

The gels were then inserted into a Mini-PROTEAN 3 electrophoresis apparatus (Biorad, UK) and the tank was filled with SDS running buffer (section 2.1.1). Protein samples were denatured at 100 ºC for 5 min in 1 x SDS sample buffer (section 2.1.1), loaded alongside a Precision Plus Protein Standards All Blue protein marker (Biorad, UK) and run at 150 V until the dye front reached the bottom of the gel.

2.3.2 WESTERN BLOT TRANSFER AND IMMUNOBLOTTING

Western immunoblotting was used to identify and to quantify the expression of various proteins. Samples were separated as described in section 2.3.1, transferred to polyvinylidene fluoride (PVDF) membrane (Millipore, UK) and probed with specific antibodies. The PVDF membrane was pre-soaked in 100% methanol, placed on top of the SDS-PAGE gel and then sandwiched between filter paper and sponges. This stack was then placed into a Mini-Trans Blot Cell Cassette (Biorad, UK) which was then inserted into a tank containing pre-chilled western transfer buffer (section 2.1.1). The membrane was transferred at a constant current of 250 mA for 90 minutes. The successful transfer of immobilized proteins from the SDS-PAGE gel to the PVDF membrane was confirmed by the presence of the protein standard markers.

Immediately after transferring the proteins to a PVDF membrane the membrane was incubated in milk solution to prevent spurious antibody binding. The milk solution was prepared fresh by adding 5g of dried milk (Sigma, UK) to 50 ml 0.05% PBS-Tween and centrifuged at 4000 rpm for 10 minutes to remove insoluble debris from the mixture. The PVDF membrane was blocked in this milk solution for 30 minutes at room temperature and the primary antibody (typically 1:5000 dilution) was added for either 1 hour at room temperature or overnight at 4°C. Unbound primary antibody was removed from the membrane by three, 5 minute washes of 15 ml PBST. The membrane was then incubated in HRP conjugated secondary antibody (diluted in 15 ml PBST + milk) for 1 hour at room temperature. Unbound secondary antibody was again removed by three, 5 minute washes of 15 ml PBST. All blocking, washing and antibody probing steps were performed under gentle agitation.

2.3.3 ENHANCED CHEMILUMINESCENCE (ECL)

Following primary and HRP-labelled-secondary antibody incubation protein bands were visualised by Enhanced Chemiluminescence (ECL). The West Dura enhanced chemiluminescence reagent kit (Pierce, UK) was used according to the manufacturer's instructions. Briefly, the HRP enzyme (attached to the secondary antibody) catalyses the reaction between the two substrates within the ECL kit (peroxide buffer and luminol/enhancer solution), emitting light which was detected by Kodak Chemiluminescence BioMax light x-ray film. Exposure of the membrane to the film typically lasted for 5 – 30 seconds to generate a strong signal on the film. The film was then immersed in Kodak GBX developer for 2 minutes, and immersed in water before being fixed in Kodak GBX fixer for 2 minutes. Finally, the film was rinsed in water before being dried using a photo film drier.

2.3.4 COOMASSIE STAINING

Coomassie Brilliant Blue R-250 stain was prepared as described (2.1.1) above and used to visualise proteins in a SDS-PAGE gel. Following gel electrophoresis the SDS-PAGE gel was immersed in pre-boiled Coomassie stain and subjected to gentle agitation for 10 minutes. The gel was then transferred to deionised water and allowed to destain, with regular changes of water, until the background was clear. This technique allows detection of bands of ~15 ng. The gel was then dried using a GelAir Drying System (Biorad, UK).

2.3.5 PROTEIN QUANTITATION

Protein concentrations were determined using the BCA (bicinchoninic acid) kit (Pierce, UK). The manufacturer's instructions were followed.

2.4 Purification of GST and HIS_6-tagged proteins

2.4.1 Recombinant protein expression conditions

All recombinant SM and SNARE proteins used in this study were expressed under standard conditions. A 50 ml solution of 2xTY + 0.1 mg/ml (section 2.1.1) of the appropriate antibiotic was inoculated with a single colony of either BL21 (DE3) or M15 (pREP4) cells expressing the relevant plasmid. The culture was grown for 7 hours at 37 ºC with shaking at 200 rpm and then used to inoculate 1 L of 2x TY media + 0.1 mg/ml antibiotic in a 2 L flask. After 2 hours of growth at 37 ºC with shaking at 200 rpm, IPTG was added at a final concentration of 1 mM to induce protein expression. Following the addition of IPTG, the temperature was reduced to 19 ºC and the bacteria was grown overnight (~16 hours) with shaking at 200 rpm.

2.4.2 Preparation of bacterial lysates for GST protein expression

Following the overnight expression of the glutathione S-transferase (GST) fusion proteins, 1 L bacterial cultures were centrifuged at 4,000 x*g* for 20 min at 4 ºC and the supernatant discarded. All procedures concerning the purification of bacterial lysates were carried out at 4 ºC and using cold solutions. The bacterial pellet was resuspended in 5 ml of chilled buffer A (section 2.1.1) + EDTA free protease inhibitor tablets (Roche, UK) and transferred to a 50 ml tube. Triton X-100 was added to a final concentration of 2% (v/v) and cells were lysed by sonication for 30 seconds (2 x 15s pulses) and incubated at 4 ºC for 20 minutes with rotation. The mixture was transferred to a centrifuge tube and insoluble material was pelleted by centrifugation at 15,000 x*g* for 30 min at 4 ºC.

2.4.2.1 Isolation of GST-tagged proteins

The purification of GST fusion proteins was performed using sepharose beads coated with glutathione. Glutathione sepharose beads (0.5 ml) (GE Healthcare, UK) were prepared by washing once in buffer A + 1 mM EDTA (section 2.1.1) and gently centrifuging (200 x*g*, 1 min) to remove the preservative solution. The buffer was then removed from the beads and replaced with 15ml lysed bacterial supernatant (section 2.4.2) and incubated at 4 ºC with rotation for 2 hours. The GST-fusion protein glutathione complex was washed by

centrifugation at 200 x*g* with 3 x 1 min washes with 15 ml of buffer A to remove unbound protein. After washing the beads were re-suspended in 7.5 ml of buffer A. SDS-polyacrylamide gel electrophoresis (section 2.3.1) was used to analyse typically 20 µl of the GST-fusion protein glutathione complex bead slurry to assess protein yield and to equalise future loading. Glycerol was then added to the bead slurry to a final volume of 15 ml and the mix was stored at -20 ºC until required.

2.4.3 PREPARATION OF BACTERIAL LYSATES FOR HIS_6-TAGGED PROTEIN EXPRESSION

Bacterial cultures expressing His_6 fusion proteins encoded by pQE-30 vectors were prepared as for GST tagged proteins (section 2.4.2), the only difference being in the buffer used (Buffer B, section 2.1.1).

2.4.3.1 PURIFICATION AND ELUTION OF HIS_6-TAGGED PROTEINS

His_6 fusion proteins were purified on a nickel chelating affinity column. All procedures were carried out at 4 ºC and all buffers were kept cold. 1 ml of Profinity Ni-Charged Resin (Biorad, UK) was transferred to a 15 ml Falcon tube and washed once with buffer B (section 2.1.1) by gentle centrifugation. The lysed bacterial supernatant (section 2.4.4) was transferred to the tube containing the resin slurry and incubated at 4 ºC with rotation for 2 hours. The His_6-fusion protein resin complex was washed by centrifugation at 200 x*g*, with 3 x 1 min washes with buffer B (section 2.1.1). The complex was then re-suspended in 7.5 ml buffer B and 20 µl of the His_6-fusion protein resin complex slurry was analysed by SDS-polyacrylamide gel electrophoresis (section 2.3.1). Finally, 7.5 ml of glycerol was added to the resin complex and the solution was mixed and stored at -20 ºC until required.

To elute the His_6 fusion proteins and remove unbound material from Ni^{2+} charged resin the beads were washed with 15 ml buffer B + 20 mM imidazole. The samples were added to 0.45 µm spin columns (Spin X, Corning Costar, UK) and washed with buffer B. The protein was eluted with 3 washes with a buffer containing excess imidazole (20 mM HEPES (pH 7.4), 100 mM NaCl, 300 mM imidazole, 0.1% (v/v) TX-100). Eluted protein

samples were solubilised in sample buffer and analysed by SDS- polyacrylamide gel electrophoresis (section 2.3.1).

2.4.4 Purification of brain derived proteins

All procedures to prepare brain extracts were performed at 4 ºC using cold solutions. Adult rats were culled according to Home Office regulations under Schedule 1. Rat brain lysates were prepared by homogenising whole rat brains in 6 ml of buffer A containing Complete Protease Inhibitor (EDTA free) (Roche) (section 2.1.1) using a glass homogeniser. Lysate was then transferred to a 15 ml tube and buffer A (section 2.1.1) added to a final volume of 10 ml. Triton X-100 was added to a final concentration of 2% (v/v) and the lysate was placed at 4 ºC for 20 minutes with mild rotation. Cellular debris was removed by ultracentrifugation using a Beckman TLA-100 rotor at 100,000 x*g* for 45 minutes at 4 ºC. Freshly prepared rat brain lysate was always used immediately.

2.5 Analysis of protein-protein interactions

2.5.1 Protein-protein binding assays

To study protein-protein interactions at a biochemical level we employed pull-down assays. Briefly, Glutathione S-transferase (GST) fusion proteins (table 2.4) were expressed in BL21 *E. coli* cells using standard methods (section 2.2.6). Eluted purified proteins or rat brain lysates were incubated with immobilised GST-Syntaxin (and variants) and incubated for 2 hours at 4 ºC with rotation. Unbound material was discarded by centrifugation in a table top micro-centrifuge at 13,000 x *g*. Beads were then washed 4 times in 1 ml of buffer A (section 2.1.1) and eluted in sample buffer (section 2.1.1) for SDS-polyacrylamide gel electrophoresis. Electrophoresed samples were transferred to PVDF membranes for immunoblotting with the appropriate antibodies (section 2.3.2) or alternatively membranes were stained with Coomassie to reveal the extent of protein binding (section 2.3.4).

2.5.2 PROTEIN PURIFICATION FOR FLUORESCENCE CORRELATION SPECTROSCOPY

Coding sequences for EGFP (Clontech pEGFP-N1) and mCherry (Clontech pmCherry-N1) were amplified by PCR with added 5' and 3' restriction sites. A poly-histidine tag was also added to carboxyl terminal of the fluorescent protein during PCR. PCR fragments were then inserted into the bacterial expression plasmid pGEX-KG for Glutathione-S-transferase (GST) fusion. EGFP fused to mCherry was created by ligation of EGFP into EcoRI and SalI sites of the newly constructed pGEX-KG_mCherry plasmid. Recombinant fluorescent proteins were expressed in *E.coli* and purified using affinity, ion-exchange and size exclusion chromatography. Affinity chromatography was carried out using GST and His-tag purification. GST purification was performed first by incubation of clarified bacterial lysate with Glutathione-Sepharose beads (GE Healthcare). Beads were washed twice with 500 mM NaCl in buffer A (20 mM Tris pH 7.4, 1 mM EDTA and 0.1% TX-100) and twice with 150 mM NaCl in buffer A (section 2.1.1). A final washing step was done in low salt buffer A excluding EDTA followed by thrombin (Sigma) cleavage to elute the bound protein. His-Tag purification was performed on a HiTrap ™ FF nickel chelating column (GE Healthcare) equilibrated with 20 mM imidazole in buffer B (20 mM Tris pH 7.4 and 150 mM NaCl) followed by a gradient elution with 500 mM imidazole in buffer B . The His tag eluted proteins were further purified by ion exchange using a Mono Q™ 5/50 GL column equilibrated with 25 mM NaCl in 20 mM Tris pH 8.5 and eluted with 1 M NaCl in 20 mM Tris pH 8.5. Gel filtration was carried out on a HiLoad™ 16/60 Superdex 200 column equilibrated with buffer A. All fractions were analysed by SDS-PAGE and Coomassie staining and fractions containing fluorescent proteins were concentrated with a Vivispin 15R (Sartorius Stedim) before proceeding to subsequent purification steps. Protein concentration was measured using a Nanodrop A 280 module with entered values for protein molecular weight and molar extinction coefficient.

2.5.3 PROTEIN STRUCTURAL DATA

The structural alignment of munc18-1 was based on the crystal structure (PDB 3C98, (Burkhardt et al, 2008)) and was generated by aligning the amino acid sequences of 191 predicted SM proteins. The degree of amino acid conservation was shown on a colour

coded scale (red – low, blue – high conservation). All illustrations were generated using PyMol software.

2.6 CELL CULTURE

All cell culture reagents were supplied by Invitrogen (Paisley, UK) unless otherwise stated. All plasticware was Greiner branded products (Greiner, UK).

2.6.1 ROUTINE PC12 CELL CULTURE

Wild-type and KD43 PC12 cells were maintained at 37 ºC in 7.5% (v/v) CO_2, 92.5% (v/v) air. Wild-type PC12 cells and KD43 PC12 cells were maintained in Advanced RPMI 1640 (section 2.1.1) and passaged twice weekly. PC12 cells were rinsed off collagen-coated flasks using 5 ml of versene. The cell suspension was diluted with 50 ml medium and centrifuged at 500 x*g* for 5 min at room temperature. Medium was then removed and the cells re-suspended in 12 ml media. Cells were re-seeded into collagen-coated flasks at a 1:3 dilution. For imaging purposes, cells were seeded onto glass coverslips in 6 well plates at a density of approximately 10^6 cells/ml.

2.6.2 CLEANING AND COATING OF GLASS COVERSLIPS

All coverslips used in imaging experiments were thoroughly cleaned before poly-D-lysine coating. Dust and foreign material was removed from coverslips by washing them with 100 mM NaOH + 0.1% (v/v) Decon- 90 detergent in a sonicator bath for 30 secs. Following sonication, the coverslips were washed 3 times with double distilled H_2O, once with 100% ethanol and once with 100% acetone. Coverslips were allowed to air dry before immersed in Poly-D-lysine (PDL) at a final concentration of 50 µg/ml for 1 hour at room temperature. Coverslips were then washed with sterile distilled water to remove excess PDL and allowed to air dry under a UV light source.

2.6.3 PC12 CELL TRANSFECTIONS

For the effective delivery of plasmid DNA into PC12 cells, cell transfections were performed using Lipofectamine 2000 (Invitrogen, UK). PC12 cells were plated onto 30 mm coverslips at the desired density (section 2.6.1) twenty four hours prior to Lipofectamine 2000 (Invitrogen, UK) transfection. Manufacturer's instructions were followed.

2.6.4 PRIMARY EMBRYONIC CORTICAL CELL CULTURE - CLEANING AND COATING OF GLASS COVERSLIPS

25 mm coverslips were autoclaved at 120 °C for 1 hour and incubated in filter sterilised Poly-D-lysine at a final concentration of 50 µg/ml at room temperature under gentle agitation. Coverslips were left to air dry in a sterile environment and used when required. At least two hours before dissection a 50 µl droplet of 10 µg/ml laminin was placed into the middle of previously PDL-coated coverslips and transferred to 37°C incubator.

2.6.5 DISSECTION AND PRIMARY CELL MAINTENANCE

Embryonic (18) cortical neurons were prepared using Sprague Dawley rats which were killed according to Home Office Schedule 1 regulations. The abdomen of the rat was opened and both uterine horns containing the embryos were removed and placed in a solution containing ice-cold PBS + 1% penicillin/streptomycin. Embryos were then decapitated and heads were dissected to isolate individual cortices. Olfactory bulbs and meninges were carefully removed and the cortical tissue was transferred to enzyme tubes containing pre-warmed papain diluted to 10units/ml in sterile PBS. Enzyme digestion took place in a water bath set to 37 °C for 20 mins. Following tissue digestion excess papain solution was removed and replaced with 2 ml pre-warmed supplemented DMEM (section 2.1.1). Tissue was disaggregated and any precipitated DNA was removed. DMEM media (section 2.1.1) was then added to a final volume of 10 ml and the cell suspension was centrifuged at room temperature at 250 x*g* for 3.5 minutes. Supernatant was then removed and the resulting pellet was re-suspended in pre-warmed full Neurobasal (NBA) medium (typically 1 ml NBA per head dissected) (section 2.1.1). A

cell count was performed using a haemacytometer and the suspension was diluted to 10^7 cells/ml. Cells were plated into the laminin spot at the desired density, placed in a 37°C incubator and topped up with 2 ml full Neurobasal medium after 1.5 hours. After 24 - 72 hours *in vitro* Ara-C (Invitrogen) was added to a final concentration of 1 µM.

2.6.6 Primary embryonic cortical cell transfections

Cortical neurons were transfected at day *in vitro* (DIV 10-12) with Lipofectamine 2000. Twenty minutes before transfections full NBA was removed from the cells, transferred to a falcon tube and placed back into the 37°C incubator. Pre-warmed MEM (section 2.1.1) was added to the neurons and transfections were carried out according to the manufacturer's instructions. In contrast to the PC12 cell transfections 1 µl/well Lipofectamine 2000 and 2 µg DNA was used due to the apparent difference in sensitivity of each cell type. The transfection mixture was left on for 2 hours and then removed. Cells were washed twice in pre-warmed MEM and then immersed in the pre-conditioned full NBA that was previously removed.

2.7 Sample Preparation for Microscopy

2.7.1 Cell fixation with paraformaldehyde

For immunofluorescence, both PC12 cells and primary cortical neurons were fixed with 4% (w/v) paraformaldehyde (PFA). PFA was prepared by adding PFA powder (4 g) to double distilled sterile water (50 ml), heated to 60 °C, and cleared by the addition of 1 M NaOH. This stock solution was diluted with phosphate buffered saline (2 x PBS) (50 ml). Culture media was aspirated off and cells adhering to coated coverslips were gently washed twice with 1 x PBS (section 2.1.1) and then fixed with 4% (w/v) PFA for 20 min. PFA was then removed by aspiration and the cells were washed twice with 1 x PBS. Cells were then incubated with 50 mM NH_4Cl for 10 min in order to quench cellular autofluorescence. The cells were again washed twice with 1 x PBS and were either mounted on slides using mowiol anti-fade medium (Calbiochem, UK) or subjected to immunofluorescence staining.

2.7.2 IMMUNOFLUORESCENCE LABELLING

Following fixation with 4% (w/v) paraformaldehyde (section 2.7.1), cells were immunostained using the relevant primary and secondary antibodies. Cells were incubated in 0.5% (v/v) Triton X-100 detergent diluted in 1 x PBS (section 2.1.1) for 4 min in order to permeabilise the cell membrane. Neuronal cells were typically permeabilised for 3 min. Cells were then washed twice with 1 x PBS and incubated in 0.5% (w/v) fish skin gelatine for 30 minutes to prevent spurious antibody binding. Primary antibody (typically 1:1000 dilution), diluted in 1 x PBS supplemented with 0.5% (w/v) fish skin gelatine, was added to the cells and left to incubate for 3 hours at room temperature. The cells were washed twice with 0.5% (w/v) fish skin gelatine diluted in 1 x PBS and then stained with the conjugated secondary antibody (typically 1:1000 dilution) diluted in 1 x PBS supplemented with 0.5% (w/v) fish skin gelatine for 1 hour at room temperature. The secondary antibody was removed and the cells were washed at least 3 times with 1 x PBS in order to remove excess and unbound fluorescent secondary antibody. Lastly, cells were gently washed in double distilled H_2O to remove residual NaCl from the PBS, left to air dry and mounted on microscopic slides with mowiol anti-fade medium (Calbiochem, UK).

2.8 MICROSCOPY TECHNIQUES

2.8.1 THE POINT SPREAD FUNCTION (PSF)

The term 'resolution' is defined as the ability of an optical imaging system to distinguish between two objects. All conventional imaging systems, including widefield and confocal microscopy, are limited in the resolution that they can achieve by a number of physical properties. These physical factors include the wavelength of light used and the numerical aperture (NA) of the optical technique, a dimensionless number corresponding to the amount of light the microscope can collect. During image acquisition all imaging techniques are only capable of collecting a fraction of light emitted by a single source of light. Due to this inherent restriction not enough positional information is gathered in order to focus this light into a perfect three-dimensional image of the point. Instead, the image generated appears widened and spread into a three-dimensional diffraction pattern. The Point Spread Function (PSF) of a single source of light is therefore described as the three-dimensional diffraction pattern that it generates (Pawley, 1995). This spread of light

generated when light hits the sample is the reason why images acquired through optical means is not an accurate representation of what the sample actually looks like. There are two main reasons for this. Firstly, electronic noise aberrations from the microscope will force the spread of the image and secondly, diffraction limitations of the objective also results in a widened, distorted image.

An x-y slice through the centre of the PSF generated by an image can be seen as a set of concentric rings: the so-called Airy Disks. The width of these disks is used to define the theoretical maximum resolution of an imaging system and can be used as a direct indicator of the quality of an imaging system (Pawley, 1995; Müller, 2002). When two objects are sufficiently separated their images can be distinguished from each other on the basis of the variation in image intensity. However, as the minimum distance between objects decreases the intensity distribution, or PSFs, of the two points overlap. This overlap results in an image of a single larger or brighter object rather than two separate objects (Pawley, 1995; Müller, 2002). An image generated by a microscope is therefore composed of the superposition of PSFs from all the objects which have dimensions below the resolution of the system, each scaled according to the intensity of the corresponding point (Pawley, 1995). Thus, if resolution is the minimum separation distance at which the two objects can be distinguished, it is the width of the PSF that defines the limit of resolution.

2.8.2 CONFOCAL LASER SCANNING MICROSCOPY (CLSM)

All confocal data, apart from neuronal FCS data, were acquired on a Zeiss LSM510 Axiovert confocal laser scanning inverted microscope equipped with an LSM510 scanning head. The Zeiss LSM510 was fitted with four lasers, an Argon laser tuneable to 458 nm, 477 nm, 488 nm and 514 nm, a 543 nm He-Ne1 laser, a 633 nm He-Ne2 laser, and a pulsed excitation source at 800 nm (MIRA 900 Ti:Sapphire femtosecond pulsed laser with a coupled VERDI 10-watt pump laser (Coherent).

All FCS recordings were acquired using a Leica SP5 SMD (single molecule detection) laser scanning confocal microscope using a Zeiss C-Apochromat 1.2 NA X63 water-corrected immersion objective and 488 nm or 561 nm CW lasers. Photon fluctuation data

routed through a Picoquant PRT 400 router were acquired at microsecond rates using external Single Photon Avalanche Photodiodes (SpADs; MicroPhoton Devices, Italy). Band pass (BP) and long pass (LP) emission filters were used in both systems to only allow desired wavelengths of light to reach the objective. PMT detector gain and laser power were set manually in order to balance image brightness versus noise. Digital scan zoom was set to acquire at Nyquist sampling rates to improve resolution dependent upon the chosen objective. Using dual laser excitation, separate fluorescence emission channels were collected. Data were acquired using a 1024 X 1024 pixel image size, using a Zeiss Plan NeoFLUAR 1.4 numerical aperture (NA) 63x oil immersion lens. For all microscopy, live cells were maintained at 37 ºC in 5% (v/v) CO_2, 95% (v/v) air in a POC chamber (LaCon).

2.8.3 Total Internal Reflection Fluorescence Microscopy (TIRFM)

All TIRFM experiments used an Olympus CellR widefield TIRFM microscope equipped with 488 nm and 561 nm diode laser lines which were focussed into a motorised inverted epifluorescence microscope (IX81, Olympus, UK) through separate condensers. A micrometer screw in the illuminator was used to adjust the position of the laser beam in order to reach the critical angle for TIRF illumination. Laser light was also used for widefield illumination. The laser beam travelling through the objective exits the front lens at a high incident angle limited by the numerical aperture. The system was equipped with excitation and emission filters allowing rapid sequential imaging of red and green fluorescent emission. Data were acquired at a 512 x 512 pixel image size using a Hamamatsu ImageEM EMCCD with an Olympus PLAN APO 45 NA 60x oil immersion objective lens. For TIRFM imaging, cortical neurons and PC12 cells were plated on PDL coated coverslips (section 2.6.1 and section 2.6.5). All imaging was performed using live cells maintained at 37 ºC in 5% (v/v) CO_2, 95% (v/v) or cells fixed with 4% (w/v) paraformaldehyde and subsequently immunostained (section 2.7.2) and imaged in UV-sterilised PBS.

2.8.4 PHOTOACTIVATABLE LOCALISATION MICROSCOPY (PALM)

In this study PALM data was acquired in both fixed and live neuronal and PC12 cells transfected with plasmids tagged with PA-mCherry. PALM acquisition involved cycles of brief activation at 405 nm followed by rapid imaging in TIRF mode at 561 nm. All PALM experiments were performed using an Olympus IX-81 microscope equipped with Olympus Cell^R acquisition software, an ImageEM EM-CCD 512x512 camera (Hamamatsu UK) and an Olympus 150X UAPO 1.45NA oil lens with a resulting pixel size in the image of 106 nm. All single molecule coordinates were obtained using Matlab using a fitting and localisation routine kindly supplied by Dr Samuel Hess (Maine). Live PALM experiments required a lower 405 nm laser intensity, ensuring an even sparser distribution of single molecules during each activation and bleaching cycle. Point spread functions arising from single molecules were localised and tracked using custom written Matlab scripts. All cells for live PALM were maintained at 37 °C in 5% (v/v) CO_2, 95% (v/v) air in a 'POC' chamber (LaCon, Germany). Fixed cells were imaged in pre-bleached PBS and live cells were imaged in phenol-free supplemented culture media.

2.8.5 GROUND STATE DEPLETION FOLLOWED BY INDIVIDUAL MOLECULE RETURN (GSDIM)

All GSDIM experiments were performed on an Olympus IX-81 microscope equipped with Olympus Cell^R acquisition software, an ImageEM EM-CCD 512x512 camera (Hamamatsu UK) and an Olympus 150X UAPO 1.45NA oil lens with a resulting pixel size of 106 nm. Endogenous proteins were immunolabelled, after 90 minute fixation in 4% (section 2.7.2) with commercially available primary antibodies and Alexa-647-conjugated anti-IgG (Invitrogen). Alexa-647 was found to have the greatest propensity to enter a dark 'triplet' state using high intensity 640 nm illumination in an oxygen-depleting buffer (section 2.1.1). Point spread functions arising from single molecules of Alexa-647 were identified, localised and images rendered using a MatLab script written by Samuel Hess (Maine).

2.8.6 TIME CORRELATED SINGLE-PHOTON COUNTING FLUORESCENCE LIFETIME IMAGING MICROSCOPY (TCSPC FLIM)

TCSPC measurements were acquired using a Zeiss LSM510 Axiovert confocal laser scanning microscope equipped with a pulsed excitation source (MIRA 900 Ti:Sapphire femto-second pulsed laser coupled with a VERDI 10W pump laser (Coherent)) capable of delivering pulses of photons at a repetition rate of 80 MHz (Duncan et al, 2004). Recordings were made under 800–820 nm two-photon excitation, which efficiently excited cerulean without any measurable excitation or emission from EYFP, using a non-descanned detector (R3809U-50) multichannel plate-photomultiplier tube or a fast photomultiplier tube (H7422; both Hamamatsu Photonics UK) coupled directly to the rear port of the microscope. TCSPC recordings were acquired for 60 s with mean photon counts between 10^5 and 10^6 counts per second. Images were recorded at 256 × 256 pixels from a 1024 × 1024 image scan with 256 time bins over a 12-ns period (Duncan et al, 2004), using a Zeiss Plan NeoFLUAR 1.4 NA 63x oil immersion objective lens. Off-line FLIM data analysis used pixel-based fitting software (SPCImage, Becker & Hickl). The optimization of the fit parameters was performed by using the Levenberg-Marquardt algorithm, minimizing the weighted χ-square quantity and thus enabling the separation of the interacting and non-interacting FRET components. The long fluorescence lifetime component τ_2 was determined by control assays with cerulean expressed alongside dark (non-interacting) EYFP. Long lifetimes for each experiment were fixed. The number of photons given off by the sample decreasing over time results in a decay curve which can be fit to provide a measure of the lifetime of the fluorophore. During all FRET experiments neurons and KD43 PC12 cells were bathed in phenol-free supplemented culture media (section 2.1.1) and maintained at 37 °C in 5% (v/v) CO_2, 95% (v/v) air in a POC chamber (LaCon). To stimulate the neuronal cells 1 μM ionomycin (Invitrogen) was added immediately prior to FRET recordings with all acquisition parameters kept constant.

2.8.7 FLUORESCENCE CORRELATION SPECTROSCOPY (FCS)

All FCS recordings were acquired using a Leica SP5 SMD (single molecule detection) laser scanning confocal microscope using a 63X 1.2NA HCX PL Apo water lens and 488 nm or 561 nm CW lasers. Photon fluctuation data routed through a Picoquant PRT 400

router were acquired at microsecond rates using external Single Photon Avalanche Photodiodes (SpADs; MicroPhoton Devices, Italy). Neurons were transfected at DIV 10-12 (section 2.7.3), imaged at DIV 11-13 to ensure weak plasmid expression and placed in a custom made POC chamber with embedded platinum wires to deliver a stimulus. Cells undergoing electrical stimulation were immersed in stimulation buffer (section 2.1.1) and stimulated at 20 Hz for 20 s allowing all FCS data to be acquired during the stimulation train. Cells were also loaded with a Ca^{2+} indicator (Fluo-5F, 1 μM) in clear NBA media for 15 minutes at 37 °C in order to record the intracellular calcium rise during the FCS recordings. All cells imaged were maintained at 37 ºC in 5% (v/v) CO_2, 95% (v/v) air and analysis of all FCS data was performed using Leica software.

2.8.8 FM1-43 DYE IMAGING

FM dye imaging is a popular method used to monitor the rate of synaptic vesicle recycling. Recording the fluorescence changes of FM dyes under different stimulation paradigms quantifies the extent of exocytosis of distinct pools of synaptic vesicles. Embryonic cortical neurons were maintained for 12 days *in vitro* (DIV 12), transfected (section 2.6.6) and typically imaged on DIV 14-15. Cells were placed in a plastic imaging chamber and immersed in imaging buffer (section 2.1.1). Invaginating membrane was loaded using FM1-43 (10 μM) by stimulating vesicle recycling with a constant low frequency electrical stimulation (10 Hz, 60 s). This stimulation was delivered using platinum wires embedded in the imaging chamber. Cells were then washed for 2 minutes with imaging buffer (section 2.1.1) and left to recover for 8 minutes. Following the rest period, FM dye was unloaded from nerve terminals using either 60 action potentials (30 Hz) for 2 s to release the readily releasable pool of vesicles and 2 X 400 action potentials (40 Hz) for 10 s to unload the reserve pool of vesicles. Cells were left to recover for 40 s between stimulations. Untransfected cells in the same field of view served as internal controls. Dye unloading was visualised using a Nikon Diaphot-TMD epifluorescence microscope and 40 X oil objective at 495 nm excitation and 550 nm emission. Images were visualised using a Hamamatsu Orca-ER CCD digital camera and analysed using offline imaging software (ImageJ).

2.9 Image Processing and Analysis

2.9.1 Nyquist Sampling Rates

In order to capture all the information generated by a signal a microscopic system needs to sample at an optimal frequency. If the sampling rate interval in the *x*, *y* and *z* direction is either too fast or too slow aliasing occurs, a term referring to when a signal is sampled at a rate that is insufficient to capture the changes in a signal. The sampling rate used in this thesis was set at 2.3 times that of the resolvable spatial frequency which conforms to the Nyquist sampling theorem (Pawley, 2006). The Nyquist sampling frequency should be at least twice the highest frequency contained in the signal and therefore represents the minimal sampling at which a sample must be recorded to ensure that all the information present is represented in the samples. In order to adhere to Nyquist sampling rate using a confocal system the excitation wavelength, the numerical aperture of the objective, and the refractive indices of the immersion medium were all set correctly.

2.9.2 Image Deconvolution

All three-dimensional image stacks generated using a confocal microscope were deconvolved, an algorithm-based process aimed at reversing signal degradation, namely axial distortion and noise degradation (Inoué, 1995; Pawley, 1995; McNally et al, 1999; Pawley, 2006). Deconvolution is a computational image processing technique that is routinely used for improving the contrast and resolution of microscopic images by reversing the blurring which can be caused by diffraction limitations of the objective. In short, deconvolution recreates and restores the original signal before signal distortion, or convolution, occurs. Image deconvolution uses a number of deconvolution algorithms alongside theoretically or experimentally measured PSF dimensions. Theoretical PSF are commonly used however it is possible to experimentally calculate the PSF in a microscope system by measuring the image of a sub-resolution spherical bead. A combination of PSF values and tailored algorithms restores the original image by redistributing out-of-focus fluorescence and background signals by resolving the original distribution of point sources of light from the summed, overlapping PSFs (McNally et al, 1999; Sibarita, 2005; Pawley, 2006). Deconvolution has been shown to be of great importance in a number of image analysis techniques, such as co-localisation (Bolte & Cordelieres, 2006). Image data

acquired at Nyquist sampling rates in this thesis was deconvolved using Huygens software (Scientific Volume Imaging, The Netherlands), using a theoretical PSF calculated from the microscope parameters, and the resulting image data were analysed using NIH Image J software.

2.9.3 Quantification of protein co-localisation

Protein colocalisation is a term used to describe the presence of two or more distinct fluorescent molecules in the same volume. In this thesis, quantitative co-localisation analysis was performed to analyse the spatial distribution of two fluorescent proteins (either fluorescently tagged or through direct immunofluorescent labelling) within a cell.

All image co-localisation analysis was conducted on deconvolved 3D images (section 2.9.2). Quantitative protein colocalisation analysis, using ImageJ software, was displayed in a qualitative manner by merging the red and green channels together in order to represent overlapping pixels or areas of coincidence. A two-dimensional histogram represents the intensity for each channel in each voxel with a colour scale representing frequency. This method was applied to every voxel in the three-dimensional image stack, with the colour scale of the histogram corresponding to the frequency of voxels for each pair of intensity values. The more linear the histogram is, the closer the fluorescence intensity ratio between both channels and therefore the higher the colocalisation between both proteins. This histogram was fit by linear least-squares regression and yielded either a Pearson's correlation coefficient. From this fit, weighted residuals for each voxel were calculated and displayed as a 'residual map' to highlight areas of fluorescence channel covariance. The residual maps were generated by calculating the residual of each voxel from the linear regression fit to the intensities of each channel from all voxels.

The ImageJ co-localisation threshold plugin was used to calculate the linear regression equation of best fit ($y = mx + b$). The x axis channel (green) was used to generate a predicted y axis channel (red) using the line of best fit. The difference between the observed y axis channel and the predicted y axis channel was then calculated using the following equation:

$$\text{Residual} \quad \frac{\text{Observed - Predicted}}{\text{Observed + Predicted}}$$

For display, the residual was shown on a Hue Saturation Brightness (HSB) colour scale, where Hue was defined by the residual, Brightness was the combined intensities of channels 1 and 2, and Saturation was the maximum value of 255. Residual maps are displayed on a colour scale from -1 to 1 with cyan corresponding to a zero residual.

Pearson's correlation coefficient was used to quantify the co-localisation between two separate channels. Pearson's correlation coefficient (R) measures the intensity-dependent correlation between two channels and provides a value ranging from -1 to 1. This R value reflects the degree of linear relationship between the two variables, with the value of 1 representing perfect co-localisation between channels.

2.9.4 FLIM DATA ANALYSIS AND FRET CALCULATIONS

Offline TCSPC-FLIM data analysis used pixel-based fitting software (SPCImage, Becker & Hickl). Data generated was fit to either a mono-exponential or a bi-exponential decay depending on the experiment. An adaptive offset correction was calculated from the average number of photons per channel preceding the rising part of the fluorescence trace. This calculation ensured detector noise and background room light did not contribute significantly to photon counts. To fit the parameters of the multi-exponential decay to the fluorescence decay trace measured by the system, a convolution with the instrumental response function was carried out. The optimization of the fit parameters was performed by using the Levenberg-Marquardt algorithm, minimizing the weighted χ-square quantity and thus enabling the separation of the interacting and non-interacting FRET components. As a control the long lifetime component $\tau 2$ was determined by expressing cerulean with dark (non-interacting) EYFP. This value was subsequently used as a fixed $\tau 2$ lifetime for all other experiments. No FRET was detected in any of the control experiments.

2.9.5 PALM ANALYSIS

All single molecule and vesicle coordinates were obtained using Matlab using a fitting and localisation routine kindly supplied by Dr Samuel Hess (Maine). Custom written scripts were used to perform Ripleys L function and nearest neighbour analysis (Ondrej Mandula, University of Edinburgh). sptPALM data were analysed using custom written algorithms for automated particle detection and tracking. These particle detection algorithms build on the recently proposed concept of particle probability (PP) image (Yang et al, 2010), which measures the critical visual features of particles in a statistical manner. By combining the concept of PP images with a new refinement approach to obtain more accurate particle features, this novel particle detection and tracking method acts to improve particle tracking in dense particle fields under low signal-to-noise ratio and low contrast environments.

After obtaining particle tracking results using particle detection and tracking codes, two steps were employed to produce density and speed contour maps. Firstly, to guarantee sub-pixel precision of each particle trajectory, linear interpolation methods were used to estimate particle coordinates between consecutive image frames. Secondly, the numbers of particles trajectories were counted in each pixel of an image, generating contour maps containing molecular densities. Contour maps representing the average molecular speed of particles were produced by calculating the mean speed of each molecule in every pixel of an image. The difference contour maps were generated by normalising the density and speed contour maps and calculating the difference between the normalised figures. The rose diagrams, presented in a circular format with each concentric circle representing a different frequency of direction and colour-coded to display ranges of molecular directionality were produced using Matlab functions.

2.9.6 VESICLE TURNOVER QUANTITATION

FM dye unload was recorded as a time stack using simplePCI software (Hamamatsu). ImageJ software performed subsequent analysis. FM dye unload from transfected neurons was compared to dye release from internal controls, non-transfected neurons. In order to locate actively recycling synapses an image of a transfected neuron was overlaid with an image of FM puncta and those FM puncta that merged with a neurite were chosen for

analysis. The ImageJ software plugin, time series analyser, was used to measure the change in fluorescence of the FM dye at defined regions of interest. Traces were normalised (between 1 and 0) to the total change in fluorescence, i.e. the size of the total recycling pool of synaptic vesicles. Synaptic vesicle pool sizes were then determined by the changes in FM dye fluorescence upon different stimulation paradigms.

2.9.7 FCS DATA ANALYSIS

Photon fluctuation analysis and FCS auto-and cross-correlation data were performed using SymphoTime v5.4.4 software (Picoquant GmbH, Germany). To quantify rates of diffusion, the value of kappa (the ratio of the axial and waist excitation spot dimensions) was estimated using recombinant fluorescent protein standards. Briefly, purified EGFP and mCherry proteins (section 2.5.2), or EGFP fused to mCherry protein at defined nanomolar concentrations were suspended in 150 mM NaCl, 20 mM Tris pH7.4, 1 mM DTT and 0.1% (v/v) Tween 20 in LabTek borosilicate glass bottomed chambers. Parfocality between 488 nm and 561 nm excitation was achieved by adjusting the objective correction ring to maximise photon counts in each router channel. FCS data from these defined samples were fitted with triplet-state diffusion models informed with concentration and expected diffusion rates and the resultant value for kappa were used in subsequent fitting from experimental data from the same day.

CHAPTER 3:

THE MOLECULAR AND CELLULAR BIOLOGY OF THE MUNC18-1-SYNTAXIN-N-TERMINAL INTERACTION

3.1 INTRODUCTION

Key insights which helped to elucidate SM protein function came from studies of SNAREs and SM proteins from a number of different membrane compartments. The yeast SM proteins, Sec1p and Sly1p, previously implicated in membrane fusion, were shown to interact with their cognate syntaxin within the ternary SNARE complex rather than to isolated syntaxin (Carr et al., 1999; Bracher and Weissenhorn, 2002; Togneri et al, 2006). Another yeast SM protein, Vps45p, has been shown to bind to Tlg2p, its cognate syntaxin, both in the monomeric state and in the ternary SNARE complex (Bryant and James, 2001). In contrast, mammalian SM protein, munc18-1, was initially identified through its tight and highly specific interaction with monomeric syntaxin (Hata et al, 1993; Pevsner et al, 1994b). It was later shown that all syntaxins contain an H_{abc} domain, a motif which occludes its SNARE motif and downstream SNARE complex formation (Dulubova et al, 2001, 2002), suggesting the possibility that a closed conformation is not a general feature of syntaxins (Dulubova et al, 2001, 2002). In support of this, syntaxins from membrane bound cellular compartments like the ER, Golgi, *trans*-Golgi network and early endosomes were found to have a strong affinity for their cognate SM proteins through an N-terminal peptide, an interaction that is compatible with SNARE complex assembly (Dulubova et al, 2001, 2002; Yamaguchi et al, 2002).

The confusion surrounding SM-syntaxin interactions was recently resolved following the solving of the crystal structures of both munc18-1 and Sly1p, in complex with their cognate syntaxins (Misura et al, 2000; Bracher and Weissenhorn, 2002; Burkhardt et al, 2008). Comparison of both crystal structures revealed two distinct binding motifs between syntaxins and their respective SM protein. Sed5p, a yeast syntaxin, was found to only interact with the extreme N-terminal domain of Slylp (Bracher and Weissenhorn, 2002) whereas syntaxin binds to domains 1 and 3 of munc18-1 and occupies most of the 'arch' of munc18-1 (Misura et al, 2000). Therefore, despite both SM proteins adopting similar 3-D conformations they bind to their cognate syntaxins via more than one distinct mechanism.

Munc18-1 is able to interact with syntaxin in two possible conformations. First, munc18-1 can bind and stabilise syntaxin in a closed conformation in which the Habc domain of syntaxin folds back and occludes the SNARE motif (Pevsner et al, 1994b, Dulubova et al,

1999). By locking syntaxin in a closed conformation SNARE complex assembly is inhibited, the main reason why munc18-1 was initially labelled as an inhibitor of vesicle exocytosis (Pevsner et al, 1994b; Yang et al, 2000). A second SM protein binding site is located at the extreme N-terminus of syntaxin, a highly conserved N-peptide characterised by two to three charged residues followed by a hydrophobic leucine or phenylalanine residue which insert into a peripheral pocket of the SM protein (Bracher and Weissenhorn, 2002; Hu et al, 2007; Burkhardt et al, 2008). The N-terminal binding mode, initially discovered in the Golgi and endocytic SNAREs (Dulubova et al, 2002; Yamaguchi et al, 2002), was later found to be prevalent among SM–syntaxin pairs (Misura et al, 2000; Yang et al, 2000; Rickman et al, 2007). Munc18-1 can also interact with the ternary SNARE complex via 'open' syntaxin, a binding mode that involves the same N-terminal binding motif in syntaxin, with differences in the conformation and additional interactions adopted by the syntaxin molecule (Rickman et al, 2007; Shen et al, 2007). Therefore the finding that SM homologues interact with their cognate syntaxins via at least two distinct mechanisms has partially explained the apparently contradictory findings regarding the functionality of SM proteins.

Recent *in vitro* reconstitution experiments established a role for munc18-1 in accelerating SNARE-driven liposome fusion, revealed by selectively dissecting both binding modes (Shen et al, 2007). By selectively impairing N-terminal peptide interaction and SNARE complex binding the stimulatory action of munc18-1 was eliminated, an effect that was not reported using mutations that only interfered with closed syntaxin binding (Shen et al, 2007). These *in vitro* results therefore suggest that the interaction of munc18-1 with the N-terminus of syntaxin is critical for efficient neuronal exocytosis. In the same year it was shown that the two mechanistically distinct modes of binding between munc18-1 and syntaxin are both functionally and spatially distinct (Rickman et al, 2007). By separately analysing each binding mode these studies were able to assign a specific biological function to the munc18-1-syntaxin N-terminal interaction, an approach used in this experimental part of the thesis.

Despite a large body of work focusing on the interaction between munc18-1 and the N-peptide of syntaxin, little is actually known about the key residues mediating this highly specific interaction. Another facet of this interaction which is also largely unknown is

what function these key residues play in a cellular environment. Structural analysis discussed above has revealed potential residues key to mediating this interaction, key residues that must be tested experimentally. A recent study used a site directed mutagenesis approach to elucidate the key residues involved in mediating N-terminal interaction and reported that it had a limited influence on neuroendocrine exocytosis (Malintan et al, 2009). However, mutations selected in this study were shown to have a low degree of evolutionary conservation and therefore not appropriate constructs to investigate the functionality of the N-terminal interaction (Malintan et al, 2009). The available structural information on SM-SNARE protein binding modes has now enabled the design of mutations that disable these interactions, an approach used in this study.

This chapter describes the dissection of both closed form and N-terminal binding *in vitro*, a mutagenesis approach aimed at highlighting the extent of N-terminal binding utilised between munc18-1 and syntaxin *in vitro*. This chapter also describes new and rationally designed mutants of munc18-1 that quantifiably disrupt N-terminal interaction *in vitro*, highlighting residues important in maintaining an N-terminal interaction with syntaxin. Here it is shown that mutating the hydrophobic pocket of munc18-1 and specifically residue I127, highlighted by SM protein conservation maps, results in a reduction in *in vitro* binding to syntaxin. The next experiment was to investigate whether perturbing the N-terminal interaction *in vitro* result in a corresponding effect in a cellular environment. Using both confocal microscopy and TCSPC FLIM it is further demonstrated that mutating specific residues of the hydrophobic pocket of munc18-1 resulted in changes in both munc18-1 and syntaxin protein localisation and interaction.

3.2 Dissection of Munc18-1-Syntaxin interaction modes *in vitro*.

To determine the extent of binding modes between munc18-1 and syntaxin *in vitro* syntaxin mutant constructs were used in order to isolate closed form and N-terminal interactions biochemically. It has already been reported that truncation of the first seven amino acids of the N-terminus of syntaxin (GST-Syx_{7-261}) can disrupt N-terminal interactions with munc18-1 (Rickman et al, 2007). To perturb closed form binding truncations of the SNARE helix of syntaxin were designed based on the close interaction of this region with munc18-1 in closed form interactions (Burkhardt et al, 2008). Two

truncations were used: removal of the syntaxin C terminus up to the ionic layer of the SNARE helix (GST-$Syx_{1–225}$) and a complete removal of the SNARE helix (GST-$Syx_{1–213}$). To examine the influence of these mutations and their combinations syntaxin constructs were immobilized on glutathione sepharose beads and incubated with fresh brain lysate (section 2.4) for 2 hours at 4 ºC. Following standard washing procedures, bound material was analysed by SDS-PAGE and subsequent Coomassie staining.

Upon incubation, native munc18-1 readily bound to wild type syntaxin (GST-Syx_{1-261}; Figure 3.1). Truncation of the N-terminus of syntaxin (GST-$Syx_{7–261}$) caused a small decrease in the amount of bound munc18-1 detected. Munc18-1 binding following truncation of syntaxin to the ionic layer (GST-$Syx_{1–225}$) was also detected but at decreased levels as a result of loss of closed form binding (Figure 3.1). No interactions were detected following removal of the whole SNARE helix of syntaxin (GST-$Syx_{1–213}$). Importantly, the combination of the N-terminal truncation and the ionic layer truncation (GST-$Syx_{7–225}$) resulted in the complete removal of detectable munc18-1 binding through ablation of both binding modes (Figure 3.1). N-terminal binding to GST-$Syx_{1–225}$ was also eliminated in a high salt buffer, highlighting the considerable ionic nature of this interaction in contrast to closed from interaction (GST-$Syx_{7–261}$). By specifically isolating munc18-1-syntaxin binding modes it was possible to test which residues of munc18-1 were important in mediating N-terminal binding to purified GST-syntaxin *in vitro*.

3.1

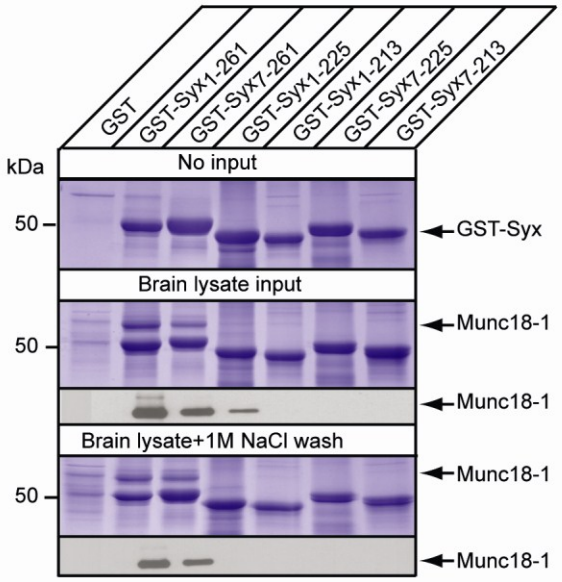

Figure 3.1. *Dissection of munc18-1-syntaxin binding modes*. Truncation of the N-terminus [syntaxin$_{7\text{-}261}$] or removal of the ionic layer [syntaxin $_{1\text{-}225}$] of syntaxin revealed the extent of closed form or N-terminal binding respectively. The combination of these truncations or removal of the entire SNARE helix of syntaxin [syntaxin $_{1\text{-}213}$] eliminated detectable binding of munc18-1. N-terminal binding [syntaxin $_{1\text{-}225}$] was sensitive to a high ionic strength wash. Bound material was analysed by SDS PAGE and Coomassie staining or Western blotting.

3.3 IDENTIFICATION OF RESIDUES CONTAINED WITHIN THE HYDROPHOBIC POCKET OF MUNC18-1 IMPORTANT IN MEDIATING N-TERMINAL INTERACTION.

The approach used in order to identify residues within the hydrophobic pocket of munc18-1, well placed to mediate an N-terminal interaction with syntaxin, was to examine the amino acid sequence of members of the SM protein family. Evolutionary conservation of amino acids, with relation to the three-dimensional protein structure is indicative of an essential function (Madabushi et al, 2002). The amino acid sequences of 191 predicted SM proteins were aligned, mapping the degree of conservation on to the crystal structure of munc18-1 bound to syntaxin (Figure 3.2, Burkhardt et al, 2008). This approach highlighted the amino acids lining the N-terminal binding pocket on munc18-1 and indicated E132 and D112 as being potential candidates. Both residues are expected to form hydrogen bonds to the N-terminal motif of syntaxin. Another potential residue important in mediating N-terminal interaction was I127, a residue forming one side of the hydrophobic pocket (Figure 3.2B, Burkhardt et al, 2008). Two-point mutations for each amino acid (I127A/I127F, E132A/E132K, and D112A/D112K) were subsequently constructed using site directed mutagenesis (section 2.2.2) to investigate their individual contributions in regulating the level of binding to the N-terminus of syntaxin *in vitro*.

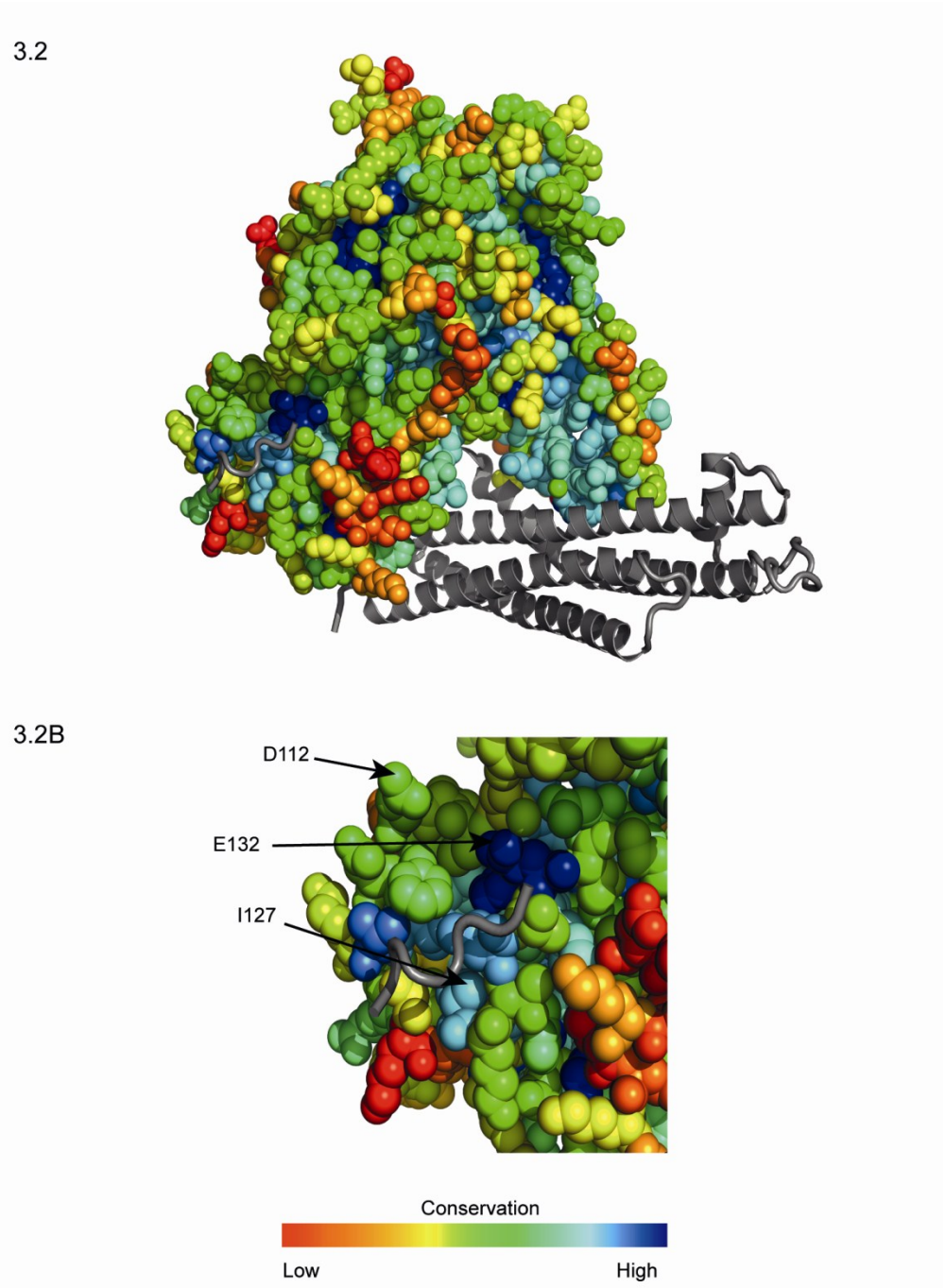

Figure 3.2. *Site directed mutagenesis predicted to disrupt N-terminal syntaxin interaction.* Structural alignment of munc18-1 (space fill, based on crystal structure PDB 3C98 (Burkhardt et al, 2008)) bound to syntaxin (grey helices) with amino acid conservation shown on a colour coded scale (red – low, blue – high conservation). 3.2B. Amino acids D112, E132 and I127, predicted to disrupt N-terminal binding, are highlighted on an enlarged view.

To determine whether these munc18-1 point mutations specifically disrupted N-terminal interaction with syntaxin *in vitro*, bacterial lysates containing His-tagged munc18-1, and mutant forms, were incubated with GST-syntaxin immobilized on beads (section 2.4.3). GST-$Syx_{7–261}$ was used to examine the impact of munc18-1 mutations on closed form binding and GST-$Syx_{1–225}$ to assess perturbations of N-terminal binding. Levels of *in vitro* binding were analysed using SDS-PAGE and Coomassie staining (section 2.3.1 and 2.3.4). Mutants munc18-1[I127A], munc18-1[I127F] and munc18-1[E132A] resulted in the largest reduction in the level of N-terminal binding compared with wild-type munc18-1 *in vitro* (Figure 3.3). No reduction in the extent of N-terminal binding was observed using mutants munc18-1[E132K], munc18-1[D112A] and munc18-1[D112K] (Figure 3.3). This biochemical approach highlighted key residues in the hydrophobic pocket of munc18-1 that were important in regulating the extent of N-terminal binding to syntaxin *in vitro*.

3.3

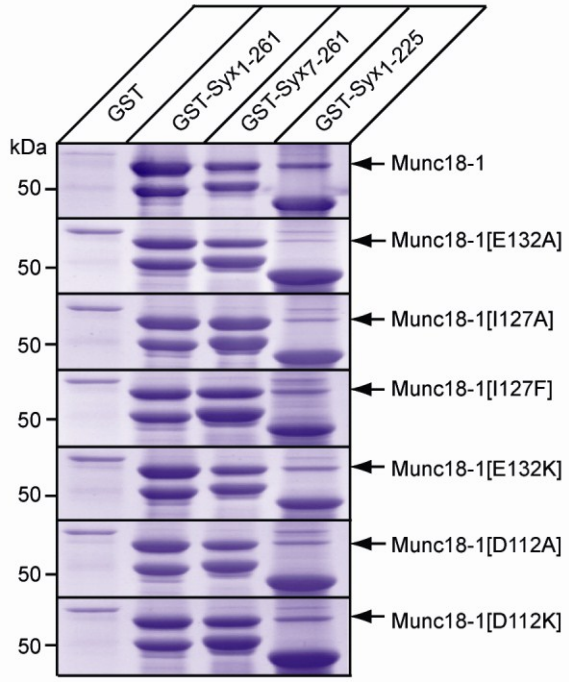

Figure 3.3. *Identification of munc18-1 residues important for mediating N-terminal interaction.* GST- syntaxin $_{7\text{-}261}$ (closed form binding only) and GST-syntaxin $_{1\text{-}225}$ (N-terminal binding only) fusion proteins were immobilised on Glutathione Sepharose beads and incubated with bacterial lysate containing His$_6$-munc18-1, or its mutant forms. Bound material was analysed by SDS PAGE and Coomassie staining. Mutations which resulted in the biggest reduction in munc18-1 binding visualised by Coomassie staining were selected for further experimentation i.e. munc18-1[I127A], munc18-1[I127F] and munc18-1[E132A].

Proteins participate in extensive networks of interactions which are able to assemble and disassemble in concert with a change in intra-, inter and extracellular cues. A preliminary step in understanding protein interaction and function is to determine which proteins interact with each other, thereby identifying relevant biological pathways. The GST pull-down technique is a common biochemical tool used for protein interaction analysis and has become an invaluable tool in studying cellular pathways via protein-protein interactions. After observing an *in vitro* effect using pulldown assays on N-terminal binding with munc18-1[I127A], munc18-1[I127F] and munc18-1[E132A], it was important to investigate whether these munc18-1 mutants had a similar effect in a cellular context. As mutants munc18-1[D112A], munc18-1[D112K] and munc18-1[E132K] had no identifiable effect on N-terminal binding in this *in vitro* assay, they were excluded from further study.

3.4 CHARACTERISATION OF MUNC18-1 SILENCED KD43 PC12 CELLS.

All experiments performed on cell lines in this thesis used munc18-silenced PC12 cells (KD43), a kind gift from Dr Sugita, Toronto Western Research Institute, Canada. This null munc18-1 background provided an excellent cellular model in order to precisely probe the downstream cellular effects on ablating N-terminal interaction between munc18-1 and syntaxin. This model system also ensured that any effects observed using N-terminal munc18-1 mutants were not an artefact of munc18-1 over-expression. Stable KD43 PC12 cells were generated using a munc18-1 knockdown plasmid (pSuper-Munc18-1-3), which selectively targeted residues 246-264 in the rat munc18-1 gene (Arunachalam et al, 2008). Cells successfully transfected with the munc18-1 knockdown plasmid were selected for using puromycin. To verify that the KD43 PC12 cells lacked endogenous munc18-1 cells were subjected to immunoblot analysis. The lysates from three 95% confluent 75 cm^2 flasks containing KD43 PC12 cells were combined and probed using various antibodies. Total protein was quantified using SDS-PAGE and immunoblotting techniques (Figure 3.4; section 2.3.1 and 2.3.2).

Immunoblot analysis revealed that total munc18-1 protein (BD-munc18-1) was knocked down by approximately 90% (Figure 3.4B). A 30% reduction in the expression of

syntaxin (HPC-1) and no change in SNAP-25 expression (SM1-81) was also found, a similar finding to the initial characterisation of these cells (Figure 3.4; Arunachalam et al, 2008). A reduction in the expression of syntaxin upon the deletion of its cognate SM protein has been previously shown in *S. cerevisiae* cells (Bryant and James, 2001) and munc18-1 null embryonic murine chromaffin cells (Voets et al, 2001). KD43 PC12 cells, unlike neurons from munc18-1 null mice (Voets et al, 2001), exhibited no problems in survival or growth. This relatively healthy model system therefore provided an excellent model system in order to conduct detailed analyses of the localisation and interaction of N-terminal munc18-1 mutants with syntaxin.

3.4

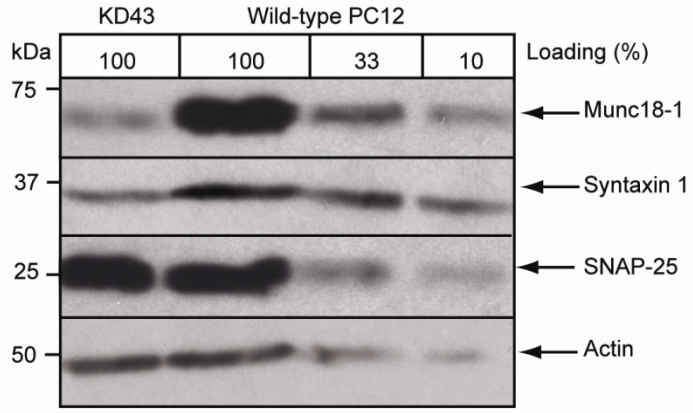

3.4B

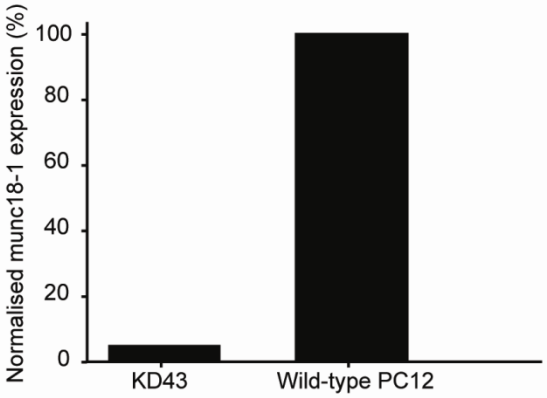

Figure 3.4. *Quantification of munc18-1 knockdown by shRNA in KD43 PC12 cells*. Dilutions of KD43 PC12 cell extract was analysed by SDS-PAGE and immunoblotting using anti-munc18-1, syntaxin1a, SNAP-25 and actin (loading control). Protein signal was detected using an enhanced chemiluminescence detection system and quantified using ImageJ. Numbers on the left indicate the positions of molecular weight markers. 3.4B. Quantification of total munc18-1 protein expression in both wild-type PC12 and KD43 PC12 cells. Lysates from three separate experiments were combined revealing that total munc18-1 protein was knocked down by approximately 95% compared to wild-type PC12 cells.

3.5 MUTATIONS IN THE HYDROPHOBIC POCKET OF MUNC18-1 RESULT IN A CHANGE IN ITS CO-LOCALISATION WITH SYNTAXIN IN CELLS.

To investigate the effect of perturbing N-terminal interaction in a cellular context, a quantitative approach was used to examine co-localisation between the two proteins in KD43 PC12 cells. In order to maintain a stable transfection of KD43 PC12 cells using fluorescently tagged munc18-1 constructs, six silent nucleotide mutations (GTCCGTGCACAGCCTGATC) were engineered within the target sequence of the munc18-1 gene. These silent mutations would have no effect on the coding sequence of munc18-1 and therefore prevent these constructs from being recognised and degraded by the shRNA present within the KD43 PC12 cells. shRNA-resistant fluorescent fusion proteins of munc18-1 and mutants were then transfected into KD43 PC12 cells in combination with syntaxin and fluorescence intensity co-variance analysis was performed (Figure 3.5, section 2.9.3).

Quantitative protein co-localisation analysis was conducted on intact, live KD43 PC12 cells to avoid a possible change in the cellular distribution of munc18-1 and syntaxin upon chemical fixation. Figure 3.5 shows a merged image of both fluorescent channels (munc18-1 in *red* and syntaxin in *green*) and displayed areas of high protein coincidence in yellow hues. The intensity of each voxel in the image was plotted as a two-dimensional histogram in order to represent the correlation in intensities. Any deviation from the linear fit of the histogram was used to produce a residual map that corresponded to covariance between the two channels. Regions which exhibit high protein covariance are coloured in cyan with any deviation from this fit appearing towards either end of the colour spectrum. As shown in the images covariance analysis revealed that both wild-type munc18-1 and syntaxin exhibited a plasma membrane distribution with a high level of protein co-localisation (Figure 3.5). The importance of munc18-1 in trafficking syntaxin to the cell surface has been previously demonstrated in these KD43 PC12 cells (Arunachalam et al, 2008). In fact, in the absence of munc18-1, syntaxin resides primarily in the perinuclear region of the cells, demonstrating the fundamental importance of munc18-1 in trafficking syntaxin to the plasma membrane (Rowe et al, 2001; Medine et al, 2007; Arunachalam et al, 2008).

When syntaxin was co-expressed with an N-terminal munc18-1 mutant the localisation of both proteins changed depending on the specific point mutation introduced. Co-localisation analysis confirmed that mutants munc18-1[I127A], munc18-1[I127F] and munc18-1[E132A,] that previously disrupted N-terminal interaction *in vitro,* (Figure 3.3) also had a significant effect on syntaxin intracellular localisation (Figure 3.5). Munc18[I127A] had the most significant influence with both proteins adopting more of an intracellular distribution, highlighting this residue as being key in the trafficking of both proteins to the plasma membrane.

The data quantified for wild-type or mutants of munc18-1 in KD43 PC12 cells are expressed as Pearson's correlation coefficient (R) values. As previously described, wild-type proteins exhibited a predominant membrane localisation with a high degree of protein co-localisation (R = 0.94 ± 0.01, mean ± S.E.M, n = 6). N-terminal mutants munc18-1[E132A] (R = 0.86 ± 0.02, mean ± S.E.M, n = 5) and munc18-1[I127F] (R = 0.84 ± 0.02, mean ± S.E.M, n = 5) resulted in a significant reduction (One way ANOVA) in the covariance of both proteins on the plasma membrane. The expression of munc18-1[I127A] (R = 0.81 ± 0.03, mean ± S.E.M, n = 4) resulted in the partial trapping of syntaxin in intracellular compartments (Figure 3.5) and therefore the most significant effect on their co-localisation when compared to wild-type munc18-1 (Figure 3.5B). Taken together, these data from living KD43 PC12 cells indicates that a reduction in the extent of N-terminal binding *in vitro* using mutants munc18-1[E132A], munc18-1[I127A] and munc18-1[I127F] results in a concomitant downstream effect on the co-localisation of munc18-1 and syntaxin in a cellular environment. Moreover, reducing the affinity between the N-terminal peptide of syntaxin and munc18-1 significantly affects the trafficking of both proteins to the plasma membrane.

3.5

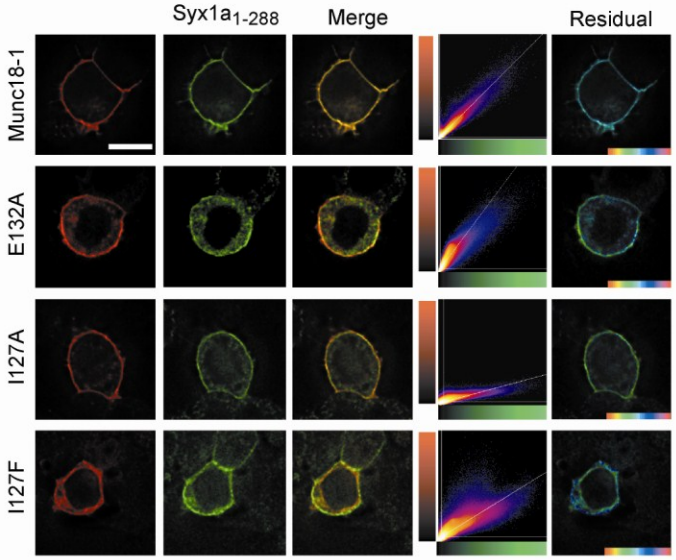

3.5B

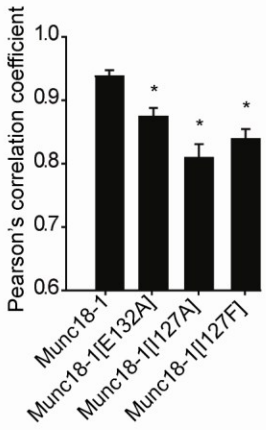

Figure 3.5. *Munc18-1 colocalisation with syntaxin in live cells is altered upon the specific disruption of N-terminal binding.* Wild-type or mutant mCherry-munc18-1 (red), and mCer-syntaxin (green) were expressed in munc18-1-silenced PC-12 cells (KD43), imaged by confocal laser scanning microscopy (CLSM) and subsequently deconvolved using Huygens deconvolution software. The merge image shows areas of coincidence in yellow hues. The 2-D histogram represents the intensity for each channel in each voxel with a colour scale representing frequency. The residual map displays weighted residuals from the line fit to the histogram, thus indicating fluorescence channel covariance. The hue is from -1 to 1 with cyan corresponding to a zero residual. Scale bar: 5 µm. 3.5B Combined covariance analysis of cerulean-syntaxin, mCherry-munc18-1 and mCherry-munc18-1 mutants. Mean Pearson's coefficients are shown ($n > 6$, mean ± S.E.M, One way ANOVA). Asterisks indicate $p > 0.05$.

The data generated by protein co-localisation studies is a good indicator of whether two proteins are sharing a similar space. However, this co-localisation data is limited by the resolution, maximally 178 nm laterally, of the microscope used, thus making it impossible to detect an interaction between two proteins. Therefore, the next step was to combine these co-localisation data with studies of TCSPC-FLIM and FRET to determine regions of interest within the cells where N-terminal interaction predominates.

3.6 PERTURBING N-TERMINAL BINDING AFFECTS THE INTERACTION STATUS OF MUNC18-1 AND SYNTAXIN.

In order to probe where the munc18-1-syntaxin N-terminal interaction is predominately utilised within a cellular environment, Time Correlated Single Photon Counting (TCSPC) FLIM was employed (section 2.8.6). FLIM quantifies the fluorescence lifetime of a fluorophore and is a direct measure of Förster resonance energy transfer (FRET) between acceptor, munc18-1, and donor, syntaxin, molecules. Fluorescence lifetime values of a donor molecule can be largely influenced by the presence of an acceptor molecule, a second fluorophore with the appropriate spectral properties to allow the absorption of energy from the donor molecule, through FRET (Lakowicz et al, 1994; Bastiaens and Squire, 1999). Therefore, a quenching of the donor fluorescence lifetime can be used to measure a FRET interaction with the acceptor fluorophore. By quantifying this interaction in every pixel of an image the fraction of non-interacting and interacting donor fluorescence lifetimes can be resolved (Duncan et al, 2004).

As a control, mCerulean-syntaxin was expressed with unfused munc18-1 and EYFP in KD43 PC-12 cells (Figure 3.6A). This analysis revealed a principally plasma membrane localisation of syntaxin with some labelling of intracellular compartments, as reported previously (Medine et al, 2007; Rickman et al, 2007). Without the presence of an acceptor molecule mCerulean donor fluorescence exhibited a mono-exponential decay function, and the FLIM map showed a single exponential fluorescence lifetime within cells of 2310 ± 151 ps (mean ± S.E.M, n = 10) (Figure 3.6A). Upon plotting this data as a frequency distribution histogram, this single fluorescence lifetime was evident (Figure 3.6A).

In the presence of a proximal FRET acceptor, EYFP, fused to munc18-1 the fluorescence lifetime could no longer be fitted by a mono-exponential decay function (Figure 3.6B). FLIM analysis showed a statistically significant quenching of the mean fluorescence lifetime of donor mCerulean-syntaxin to 1563 ± 65 ps (mean ± S.E.M, n = 6, One way ANOVA) in the presence of EYFP-munc18 (Figure 3.6B), indicative of FRET. These FRET data could now be fit by a bi-exponential decay function and the FLIM map revealed a quenched donor fluorescence lifetime. This analysis confirmed that munc18-1 and syntaxin interact on the plasma membrane (Figure 3.6B).

The expression of munc18[I127A] resulted in significantly less quenching of the donor fluorescence lifetime from 2310 ± 151 ps (mean ± S.E.M, n = 10) to 2062 ± 70 ps (mean ± S.E.M, t test, $p < 0.05$, n = 5), indicating either reduced interaction or altered conformation of interaction (Figure 3.6D). Mutants munc18-1[I127F] (1994 ± 85 ps (mean ± S.E.M, n = 6, Figure 3.6E) and munc18-1[E132A] (1976 ± 205 ps (mean ± S.E.M, n = 7, Figure 3.6C)) resulted in more of a donor lifetime quenching, indicating that they were involved in a stronger and more stable interaction. Plotting every pixel in the image but assigning donor fluorescence lifetime value a colour revealed that areas on the plasma membrane contained significantly less energy transfer, confirming that N-terminal interaction predominates at the cell surface (Figure 3.6). This result supports previous work demonstrating that distinct modes of munc18-1 and syntaxin interaction occur at distinct cellular locations, with the N-terminal interaction predominating at the plasma membrane (Rickman et al, 2007).

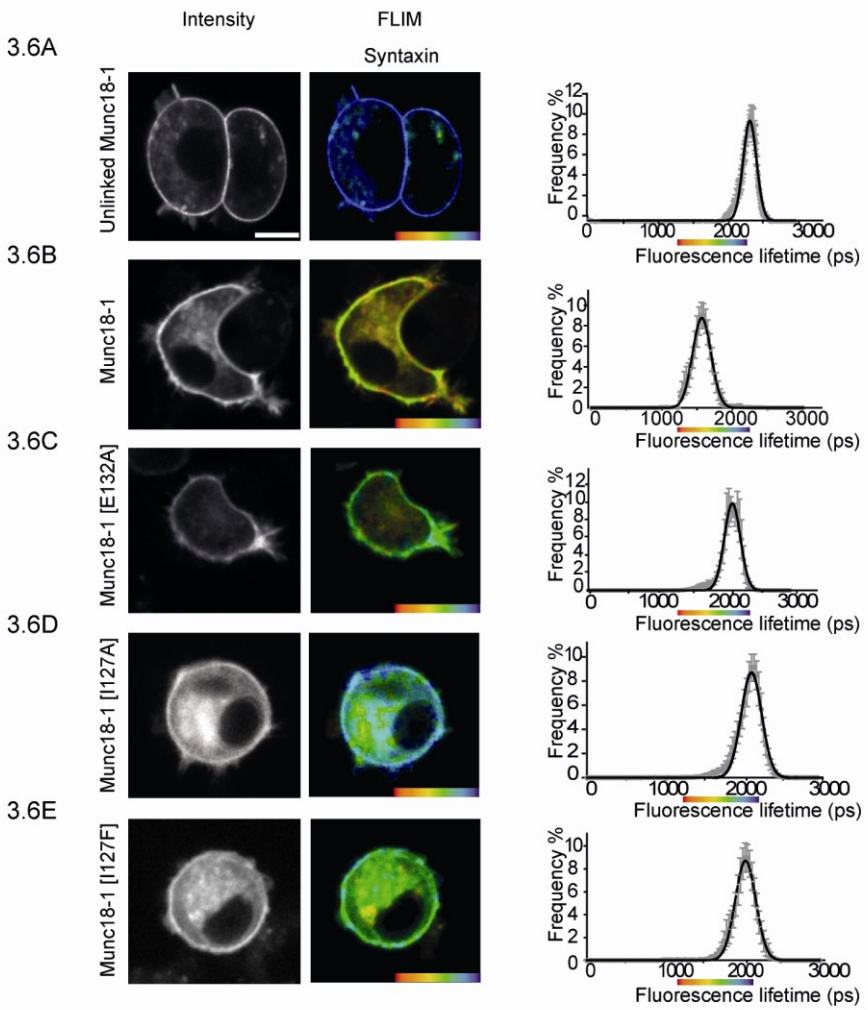

Figure 3.6. *Targeted disruption of N-terminal interaction resulted in a change in interaction with syntaxin in live cells*. KD43 PC12 cells were transfected to co-express mCer-syntaxin, with unfused EYFP and munc18-1 (3.6A). Without a proximal fluorescent acceptor, mCer-syntaxin had both a plasma membrane and intracellular membrane distribution and a long fluorescence lifetime (2310 ± 151 ps (mean ± SEM, n = 10 cells). mCer-syntaxin, in the presence of EYFP-munc18-1, also exhibited a plasma membrane and intracellular membrane distribution and a significantly shorter fluorescence lifetime (1563 ± 65 ps (mean ± SEM, n = 6 cells) (3.6B). FLIM revealed that munc18-1 mutants resulted in a quenching of the fluorescence lifetime to a lesser extent compared to wildtype munc18-1 and a modest change in their interaction at the plasma membrane (3.6C-E). Munc18-1[I127A] resulted in a partial trapping of syntaxin in intracellular compartments and significantly less quenching of the donor fluorescence lifetime to 2062 ± 70 ps (mean ± SEM, t-test, p <0.05, n =5 cells) compared to the other munc18-1 mutants (3.6D). The colour scale represents the fluorescence lifetime fluorescence on a range from 1250 ps (red) to 2250 ps (blue) and brightness represents intensity. The weighted mean fluorescence lifetime values were plotted as a frequency distribution histogram. Scale bar: 5 µm.

3.7 CONCLUSION.

Using biochemistry, crystallography and optical imaging techniques, it has been previously shown that munc18-1 can interact with syntaxin through two discrete modes of binding, closed form and N-terminal. Munc18-1 has been shown to readily bind to an open mutant of syntaxin, a mutant unable to adopt its closed conformation, with high affinity (K_d = 5 nM) (Medine et al, 2007). This binding assay, and a number of other studies, therefore indicates that munc18-1 can interact with syntaxin via a second mode, through the extreme N-peptide of syntaxin (Misura et al, 2000; Yang et al, 2000; Rickman et al, 2007).

By biochemically separating the binding modes between munc18-1 and syntaxin this study revealed the extent of closed and N-terminal binding occurring in an *in vitro* setting. From these findings it is clear that munc18-1 can interact with syntaxin via two mechanistic modes, interactions that have been reported to be both functionally and spatially distinct (Rickman et al, 2007). By dissecting both forms of interaction this study was able to specifically probe the effect of the munc18-1 point mutations specifically on the extent of N-terminal binding. Without separating binding modes the effect reported using these N-terminal mutants on total munc18-1 binding would have been lost. Using GST-Syx_{1-225} in combination with various munc18-1 mutants the extent of disruption of N-terminal binding *in vitro* was revealed, with munc18-1[I127A], munc18-1[I127F] and munc18-1[E132A] resulting in the largest reduction in binding to syntaxin. These *in vitro* binding assays also demonstrated that N-terminal binding involves a number of ionic interactions, in contrast with closed form binding. These preliminary findings highlighted which munc18-1 residues were the most important in facilitating the N-terminal interaction *in vitro* and acted as a platform for further investigation within cells.

This study also employed both protein colocalisation and TCSPC FLIM in order to investigate whether the *in vitro* effects of perturbing the N-terminal interaction between munc18-1 and syntaxin were translated into a downstream function within a cellular environment. Protein co-localisation studies revealed that perturbing N-terminal interaction resulted in the less efficient trafficking of syntaxin to the plasma membrane,

presumably to sites of fusion. This is in agreement with a previous study showing that removing the N-terminus of syntaxin affected the trafficking of both munc18-1 and syntaxin to the plasma membrane (Rickman et al, 2007). A number of studies have shown that the binding of syntaxin to munc18-1 is critical for its efficient trafficking to the plasma membrane in specialised secretory cells (Rowe et al, 2001; Martinez-Arca et al, 2003; Medine et al, 2007; Arunachalam et al, 2008). However, in contrast it has also been demonstrated that syntaxin can traffic to the plasma membrane (albeit inefficiently) and synapses in the absence of munc18-1 in PC12 cells and neurons respectively (Schutz et al, 2005; Toonen et al, 2005). Perhaps the mere fact that syntaxin exists in excess over munc18-1 (Schutz et al, 2005) in PC12 cells has been used to argue against a role for munc18-1 in syntaxin trafficking. A possible explanation for this discrepancy is the fact that genetically deleting munc18-1 still leaves other perhaps redundant munc18 isoforms present and also results in a concomitant fall in syntaxin in a variety of cells (Verhage et al, 2000; Toonen et al, 2005; Arunachalam et al, 2008). However pulse-chase analysis in HEK293 cells suggested that munc18-1 directly promotes the stability of syntaxin (Toonen et al, 2005) and in its absence syntaxin forms ectopic complexes with other intracellular SNAREs (Medine et al, 2007), consistent with a chaperone function.

Recently, studies have mutated amino acids in or around the hydrophobic region of munc18-1 and concluded that N-terminal interaction plays no part in catalyzing neuroendocrine vesicle exocytosis (Arunachalam et al, 2008; Han et al, 2009; Malintan et al, 2009). One of the munc18-1 amino acid residues targeted in these studies and also analysed here (munc18-1[E132A], Malintan et al, 2009) was observed to have only modest effects on co-localisation with syntaxin compared with munc18-1[I127A]. An additional mutation used in the above study (munc18-1[F115E]) was observed to have a low degree of evolutionary conservation (Figure 3.2), a poor candidate for subsequent study. Therefore, studies may have concluded that the N-terminus of syntaxin has no functional role within a cell due to the fact that researchers have not selected conserved residues, indicative of essential function (Madabushi et al, 2002).

Protein co-localisation analysis revealed that N-terminal binding plays a role in trafficking syntaxin to the plasma membrane and maintaining an interaction once there, as previously reported (Rickman et al, 2007; Arunachalam et al, 2008). In this study residue I127 has

been shown to be the most significant residue in forming a tight interaction with syntaxin *in vitro* and in determining the level of interaction between both proteins in cells. A reduced interaction, detected by TCSPC FLIM, is a likely explanation for why munc18-1 and syntaxin are not trafficked efficiently to the plasma membrane, instead becoming trapped in intracellular compartments. In support of this hypothesis a study using munc18-1 mutants carrying mutations in the syntaxin-binding region shows that the membrane association of munc18-1 is dependent on direct binding to syntaxin (Schütz et al, 2005). Therefore, by ablating the N-terminal interaction between munc18-1 and syntaxin, both proteins are unable to reach the plasma membrane as efficiently and do not interact once there in a stable form.

It remains to be established what the functional significance is of this altered localisation and interaction between munc18-1 and syntaxin. It has been shown that perturbing the interaction of munc18-1 and syntaxin not only affects their membrane association but also inhibits neurotransmitter and hormonal release upstream of the individual fusion event (Schütz et al, 2005; Rickman and Duncan, 2010). This implies that without a stable interaction between munc18-1 and syntaxin, downstream vesicle exocytosis is impacted upon. The next study in the following chapter involved investigating the effect of N-terminal binding on downstream neuroendocrine large dense core vesicle kinetics and fusion and whether or not this mode of binding had similar effects in neuronal counterparts.

CHAPTER 4:

THE FUNCTION OF THE MUNC18-1-SYNTAXIN-N-TERMINAL INTERACTION

4.1 INTRODUCTION

Intracellular membrane fusion is the basis of a number of fundamental biological processes, from organelle preservation and maintenance to cellular secretion. Munc18-1 was originally defined as an inhibitor of this reaction following the observation that it prevented syntaxin from forming the SNARE fusion complex (Pevsner et al, 1994b; Dulubova et al, 1999). This hypothesis was at considerable odds with previous genetic experiments which implied a more positive role for munc18-1 (reviewed in Toonen and Verhage, 2007). The discrepancy surrounding the function of munc18-1 was resolved upon the discovery that munc18-1 interacted with syntaxin via two distinct binding modes (Burgoyne and Morgan, 2007; Dulubova et al, 2007; Rickman et al, 2007; Shen et al, 2007). The initial characterisation of the N-terminal mode of binding was the topic of considerable debate, primarily due to the fact that munc18-1 was shown to be unable to interact with the N-terminus of syntaxin (Calakos et al, 1994), unlike its homologues (Misura et al, 2000; Yang et al, 2000; Rickman et al, 2007). However it is noteworthy to mention that early clones of syntaxin that were widely used to measure protein-protein interactions *in vitro* lacked a conserved N-terminal region (Calakos et al, 1994).

Over the last decade a huge amount of research has focussed on elucidating the functionality of munc18-1-syntaxin-N-terminal binding. To date, N-terminal binding has been shown to stimulate vesicle mobilization (Rickman and Duncan, 2010), SNARE complex binding (Dulubova et al, 2007) and assembly (Shen et al, 2007; Rathore et al, 2010; Schollmeier et al, 2011), synaptic fusion in the calyx of Held (Khvotchev et al, 2007) and synaptic vesicle priming (Deak et al, 2009). Recently, the SNARE complex together with the N-terminal peptide of syntaxin was shown to constitute the minimal requirement for munc18-1 association and activation, whereas the remaining SNARE sequences, including the syntaxin-1 Habc domain, are expendable (Shen et al, 2010). There are a number of hypotheses that exist regarding how the N-peptide motif acts together with munc18-1 and the SNARE complex to drive bilayer fusion. The N-peptide motif may provide an additional binding surface to stabilize an otherwise low-affinity interaction between munc18-1 and the SNARE complex, allosterically activate munc18-1 or simply recruit the SM protein to its cognate SNARE syntaxin (Shen et al, 2007; Toonen and Verhage, 2007; Burgoyne et al, 2009; Carr and Rizo, 2010). A recent study

discounted the possibility that N-terminal binding could activate a conformational change in syntaxin as it was shown to regulate fusion when completely spatially separated from the SNARE complex (Rathore et al, 2010).

Despite the essential roles played by the N-terminal peptide in metazoan membrane fusion, the N-peptide motif of syntaxin appears to be superfluous in a number of yeast fusion pathways (Peng and Gallwitz, 2004; Carpp et al, 2006). Furthermore, N-terminal binding is absent in the yeast SM proteins Sec1p and Vps33p (Pieren et al, 2010; Wickner, 2010). A possible explanation for these functional discrepancies could relate to the fact that the yeast SM protein Vps45p may have evolved a higher affinity for its cognate syntaxin (Carpp et al, 2006; Furgason et al, 2009). Therefore, N-terminal binding may be dispensable for the assembly of the yeast endocytic fusion complex and bilayer unification, unlike its mammalian counterparts. SM homologues possess both disparate modes of binding and regulatory effects, therefore leaving a hypothetical question mark over the precise functional role of the munc18-1-syntaxin-N-terminal interaction.

This chapter describes how perturbing N-terminal interaction, specifically mediated by disrupting residue I127 of the hydrophobic pocket of munc18-1, restricted vesicle kinetics at the plasma membrane under TIRF microscopy. By limiting the dynamics of membrane proximal vesicles a concomitant reduction in vesicle exocytosis was also recorded. To elucidate whether changes in vesicle dynamics and fusion capabilities were a result of an altered association between munc18-1 and syntaxin at the plasma membrane, their interaction status was quantified. Quantification of the munc18-1-syntaxin interaction at the base of a neuroendocrine cell upon N-terminal ablation revealed that this binding mode is not required for vesicle-membrane association and the spatial arrangement of membrane proximal vesicles. Instead, disturbing N-terminal interaction resulted in a reduced size of a distinct pool of fusion competent vesicles at the plasma membrane, a probable explanation for reduced vesicle exocytosis.

Aside from neuroendocrine cells, the munc18-1-syntaxin-N-terminal interaction has been shown to play a role in neuronal exocytosis and SNARE assembly (Khvotchev et al, 2007; Johnson et al, 2009; Rathore et al, 2010). This study therefore also set out to investigate where N-terminal binding is utilised within a neuron and whether this form of interaction

was important in catalyzing synaptic vesicle fusion. By specifically probing for phosphorylated syntaxin at residue serine[14], a key site for the regulation of munc18-1-syntaxin N-terminal binding, this study shows that phosphorylated syntaxin is not localised to synaptic sites in a neuron, compared with unphosphorylated syntaxin. Using phosphosyntaxin-specific antibodies this study also demonstrates that the phosphorylation of syntaxin at serine[14] in neuronal cells is not activity dependent but required for the efficient fusion of synaptic vesicles specifically residing in the readily releasable pool.

4.2 Modulation of vesicle dynamics at the plasma membrane by the munc18-syntaxin-N-terminal interaction.

It has been previously reported that the phosphorylation of syntaxin can modulate its interaction with munc18-1. Following the finding that serine-14 was a target for casein kinase II (CKII) (Risinger and Bennett, 1999; Foletti et al, 2000) it was shown, using a series of phosphomimetic and phospho-null mutations, that this site was a key regulator of the N-terminal interaction between munc18-1 and syntaxin (Rickman and Duncan, 2010). Disrupting munc18-1-syntaxin-N-terminal binding, through phosphomimetic mutation of syntaxin at serine-14, resulted in the increased average immobilization of secretory vesicles, rendering them unable to support membrane fusion (Rickman and Duncan, 2010). This finding agrees well with the idea that vesicular mobility is enhanced directly preceding fusion (Degtyar et al, 2007). The first part of this chapter therefore investigated whether mutation of the munc18-1 hydrophobic pocket, and a concomitant reduction in N-terminal binding with syntaxin, resulted in similar downstream effects, specifically on single vesicle kinetics and their fusion capabilities. In order to attain both high spatial and temporal axial resolution at the single-vesicle level Total Internal Reflection Fluorescence Microscopy (TIRFM) was employed (Axelrod, 2001). TIRFM selectively illuminates and excites fluorophores immediately adjacent to the glass-water interface, penetrating into the sample to a depth of approximately 150 nm. TIRFM is therefore an ideal technique for recording events specifically occurring at the plasma membrane, for example, the behaviour of membrane proximal secretory vesicles.

Vesicles, expressing a fluorescent cargo marker, NPY-mCherry, were tracked under TIRF illumination at physiological temperatures in munc18-1-silenced PC12 cells (KD43)

expressing either wild-type munc18-1, a munc18-1 N-terminal mutant or lacking the expression of both exogenous (and endogenous) munc18-1 (unrescued). Syntaxin was always co-expressed alongside munc18-1. Fluorescent vesicles were tracked using Imaris software (Bitplane) and at least five cells from each condition were combined to give an average of a number of measured parameters (Figure 4.1). Fluorescent vesicles contained within cells not expressing munc18-1 or syntaxin (unrescued) travelled at an average speed of 0.81 ± 0.06 μm/s (n = 8) with an average track length of 4.03 ± 0.13 μm (n = 8). Analysis of track displacement values, the distance calculated between the start and end of the vesicle track, indicated whether a vesicle was 'tethered' at the plasma membrane or whether it displayed more of a scanning behaviour, presumably of sites of fusion. Vesicles within KD43 cells only expressing a fluorescent vesicle marker, NPY, displayed an average displacement value of 0.17 ± 0.004 μm, (n = 8) (Figure 4.1B).

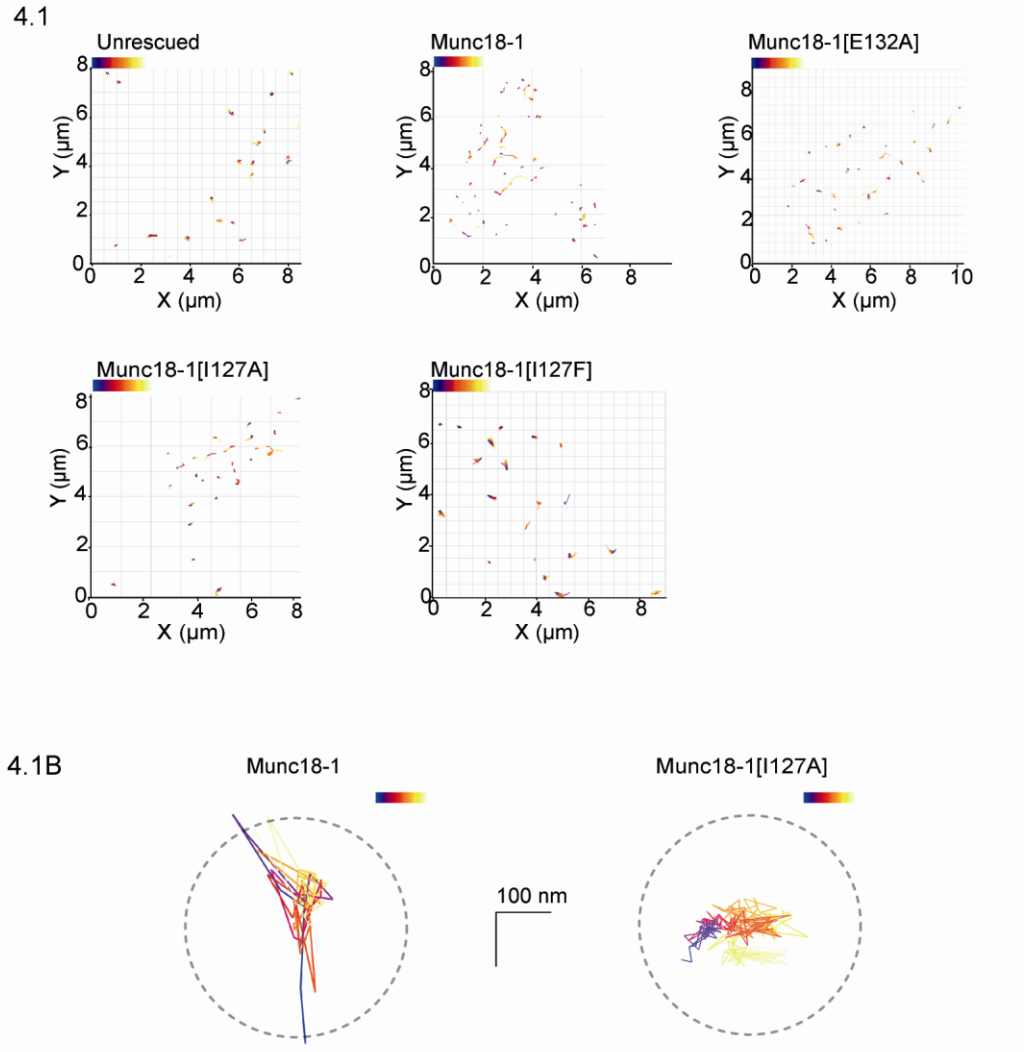

Figure 4.1. *Vesicle dynamics at the plasma membrane are modulated by munc18-1-syntaxin-N-terminal interaction*. Fluorescent NPY labelled vesicles were tracked under TIRF illumination using an evanescent wave in KD43 PC12 cells either unrescued or expressing wild-type or mutant munc18-1. Individual vesicle trajectories are shown as tracks with colour corresponding to time during acquisition (blue – start to red – end). 4.1B Examples most closely matching the mean track displacement for munc18-1 and munc18-1[I127A] rescued cells are shown. The dashed circle corresponds to a vesicle diameter of 400 nm.

Vesicles contained within KD43 PC12 cells expressing both wild-type munc18-1 and syntaxin exhibited a significantly longer track displacement of 0.21 ± 0.01 μm (n = 6 cells) with an average track length of 4.8 ± 0.17 μm (n = 6 cells; Figure 4.2). The speeds at which vesicles were travelling in unrescued and wild-type munc18-1 rescued KD43 cells were not statistically different. Vesicular speed is therefore not dictated by munc18-1; instead membrane proximal vesicles require a stable expression of munc18-1 molecules in order to successfully 'scan' the plasma membrane, most probably in search of SNARE mediated fusion sites.

4.2

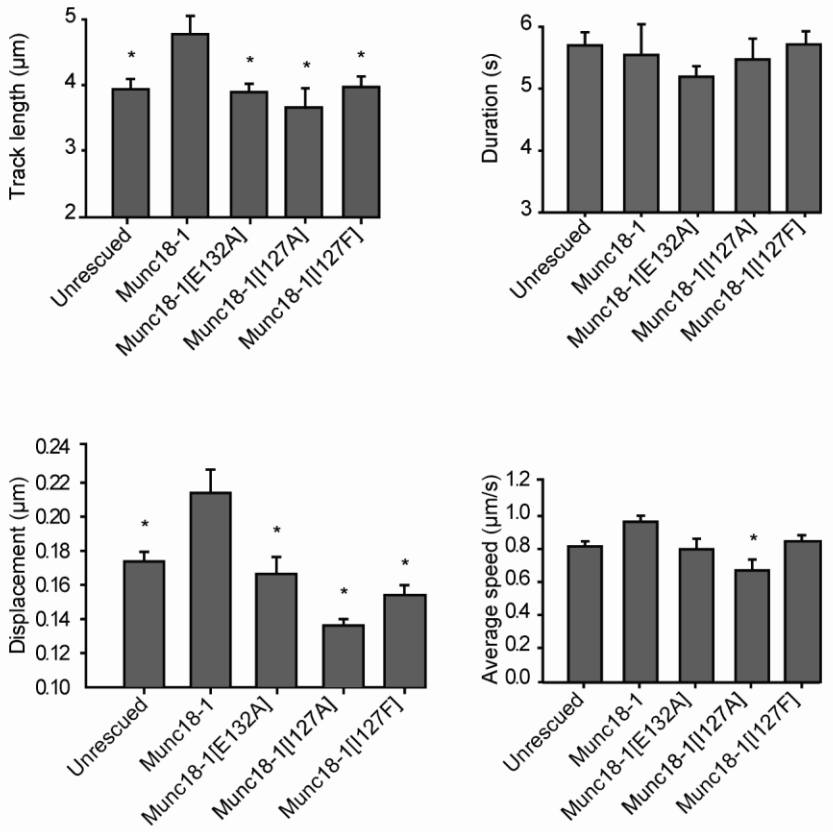

Figure 4.2. *Perturbing N-terminal interaction specifically affects vesicle kinetics*. Individual tracks were measured for track length, mean vesicle speed and vesicle track displacement (>250 tracks per cell, n = 5 cells). Rescue with munc18-1[I127A] resulted in a reduction in all parameters measured, track length, displacement and speed compared to wild-type munc18-1 (n = 5, mean ± S.E.M, One way ANOVA, asterisks indicate $p < 0.05$).

It was previously shown in Chapter 3 that perturbing the N-terminal interaction (using munc18-1[I127A]) resulted in a mis-localisation of, and reduced interaction between, munc18-1 and syntaxin (Figure 3.5 and 3.6). Following on from this earlier finding this chapter investigated whether a change in the localisation and interaction of munc18-1 and syntaxin affected downstream cellular events, for example, secretory vesicle behaviour. Employing mutant proteins, munc18-1[I127A], munc18-1[I127F] and munc18-1[E132A] alongside syntaxin and fluorescently labelled vesicles in KD43 PC12 cells revealed a significant change in a number of vesicle parameters. All munc18-1 mutants resulted in restricted vesicle track lengths and displacement values, with munc18-1[I127A] reducing vesicle displacement by approximately 40% from 0.21 ± 0.01 μm (n = 6 cells) in wild-type cells to 0.13 ± 0.01 μm (n = 5 cells; $p < 0.05$, one-way ANOVA, Figure 4.1B and 4.2). Munc18-1[I127A], the mutant with the most significant effect on syntaxin localisation and interaction (Figure 3.5 and 3.6), was also the only mutant to have an effect on the average speed of fluorescently labelled vesicles. The speed of vesicles was reduced from 0.96 ± 0.06 μms-1 (n = 6 cells) in wild-type munc18-1 expressing cells to 0.70 ± 0.02 μms-1 (n = 5 cells, Figure 4.2). This result supports the idea that N-terminal interaction imparts a kinetic advantage to a secretory vesicle and is an important modulator in their dynamics, as previously shown (Rickman and Duncan, 2010). Importantly the duration vesicle tracks were recorded under TIRFM illumination was not statistically significant; indicating that an effect seen with munc18-1 mutants was not caused by a difference in the amount of time a vesicle was visible and tracked for. On average vesicles were tracked for 5.34 ± 0.12 s and those vesicles that were not tracked for at least 150 ms (3 frames) were discounted from further analysis.

The effect on vesicle kinetics was less pronounced using munc18-1[I127A] compared with syntaxin[S14E], with the latter mutant resulting in the total immobilization of vesicles at the plasma membrane (Rickman and Duncan, 2010). This indicates that residue I127 is not solely responsible, and could therefore be partially redundant, for mediating the munc18-1-syntaxin-N-terminal interaction. Another likely reason for the difference in phenotypes is the idea that the phosphorylation of the N-terminus of syntaxin is a more important regulator of the munc18-1-syntaxin interaction and its preservation is more crucial in modulating vesicle dynamics at the plasma membrane.

Taken together, these findings indicate that perturbing N-terminal interaction between munc18-1 and syntaxin, most significantly using munc18-1[I127A], resulted in a) partial trapping of syntaxin in intracellular compartments, b) reduced munc18-1-syntaxin interaction and c) a loss of vesicle mobility at the plasma membrane. Vesicular fusion involves a number of highly orchestrated interactions between large cohorts of proteins, proteins which are spatially and temporally regulated within the process. So, if munc18-1[I127A] is disrupting a number of key steps required for efficient SNARE mediated fusion, for example, munc18-1-syntaxin trafficking and vesicle mobility, it may also be having a detrimental effect on single secretory vesicle fusion capabilities. For the remaining chapters of this thesis mutant munc18-1[I127A] will only be focussed on as it has consistently resulted in the largest effect on N-terminal binding both *in vitro* and in live cells.

4.3 Mode of interaction of munc18-1 with syntaxin influences vesicle fusion probability at the plasma membrane.

For many years it was postulated that secretory vesicles are stably bound to the plasma membrane before undergoing membrane fusion (Bittner and Holz, 1992; Xu et al, 1999). This theory was recently challenged by the finding that secretory vesicles, instead of being stably docked before exocytosis, undergo molecular-scale movements within several hundred milliseconds of agonist-induced fusion (Degtyar et al, 2007). It is possible that this sudden change in organelle movement increases the probability of productive interactions with the SNARE complex and plasma membrane. Molecular movements displayed by membrane bound vesicles have been postulated to be regulated by Ca^{2+}, ATP (Allersma et al, 2006) and by various proteins (Tsuboi and Fukuda, 2006). In fact, synaptotagmin-like protein 4-a (Slp4-a) has been shown to interact with the munc18-1-syntaxin complex to support the docking of dense-core vesicles at the plasma membrane in PC12 cells (Tsuboi and Fukuda, 2006). Furthermore, it has been repeatedly shown that munc18-1 promotes the docking of secretory vesicles in a variety of cells (Voets et al, 2001; Arunachalam et al, 2008; de Wit, 2010; Han et al, 2011). Therefore, the docking and fusion of secretory vesicles is dependent on the presence of munc18-1, its stable interaction with syntaxin and minute vesicular movements immediately prior to stimulation. Consequently, by reducing the speed and distance travelled by membrane

proximal secretory vesicles upon N-terminal perturbation, using munc18-1[I127A], there must be a downstream effect on the fusion capability of a single secretory vesicle.

To examine whether a change in vesicle behaviour affected downstream membrane fusion, single-vesicle fusion events, using a pH-sensitive EGFP-NPY probe (Rickman and Duncan, 2010), were analysed (Figure 4.3). In the single-vesicle fusion assay, secretion is observed as a rapid transient increase in fluorescence intensity due to a change in the pH of the microenvironment upon fusion. Fusion events were calculated as the percentage of the total number of vesicles visible at the start of the 3 minute recording that underwent fusion after stimulation with 300 μM ATP (Figure 4.3, shown by arrows). In the absence of munc18-1, stimulated exocytosis in KD43 PC12 cells was not significantly different from basal secretion observed in single-vesicle fusion assays, as shown previously (Arunachalam et al, 2008) (Figure 4.3B). Similarly, the genetic deletion of munc18-1 in mouse chromaffin cells results in the reduction of calcium-dependent LDCV exocytosis by 10-fold (Voets et al, 2001). Furthermore it was reported that the kinetic properties of the remaining single fusion events in chromaffin cells were not different from wild-type controls (Voets et al, 2001), a parameter not investigated in this study.

4.3

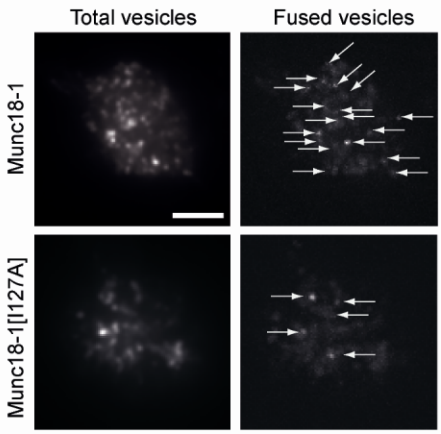

4.3B

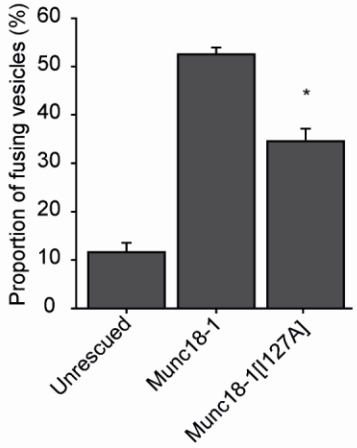

Figure 4.3. *N-terminal interaction is required for maximal vesicular exocytosis at the plasma membrane*. The total number of NPY-labelled vesicles at the beginning of the experiment (*left panels*) compared with the number of fusion events (*right panels*). Individual fusion events were detected by analysing the rate of fluorescence intensity change during the recording using ImageJ. Arrows indicate single vesicle fusion events detected throughout the entire recording period of 3 minutes. Fusion events were calculated as the percentage of the total number of vesicles visible at the start of the recording that underwent fusion after stimulation with 300µM ATP. Rescue with munc18-1[I127A] elicits fewer fusion events compared to wild-type munc18-1. Scale bar 5 µm. 4.3B. Exocytosis is reduced by shRNA knockdown of munc18-1 and is only partly rescued by munc18-1[I127A] compared to wild-type munc18-1. Error bars are SEM (One way ANOVA, $n = 4$, asterisk indicates $p < 0.05$).

Exocytosis in KD43 PC12 cells was fully rescued (to levels observed in native PC12 cells) by introducing a fluorescent fusion of wild-type munc18-1 (Figure 4.3B). The extent of exocytosis recorded in this study is in agreement with the initial characterisation of these KD43 PC12 cells (Arunachalam et al, 2008). This result indicates a requirement for munc18-1 in exocytosis, as observed previously (Verhage et al, 2000). Importantly, the fluorescent munc18-1 probe used in this thesis was functional and the expression level is sufficient for full fusion capacity.

Mutant munc18-1[I127A] resulted in the partial rescue of exocytosis in KD43 PC12 cells (Figure 4.3B), with only 32 ± 1.8 % (n = 6 cells) of vesicles fusing with the plasma membrane, compared with 51 ± 0.9 % (n = 5 cells) in wild-type munc18-1 expressing cells. The extent of vesicle exocytosis was significantly different in KD43 PC12 cells expressing wild-type munc18-1 and munc18-1[I127A] ($p < 0.05$, Mann-Whitney U). Therefore, mutating the hydrophobic pocket of munc18-1 to quantifiably disrupt N-terminal interaction with syntaxin not only results in significant changes in vesicle dynamics, but also negatively impacts on single vesicle fusion efficiency. It has been shown in Chapter 3 that disrupting N-terminal binding between munc18-1 and syntaxin results in a weakened interaction specifically at the plasma membrane. Therefore, the next question to address was whether disrupting N-terminal interaction affected munc18-1-syntaxin interaction specifically at the base of the cell, the site where these secretory vesicles are residing and eventually undergo fusion.

4.4 Perturbing N-terminal binding disrupts munc18-1-syntaxin interaction specifically at the plasma membrane.

To understand further the molecular interactions underlying this spatially restricted N-terminal interaction-enhanced exocytosis, munc18-1-syntaxin interaction, specifically at the base of the cell using TCSPC FLIM, was quantified (Figure 4.4). FLIM maps reveal that munc18-1 and syntaxin interact across the entire plasma membrane and these interactions have membrane-proximal vesicles associated with all areas of the cell surface. These data revealed that disrupting the N-terminal mode of interaction between munc18-1 and syntaxin, using munc18-1[I127A], decreases the amount of interaction detected, specifically within large areas at the plasma membrane (right panels, non-interacting

proteins shown in grayscale). Notably, areas of the plasma membrane that have a reduced munc18-1-syntaxin interaction are not avoided by membrane-proximal secretory vesicles. This finding indicates that N-terminal interaction is not required *per se* for vesicle-membrane association, at least within sub 100 nm axial distances. Taken together, these findings show that munc18-1 interacts with the N-peptide of syntaxin at the plasma membrane and that the spatial distribution of vesicles is not controlled by N-terminal interaction as their localisation is unaltered. Therefore, the reduced exocytotic events upon N-terminal ablation are not due to a re-positioning of secretory vesicles.

4.4

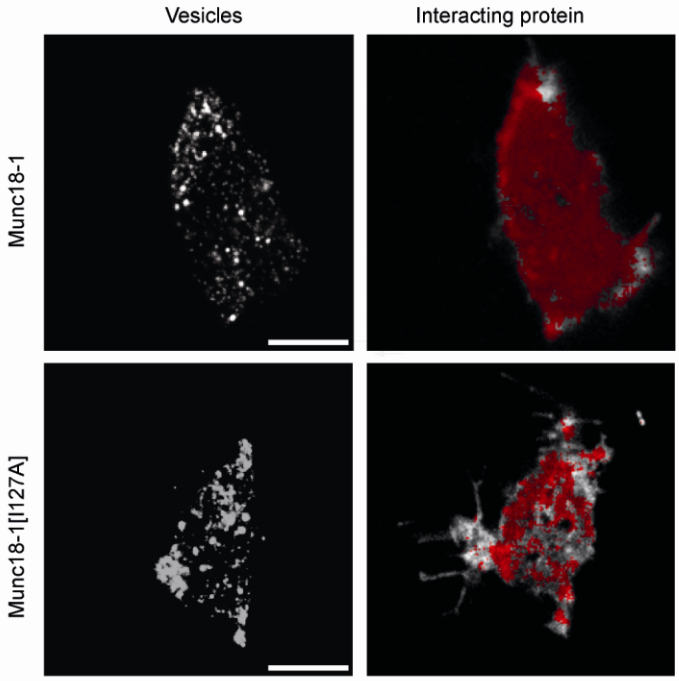

Figure 4.4. *Perturbing N-terminal interaction reduces munc18-1-syntaxin interaction at the cell surface but does not affect the spatial distribution of vesicles*. FLIM was used to quantify interaction changes specifically at the plasma membrane upon disruption of N-terminal binding, correlated with vesicle position. FLIM maps reveal that munc18-1[I127A] decreases the amount of interaction detected, specifically within large areas at the plasma membrane (*right panels*). Pixels containing donor fluorescence lifetime values >2 standard deviations below the mean, non-interacting control values obtained are shown (*red*). Pixels containing donor fluorescence lifetime values consistent with non-interacting syntaxin are shown (*grayscale*). Scale bar, 5 μm.

By disrupting the N-terminal interaction between munc18-1 and syntaxin this study has shown that a reduction in vesicle dynamics at the plasma membrane results in a concomitant fall in the level of vesicle fusion. The link(s) between how N-terminal binding impacts on vesicle exocytosis is still unknown. Previously in this chapter vesicle kinetics were analysed by calculating a mean account of their behaviours from at least five different cells (Figure 4.2). By combining datasets and producing an average of vesicle displacement, track length and speed it is possible that the more subtle effects of N-terminal interaction on single secretory vesicle dynamics were being lost. To fully investigate the impact of N-terminal interaction on single secretory vesicles the behaviour of every vesicle (as opposed to the mean behaviour previously analysed) in both wild-type- and mutant-rescued KD43 PC12 cells was analysed in detail.

4.5 N-TERMINAL INTERACTION ACTS ON A SPECIFIC POOL OF VESICLES AND IMPARTS A GREATLY INCREASED FUSION PROBABILITY.

By taking a cell by cell approach and resolving vesicle dynamics separately, this analysis should reveal whether all of the vesicles in a sample behave in an identical manner, or whether there are different types of vesicular dynamics prior to fusion. Using this method of analysis it might then be possible to explain exactly how immobilizing vesicles on the plasma membrane resulted in a partial arrest in downstream exocytosis. Approximately 64% of single vesicles in wild-type munc18-1-rescued cells (n = 545 vesicles, n = 7 cells) had a limited displacement distance (Figure 4.5). The behaviour of these vesicles was identical to that observed in the absence of munc18-1, i.e. in unrescued munc18-1 silenced KD43 PC12 cells (Figure 4.2). This suggested that this vesicle pool had no, or few, proximal munc18-1 molecules. Cells expressing wild-type munc18-1 and syntaxin revealed a smaller, more mobile pool of vesicles, comprising 37% of the total vesicle complement which had a greatly increased likelihood of proceeding to membrane fusion (Figure 4.5). In total, 75 ± 3% of all single vesicle fusion events (at least 60 fusion events from 6 cells) arose from vesicles contained within this minority pool. In fact, the fusion probability of vesicles contained within this minority pool was enhanced by approximately 5 times.

4.5

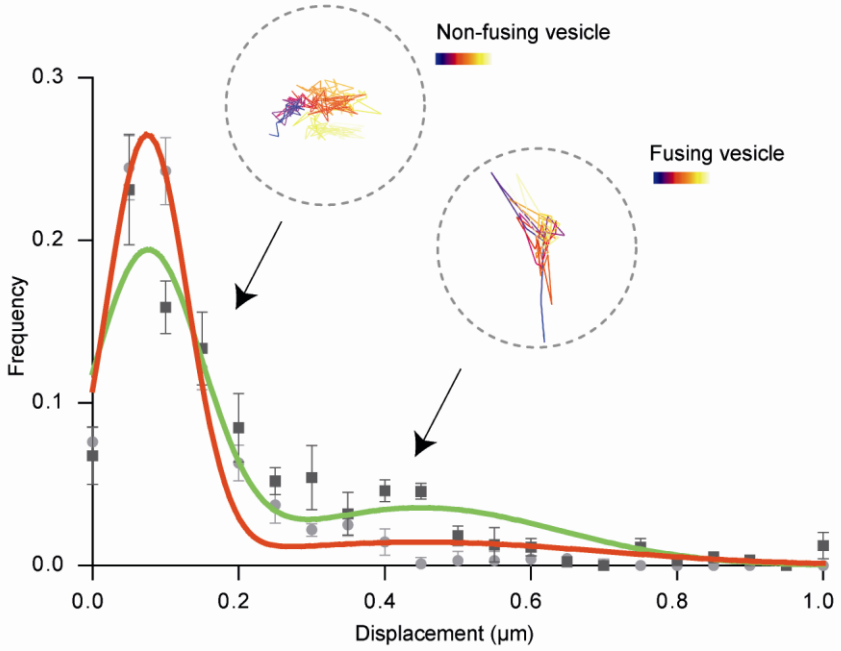

Figure 4.5. *N-terminal interactions increase the fusion likelihood in a specific pool of vesicles*. The histogram shows the measured vesicle displacements from wild-type munc18-1 (*dark gray*) and munc18-1[I127A]-rescued KD43 PC12 cells (*light grey*), best fit by a double Gaussian function (munc18-1: green, munc18-1[I127A]: red). The majority of non-fusing vesicles have a limited displacement distance whereas a second, more highly mobile pool of vesicles has an increased likelihood of exocytosis. Both distributions are bimodal, with a significant decrease in the magnitude of the higher mobility, fusion-competent pool of vesicles in the mutant cells (mean ± SEM, $n = 4$ cells; sum of squares F-test, $p < 0.05$).

To further identify any role that N-terminal interaction may have in delineating this vesicle behaviour and fusion likelihood, data with those acquired from munc18-1[I127A]-rescued cells was analysed. There was a significant decrease, revealed by a sum of squares special F-test ($p < 0.001$, $n = 4$ cells), in the magnitude of this higher fusion probability pool of vesicles when N-terminal interaction was disrupted, from 37% to 4% of the total vesicle complement (Figure 4.5). These findings correlate with the decrease in exocytosis in munc18-1[I127A]-rescued cells. Disruption of N-terminal interaction, as well as having an effect on vesicle pool mobility, also interferes with exocytosis from this pool. It is noteworthy to mention that the complete removal of this more mobile pool of vesicles was seen upon phosphomimetic mutation of syntaxin serine[14], when these data were analysed in this manner (Figure 4.6). This fits well with the observation that syntaxin[S14E] resulted in the total immobilization of membrane proximal secretory vesicles and inhibition of membrane exocytosis (Rickman and Duncan, 2010). The simplest explanation for these observations is that N-terminal interaction is required for events immediately postdocking and preceding exocytosis.

4.6

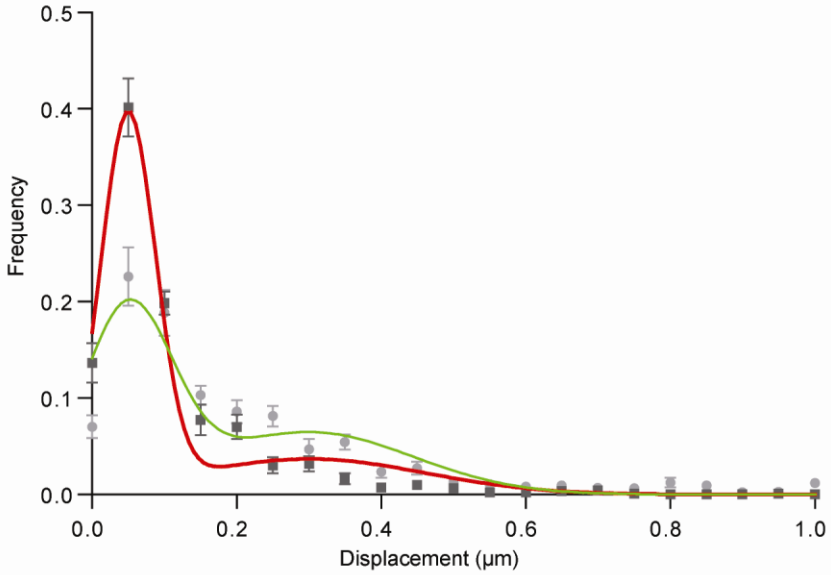

Figure 4.6. *N-terminal interactions are critical for the fusion of a subset of secretory vesicles.* The histogram shows the measured vesicle displacements from wild-type syntaxin (*dark gray*) and syntaxin[S14E] in wild-type PC12 cells (*light grey*), best fit by a double Gaussian function (syntaxin: green, syntaxin[S14E]: red). A large percentage of secretory vesicles within cells expressing wild-type syntaxin have a restricted displacement distance whereas a second, more highly mobile pool of vesicles has an increased likelihood of exocytosis. Both distributions are bimodal, with a significant decrease in the magnitude of the higher mobility, fusion-competent pool of vesicles in the mutant cells (mean ± SEM, n = 4 cells; sum of squares F-test, p <0.05). Data provided by Colin Rickman, Heriot Watt University (Rickman and Duncan, 2010).

From this study two distinct pools of vesicles can be identified, based on their relative mobility; the majority of fusion events arise from a minority pool of relatively mobile membrane proximal vesicles, which in turn relies on N-terminal interactions. Disrupting this interaction reduces the magnitude of this pool and thus immobilizes almost all vesicles at the membrane. Therefore, the presence of munc18-1 molecules, engaged in regulated N-terminal interaction with syntaxin, exerts a strong positive effect on a specific postdocking pool of vesicles, increasing the probability of fusion by a factor of 5 (Smyth et al, 2010).

4.6 PHOSPHORYLATION OF SYNTAXIN AT SERINE^{14} REDUCES ITS CO-LOCALISATION WITH SYNAPTIC TERMINALS.

Over the last decade there has been a huge interest in further characterising N-terminal binding and its functionality in neuronal cells. However, further understanding in an *in* or *ex vivo* setting has been hindered by the fact that munc18-1– and syntaxin-deficient neurons die early (Verhage et al, 2000; de Wit, 2006) and are thus difficult to analyse. To overcome this problem a recent study used lentiviral expression of munc18-1 in neurons from munc18-1 knockout mice and concluded that interactions of munc18-1 with the SNARE complex via N-terminal binding are critical for SNARE complex binding and the priming of synaptic vesicles (Deak et al, 2009). Another study tested the importance of the N-peptide of syntaxin in a physiologically relevant system, using large nerve terminals in the calyx of Held synapse. This study showed that the binding of the syntaxin N-terminus to munc18-1 is also essential for synaptic vesicle fusion (Khvotchev et al, 2007). Furthermore, within the nervous system of the *C.elegans* it has been shown that binding of the SM protein unc-18 to closed syntaxin is dispensable for membrane fusion, whereas interaction with the syntaxin N-terminus is essential for neuronal exocytosis *in vivo* (Johnson et al, 2009).

The characterisation of the munc18-1-syntaxin N-terminal interaction could provide a new target for regulation (Dulubova et al, 2007; Rickman et al, 2007). Following the finding that syntaxin is phosphorylated *in vivo* by casein kinase II (CKII) (Foletti et al, 2000) it was shown that serine^{14} was a target for CKII (Risinger and Bennett, 1999; Foletti et al, 2000). Using phosphosyntaxin-specific antibodies this study reported that the phosphorylation on serine^{14} of syntaxin was developmentally regulated *in vivo*, rising to a

level of 40% of the total syntaxin in adult rat brains (Foletti et al, 2000). Interestingly, it was shown that phosphorylated syntaxin at serine^{14} localises to discrete domains of the axonal plasma membrane that do not correspond to synaptic sites. The authors of this study were unable to provide a mechanism that was in turn regulated by this modification and notably only employed syntaxin constructs which lacked N-terminal amino acids (Foletti et al, 2000). Importantly, this site is well positioned to potentially influence the N-terminal interaction of syntaxin with munc18-1.

This study firstly set out to test whether phosphorylated endogenous syntaxin is localised outside of synaptic terminals in dissociated embryonic rat cortical neurons, instead of previously used rat brain slices. An anti-syntaxin (phospho-serine^{14}) antibody that specifically recognizes a casein kinase II-mediated phosphorylation on serine^{14} of syntaxin 1 was supplied by Abcam. This antibody was generated using a peptide corresponding to amino acids 9–19 of syntaxin 1A (RTAKDSDDDDD) (Bennett et al, 1992) and synthesized with a phosphoserine at position 14 and an additional cysteine residue at the C terminus. Embryonic cortical neurons at day *in vitro* (DIV) 14 were fixed with 4% paraformaldehyde (section 2.7.1) and subsequently immunolabelled with syntaxin 1a monoclonal antibody (clone HPC-1) or syntaxin-serine^{14}-phosphospecific antibody and synapsin (Table 2.1). Cells were further labelled with Fab fragment secondary fluorescent antibodies specific to the primary antibody used (section 2.7.2) (Figure 4.7).

Embryonic cortical neurons were imaged using confocal microscopy and data deconvolution techniques were performed on acquired Z axis stacks (section 2.8.2 and 2.9.2). Quantitative co-localisation studies (section 2.9.3) of phosphorylated and unphosphorylated syntaxin indicated that endogenous and unphosphorylated syntaxin labelling was highly concentrated in synaptic terminals with a Pearson's correlation coefficient of R = 0.90 ± 0.008, n = 8 cells (Figure 4.7B). The dense accumulation of syntaxin at synaptic terminals agrees with previous reports suggesting that syntaxin forms clusters on the plasma membrane in a variety of cell types (Bennett et al, 1992; Lang et al, 2001; Sieber et al, 2007). Neurons immunolabelled with the phospho-specific syntaxin antibody revealed a significant reduction in co-localisation with synapsin, a synaptic terminal marker (R = 0.83 ± 0.019, n = 6 cells; One way ANOVA $p < 0.05$). This value was not significantly different from the Pearson's Correlation Coefficient calculated for

the covariance of unphosphorylated and phosphorylated syntaxin (R = 0.80 ± 0.013, *n* = 11 cells, Figure 4.7B). The colocalisation of β-tubulin and synapsin represented a negative control (R = 0.66 ± 0.03, *n* = 9 cells). This finding supports previous immunohistochemistry experiments which revealed that phosphorylated syntaxin, despite being concentrated in puncta on a subset of axons, was not enriched at synaptic sites, in contrast to unphosphorylated syntaxin (Foletti et al, 2000). These results suggest a role for casein kinase II and phospho-syntaxin in defining specific subdomains for a subset of vesicles which are segregated from the synaptic active zones.

4.7

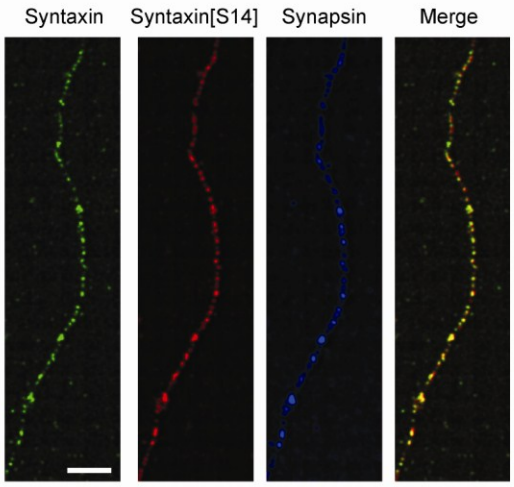

4.7B

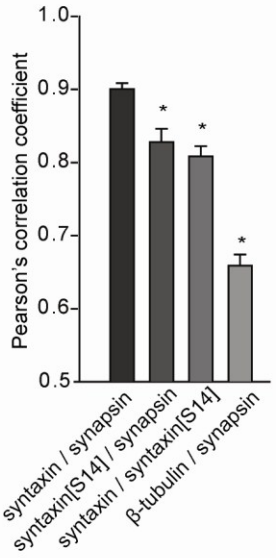

Figure 4.7. *Specific phosphorylation of syntaxin at residue serine*[14] *results in a reduction in its localisation with synapses*. DIV 14 embryonic cortical neurons were fixed and immunolabelled with syntaxin (HPC-1), phospho-specific syntaxin[S14E] and synapsin and imaged by confocal laser scanning microscopy (CLSM). Resulting images were subsequently deconvolved using Huygens deconvolution software. Immunolabelling syntaxin with a S14 phospho-specific antibody (Abcam) revealed that phosphorylated syntaxin co-localises with synapsin, a synaptic marker, to a lesser extent compared to syntaxin. A merge image of syntaxin and phospho-specific syntaxin[S14E] indicates the extent of their co-localisation. Scale bar: 5 µm. 4.7B Combined covariance analysis of syntaxin, syntaxin[S14E], synapsin and β-tubulin (negative control). Mean Pearson's correlation coefficients are shown (n >5, mean ± S.E.M, One way ANOVA, asterisks indicate $p < 0.03$).

Over the last decade a number of kinases, proteins and fatty acids have been demonstrated to regulate the dynamic interaction between munc18-1 and syntaxin (Fugita et al, 1996; Craig et al, 2003; Rickman and Davletov, 2005; Connell et al, 2007). One of the proposed regulators of this interaction, acting in an activity dependent manner, is protein kinase C (PKC). It has been shown that munc18-1 is a substrate for protein kinase C (PKC) (Fugita et al, 1996; Craig et al, 2003) and that PKC activation can be triggered upon neuronal depolarisation (de Vries et al, 2000). PKC phosphorylation is thought to be essential for the regulation of exocytosis (Barclay et al, 2003) as the phosphorylation of munc18-1 by PKC reduces its affinity for closed syntaxin (Fujita et al, 1996; Toonen and Verhage, 2007). Therefore, the next question in this study was to address whether the phosphorylation of syntaxin, specifically at serine^{14}, was regulated by neuronal activity.

4.7 THE PHOSPHORYLATION OF SYNTAXIN AT SERINE^{14} IS NOT ACTIVITY DEPENDENT.

In order to determine whether the regulation of syntaxin phosphorylation, specifically at serine^{14}, is regulated by synaptic activity neuronal cultures were subjected to different ionic treatments *in vitro*. Dissociated DIV 14 embryonic cortical neurons were exposed to either a treatment which would stimulate neurotransmitter release (50 mM KCl) or a control treatment containing 2.5 mM of KCl. Cells were incubated for 1 minute in their corresponding buffers and immediately lysed in SDS-sample buffer. Protein expression was determined by SDS-PAGE and immunoblotting using syntaxin (HPC-1), syntaxin phospho-serine^{14} and synaptophysin, a loading control (section 2.3.1 and 2.3.2, Figure 4.8). No significant difference in the levels of proteins between the unstimulated and stimulated conditions was found, indicating that the phosphorylation of syntaxin on serine^{14} is not regulated by neuronal activity (Figure 4.8B). This finding also supports a previous study which failed to detect a change in the phosphorylation status of syntaxin upon neuronal depolarisation (Foletti et al, 2000).

4.8

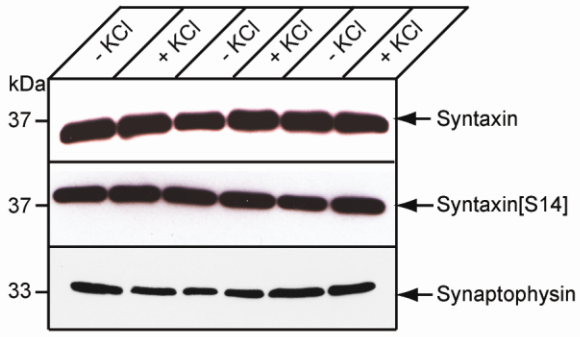

4.8B

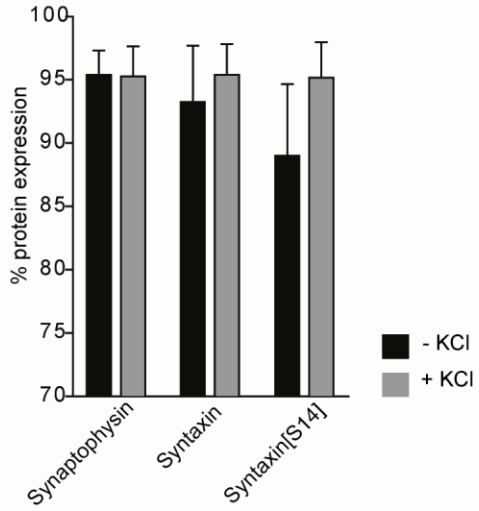

Figure 4.8. *The phosphorylation of syntaxin at residue serine*[14] *is not activity dependent*. Dissociated DIV 14 embryonic cortical neurons were exposed to either a treatment which would stimulate synaptic transmission (50 mM KCl) or a control treatment containing 2.5 mM of KCl. Cells were incubated for 1 minute in their corresponding buffers, immediately lysed in SDS-sample buffer and protein signal was analysed using SDS-PAGE and immunoblotting. Membranes were probed with anti-syntaxin (HPC-1), phospho-syntaxin[S14] and synaptophysin (loading control) and protein levels were quantified using ImageJ. Numbers on the left indicate the positions of molecular weight markers. 4.8B Quantification of protein blots revealed no significant difference in the levels of proteins between unstimulated and stimulated conditions (n = 6, mean ± S.E.M).

The negligible change in the phosphorylation status of syntaxin following synaptic stimulation suggests that casein kinase II-mediated phosphorylation is unable to induce an immediate response that is required for efficient neurotransmission. This finding is in contrast to the regulation of synapsin, a presynaptic protein, which undergoes a rapid change in its phosphorylation state after stimulation (Greengard et al, 1993). Serine^{14}, previously labelled as a regulator of the munc18-1-syntaxin N-terminal interaction (Rickman and Duncan, 2010), must be itself regulated via a different mechanism, perhaps by other proteins or kinases.

Taken together these findings suggest that phosphorylated syntaxin at serine^{14}, a regulator of the munc18-1-syntaxin-N-terminal interaction (Rickman and Duncan, 2010), resides outside of the active zone and is not regulated by neurotransmission. It is possible that phosphorylated syntaxin could be labelling plasma membrane domains where exocytosis of synaptic vesicles is inhibited, domains where non-classical inter-cellular communication between neurons could occur. The phosphorylation of syntaxin at serine^{14} could therefore be a regulatory mechanism to impart a difference between fusion and non-fusion sites across a neuron.

A recent study has shown that serine^{14} on the N-terminus of syntaxin modulates the N-terminal interaction with munc18-1 (Rickman and Duncan, 2010). By specifically destabilizing this phosphorylation site it was shown that secretory vesicles within PC12 cells displayed enhanced immobilization at the plasma membrane with a resulting inhibition of exocytosis (Rickman and Duncan, 2010). Taking this result into consideration, the next facet of this interaction was to determine whether this phosphorylation site, and more importantly, N-terminal binding between munc18-1 and syntaxin, was also critical to the process of exocytosis in a neuronal cell.

4.8 Disrupting the phosphorylation status of the N-terminus of syntaxin reduces the size of the readily releasable pool of synaptic vesicles.

Inter- and intra- neuronal communication is operated by neurotransmitters stored in synaptic vesicles and released to the extracellular space by regulated exocytosis. Synaptic

vesicles are virtually indistinguishable in ultrastructural examinations but nevertheless exhibit both functional and spatial heterogeneity in physiological studies (Rosenmund and Stevens, 1996; Von Gersdorff and Matthews, 1997; Kuromi and Kidokoro, 1998). There is now an extensive amount of literature reporting that the proportion, distribution and release probabilities of synaptic vesicles are non-uniform, establishing a diversity that is thought to be vital for neuronal communication and information processing (Hessler et al, 1993; Neher and Zucker, 1993; Rosenmund et al, 1993; Murthy et al, 1997). Within central nerve terminals synaptic vesicles capable of fusing with the pre-synaptic membrane are commonly referred to as the recycling pool of vesicles (Südhof, 2000; Rizzoli and Betz, 2005). This recycling pool can be further subdivided into the readily releasable pool (RRP) and the reserve pool (RP). The RRP vesicles are positioned in close apposition to the active zone and are available for immediate release upon the arrival of a physiological stimulus (Greengard et al, 1993; Pieribone et al, 1995; Brodin et al, 1997; Kuromi and Kidokoro, 1998). The reserve pool, anatomically distinct from fusion sites, releases synaptic vesicles during periods of prolonged stimulation, its size often resembling the functional requirements of a nerve terminal (Rizzoli and Betz, 2005). In general, the magnitude of synaptic pools initially declines as the RRP is depleted, declining further as vesicles are then mobilized from the reserve pool during prolonged stimulation (Elmqvist and Quastel, 1965; Richards et al, 2003).

The ability to measure the kinetics of synaptic vesicle fusion provides an insight into some of the basics of neurotransmission. A common technique in order to visualise and measure synaptic vesicle release from nerve terminals is to use membrane-selective FM-dyes. FM-dyes FM4-64 and FM1-43 are most commonly used and belong to a class of amphiphilic styryl dyes developed by Betz and colleagues (Betz et al, 1992, 1996). FM dyes are internalized by endocytic vesicles during spontaneous or evoked activity and are subsequently distributed to various organelle membranes (Betz et al, 1992, 1996). Only when exposed to a lipophilic environment, for example the lumen of a synaptic vesicle, will FM dyes fluoresce brightly (Richards et al, 2005). FM dye concentrated within vesicles is then released into the extracellular environment during exocytosis, resulting in a nominal fluorescence signal once in the extracellular fluid. The ability of FM dyes to bind to the vesicle membrane in a reversible manner enables FM dyes to be used to study vesicle exocytosis and endocytosis in various systems. The advancement of optical

techniques has now permitted the study of synaptic vesicle cycling within nerve terminals (Betz et al, 1992; Ryan et al, 1993; Sankaranarayanan and Ryan, 2000).

Synaptic vesicles from DIV 18 embryonic cortical neurons were labelled with FM1-43 to measure their release from functionally distinct pools using pre-defined stimulation paradigms (Richards et al, 2003; Rizzoli and Betz, 2004). Resolving the changes in fluorescence, indicative of vesicle fusion, allowed for the examination of whether the munc18-1-syntaxin N-terminal interaction played a role in catalyzing synaptic vesicle exocytosis. More specifically, FM1-43 fluorescence changes in conjunction with different electrical stimulations enabled this study to probe whether this interaction was important in facilitating the fusion of synaptic vesicles residing in a distinct pool in central nerve terminals.

Embryonic cortical neurons were transfected with mCherry-munc18-1 and Cerulean-syntaxin at DIV 14. On DIV 18 embryonic cortical neurons expressing munc18-1 and syntaxin were labelled with FM1-43 dye (10 μM) using 600 action potentials (10 Hz) for 60s. Successful FM1-43 dye uptake into the membranes of synaptic vesicles was confirmed upon fluorescent puncta labelling. Following FM dye uptake neurons were washed in order to remove external dye from the plasma membrane and allowed to rest within the stimulation buffer (section 2.1.1) for a further 8 minutes. FM1-43 dye was subsequently unloaded using 60 action potentials (30 Hz) for 2s (RRP release) and 2 X 400 action potentials (40 Hz) for 10s (reserve pool) (Richards et al, 2003; Rizzoli and Betz, 2004). Fluorescent images were captured at 4 s intervals and processed offline using ImageJ 1.43 software (NIH). Regions of interest of identical size were placed over nerve terminals that displayed a decrease in fluorescence on stimulation and the total fluorescence intensity was monitored over time. Fluorescence traces were normalised (between 1 and 0) to the size of the recycling pool (RRP+RP) for each nerve terminal (Figure 4.9A-C). The fluorescence decay of FM dyes in control, non-transfected boutons, served as an internal control. Importantly, the over-expression of wild-type munc18-1 and syntaxin had no effect on the rate and extent of vesicle exocytosis, as compared to the non-transfected internal control (Figure 4.9A).

4.9A

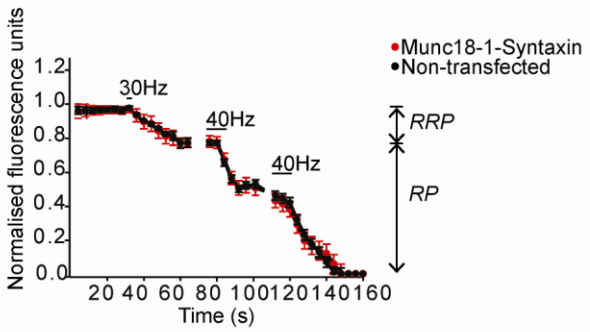

4.9B

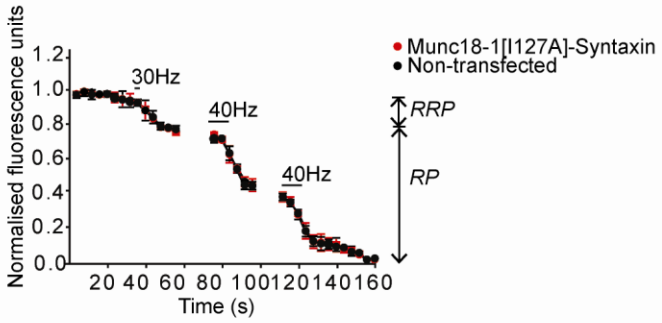

4.9C

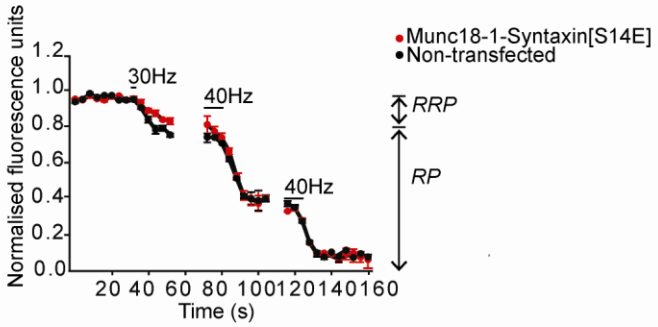

Figure 4.9. *Disrupting the phosphorylation status of the N-terminus of syntaxin reduces the size of the readily releasable pool of synaptic vesicles*. 4.9A. DIV 18 embryonic cortical neurons expressing mCherry-munc18-1 and mCer-syntaxin were immersed in buffer and loaded with FM 1-43(10 μM) using 600 action potentials (10 Hz) for 60 s. FM dye was subsequently unloaded using 60 action potentials (30 Hz) for 2 s (RRP release) and 2 X 400 action potentials (40 Hz) for 10 s (reserve pool). Representative traces of the average fluorescence decay are shown with fluorescence decay calculated using ImageJ. Traces were normalised (between 1 and 0) to the size of the recycling pool (RRP+RP) for each nerve terminal. The relative sizes of the RRP and RP are indicated by arrows and unloading stimulations are represented by horizontal bars. The same imaging protocol and analysis was carried out on DIV 14 embryonic cortical neurons expressing mCherry-munc18-1[I127A]/mCer-syntaxin (4.9B) and mCherry-munc18-1/mCer-syntaxin[S14E] (4.9C) (n = 150 nerve terminals).

The same imaging protocol and analysis was carried out on DIV 18 embryonic cortical neurons expressing mCherry-munc18-1[I127A]/mCer-syntaxin (Figure 4.9B) and mCherry-munc18-1/mCer-syntaxin[S14E] (Figure 4.9C) to study whether N-terminal interaction was important in the fusion efficiency of synaptic vesicles, as compared to their neuroendocrine counterparts (Figure 4.3). As shown in figures 4.9B and 4.10, there was no significant change in the size of both the RRP (first stimulus) and RP (second and third stimulus) in cortical neurons expressing munc18-1[I127A] alongside wild-type syntaxin. This analysis revealed that the size of the readily releasable pool was 18 ± 2.23 % (n = 3 experiments) of the total recycling pool of vesicles with 82 ± 1.93 % (n = 3 experiments) of synaptic vesicles within the reserve pool in munc18-1[I127A] expressing cells (Figure 4.10). The extent of vesicle release from both pools was almost identical to cells expressing wild-type munc18-1 and syntaxin. This finding is in agreement with a finding earlier this year suggesting that interfering with the binding of munc18-1 to the N-peptide of syntaxin is not involved in maintaining the normal docking, priming and fusion of synaptic vesicles in munc18-1 null mutant neurons (Meijer et al, 2012). Null neurons rescued with either munc18-1[F115E], a construct predicted to disrupt N-terminal binding, or wild-type munc18-1 had the same size of RRP, indicating that the N-peptide is not required for normal synaptic transmission (Meijer et al, 2012).

In contrast, the expression of syntaxin[S14E] alongside wild-type munc18-1 resulted in a significant reduction in the size of the readily releasable pool upon stimulation compared with non-transfected neurons in the same field (Figure 4.9C). Quantification of fluorescence changes showed that the proportion of fusing vesicles within the RRP was reduced whereas the size of the RP was unaffected. The extent of the RRP size was reduced to 12 ± 3.42% (n = 4) with an RP size of 88 ± 3.08% (n = 4) of the total pool of synaptic vesicles (Figure 4.10). Together, these results suggest that residue I127A interaction looks to be largely dispensable whereas an intact N-terminal casein kinase II phosphorylation site is crucial for mobilising vesicles residing within the RRP. A number of studies can be used to explain why the N-terminal interaction, specifically mediated through residue serine[14], plays more of a role in synaptic vesicle exocytosis. It has been previously shown that mutations in the UNC-18 protein which selectively abolish the N-peptide interaction (F113R and L116K) in unc-18 null *C. elegans* neurons result in a sustained defect in regulated exocytosis (McEwen and Kaplan, 2008; Johnson et al, 2009).

However, in munc18-1 silenced PC12 cells the same munc18-1 mutants almost completely rescue exocytosis (Han et al, 2009; Malintan et al, 2009), suggesting a more subtle role of these particular residues of the N-peptide in driving dense core vesicle exocytosis. Therefore, munc18-1[I127A] may be playing a more pronounced role in neuroendocrine cells but is superfluous to RRP synaptic vesicle exocytosis. In contrast, the serine^{14} phosphorylation site on the N-peptide of syntaxin, important in neuroendocrine exocytosis (Rickman and Duncan, 2010) and RRP mobilisation reported in this study, may orchestrate a number of additional upstream actions involved in the regulation of different mechanisms, protein (N-terminal) interactions and pathways that are involved in catalysing the release of synaptic vesicles immediately adjacent to the active zone.

4.10

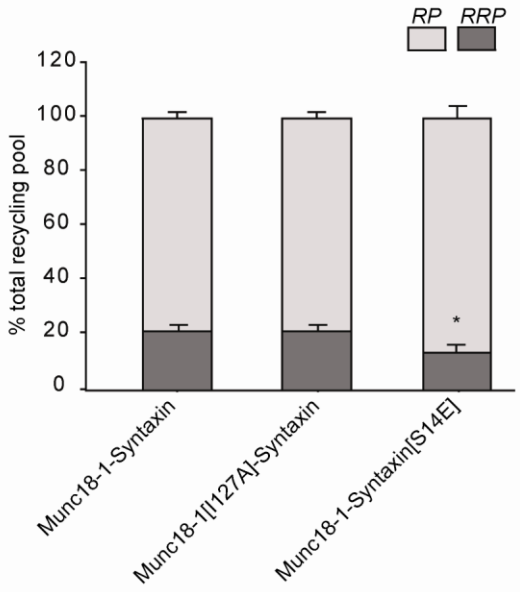

Figure 4.10. *Destabilizing the phosphorylation site on syntaxin (serine* ^{14}*) results in a reduction in the proportion of readily releasable vesicles able to fuse with the plasma membrane*. The average proportion of the RRP and RP as a percentage of the entire synaptic vesicle recycling pool is shown (RRP - dark grey bars, RP - light grey bars). Mutating the casein kinase II phosphorylation site on the N-terminus of syntaxin (S14E) resulted in a significant decrease in the size of the readily releasable pool of vesicles compared to wild-type munc18-1 and syntaxin (n = 4 separate experiments, mean ± S.E.M, One way ANOVA (Newman-Keuls multiple comparison post hoc test, asterisks indicate $p < 0.05$).

4.9 CONCLUSION

Despite intensive research the molecular mechanisms involved in the lifecycle of a membrane bound vesicle, from transport to fusion, remains poorly defined. It is thought that munc18-1 acts to promote docking, as in its absence there is a large reduction in the number of vesicles found immediately adjacent to the plasma membrane of neuroendocrine cells (Voets et al, 2001; Toonen et al, 2006; Verhage and Sørensen, 2008), but not in synapses (de Wit et al, 2006). More recently, it was suggested that syntaxin is involved in docking (de Wit et al, 2006) and that t-SNARE heterodimer intermediates act as an acceptor for synaptotagmin (Rickman and Davletov, 2003; Rickman et al, 2004), forming a docking assembly. In this situation, munc18-1 has been suggested to act as an ancillary t-SNARE heterodimer-stabilizing factor (de Wit et al, 2009). It is now clear that munc18-1 is an important factor in the process of both vesicle docking and membrane fusion (i.e. postdocking), but the molecular mechanism of its action at the membrane remains undefined.

This chapter presents findings showing that mutating the hydrophobic pocket of munc18-1 to quantifiably disrupt N-terminal interaction with syntaxin results in significant changes in vesicle dynamics and fusion efficiency. This is in contrast with recent studies finding that the N-terminal peptide is dispensable in neuroendocrine exocytosis (Arunachalam et al, 2008; Han et al, 2009; Malintan et al, 2009). This controversy can be explained by the fact that poorly conserved residues of the hydrophobic pocket of munc18-1 were selected for study and likely to play no significant role in mediating this interaction. Furthermore, earlier this year Verhage and colleagues reported that the N-peptide of munc18-1 is dispensable for synaptic transmission (Meijer et al, 2012). This study went on to suggest that binding to assembled SNARE complexes in order to drive membrane fusion may be a central aspect of some SM proteins (Carr et al, 1999; Togneri et al, 2006; McEwen and Kaplan, 2008), but is not a universal feature of all SM proteins. Despite dismissing a role of the N-terminal interaction the authors of this study reported a slight difference in the ratio between synaptic responses to stimuli given at various time intervals i.e. release probability (Meijer et al, 2012). This finding tentatively suggests that the binding of munc18-1 to the SNARE complex via the N-terminal peptide may be playing a more subtle and unpronounced role in synaptic transmission. In addition, it may well be that the

contribution of N-peptide binding and its inter-dependence on closed form interaction is likely to be different in divergent systems, partially explaining the different effects documented upon disruption (Khvotchev et al, 2007; Shen et al, 2007; Deak et al, 2009; Johnson et al, 2009; Rickman and Duncan, 2010). This chapter also presents evidence to suggest that two distinct pools of vesicles can be identified in neuroendocrine cells. These pools are based on their relative mobility; the majority of fusion events arise from a minority pool of relatively mobile membrane proximal vesicles, which in turn relies on N-terminal interactions.

Despite extensive investigation into munc18-1-syntaxin-N-terminal binding it is still unknown how this mode of interaction between a t-SNARE and an SM protein affects prefusion vesicle dynamics. At present it is thought that munc18-1 may be part of a larger "docking complex," acting somehow to stabilize the t-SNARE heterodimer (de Wit et al, 2009). Based on current understanding, this interaction with the assembled SNARE complex would require munc18-1 to associate with syntaxin via N-terminal interaction. In fact it was recently shown that the 4-helical SNARE bundle, containing the syntaxin N-peptide region, is the minimal complement required for munc18-1-mediated stimulation of membrane fusion *in vitro* (Shen et al, 2010). By destabilizing the N-terminal interaction this study highlighted that residue I127 is a key player in regulating vesicle mobility and membrane fusion, i.e. events immediately postdocking and preceding exocytosis.

Both SNAREs and SNARE regulatory proteins are phosphorylated *in vitro* (Gerst, 1999; Lin and Scheller, 2000). What remains to be resolved is when this phosphorylation occurs, what regulatory mechanism controls the phosphorylation of SNAREs and their partners and its downstream functional significance *in vivo*. Regulation of plasma membrane dynamics and turnover is critical to the function of the nervous system in many ways, for example, axonal outgrowth and synaptogenesis. Given the essential role of SNARE-mediated vesicular fusion in the functions of various membrane compartments, it is crucial to understand how SNAREs are themselves regulated. The three neuronal SNAREs have been previously shown to be phosphorylated *in vitro* by different kinases: synaptobrevin by Ca^{2+}- and calmodulin-dependent protein kinase II (Hirling and Scheller, 1996), syntaxin 1 by casein kinase II (Bennett et al, 1993) and SNAP-25 by protein kinase A (Risinger and Bennett, 1999).

This chapter investigated the phosphorylation of syntaxin on residue serine^{14} by casein kinase II using phosphosyntaxin-specific antibodies. Phosphorylated syntaxin appears to reside in specific domains along axons, domains that are separate from active zones and synapsin localisation, in agreement with a previous report (Folleti et al, 2000). The disparity between the neuronal localisation of phosphorylated and unphosphoryated syntaxin may provide a signalling pathway to differentiate between functional and non-functional synapses, a regulatory mechanism in order to prevent indiscriminate fusion outside pre-defined areas. This idea fits with the observation that the upregulation of syntaxin phosphorylation coincided with an increase in the expression of synaptic vesicle proteins and the maturation of synapses (Folleti et al, 2000). Taking the differential expression and localisation of phosphorylated syntaxin into account, it would be of interest to investigate whether there are phosphorylated and non-phosphorylated syntaxin 'hotspots' across the plasma membrane of a neurosecretory cell. It would be conceivable to think that disrupting the phosphorylation of syntaxin could alter the architecture of the plasma membrane, specifically productive fusion sites, resulting in a loss and mis-regulation of exocytotic events. This hypothesis may help to explain why vesicle mobility and fusion was arrested in neuroendocrine cells upon phosphomimetic disruption of serine^{14} (Rickman and Duncan, 2010).

The next facet of the N-terminal interaction within neuronal cells investigated was whether its regulation was activity dependent. The phosphorylation of serine^{14} has been previously shown to be important in mediating the N-terminal interaction between munc18-1 and syntaxin (Rickman and Duncan, 2010). These findings demonstrated that the extent of syntaxin phosphorylation, specifically on residue serine^{14}, is not regulated by synaptic transmission, in agreement with Foletti et al (2000). Therefore, despite the abundance of neuronal syntaxin and the extent of its phosphorylation, the casein kinase II site is not a likely regulator of an activity-induced response that could rapidly induce vesicular fusion.

The interaction between munc18-1 and the N-terminal peptide of syntaxin has been repeatedly shown to be a critical factor in driving SNARE complex assembly and membrane fusion in purified *in vitro* systems (Dulubova et al 2007; Rickman et al, 2007; Shen et al, 2007, 2010). In cultured neuronal systems it has also been shown that N-

terminal binding is critical for SNARE complex binding and both the 'priming' and fusion of synaptic vesicles (Khvotchev et al, 2007; Deak et al, 2009; Johnson et al, 2009). Furthermore, the N-peptide has been shown to inhibit vesicle fusion if over-expressed in a number of different systems (Yamaguchi et al, 2002; Dulubova et al, 2003; Williams et al, 2004; Khvotchev et al, 2007). In support of both *in vitro* and *ex vivo* studies it has also been shown in a neuroendocrine model that perturbing N-terminal binding between munc18-1 and syntaxin (syntaxin[S14E]) renders secretory vesicles immobile and unable to support membrane fusion (Rickman and Duncan, 2010). Using the same phosphomimetic syntaxin mutant as the latter study the importance of the N-terminal interaction in catalyzing synaptic vesicle fusion was explored. In order to probe whether phosphorylation of this N-terminal peptide was acting specifically on a discrete pool of synaptic vesicles, different electrical stimulation paradigms were used (Richards et al, 2003; Rizzoli and Betz, 2004). FM1-43 fluorescence changes were directly correlated with stimulation intensity, thus the longer the stimulation the more sustained vesicle exocytosis and the larger the drop in fluorescence.

This study has shown that the transfection of munc18-1 and syntaxin fluorescent constructs had no detrimental effect on the extent of synaptic vesicle exocytosis or endocytosis, in comparison to non-transfected control cells (Figure 4.9A). This was also confirmed in KD43 PC12 cells as the same fluorescent munc18-1 probe used was sufficient for full fusion capacity (Figure 4.3B). Expression of munc18-1[I127A] alongside wild-type syntaxin in embryonic cortical cells did not alter the proportion of fusing vesicles residing in either the readily releasable pool or reserve pool. Interestingly, disrupting the casein kinase II phosphorylation site at the N-terminus of syntaxin resulted in both the loss of secretory vesicle movement and exocytosis in neuroendocrine cells and a reduction in the percentage of fusing vesicles residing in the RRP of central nerve terminals. This suggests that the transition of a vesicle from an immobilized to a more mobile state (on the nano-scale) is an essential step in the pathway to fusion. The idea that vesicle dynamics and exocytosis are inextricably linked fits well with the finding that vesicle motion increases on a molecular scale immediately prior to fusion (Degtyar et al, 2005). Indeed, a large majority of highly immobilized vesicles docked at the plasma membrane in bovine adrenal chromaffin cells exhibit a low degree of fusion competence (Becherer et al, 2007). Thus, perturbing the phosphorylation site on the N-peptide of

syntaxin may well impact more heavily on downstream vesicular mobilites and mechanisms involved in the pathway of full fusion by vesicles primed for immediate release (Voets et al, 2001; Deak et al, 2009). These results suggest that N-peptide binding is indeed important in regulating vesicular fusion, with an intact phosphorylation site at the N-terminus of syntaxin playing more of a prominent role. Perhaps serine^{14} has a role beyond munc18-1 and its disruption leads to an alteration in a number of protein-protein interactions and upstream pathways required for Ca^{2+}-triggered fusion.

The matter of how Ca^{2+} triggers membrane exocytosis was first raised by Katz's seminal finding showing that Ca^{2+} induces synaptic vesicle exocytosis, thereby initiating synaptic transmission (Katz and Miledi, 1967). Approximately 23 years later the discovery of synaptotagmin-1, a candidate Ca^{2+}-sensor for synaptic exocytosis, was made (Perin et al, 1990). Over the last 20 years there has been overwhelming evidence demonstrating that synaptotagmin-1 and its homologs function as the primary Ca^{2+}-sensors in most forms of exocytosis (reviewed in Südhof, 2004). Following its identification it was shown that syntaxin and synaptotagmin interact *in vitro* (Li et al, 1995; Kee and Scheller, 1996; Rickman and Davletov, 2003; Rickman et al, 2004) and more recently it was reported that vesicles dock when synaptotagmin-1 binds to syntaxin/SNAP-25 acceptor complexes and together with munc18-1, constitute the minimal docking machinery (de Wit et al, 2009).

Taking this into consideration, it is plausible that preventing the phosphorylation of syntaxin at serine^{14} alters the fusion capabilities of readily releasable synaptic vesicles by disrupting an interaction between the N-terminal peptide of syntaxin and synaptotagmin, the putative Ca^{2+} sensor for exocytosis. Previously, NMR spectroscopy elucidated the three-dimensional structure of the N-terminal peptide of syntaxin and revealed that a highly acidic region of this peptide binds to the C2A domain of synaptotagmin I in a Ca^{2+}-dependent manner (Fernandez et al, 1998). The Ca^{2+}-binding region of the C2A domain of synaptotagmin is highly negative before Ca^{2+} binding, leading to the hypothesis that this most likely acts to prevent interaction between the N-terminal peptide of syntaxin and the C2A domain of synaptotagmin, thereby inhibiting synaptic vesicle exocytosis until Ca^{2+} influx (Fernandez et al, 1998). This interaction could therefore be serving as an electrostatic switch in the release of neurotransmitters (Fernandez et al, 1998). With synaptotagmin, syntaxin-1, SNAP-25 and munc18-1 now constituting the minimal

docking machinery a disruption between this acceptor complexes using syntaxin[S14E] could also prove to destabilize the initial association of readily releasable vesicles with the plasma membrane (de Wit et al, 2009). Interestingly, the reserve pool is unaffected by the expression of syntaxin[S14E], indicating that these transient interactions between syntaxin, munc18-1, synaptotagmin and Ca^{2+} are only required for those vesicles already docked and primed for release at the plasma membrane. These protein-protein interactions are therefore required downstream of membrane association and are essential in catalysing the final fusion event of vesicles in close apposition to the active zone of a nerve terminal. This finding may introduce another dimension to the regulation of synaptic vesicle pools, with the readily releasable and fusion competent vesicles requiring a more stable interaction between the N-terminus of syntaxin, munc18-1 and synaptotagmin.

CHAPTER 5:

THE SPATIAL ORGANISATION AND SINGLE MOLECULE KINETICS OF MUNC18-1 AT THE PLASMA MEMBRANE

5.1 INTRODUCTION

SM proteins have been shown to directly interact with their cognate trans-SNARE complexes in order to promote the rate and specificity of the membrane fusion reaction (Novick and Schekman, 1979; Hata et al, 1993; Shen et al, 2007). To date munc18-1 has been ascribed a wide range of functions; it has been shown to promote the docking of large dense core vesicles (Voets et al, 2001), regulate the 'primed' state of synaptic vesicles (Deak et al, 2009) and both the stabilization and stimulation of SNARE complex assembly immediately prior to vesicle fusion (Dulubova et al, 1999; Shen et al, 2007; Chen et al, 2008; Schollmeier et al, 2011). The positive action of munc18-1 has therefore been evidenced at a number of stages within the vesicle lifecycle, from vesicle transport to fusion. Despite these advances it still remains ambiguous how SM proteins actually function at the molecular level and how they are spatially arranged in order to execute their functions.

Using intact and exocytosis-competent PC12 cell membranes it was shown that munc18-1 is bound to the plasma membrane and concentrated at sites of docked vesicles (Zilly et al, 2006). Not surprisingly syntaxin was also found to reside in these cholesterol-dependent microdomains that determine the sites at which secretory granules dock and fuse, albeit determined using diffraction-limited imaging (Lang et al, 2001; Chamberlain et al, 2001). Lang and colleagues (2001) presented evidence demonstrating that syntaxin and SNAP-25 are concentrated in diffraction limited 200 nm large, cholesterol-rich clusters in the plasmalemma. Over the last decade a wide range of estimates concerning the number of SNARE molecules required to drive vesicle fusion now exist in the literature. A number of studies have concluded that the fusion of a single secretory vesicle requires the concerted action of three SNARE complexes (Hua and Scheller, 2001; Mohrmann et al, 2010). Alternatively, it has also been demonstrated that bilayer fusion can be executed by either a single SNARE complex (Bowen et al, 2004; van den Bogaart et al, 2010) or by anything between five to eight complexes (Han et al., 2004). More recently it was shown, using a pH-sensitive pHluorin attached to vesicle-associated synaptobrevin, that two SNARE complexes are sufficient for synaptic transmission in hippocampal neurons (Sinha et al, 2011). These different estimates are most likely due to the different *in vitro*

biochemical and fluorescence techniques employed. An obvious problem with these approximations is the fact that none of the above studies looked at the situation *in situ* or in the presence of co-expressed accessory proteins fundamental to exocytotic events. For example, synaptotagmin has been shown to influence the curvature of plasma membranes (Martens et al, 2007; Hui et al, 2009) whilst munc18-1 is thought to stimulate SNARE complex assembly immediately prior to membrane fusion (Fisher et al, 2001; Shen et al, 2007). With the exception of Sinha et al (2011), these highly purified *in vitro* assays are probably unable to accurately report the number of SNARE molecules required to drive membrane fusion in a biochemically and physiologically relevant system.

To precisely determine the quantity of exocytotic proteins required to drive exocytosis it is essential to probe a physiologically intact system on a single molecule level. For many decades, diffraction limited optical imaging was prevented from attaining resolution better than half the wavelength of light (Abbe, 1873). Due to these inherent limitations in the resolution of imaging techniques individual molecules appear much larger than they actually are. This phenomenon is due to the fact that the dispersion of light, or Point Spread Function (PSF), generated by a single light source, is spread over a large area due to chromatic aberrations and diffraction effects of the optical system (section 2.8.1). Therefore, conventional imaging techniques lack sufficient resolution in order to optically discriminate between overlapping signals and as a result only display an expanded version of labelled proteins. This fundamental drawback to light microscopy therefore prevented the visualization of cellular features smaller than 200 nm, the highest lateral resolution achievable using standard imaging techniques (Pawley, 1995). Consequently, Electron Microscopy (EM) was the only method that exceeded the resolution attainable with an optical microscope but required the fixation, dehydration and thin sectioning of a sample. So, in order to image minute cellular constituents in an unperturbed and dynamic environment, researchers had to find a way to combine the non-destructive nature of optical microscopy and the nanometer resolution of EM.

One of the first optical techniques designed to overcome both the diffraction limitation of light microscopy and the harmful processing of samples for EM was the advent of Stimulated Emission Depletion fluorescence microscopy (STED) in 1994 (Hell and Wichmann, 1994). In brief, a STED microscope resolves two adjacent objects by

transiently switching fluorescent markers between two interchangeable states using light, a concept known as Reversible Saturable Optical (Fluorescence) Transitions (RESOLFT) (Hell et al, 2003; 2009). STED microscopy, revealed to reach resolutions far below that of conventional light microscopy (Hell and Wichmann, 1994), has so far been used to map the spatial pattern of proteins in cells (Donnert et al, 2006; Sieber et al, 2007) and for the real-time imaging of synaptic vesicles in living neurons (Westphal et al, 2008). Using STED the same group that suggested syntaxin and SNAP-25 reside in 200 nm large clusters (discussed above; Lang et al, 2001) reported six years later that approximately 75 single syntaxin molecules are found in clusters of only 50-60 nm in size (Sieber et al, 2007). This discrepancy can be easily explained by considering the optical resolution of the imaging techniques used in both studies. In 2001 immunolabelled syntaxin was imaged using a standard confocal microscope, an optical technique limited to approximately 200 nm in lateral resolution (Pawley, 1995). Conversely STED microscopy, limited to a lateral resolution of approximately 50 nm, revealed that syntaxin resides in clusters of approximately 50-60 nm in size (Sieber et al, 2007). These studies serve to highlight that advances in our understanding of protein organisation have mirrored technological developments in optical microscopy.

Recently, RESOLFT microscopy was complemented by powerful optical methods that involve the sequential and stochastic activation of individual photoactivatable fluorescent probes in time (Betzig et al, 2006; Hess et al, 2006, 2009; Rust et al, 2006). Advancements in single-molecule spectroscopy in the early 1990s introduced a new approach to precisely localise the centre of a single fluorescent signal, heralding the new age of super-resolution microscopy (Moerner and Kador, 1989; Orrit and Bernard, 1990; Hess et al, 2006). In 2006 three independent techniques demonstrated that molecular scale localisation accuracy could be achieved through Photoactivated Localisation Microscopy (PALM) (Betzig et al, 2006) Stochastic Optical Reconstruction Microscopy (STORM) (Rust et al, 2006) and Fluorescence Photoactivation Localisation Microscopy (FPALM) (Schermelleh et al, 2008). In general, all three techniques achieve nano-scale resolution by activating fluorescent molecules in a temporally and spatially segregated manner, thereby avoiding PSF overlap and achieving precise positional information of each fluorescent marker.

Using the super-resolution technique PALM single molecules of SNAP-25 and syntaxin have been visualised and shown to be distributed non-randomly across the plasma membrane of specialised secretory cells (Rickman et al, 2010). Despite these advances, however, it remains unknown how munc18-1 is spatially arranged at the molecular level in order to execute its functions. Using single molecule imaging approaches and bio-informatics analyses this chapter defines, with the highest possible resolution, the molecular arrangement and kinetics of large cohorts of single munc18-1 molecules across the plasma membrane of intact munc18-1-silenced PC12 cells. This study also investigates whether perturbing the N-terminal interaction between munc18-1 and syntaxin, using munc18-1[I127A], affects the molecular organisation of both proteins.

The combination of PALM and single-particle tracking (sptPALM) has now enabled the tracking of large cohorts of single molecules in live cells (Manley et al, 2008). Analysis of single molecule trajectories, heterogeneities and behaviours provides a better understanding of protein dynamics fundamental to basic cell physiology and survival. Using this approach this study investigates the molecular kinetics of single munc18-1 molecules in live munc18-1-silenced PC12 cells. Taking the spatial arrangement and live kinetics of single munc18-1 molecules together, this chapter elucidates the molecular architecture and dynamics of munc18-1 in specialised secretory cells.

5.2 THE MOLECULAR ARRANGEMENT OF ENDOGENOUS AND EXOGENOUS MUNC18-1 REVEALED BY GSDIM.

Ground state depletion-individual molecule return (GSDIM) microscopy is a super-resolution technique designed to overcome the diffraction-limited resolution of a conventional imaging setup (Fölling et al, 2008). GSDIM achieves nano-scale resolution by regulating the number of active fluorescent probes in both time and space, thereby minimizing the likelihood that two fluorophores will spatially overlap (Figure 5.1). The technique operates by starting with the vast majority of fluorescent labels in the inactive state (Figure 5.1). By sequentially switching on fluorescent probes in time the precise localisation of thousands of sparse subsets can be achieved. This operating principle is in stark contrast to conventional diffraction limited imaging which activates all the

fluorescent reporters at once, as shown in the summed raw data in Figure 5.1B. By exploiting photoswitchable fluorophores and controlling the density of these high-contrast fluorescent probes the precise localisation of individual molecules can be determined through a statistical fit of the ideal point spread function, as seen in the localised rendered single molecule panel in Figure 5.1 (section 2.8.5).

GSDIM and total internal reflection fluorescence microscopy (TIRFM) involves immunolabelling endogenous munc18-1 (section 2.8.2) with a fluorophore-conjugated antibody (Alexa-647), and driving this into a 'dark-state' using laser illumination in the presence of a reducing buffer (section 2.1.1, Fölling et al, 2008). Single Alexa-647-conjugated antibodies, bound to immunolabelled munc18-1 molecules spontaneously re-emerge from this dark state, permitting the localisation of individual molecules separated in a time stack (Figure 5.1B).

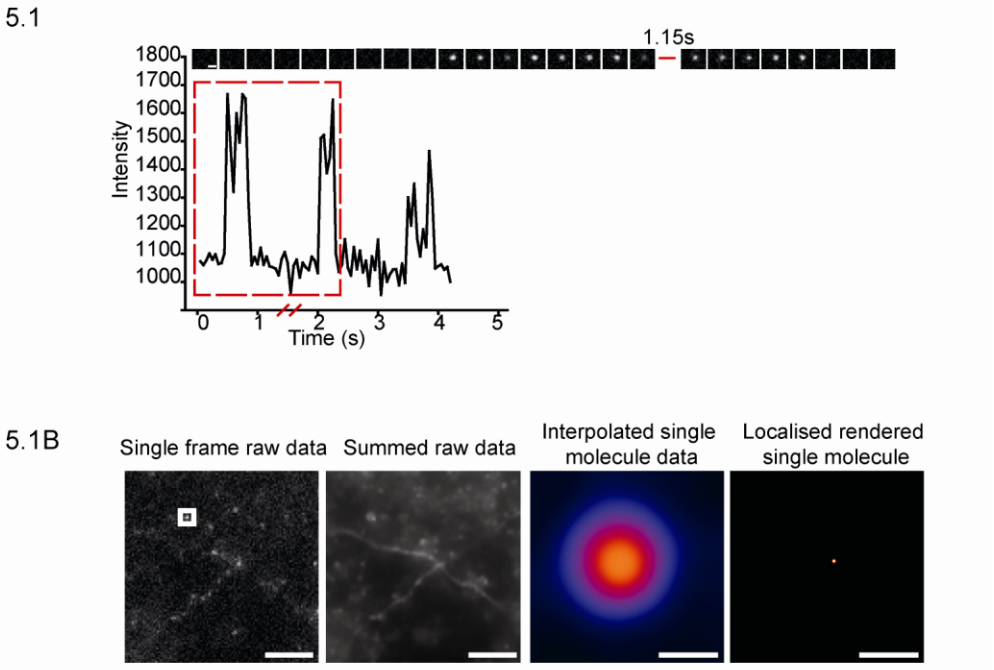

Figure 5.1. *Visualising single munc18-1 and syntaxin molecules in fixed KD43 PC12 cells.* GSDIM was used to probe the single molecule arrangement of munc18-1 and syntaxin across the base of neuroendocrine cells. Sequential frames of a single, GSDIM signal from a single Alexa647-conjugated secondary antibody, labeling immunodetected munc18-1. Each frame is a 300 ms integration. Signals from a single molecule persist for several exposures before photo destruction. The montage of images has also been represented as a fluorescence intensity plot, where the red box indicates the time-frame contained in the montage. The plot illustrates that repetitive GSDIM signals may arise from the same points in the dataset, making it impossible to count single molecules. 5.1B. A single frame of raw GSDIM data showing single Alexa-647 labelled munc18-1 molecules (first panel), with the summed raw data panel showing a sum of all the single molecule signals acquired during the entire recording, scale bar, 5µm. The region of interest in the first panel relates to the rest of the panels in the figure. An interpolated image of averaged detectable fluorescence in all frames displayed as an intensity plot shown in false colour (black – low intensity – red – high intensity), scale bar, 250 nm. The localised rendered single molecule panel represents the centroided and rendered single munc18-1 molecule represented by the signal in the third panel, scale bar, 250 nm.

Wild-type PC12 cells were chemically fixed using 4% paraformaldehyde for 60 minutes to ensure complete immobilization (Sieber et al, 2007) and munc18-1 was immunolabelled with Alexa-647 and subsequently processed for GSDIM. The extended fixation period was to immobilise as much as possible the molecules under study to minimise potential movement or antibody patching artifacts (Sieber et al, 2007). Munc18-1 molecules were seen to be concentrated in areas of high and low densities across the plasma membrane (Figure 5.2).

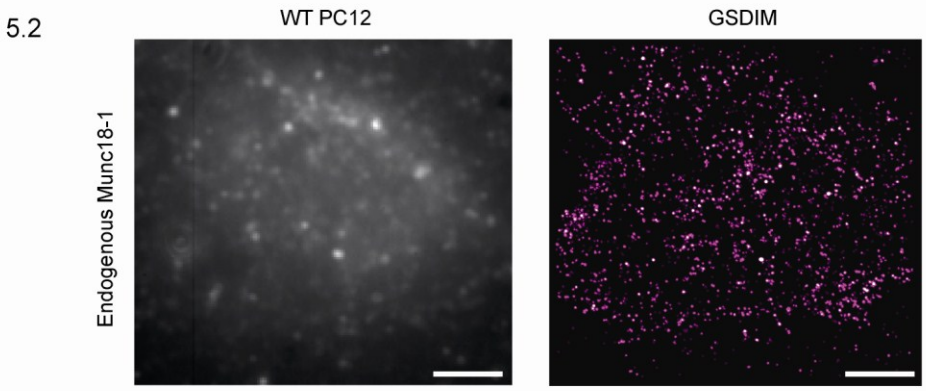

Figure 5.2. *Endogenous munc18-1 is distributed heterogeneously across the plasma membrane.* All frames containing Alexa647-munc18-1 signals from single molecules were summed and displayed as an intensity image to approximate a diffraction limited image (greyscale, *left panel*). A representative GSDIM map of immunolabelled Alexa647-munc18-1 in wild-type PC12 cells (*right panel*, magenta). Munc18-1 single molecules are arranged in a heterogeneous manner across the plasma membrane. Scale bar 5 μm.

It has already been shown in chapter 4 that KD43 PC12 cells expressing heterologous munc18-1 is sufficient to fully restore exocytosis (comparable to wild-type levels, Smyth et al, 2010, Figure 4.3). Therefore, this investigation next determined whether rescuing munc18-1 silenced PC12 cells with exogenously expressed fluorescent munc18-1 resulted in a similar molecular distribution. KD43 PC12 cells were transfected with munc18-1 and syntaxin, fixed and exogenous munc18-1 was immunolabelled with Alexa-647. GSDIM imaging also revealed munc18-1 to be concentrated in specific areas across the plasma membrane and thus subject to similar targeting and localisation compared to endogenous munc18-1 (Figure 5.3).

It was previously shown in chapter 4 that disrupting specifically the interaction between munc18-1 and the N-peptide of syntaxin resulted in a reduction in single vesicle mobility (Figure 4.1) and fusion capabilities (Figure 4.3, Smyth et al, 2010). Therefore, it was also important to investigate whether these downstream effects were a result of a concomitant change in the spatial arrangement of munc18-1 molecules on a molecular level. KD43 PC12 cells were transfected with munc18-1[I127A] and syntaxin, fixed and exogenous munc18-1 was immunolabelled with Alexa-647. GSDIM imaging reported that there was no obvious disruption in the localisation of single munc18-1[I127A] molecules as compared with wild-type munc18-1, with both proteins arranged in a spatially heterogeneous fashion on the cell surface (Figure 5.3B).

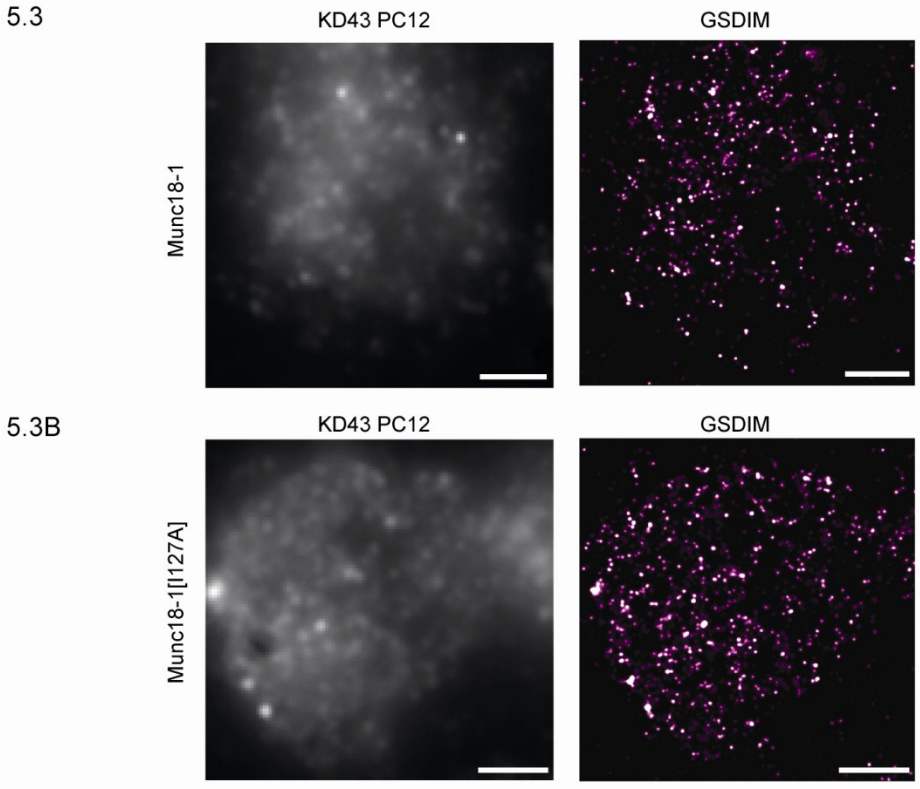

Figure 5.3. *Exogenous munc18-1 and munc18-1[I127A] are organised in a non-uniform pattern across the plasma membrane.* KD43 PC12 cells were transfected with munc18-1 and syntaxin for 48 hours, fixed and immunolabelled with Alexa-647-munc18-1. Exogenously expressed munc18-1, as compared to endogenous munc18-1, displayed a non-uniform distribution. 5.3B. KD43 PC12 cells transfected with munc18-1[I127A] and immunolabelled with Alexa-647-munc18-1 also had a heterogeneous arrangement across the plasma membrane, as compared to endogenous munc18-1. Scale bar 5 μm.

Functions of munc18-1 include docking secretory vesicles at the plasma membrane (Voets et al, 2001) and the catalysis of their final fusion (Novick et al, 1980; Dascher et al, 1991; Gengyo-Ando et al, 1993; Harrison et al, 1994; Verhage et al, 2000) but it remains unknown how it is spatially organised on the plasma membrane in order to help drive vesicular fusion. Munc18-1 has been localised on a gross microscopic scale to the plasma membrane of secretory cells several times (Zilly et al, 2006; Medine et al, 2007; Rickman et al, 2007), with this membrane association mediated principally by interaction with syntaxin (Rickman et al, 2007). Taking the functions of munc18-1 into consideration, it is reasonable to assume that some, if not most, munc18-1 is arranged in close proximity to membrane proximal vesicles in order to drive their fusion.

To probe the spatial relationship between single endogenous munc18-1 molecules and membrane proximal secretory vesicles this thesis used GSDIM and total internal reflection fluorescence microscopy (TIRFM). Wild-type PC12 cells were fixed, immunolabelled with Alexa-647-munc18-1 and Alexa-488-synaptotagmin, a marker of the vesicular membrane, and processed for GSDIM. Surprisingly, in light of current hypotheses regarding munc18-1 and its proposed function, secretory vesicles did not co-locate with the areas of higher munc18-1 density (Figure 5.4). Instead of being found in molecular contact with a secretory vesicle, munc18-1 was enriched in the 'gaps' between where vesicles were docked at the plasma membrane. This finding is in agreement with a recent study also finding that most syntaxin clusters did not coincide with secretory vesicles (Barg et al, 2010). However, calculating how these image data would have appeared if imaged using diffraction-limited fluorescence microscopy resulted in an image demonstrating partial overlap between munc18-1 and synaptotagmin, in agreement with a previous study (Figure 5.4; De Wit et al, 2009). As before, it was next important to ascertain whether the spatial arrangement of exogenous munc18-1 molecules and endogenous secretory vesicles was similar to that of endogenous munc18-1 within KD43 PC12 cells.

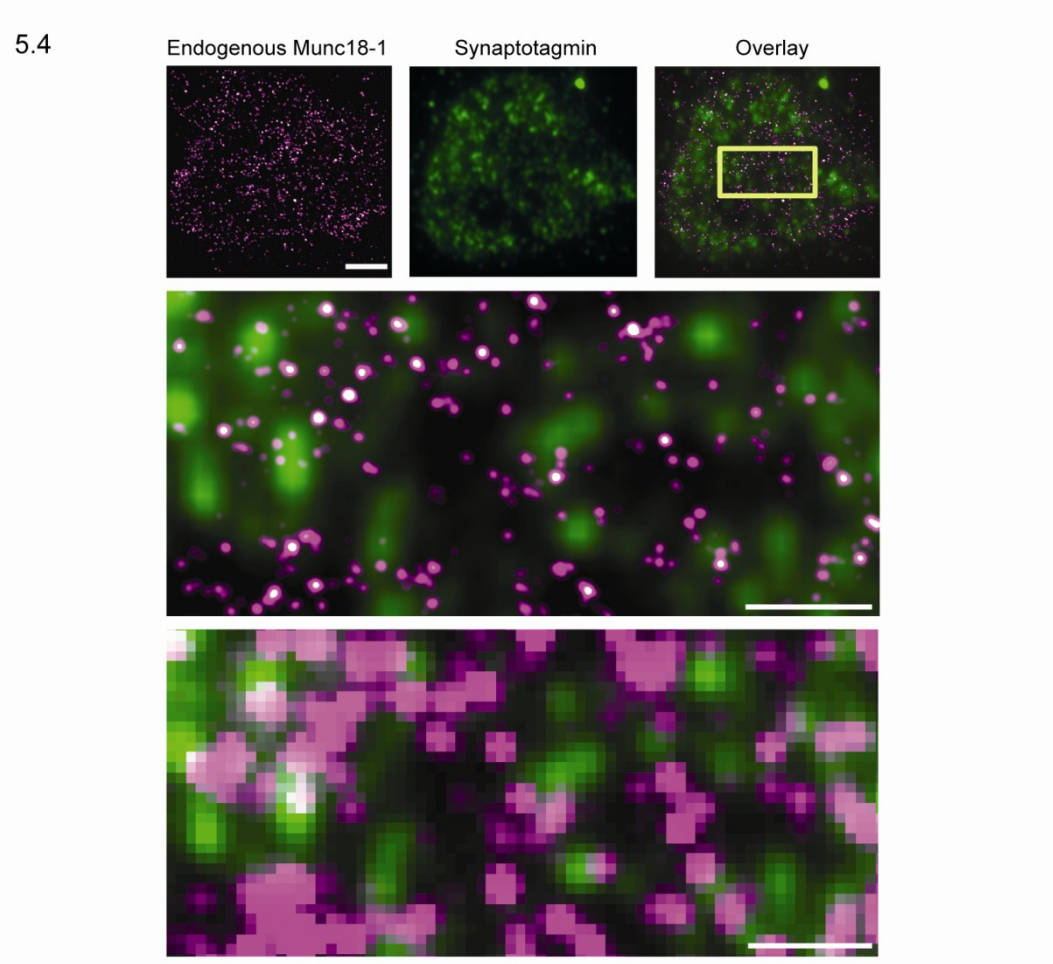

Figure 5.4. *Endogenous munc18-1 is expressed in areas of the plasma membrane largely devoid of membrane proximal vesicles*. Wild-type PC12 cells were fixed and munc18-1 and synaptotagmin were immunolabelled with Alexa-647 and Alexa-488 (to mark secretory vesicles) respectfully. TIRFM imaging shows a rendered map of single Alexa-647-munc18-1 molecules, Alexa-488-synaptotagmin-labelled secretory vesicles and an overlay of both signals, scale bar 5 µm. GSDIM imaging revealed that endogenous munc18-1 is arranged in the areas of the membrane where no labeled vesicles were present, as seen in the zoomed version, scale bar 500 nm. A convolved GSDIM map of the boxed region of Alexa647-munc18-1 molecules is displayed to approximate a diffraction limited image, highlighting that the majority of vesicles and munc18-1 molecules do not overlap, scale bar 500 nm.

KD43 PC12 cells were co-transfected with munc18-1 and syntaxin, fixed and immunolabelled with Alexa-647-munc18-1 and Alexa-488-synaptotagmin as before. GSDIM imaging reported that munc18-1 molecules were distributed heterogeneously, congregating in areas of the cell membrane that were not associated with secretory vesicles (Figure 5.5). Performing the same experiments in the presence of a munc18-1-syntaxin-N-terminal mutant resulted in no difference between this molecular pattern and that of wild-type munc18-1, suggesting that binding between munc18-1 and the N-peptide of syntaxin is not involved in targeting munc18-1 to defined sites on the plasma membrane (Figure 5.5B). Again, partial overlap is observed between secretory vesicles and munc18-1 molecules if these molecular maps are used to generate lower resolution images comparable to those of a standard fluorescent microscope.

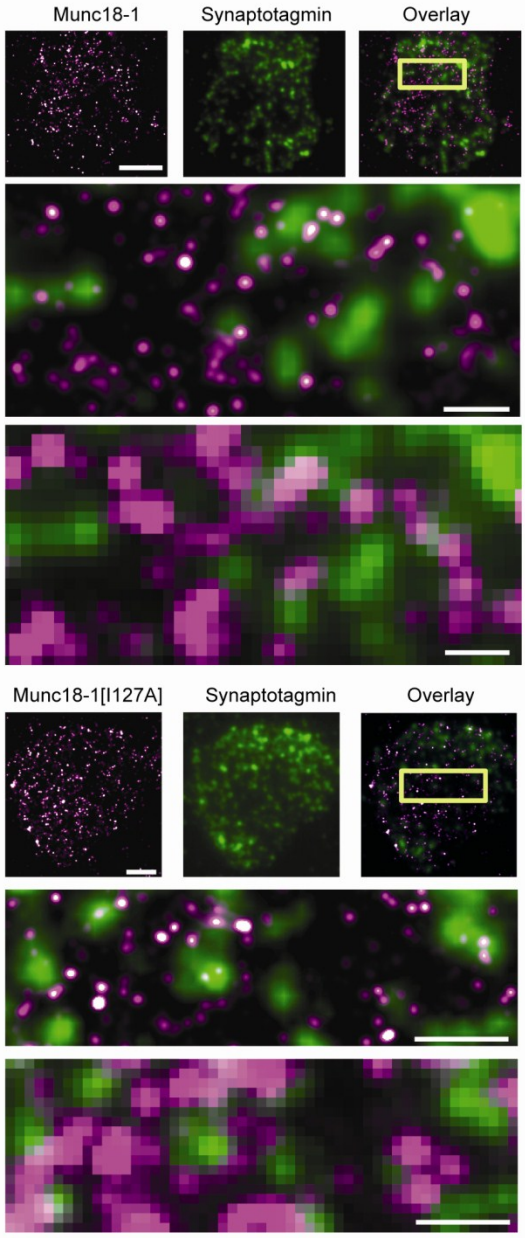

Figure 5.5. *Exogenously expressed munc18-1 and munc18-1[I127A] avoid areas of the plasma membrane where secretory vesicles reside*. KD43 PC12 cells were transfected with munc18-1, fixed after 48 hours and both munc18-1 and synaptotagmin were immunolabelled with Alexa-647 and Alexa-488 respectfully. TIRFM images show rendered single munc18-1 molecules, labelled secretory vesicles and a merged image of both signals, scale bar 5 µm. A rendered map of single molecules at a higher zoom within the boxed region of a KD43 PC12 cell displays the lack of co-clustering between munc18-1 and secretory vesicles, scale bar 500 nm. 5.5B. Perturbing the munc18-1-syntaxin-N-terminal interaction did not result in a change in the spatial arrangement of munc18-1, with munc18-1 residing in areas largely devoid of labelled membrane proximal vesicles.

Whilst GSDIM data are invaluable for defining with the highest possible resolution the spatial distribution of endogenous proteins, further statistical analysis of this is hampered by the fact that individual molecules may move reversibly from an 'off' state to being repetitively fluorescent (Figure 5.1B, Fölling et al, 2008; McEvoy et al, 2010). This means that single molecules may be counted multiple times in an analysis, as the precise coordinate of each signal will vary on the nano-scale because of photon statistics and minute sample movements. In order to overcome these limitations and acquire statistical information on the spatial patterning of exogenously expressed munc18-1 molecules this thesis next used Photoactivatable Localisation Microscopy (PALM).

5.3 THE RESOLUTION OF SINGLE MUNC18-1 MOLECULES USING PHOTOACTIVATABLE LOCALISATION MICROSCOPY (PALM).

Cells expressing proteins of interest labelled with fluorescent markers contain detailed information on the spatial arrangement of these specific target proteins accurate at the molecular level. However the precise location of fluorescently tagged proteins is lost using conventional optical microscopy, a technique limited by diffraction (Stephens and Allan, 2003). Over the last decade advancements in fluorescence microscopy have broken through this diffraction barrier and enabled the imaging of intracellular proteins with near-molecular resolution. Nanoscale imaging is now capable of determining the static structural organisation and relationship of two or more proteins of interest at the molecular level.

Photoactivation Localisation Microscopy (PALM) optically resolves fluorescent proteins to molecular resolution through the serial photo -activation and -irreversible destruction of subsets of molecules with each step optimized to ensure a sparse distribution of signals visible during each cycle (Betzig et al, 2006). At the beginning of each PALM experiment the vast majority of fluorescent labels are in an inactive, dark state where they do not contribute to sample fluorescence. Near-ultraviolet light illumination induces a chemical modification in a small fraction of quiescent molecules, activating on average less than 1% of the total population (Betzig et al, 2006). The process of photoactivation occurs in a stochastic manner and its probability is proportional to the location and intensity of the

activation laser. During the acquisition readout, activated molecules spontaneously photobleach, resulting in a reduction in the number of active molecules within the sample. Following photobleaching a new subset of molecules is transferred into an active state, a process repeated until all the molecules are depleted and molecular coordinates gathered. Over time many thousands of single molecules and their molecular coordinates are typically localised in a single experiment allowing for further statistical spatial analysis of point patterns. Finally, a composite image rendered from all the coordinates in each image can then be used to generate a super-resolution map of the fluorescently-labelled sample under investigation.

Although PALM imaging cannot provide an exact measure of the number of molecules in a sample, as it is never certain that every molecule has been localised (Hess et al, 2006; Betzig et al, 2006), it can provide a lower limit for the number of molecules per unit area (Rickman et al, 2010). Therefore, under optimal imaging conditions, it is likely that most molecules will be imaged and localised (Hess et al, 2006; Zilly et al, 2006). Point spread function signals that arise from single molecules in the sample are localised and the molecular coordinates added to a cumulative map (Figure 5.6). In contrast to GSDIM imaging, photoactivatable molecules are photo-destroyed following activation and do not spontaneously re-emerge from a 'dark state' (Figure 5.6B). Therefore, PALM records the signal from a fluorescent molecule only once, allowing for the precise localisation of a single molecule and further statistical spatial analysis (Figure 5.6B).

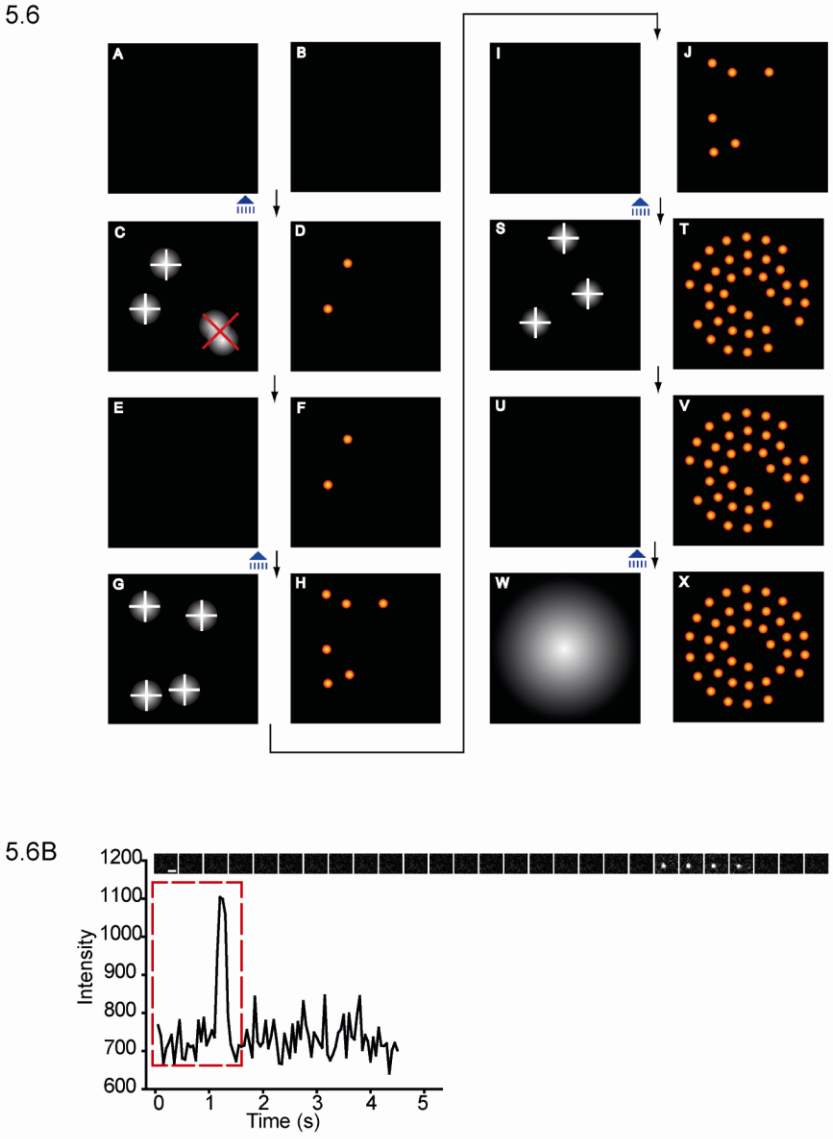

Figure 5.6. *Photoactivation Localisation Microscopy (PALM)*. PA fluorophores reside in an inactive state before being switched on by irradiation with 405 nm wavelength of light. Molecules undergo cycles of activation (405 nm), localisation (561 nm) and bleaching with each step optimised to ensure a sparse distribution of single molecules activated during each cycle. Those molecules that are too close to each other are discounted from the localisation. After a period of time, emphasised by a jump from image J to image S, a super resolution image is built up using the positional information of each single molecule. Figure generated by Amy Gray, University of Edinburgh. 5.6B. Sequential frames of a single molecule of PA-mCherry labelled munc18-1 on the plasma membrane demonstrating the quantal activation and bleaching characteristic of single fluorescent molecules. Each frame is a 300 ms integration with fluorophore activation by brief 405 nm illumination preceding the first frame, scale bar 1 μm.

This study first examined the localisation of single photoactivatable molecules of munc18-1 (Figure 5.7) and munc18-1[I127A] (Figure 5.7B) co-expressed alongside syntaxin in fixed KD43 PC12 cells. The process of photoactivation, measurement, and bleaching of these photoactivatable molecules was repeated for many cycles, often for 10^2 - 10^3 image frames depending on the expression level of the PA-fluorescent probe. At a typical frame rate of 50 ms, recordings lasted for between 20 to 30 minutes in order to acquire a complete image stack, often containing 10^2 - 10^3 localised molecules.

Positional information describing PA-mCherry-munc18-1 molecules was uniquely isolated and subsequently rendered into molecular maps, where munc18-1 molecules were seen to adopt an apparent heterogeneous distribution across the plasma membrane, in support of the data generated by GSDIM (Figure 5.7). Similarly, munc18-1[I127A] molecules appear to be concentrated into higher and lower densities (Figure 5.7B). The convolved image of all localised munc18-1 and munc18-1[I127A] molecules demonstrates that conventional, diffraction limited microscopy is unable to resolve single molecules and an accurate representation of their spatial organisation.

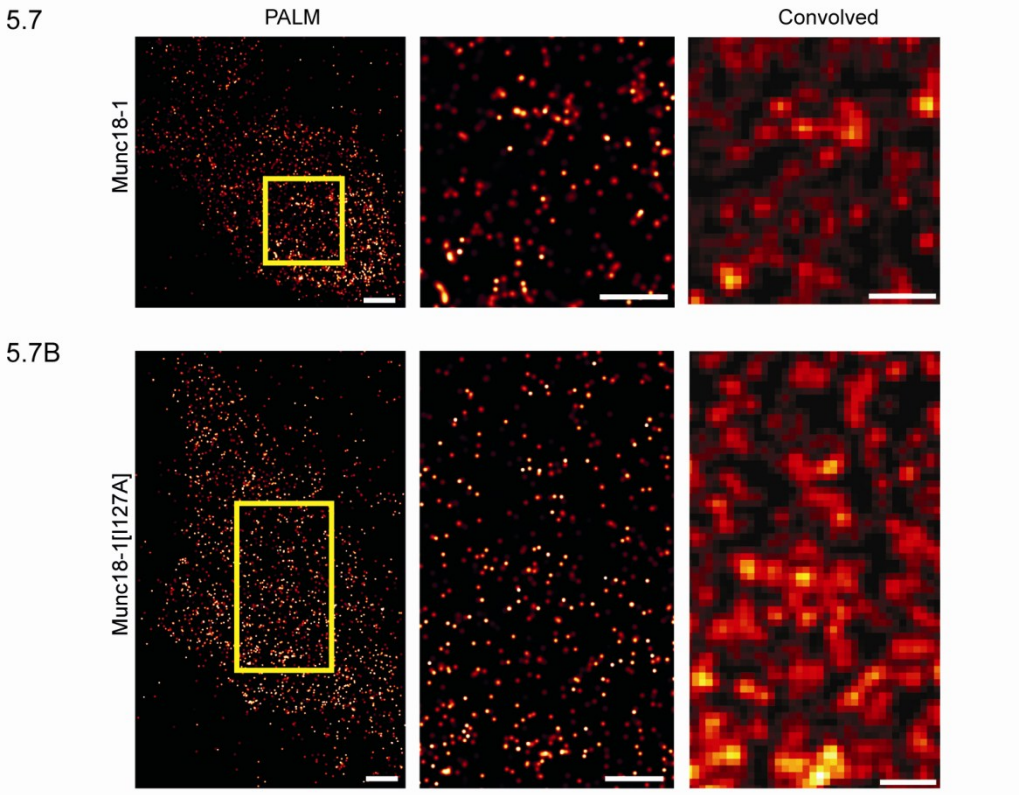

Figure 5.7. *The visualisation of single munc18-1 molecules using PALM.* TIRF-PALM of rendered PA-mCherry labelled munc18-1 (*upper panels*) or munc18-1[I127A] (*lower panels*, 5.7B) showing a non-uniform distribution on the plasma membrane, scale bar 5 µm. The boxed regions are displayed at a higher zoom together with the convolved image corresponding to the same region of interest to approximate diffraction limited imaging, scale bar 500 nm.

5.4 THE MOLECULAR DISTRIBUTION OF MUNC18-1 ACROSS A NEUROENDOCRINE PLASMA MEMBRANE IS NON-RANDOM.

Having disrupted N-terminal interactions at the plasma membrane (Chapter 4), this study set out to determine whether this specific effect resulted in, or was caused by, a spatial reorganisation of munc18-1 molecules. In order to extract positional information from fluorescent munc18-1 molecules a non-parametric statistical tool, Ripley's *K*-function, was used to analyse the spatial distribution of single munc18-1 molecules across the plasma membrane (Ripley, 1977, 1987).

Since its introduction in 1977, Ripley's *K*-function has been widely used as a tool in spatial point pattern analysis (Ripley, 1977, 1987). Since then spatial point patterns have been classified into three main classes, namely complete spatial randomness (CSR), clustering and regularity (Figure 5.8, Diggle, 2003). To analyse the spatial distributions of single molecules the *xy* coordinates of each localised molecule are counted in concentric rings across every pixel of an image (as shown in Figure 5.8) and added together in a cumulative fashion. This mathematical function is then compared with the expected line ($y=x$) under Poisson distribution of all points. When the observed Ripley's *K* value for single molecules is larger than the expected *K* value for a particular distance, the distribution is more clustered than a random distribution at that distance (Figure 5.8B). However, when the observed *K* value is smaller than the expected *K*, the distribution is more dispersed and regular than a random distribution at a particular distance. If both observed and expected frequencies are the same the distribution of molecules is completely random (Figure 5.8B).

5.8

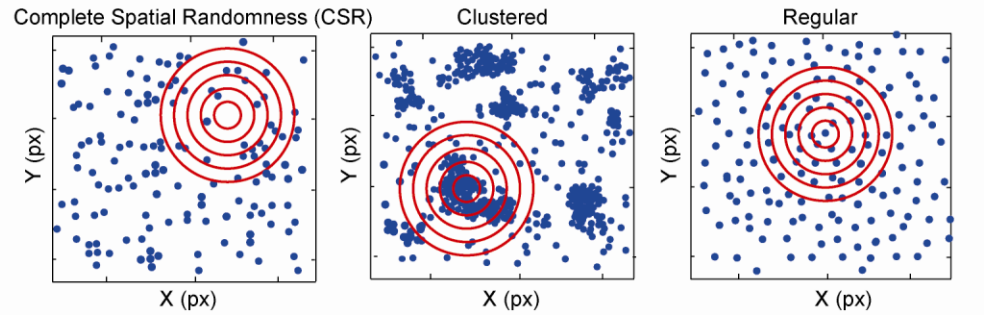

5.8B

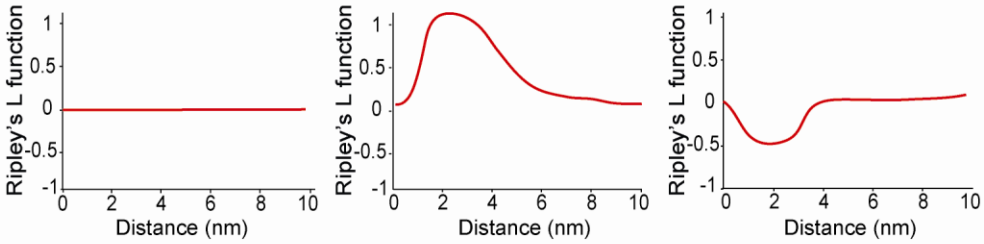

Figure 5.8. *Quantification of the spatial arrangement of single molecules*. Spatial point pattern analysis has been classified into three main classes, complete spatial randomness (CSR), clustering and regularity. The xy coordinates of each localised molecule are counted in each concentric ring, added together in a cumulative fashion and compared with the expected line (y=x) under Poisson distribution of all points. 5.8B. Molecules exhibit a clustered distribution if the observed Ripley's L value is larger than the expected K value for a particular distance. When the observed L value is smaller than the expected L, the distribution is more dispersed and regular than a random distribution at a particular distance. If both observed and expected frequencies are the same the distribution of molecules is completely random.

To analyse the spatial arrangement of munc18-1 molecules Ripley's K function followed by its L function transformation was used to compare the spatial distribution of the individual molecules to a randomized sample (constrained to the same particle number and area as the test sample, Misura et al, 2000). Both munc18-1 and munc18-1[I127A] exhibited a spatially ordered, non-random distribution across the plasma membrane of secretion-competent rescued PC12 cells (Figure 5.9 and 5.9B). This finding demonstrates that munc18-1 is subject to a higher order organisation at the molecular level, a finding previously shown with the t-SNAREs (Sieber et al, 2007; Rickman et al, 2010). It is noteworthy to mention that this study cannot conclude that munc18-1 resides in distinct clusters across the membrane as both the definition of a cluster and importantly, how many molecules makes up a cluster, remains undefined.

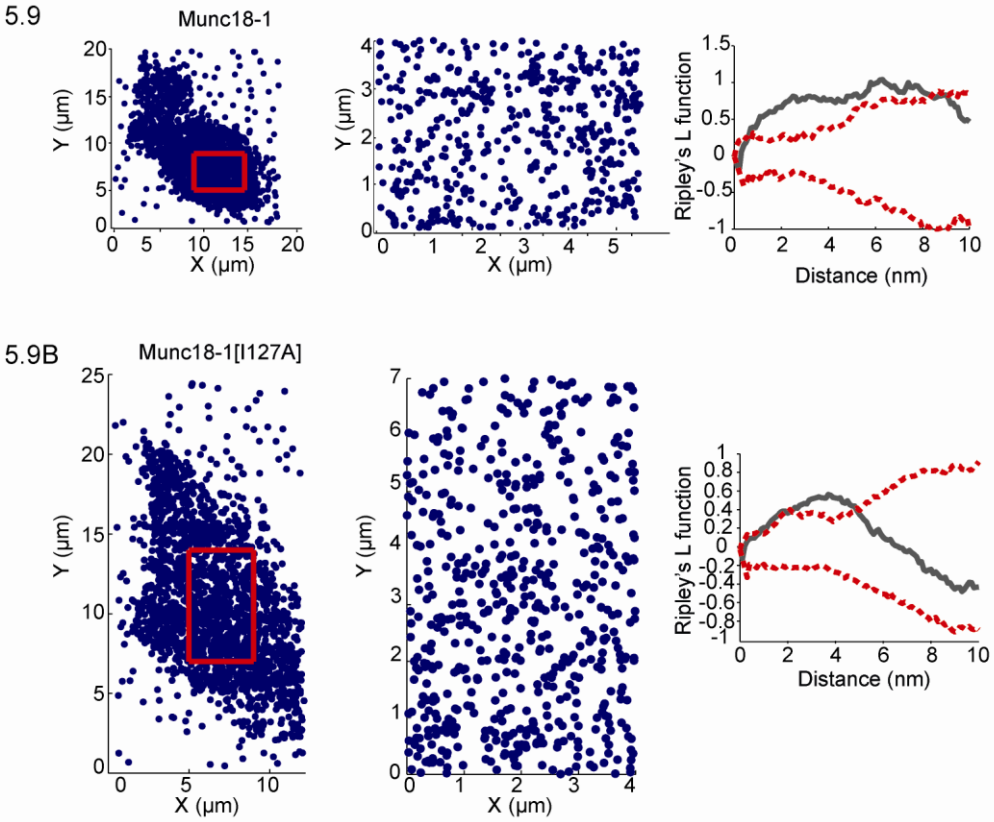

Figure 5.9. *The spatial arrangement of munc18-1 across the plasma membrane is non-random and unaffected by mode of interaction with syntaxin*. KD43 PC12 cells were transfected with syntaxin and PA-munc18-1 or PA-munc18-1[I127A] (5.9B), fixed and subjected to PALM imaging. Single molecules were localised and areas within the red boxes analysed. Each representative dataset, consisting of XY coordinates describing the localisation of individual munc18-1 molecules (accurate to <12 nm) was repeatedly randomised, and the L-function derived. Representative L-function plots (grey lines) are shown with confidence envelopes indicating the maximum and minimum L-function values from 1000 randomisations (dashed red lines). This approach compares the L-function between experimental data and an identical number of random points. Values outside the confidence envelopes indicate a non-random spatial organisation.

Recently it has been shown using PALM and Ripley's K function analyses that the molecular spatial organisation of syntaxin is non-random (Rickman et al, 2010). This thesis has already provided evidence demonstrating that by disrupting the N-terminal interaction between munc18-1 and syntaxin the spatial organisation of secretory vesicles (Figure 4.4) or single munc18-1 molecules (Figure 5.9) is not altered. Therefore, the next question to address was whether the reduced level of evoked exocytosis in the presence of a munc18-1 N-terminal mutant within KD43 PC12 cells was a result of a reorganisation of syntaxin at the molecular level.

Performing reciprocal PALM experiments and Ripley's K analyses demonstrates that single syntaxin molecules are organised into discrete molecular entities across the plasma membrane, as shown in a number of previous studies (Sieber et al, 2007; Barg et al, 2010; van den Bogaart et al, 2011; Zilly et al, 2011; Figure 5.10). The expression level of transmembrane syntaxin was also much higher at the base of a KD43 PC12 cell compared to munc18-1 (Figure 5.10, *middle panel*), in agreement with a study demonstrating that syntaxin exists in excess over munc18-1 by approximately 20 fold (Schutz et al, 2005). Furthermore, these reciprocal PALM experiments revealed that perturbing its N-terminal interaction with munc18-1 had no effect on its non-random, highly ordered distribution (Figure 5.10B). Thus, targeted disruption of the munc18-1-syntaxin-N-terminal interaction only resulted in a reorganisation of interaction with syntaxin (Figure 4.4; Smyth et al, 2010), with no change in the spatial molecular pattern at the plasma membrane.

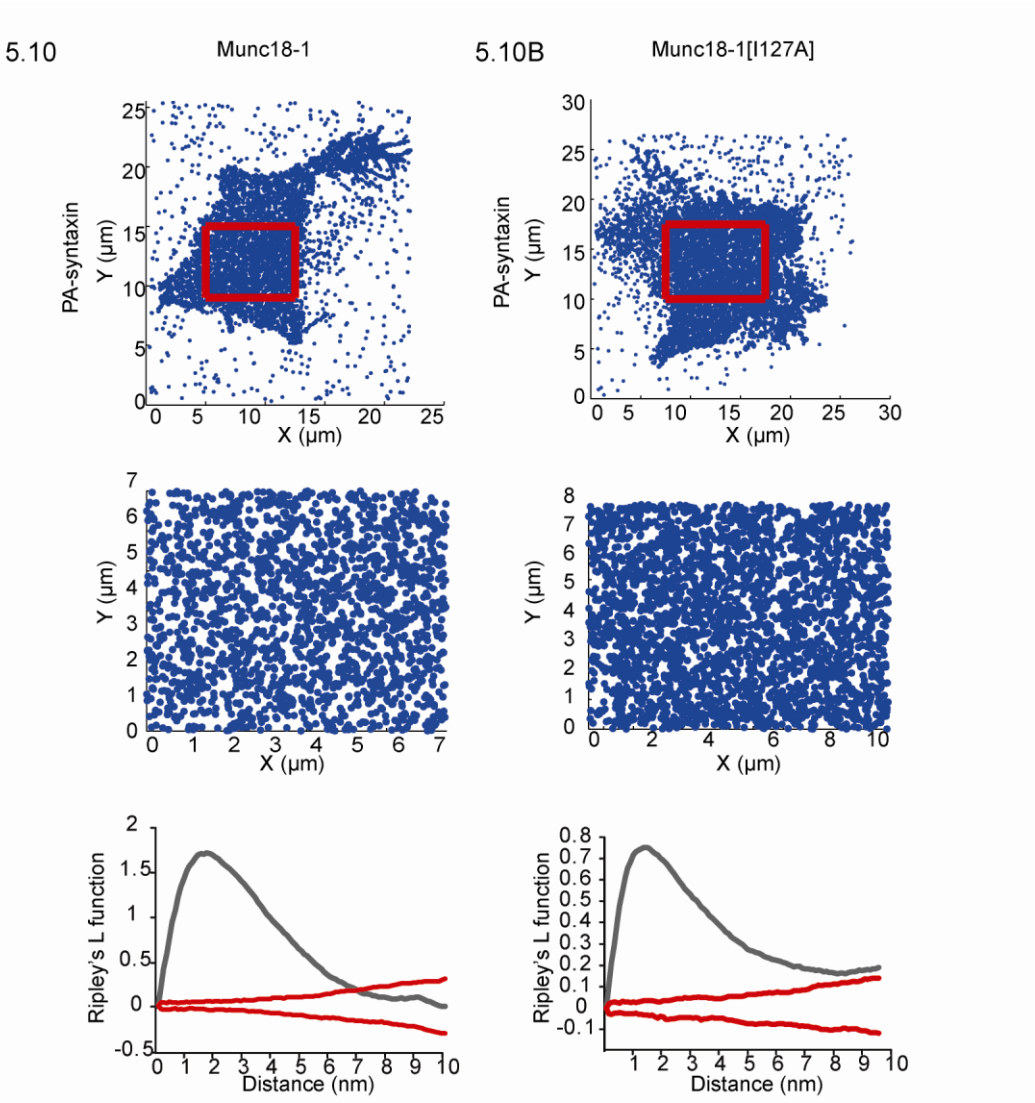

Figure 5.10. *The spatial distribution of syntaxin across the plasma membrane is unaffected by perturbing its N-terminal interaction with munc18-1.* KD43 PC12 cells were co-transfected with PA-syntaxin and either munc18-1 or munc18-1[I127A], fixed 48 hours post-transfection and imaged under PALM. The xy coordinates of detected single photoactivatable molecules were localised and Ripley's L function was used to describe their spatial arrangement. Syntaxin exhibited a highly ordered, non-random distribution in the presence of both wild-type munc18-1 and munc18-1[I127A].

In this chapter GSDIM imaging revealed that munc18-1 was found to be concentrated in areas of the plasma membrane that were devoid of secretory vesicles (Figure 5.5 and 5.5B). It can be deduced from our current understanding that for munc18-1 to act at the final stage of fusion it must be associated with syntaxin (and probably the other SNAREs) and an adjacent vesicle for exocytosis to proceed. A number of *in vitro* measurements have suggested that anything between one to eight SNARE complexes are required to drive vesicular fusion (Hua and Scheller, 2001; Han et al, 2004; Mohrmann et al, 2010; van den Bogaart et al, 2010) but no study on the number of munc18-1 molecules has ever been conducted. Using PALM and assigning xy coordinates to all single munc18-1 molecules and labelled secretory vesicles it was possible to statistically quantify the nano-scale organisation of single munc18-1 molecules in relation to their nearest secretory vesicle centre.

5.5 NEAREST NEIGHBOUR ANALYSIS OF SINGLE MUNC18-1 MOLECULES.

Nearest neighbour analysis was next performed on fluorescently labelled secretory vesicles and single munc18-1 molecules to determine their spatial arrangement in relation to one another. KD43 PC12 cells rescued with fluorescently-labelled-munc18-1, -syntaxin and -NPY, a vesicle cargo protein, were fixed and imaged using PALM. Nearest neighbour analysis was performed on immobilized samples where >97% of all cellular vesicles were labelled (Duncan et al, 2003). These newly assembled, NPY-labelled vesicles are trafficked preferentially to the plasma membrane, have the highest probability of fusion and comprise at least in part the readily releasable pool (Duncan et al, 2003). These vesicles were also localised using TIRFM, allowing visualization only within a 90 nm (FWHM) distance of a refractive index interface, thereby selectively localizing only 'morphologically docked' membrane proximal vesicles.

As before single munc18-1 molecules were activated, localised and bleached (Figure 5.11, *top left panel*). Molecules of munc18-1 (*blue*) and labelled secretory vesicles (*red*) were localised (Figure 5.11 *top right panel*) and all molecules were assigned to the centroid coordinates of their nearest secretory vesicles using nearest neighbour analysis (*bottom*

right panel). Munc18-1[I127A] expressing KD43 PC12 cells were subject to the same experimentation and analysis (Figure 5.11B).

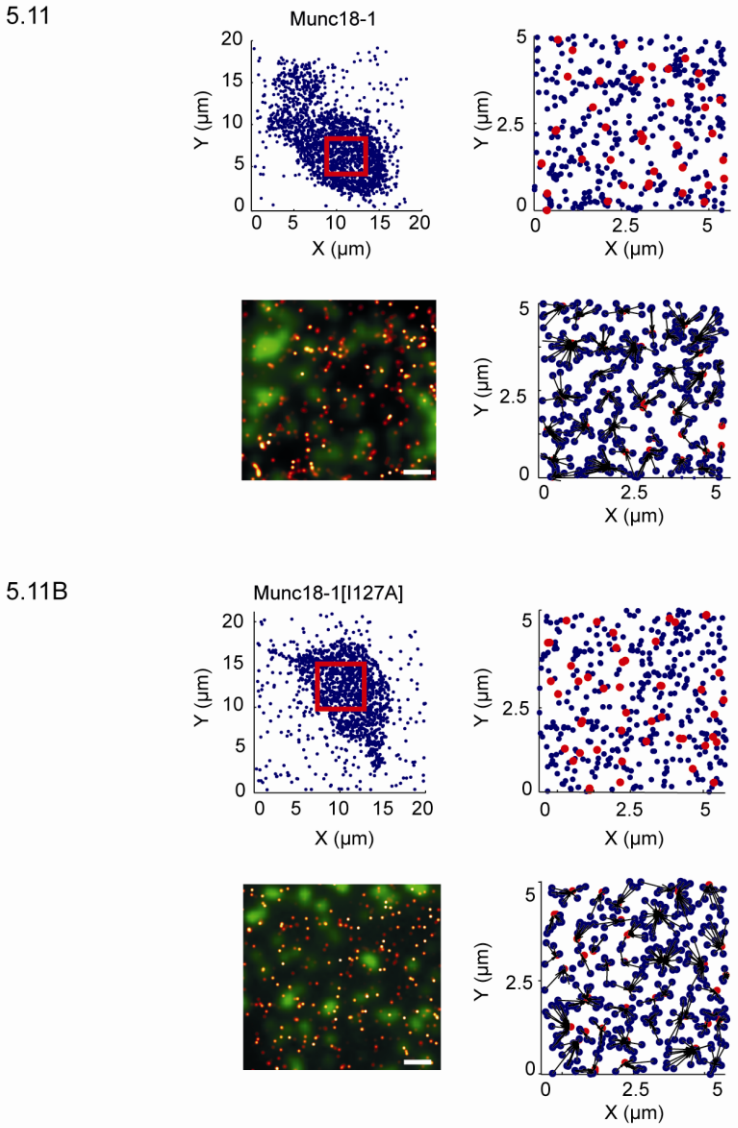

Figure 5.11. *The spatial arrangement of munc18-1 and secretory vesicles is unaffected by N-terminal interaction*. KD43 PC12 cells were transfected with munc18-1, syntaxin and a fluorescent vesicle cargo marker, NPY, and fixed 48 hours later. Single munc18-1 molecules were activated and localised and the coordinates of both single munc18-1 molecules and secretory vesicles were centroided (*top right panel*). TIRFM image showing NPY-EGFP-labeled secretory vesicles and a rendered map of single munc18-1 molecules within the boxed region at the plasma membrane (*bottom left panel*). Individual molecules were assigned to a nearest neighbour secretory vesicle. The "quiver" diagram shows single molecule co-ordinates (red spots) connected by to the centroid coordinates of their closest vesicle (*bottom right panel*). Munc18-1 *n* = 24,096 molecules, 412 vesicles. 5.11B. Munc18-1[I127A] expressing KD43 PC12 cells were subject to the same experimentation and nearest neighbour analysis. Munc18-1[127A] *n* = 20,567 molecules, 350 vesicles.

Using this cellular system the average numbers of munc18-1 molecules within 200 nm from the centre of mass of each vesicle i.e. under the equatorial diameter of a secretory vesicle, ranged between zero and a maximum of nine (Figure 5.12 and 5.13; n = 24,096 munc18-1 molecules localised to 412 vesicles, combined from n = 8 independent experiments). Ablating the N-terminal interaction between munc18-1 and syntaxin had no effect on the proportion of munc18-1 molecules within 200 nm of a vesicle. This value gives an estimation of the minimum numbers of molecules that could potentially reside underneath a membrane resident secretory vesicle.

However, allocating munc18-1 molecules that resided within 200 nm of the centroid of their nearest vesicle is perhaps not a realistic representation of the distances over which munc18-1 would be predicted to interact with the syntaxin-containing-SNARE complex to drive membrane fusion. Therefore, a sampling radii was determined based on the range over which the tSNAREs and vSNARE would be able to interact using available structural information. Using the most recent structural data regarding SNARE proteins in lipid bilayers (Ellena et al, 2009; Stein et al, 2009), the maximum separation distance over which the SNARE proteins can physically interact was calculated to be 17.8 nm (Figure 5.12B). Combining this estimate with the assumption that plasma and vesicular membranes are separated by a distance of zero nanometers (previously used to define 'docked' secretory vesicles by electron microscopy (Voets et al, 2001; de Wit et al, 2006)), the maximum distance from the centre of a secretory vesicle that the t-SNARE and v-SNARE proteins could interact was calculated to be 82.5 nm (Figure 5.12). These values therefore provide the most stringent criteria for measuring the maximum distance over which SNARE proteins are able to interact with a neighbouring vesicle in order to catalyse its fusion.

5.12

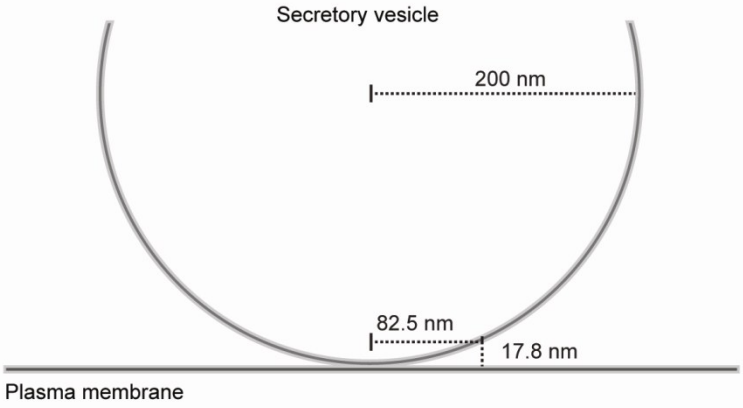

5.12B

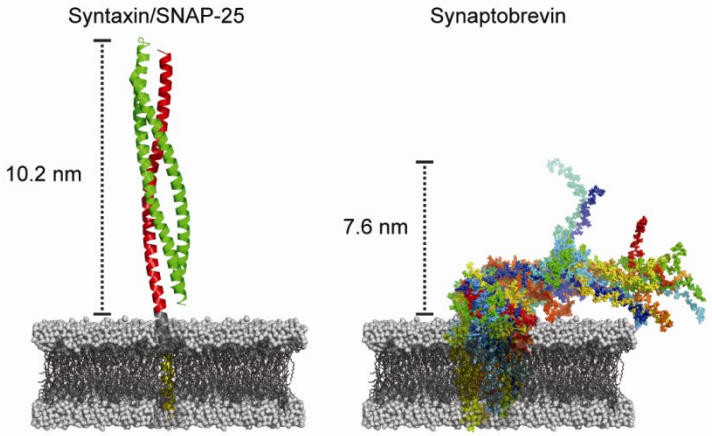

Figure 5.12. *Nearest neighbour analysis of single munc18-1 molecules and membrane proximal secretory vesicles*. The dimensions of a secretory vesicle and plasma membrane are shown to scale with a distance of of 200 nm resembling the equatorial radius of a large dense core vesicle. 5.12B. Using the most recent structural data regarding SNARE proteins in lipid bilayers, the maximum separation distance over which the SNARE proteins can physically interact was calculated to be 17.8 nm (10.2 nm + 7.6 nm). Combining this estimate with the assumption that plasma and vesicular membranes are separated by a distance of zero nanometers gave the maximum distance from the centre of a secretory vesicle that the SNARE proteins could interact as 82.5 nm. Figure generated by Colin Rickman.

Using the radius of 82.5 nm this analysis demonstrated that each vesicle had approximately a 25% probability of being physically associated with one or two munc18-1 molecules in this functionally rescued cellular system (Figure 5.13B). Furthermore neither the probability of having a munc18-1 molecule associated with a secretory vesicle, nor the number of molecules found to reside under a single vesicle was altered upon N-terminal interaction disruption (Figure 5.13B; n = 20,567 munc18-1[I127A] molecules, localised to 350 vesicles, n = 7 independent experiments). Thus, the reduction in exocytosis observed upon disruption of N-terminal binding in KD43 PC12 cells (Figure 4.3; Smyth et al, 2010) is not simply a result of a reduced number of munc18-1 molecules residing in close proximity to a secretory vesicle but rather arises from specific functional effects.

5.13

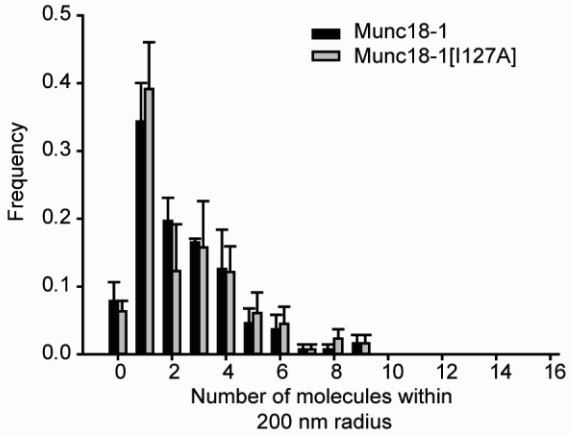

5.13B

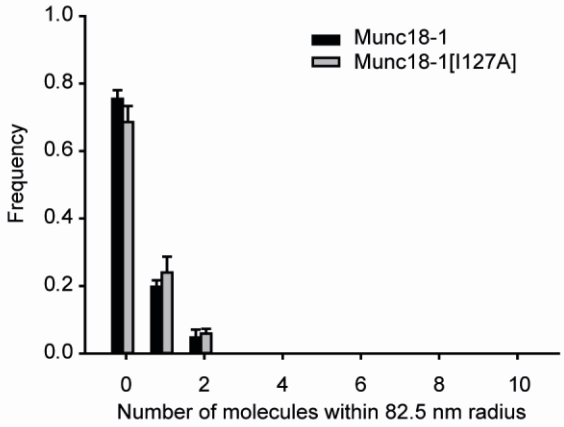

Figure 5.13. *Approximately 75% of all single secretory vesicles have no munc18-1 molecules associated.* Nearest neighbour analysis used all xy coordinates of all labelled plasma membrane secretory vesicles and localised all detected photoactivatable munc18-1 molecules. This analysis was also used to calculate the number of munc18-1 molecules within 200 nm (Figure 5.12) or 82.5 nm (Figure 5.12B) of a secretory vesicle. No significant differences exist between munc18-1 (black bars) and munc18-1[I127A] (grey bars) cell data. Error bars are S.E.M (munc18-1 expressing: 12778 molecules, 866 vesicles, n = 7 cells; munc18-1[I127A]: 10548 molecules, 740 vesicles, n = 8 cells).

To date these experiments have provided an accurate 'snapshot' of the positional information of single munc18-1 and syntaxin molecules in immobilised cells that are not thought to undergo any structural alterations. However, cellular fixation results in a huge loss of information regarding the molecular kinetics and processes existing within a biological system (Lippincott-Schwartz and Patterson, 2003). Advancements in the use of fluorescent probes, stable imaging techniques and sensitive cameras has now permitted the study of sub-cellular dynamics in live cells on a physiologically relevant time-scale. Therefore, this study next determined the mobility and spatio-temporal behaviours of individual munc18-1 molecules in living KD43 PC12 cells by analysing, and quantifying molecular movements of, large cohorts of single molecules using single particle tracking PALM (sptPALM; Manley et al, 2008; Parton et al, 2011).

5.6 Resolving single munc18-1 dynamics in live neuroendocrine cells.

The development of techniques specifically for imaging single molecules in living cells offers an opportunity to probe the dynamics of single proteins in living cellular environments (Sako et al, 2000; Nakada et al, 2003). Proteins of interest can be attached to probes such as gold beads (Kusumi et al, 1993) or fluorescent-protein chimeras (Douglass et al, 2005) and can be tracked by single particle tracking (SPT). Single particle tracking provides an insight into local membrane environments by dissecting heterogeneities in molecular behaviour (Schütz et al, 1997; Dietrich et al, 2002). To date, single particle tracking has helped to elucidate the molecular kinetics behind a number of cellular events, for example the movement of myosin V over actin filaments (Yildiz et al, 2003) to the membrane binding mechanisms of epidermal growth factors (Teramura et al, 2006). More recently the use of photoactivatable markers in conjunction with single particle tracking has enabled the quantification of the diffusion coefficient of tens of thousands of hemagglutinin molecules in living fibroblast cells (Hess et al, 2007).

Super-resolution techniques such as PALM (Betzig et al, 2006) have enabled the imaging of fluorescently labelled proteins to reveal their organisation on the nanoscale, a technique shown to be complementary to single particle tracking (Manley et al, 2008). In this study

PALM has been combined with single particle tracking (sptPALM, Manley et al, 2008) to provide a greater understanding of the complex spatio-temporal behaviours of sub-cellular munc18-1 molecules and to quantify their molecular movements (Parton et al, 2011) in living neuroendocrine cells. Live cell data are acquired in the same manner as for PALM, but with reduced activation energy (to activate fewer molecules at once), faster image frame rates and with lower excitation power, to ensure a larger number of image frames before single molecules bleach off (Manley et al, 2008). Cell viability was also maintained by reducing the excitation light intensity to avoid damaging cellular effects.

5.7 TRACKING LARGE COHORTS OF MUNC18-1 MOLECULES REVEALS HETEROGENEITIES ACROSS THE PLASMA MEMBRANE.

This study obtained information on the positions of single munc18-1 molecules by activating, localizing and bleaching many subsets of photoactivatable-mCherry fluorescent-protein chimeras within KD43 PC12 cells. For sptPALM the data acquisition rate and illumination intensities were optimized in order to maintain cell viability and activate the optimum number of fluorophores per frame. As for PALM, sptPALM was operated under total internal reflection and a high numerical aperture objective was used (Olympus 150X; 1.65 NA). Unlike traditional single-particle tracking in which all single molecules are simultaneously imaged and tracked (Douglass et al, 2005), photoactivatable fluorophores enable multiple subsets of molecules to be activated, imaged and bleached. Therefore several orders of magnitude more trajectories per cell were obtained, as opposed to traditional single-particle tracking which commonly combined 10–100 cells to obtain statistically significant single-particle tracking information (Vrljic et al, 2002; Ewers et al, 2005; Wieser et al, 2007). Therefore, by ensuring that the distance between fluorescent molecules at any one time was greater than the width of their point spread function, thousands of high-density overlapping single-molecule trajectories could be resolved and tracked (Figure 5.14). Molecules that remained visible for more than three frames were localised and their determined positions in consecutive frames were linked into tracks. Particle identification and tracking algorithms were all written and performed by Lei Yang, Heriot-Watt University, Edinburgh (Figure 5.14).

Using sptPALM the spatial distribution of proteins and the information regarding their molecular dynamics could be examined. Large cohorts of single munc18-1 (n = 5873) and munc18-1[I127A] (n = 20878) molecules were tracked in the basal plasma membrane of each cell at 37^{o}C, revealing kinetically and spatially distinct populations of molecules (Figure 5.14 and 5.14B). These images correspond to all the single molecule trajectories in consecutive frames, permitting the construction of maps containing thousands of molecular tracks across the plasma membrane. This information provides a means of obtaining spatially resolved information on cellular dynamics and local environments on the molecular scale (Figure 5.14).

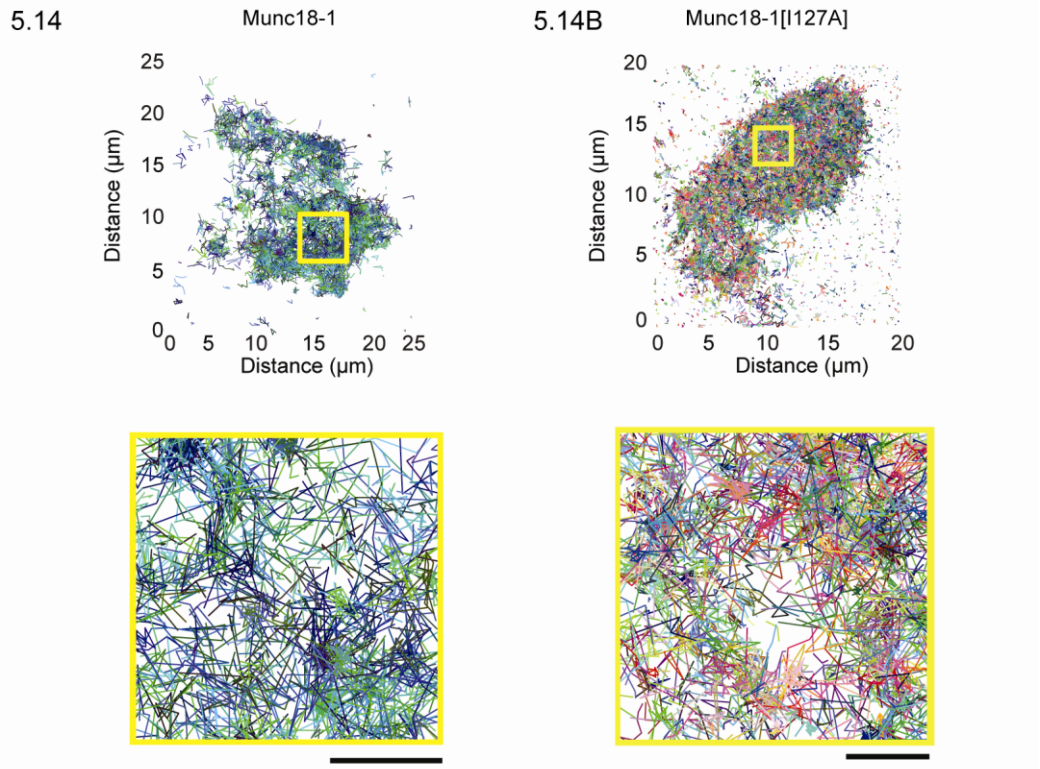

Figure 5.14. *sptPALM tracking of single munc18-1 molecules.* KD43 PC12 cells were transfected with PA-munc18-1 and syntaxin for 48 hours and then subjected to live PALM imaging. Subsets of photoactivatable fluorophores were activated under 405 nm illumination, localised and bleached. Molecules visible for more than 90 ms (3 frames) were tracked using Matlab algorithms written and performed by Lei Yang, Heriot Watt University. The tracks of single molecules in either wild-type munc18-1 (n = 5,873 molecules) or munc18-1[I127A] expressing cells (n = 20,878 molecules) with time-integrated PALM images reflecting the distribution of all molecular tracks localised to <25 nm are shown. Tracks were plotted in different colours to distinguish between individual tracks. Scale bar 2 µm, expanded image scale bar 500 nm.

5.8 MUNC18-1 MOLECULAR SPEED NEGATIVELY CORRELATES WITH DENSITY AT THE PLASMA MEMBRANE.

The technique of sptPALM enabled the dynamics of single molecules to be investigated and molecular environments to be defined within a single cell. This complex network of molecular tracks can be simplified by the generation of contour maps to provide a large-scale quantitative representation of the dynamics of munc18-1 at the plasma membrane of intact, living cells. Both munc18-1 and munc18-1[I127A] molecules exhibit a heterogeneous spatial distribution in their movement with regions of high and low density observed on the plasma membrane (Figure 5.15). This result supported the finding that munc18-1 was found to be concentrated in areas of the cell as shown by GSDIM and PALM, a distribution shown to be independent of syntaxin-N-terminal interaction.

sptPALM data was used to correlate areas of the plasma membrane that were characterised by a high density of munc18-1 molecules. Bioinformatics analyses of sptPALM data revealed that munc18-1 moves freely across the plasma membrane but displays restricted, slower motions in areas enriched with munc18-1 molecules (Figure 5.15). Conversely, munc18-1 travels at greater speed in areas of the plasma membrane that are not associated with a high concentration of munc18-1 molecules. 'Difference' contour maps were plotted in order to highlight the areas of the membrane with the largest degree of anti-correlation (section 2.9.5). These plots revealed that areas of the membrane with a higher density of munc18-1 molecules and a lower molecular speed, and vice-versa, had the greatest anti-correlation value (Figure 5.15). Furthermore, disrupting the N-terminal interaction between munc18-1 and syntaxin did not result in a change in the molecular dynamics of munc18-1, with munc18-1 molecules continuing to display reduced molecular speeds in areas of munc18-1 concentration.

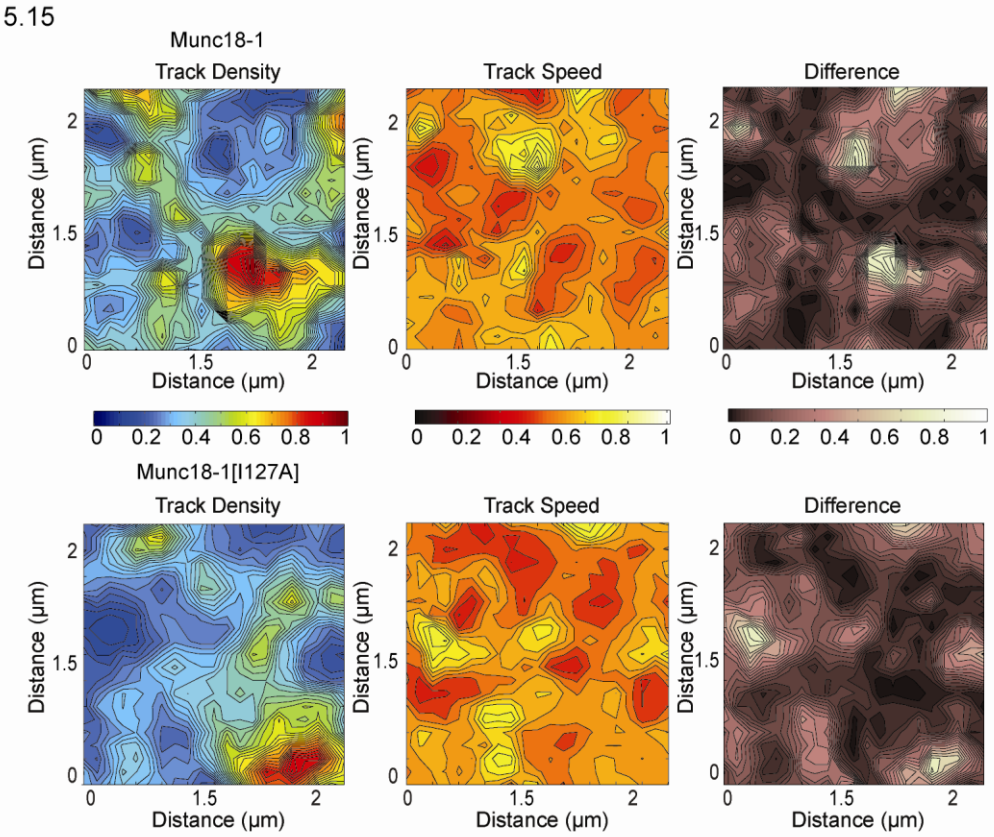

Figure 5.15. *Munc18-1 molecular density anti-correlates with molecular speed at the plasma membrane*. KD43 PC12 cells were transfected with either PA-munc18-1 or PA-munc18-1[I127A] and syntaxin for 48 hours and then subjected to live PALM imaging. Contour maps containing normalised molecular densities and speeds are shown. Difference contour maps were created by calculating the difference between the density and molecular speed across each pixel of the image. All images are on the same colour scale and correspond to the region of interest in Figure 5.14.

Diffusion maps of munc18-1 reflect the dynamics of molecules in single cells. By combining data from multiple cells, a histogram of single molecule speed coefficients was constructed (Figure 5.16; munc18-1 n = 31,566 molecules, n = 3 cells; munc18-1[I127A] n = 40,078 molecules, n = 3 cells). This confirmed that a large fraction of munc18-1 molecules exhibited a highly restricted speed, never reaching more than 3 μms^{-1} at the plasma membrane. Perturbing the N-terminal interaction between munc18-1 and syntaxin had no effect on the molecular speed of munc18-1, indicating that the syntaxin-N-peptide is perhaps not critical in the recruitment of munc18-1 to the plasma membrane, as previously suggested (Figure 5.16; Rathore et al, 2010).

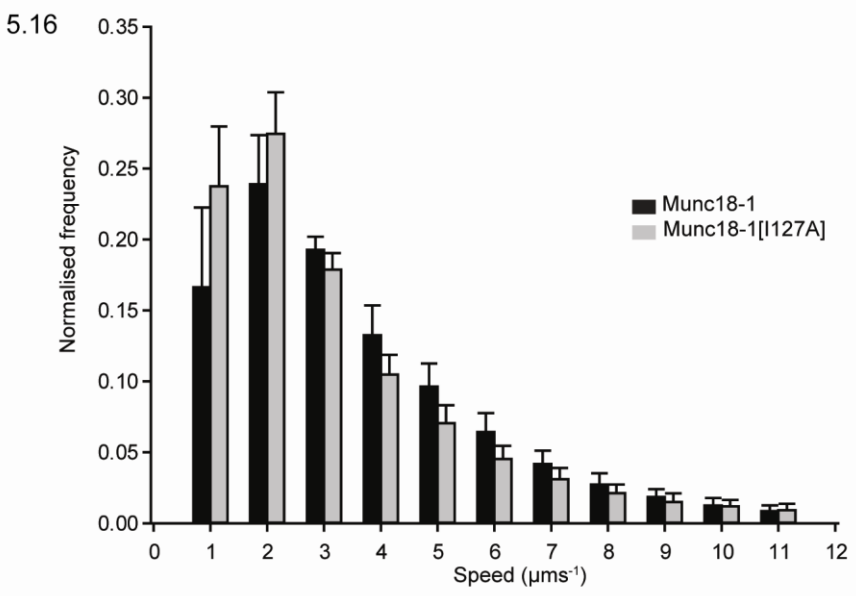

Figure 5.16. *Perturbing the N-terminal interaction with syntaxin has no effect on the speed of single munc18-1 molecules.* Speeds of all munc18-1 and munc18-1[I127A] single molecules were normalised and displayed in histogram form, revealing no significant difference using a two-way ANOVA (munc18-1 n = 31,566 molecules, n = 3 cells; munc18-1[I127A] n = 40,078 molecules, n = 3 cells).

5.9 MUNC18-1 MOLECULES MOVE BETWEEN MOLECULAR DEPOTS ON THE PLASMA MEMBRANE.

By resolving the tracks of thousands of munc18-1 molecules it was also possible to determine the trajectories and directionality of these molecules. Single particle tracking of munc18-1 combined with detailed analysis of molecular trajectories revealed no directional preference of munc18-1 molecules in their choice of initial track movements (Figure 5.17). This result indicated that munc18-1 molecules had complete freedom of directional motion regardless of an N-terminal interaction with syntaxin (Figure 5.17). The constructed 'rose diagram' shows that all molecules have an equal propensity to move in any direction in their first movement, discounting the idea that their movement is correlated with microscopic drift. It was next decided to ask a more detailed question of the munc18-1 molecular motion data; once moving in a particular direction, where do single molecules go next?

Analyzing the trajectory angle taken by every molecule at the second position of a trajectory, relative to the previous movement (i.e. incorporating a direction into the analysis), it was found that single molecules were highly likely to reverse their directions once already moving forward (Figure 5.17B). Furthermore this molecular behaviour was not dependent on an interaction with the N-terminal peptide of syntaxin (Figure 5.17B). The reason for this unusual reversing behaviour could be either due to a 'zig-zag' motion, overlying a general linear directionality, or due to a 'caged' motion, where molecules are able to move only a certain distance from their origin (Figure 5.18). These two possibilities can be distinguished by correlating track length with displacement (the direct distance between the start and the end of molecular trajectories). Analysis of track length and displacement confirmed that the immobile fraction of munc18-1 exhibits a caged, restricted motion (Figure 5.18B). The restricted kinetics of munc18-1 molecules in membrane hot-spots are likely to reflect the recruitment of munc18-1 molecules to membrane-inserted syntaxin as this is the principal mechanism for munc18-1-membrane association (Hata et al, 1993; Rowe et al, 1999, 2001; Medine et al, 2007; Arunachalam et al, 2008).

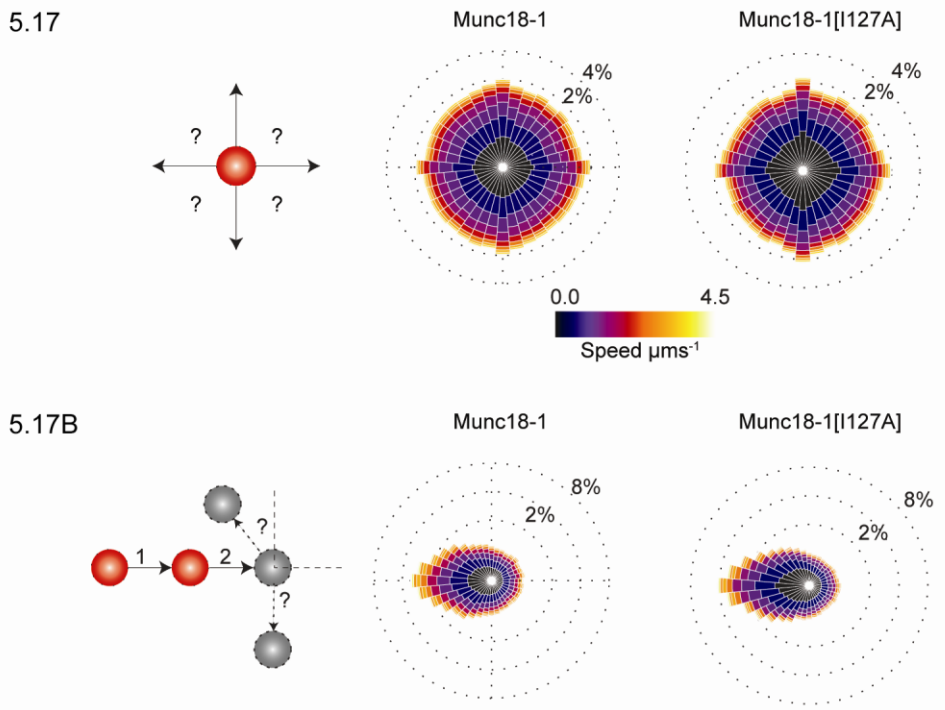

Figure 5.17. *Munc18-1 molecules reverse in direction following their initial movement*. The angle of momentum was calculated for every munc18-1 molecule tracked (n = 31,566 munc18-1 molecules), assuming no prior knowledge of direction (*cartoon, left*). A circular histogram ('Rose diagram') was generated, accumulating track angles into 36 bins and percentages indicate bin amplitude as a fraction of the total tracks. Amplitude of each bin indicates the number of tracks, colour coding is for speed (blue – slow – yellow – fast). Tracking of munc18-1 combined with detailed analysis of molecular trajectories revealed no directional preference of munc18-1 molecules in their choice of initial track movements. Perturbing N-terminal interaction had no effect on the directionality of molecules, with all molecules have an equal propensity to move in any direction in their first movement. 5.17B. Combined track angles measured between the second and third positions of every munc18-1 molecule trajectory was calculated, using a priori information of direction the angle of momentum. This analysis revealed that molecules are highly likely to reverse after moving forwards for a short distance. Rose diagrams were plotted (munc18-1, $n = 31{,}566$ molecules, $n = 3$ cells; munc18-1[I127A], $n = 40{,}078$ tracks, $n = 3$ cells) showing this behaviour is unaffected by syntaxin N-terminal interaction.

5.18

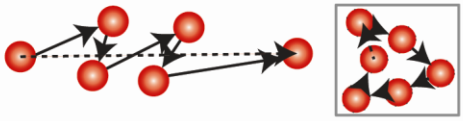

5.18B

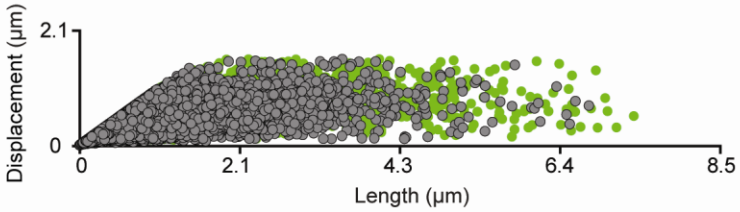

Figure 5.18. *Single munc18-1 molecules exhibit caged movement on the plasma membrane*. The reversal behaviour seen in the previous Rose diagrams could be due to a 'zig-zag' or a 'caged' motion. These two possibilities can be dissected by correlating the total track length (shown as a solid arrows) with track displacement (dashed arrow). 5.18B. These plots show that trajectories with long track lengths but short displacements are maintained both with wild-type munc18-1 and (grey points) and when N-terminal interaction is abolished (green points). Trajectory analysis revealed that the majority of munc18-1 molecules had a caged motion, never moving more than 1 µm in a single direction before reversing.

The spatio-temporal organisation of relatively immobile munc18-1 molecules into hot-spots, distinct from vesicle docking sites but interspersed with more mobile molecules, is suggestive of munc18-1 recycling between molecular depots. This question was addressed using online tracking software which averaged the directionality of hundreds of munc18-1 (n = 786 tracks) or munc18-1[I127A] (n = 1239 tracks) molecules in a 500 nm region of interest (Hamilton et al, 2010). This analysis demonstrated that munc18-1 molecular populations appeared to move in a directed way around the membrane (Figure 5.19). However, averaging the behaviours of hundreds of molecules to highlight the average trend in directionality removes variations within data sets. In order to dissect whether there was directed motion between areas of high and low munc18-1 densities this investigation extracted exemplar trajectories of fifty representative molecular tracks from KD43 PC12 cells expressing both munc18-1 and munc18-1[I127A] molecules (Figure 5.19B). Using the same region on interest and taking a more individual approach this analysis demonstrated that munc18-1 molecules move in a directed motion between areas of high and low molecular densities.

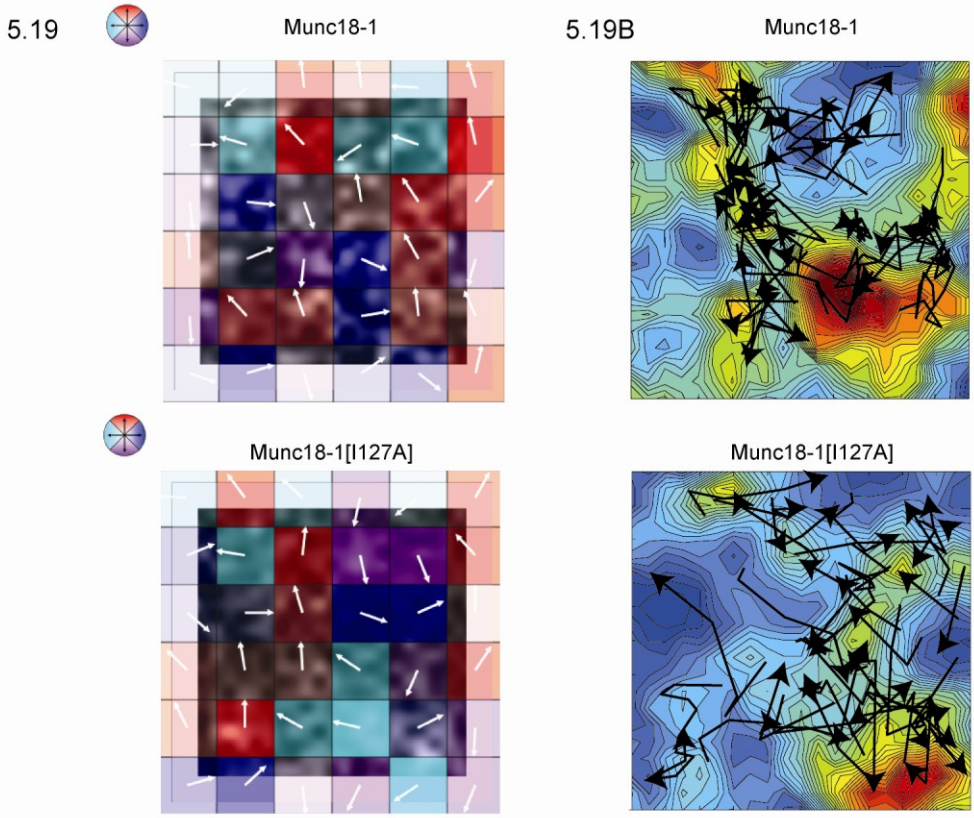

Figure 5.19. *Munc18-1 molecules move between molecular depots at the plasma membrane.* Directionality maps were generated using an online programme and show the average direction of munc18-1 (786 tracks, *upper panel*) or munc18-1[I127A] (1239 tracks, *lower panel*) molecules within each 500 nm square. Squares are colour coded for direction. 5.19B. Example trajectories of approximately 50 munc18-1 (*upper panel*) or munc18-1[I127A] (*lower panel*) molecules are superimposed onto molecular density contour maps. Single molecules appear to move between areas of high and low concentrations of munc18-1 molecules.

The eukaryotic plasma membrane is a laterally organised and highly heterogeneous structure where a number of proteins exert a multitude of cellular functions. Over the last fifteen years a number of theories have been discussed to try and explain these lateral heterogeneities or plasma membrane microdomains. Simons and Ikonen (1997) popularised the 'lipid raft' hypothesis, a theory suggesting that cholesterol clusters into lipid rafts in the exoplasmic leaflet of the plasma membrane. Since the introduction of the 'lipid raft' proposal more than 200 cellular components have been assigned to rafts, including syntaxins 1-4, SNAP-25 and VAMP 2 and 3 (Foster et al, 2003). It has also been shown that the integrity of these SNARE-rich clusters is dependent on cholesterol with major changes in the distribution of syntaxin 1 (Lang et al, 2001; Ohara-Imaizumi et al, 2004), syntaxin 3 (Low et al, 2006) and SNAP-23 (Chamberlain and Gould, 2002) upon its depletion.

Taking into account that munc18-1 interacts with syntaxin with a high affinity (Pesvner et al, 1994), it can be postulated that munc18-1 may also reside on lipid rafts through an interaction with syntaxin. Cholesterol-rich clusters are of huge functional importance as their depletion results in a disruption of exocytotic events in a number of cell types (Chamberlain et al, 2001; Lang et al, 2001; Ohara-Imaizumi et al, 2004; Wasser et al, 2007), similar to the genetic removal of munc18-1 (Verhage et al, 2000). Therefore it could be reasoned that the caged motion exhibited by munc18-1 molecules may be responsible for the endogenous and heterologous molecular distribution seen in fixed samples (Figure 5.2), where single munc18-1 molecules accumulate in distinct membrane domains through a tight interaction with syntaxin, a local barrier to the diffusion of munc18-1 molecules. Together, these findings demonstrate that a limited number of munc18-1 molecules recycle between molecular storage depots with membrane locations distinct from vesicle docking sites.

5.10 CONCLUSION

Most subcellular structures, for example, microtubules, ribosomes and vesicles, are much smaller than the limit of resolution of conventional imaging systems. Therefore the ability to both visualise individual molecules and record their large-scale organisation and

kinetics has been severely restricted. Advancements in single molecule imaging *in vitro* and in living cells (Sako et al, 2000; Nakada et al, 2003; Betzig et al, 2006; Hess et al, 2006) now offer a method for probing single protein architectures and dynamics by breaking through the diffraction barrier and imaging beneath the size limitation that it defines. Super-resolution imaging techniques including GSDIM and PALM can reveal the nanoscale organisation of fluorescently labelled proteins with a density of molecules high enough to provide structural context. In this study GSDIM and PALM imaging demonstrated that, at rest, secretory vesicles do not reside over dense areas of munc18-1 on the plasma membrane. This is surprising given that the presence of munc18-1 is vital in catalysing the fusion of opposing lipid bilayers. However, previous studies examining syntaxin clustering, which is directly relevant to the localisation of munc18-1, have observed only partial colocalisation with secretory vesicles (Lang et al, 2001; Barg et al, 2010). Furthermore, the spatial pattern of munc18-1 or syntaxin is not dictated by the N-peptide of syntaxin; ablating this interaction does not result in a molecular reorganisation. Thus, a reduction in both vesicle kinetics and fusion likelihood upon the selective disruption of the N-terminal interaction, as shown previously (Smyth et al, 2010), cannot be explained by a spatial redistribution of molecules away from vesicles across the cell surface.

For munc18-1 to act at the final stage of fusion it is intuitive to think that it must be associated with an adjacent vesicle. Data included in this chapter provide estimates for the number of munc18-1 molecules that act within 200 nm of a single vesicle level in cells; this number ranges between zero and nine. A substantial pool of vesicles in this study was found to have no adjacent munc18-1 molecule and these vesicles cannot move sufficient distances at the plasma membrane to reach their nearest neighbour munc18-1 molecule. Importantly, this limited number of munc18-1 molecules acting at a single vesicle level is sufficient to fully rescue exocytosis (Smyth et al, 2010). As munc18-1 and syntaxin (and the SNARE complex) have a 1:1 stoichiometry, this suggests that few SNARE complexes are required to drive fusion, in agreement with current estimates of the numbers of SNARE molecules required to drive exocytosis, of between 5 and 11 (Han et al, 2004; Karatekin et al, 2010). Furthermore, the majority of vesicles in this study were found to have no proximal munc18-1 molecule suggesting that few munc18-1 molecules are required for exocytosis to proceed and that despite the population of cells exhibiting full

secretion, at the single vesicle level, most vesicles remain unused. Few molecules are required for exocytosis to proceed, and it remains unknown whether the presence of multiple munc18-1 molecules (this study observed a maximum of 9 per vesicle) further enhances fusion likelihood. It remains to be seen whether multiple munc18-1-syntaxin complexes can act cooperatively to further increase release probability over the absent state. Taken together, munc18-1 molecules exist in a non-random spatial distribution, resulting in areas of low and high molecular density. Importantly it is the regions of low munc18-1 molecular density at the plasma membrane that are specifically targeted by secretory vesicles.

There are three possible scenarios to explain why munc18-1 and secretory vesicles are spatially distinct on the cell surface. Firstly, are molecules enriched in-between secretory vesicles able to move sufficient distances in order to reach the nearest vesicle and drive fusion? Comparing total track length to maximum displacement showed that despite the presence of long molecular tracks, the maximum displacement for munc18-1 was capped at approximately 1.5 μm (Figure 5.18B), making it impossible for munc18-1 molecules to travel to secretory vesicle 'docking sites' immediately prior to exocytosis. Secondly, in addition to the lateral diffusion of single munc18-1 molecules in the plasma membrane, secretory vesicles undergo both Brownian motion and have been shown to undergo a rapid movement immediately prior to fusion (Degtyar et al, 2007). The functional significance of this 'jump' in vesicular movement may be to permit a secretory vesicle to sample more individual munc18-1 molecules immediately preceding membrane exocytosis. Lastly, it may be the case that vesicular fusion occurs where munc18-1 (and presumably SNAREs) are not enriched; a theory not easily placed within the concept of SNARE mediated exocytosis. Despite directly addressing the fundamental question of why munc18-1 molecules and secretory vesicles appear to be spatially segregated, these findings provide a working model where the association of a small number of munc18-1 molecules are required to support single vesicle exocytosis and that the association, or not, of a munc18-1 molecule with the SNARE complex within a functionally relevant distance of a vesicle is a determinant of fusion probability.

In this study PALM was combined with live-cell single particle tracking (sptPALM; Manley et al, 2008) to capture the spatio-temporal complexities and heterogeneities of

single-munc18-1 molecular motions across the membrane of neurosecretory cells (Schutz et al, 1997; Dietrich et al, 2002). By overcoming a number of difficulties associated with this technique, for example high particle density and temporary particle disappearance, it is possible to gain an insight into how individual proteins drive a number of cellular events (Yildiz et al, 2003; Douglass and Vale, 2005; Teramura et al, 2006). More relevantly, decoding the kinetics of single munc18-1 molecules provides a significant clue for understanding the mechanisms that drive the behaviors governing its spatial arrangement.

In this study single-molecule motion was probed with high specificity, millisecond time resolution, and nanometer spatial resolution in a living cell using sptPALM. Single munc18-1 molecules exhibited spatially distinct diffusional behaviours across the plasma membrane of live neuroendocrine cells. Munc18-1 molecules were seen to freely explore the plasma membrane, often preferring specific areas of the planar bilayer, evidenced by a heterogeneous density of tracks. Munc18-1 molecules within areas of molecular enrichment exhibited slower speeds and confined kinetics whereas highly mobile munc18-1 molecules were found in less dense munc18-1 areas and moved in a more mobile manner. It can be speculated that munc18-1 'scans' the membrane for syntaxin molecules and upon binding to the transmembrane protein becomes immobile, possibly marking a fusion site for the docking of a large dense core vesicle. The fact that the mobility of single munc18-1 molecules is highly restricted within these plasma membrane 'hot-spots' could represent anomalous diffusion, a term used to describe a diffusion process with a non-linear relationship with time, as demonstrated for several membrane proteins and lipids (Feder et al, 1996). The interaction with munc18-1 and syntaxin in membrane domains might act as a local barrier to diffusion, caging munc18-1 in order to catalyse the fusion of a secretory vesicle.

These munc18-1-rich domains of the phospholipid bilayer might well be associated with lipid rafts as syntaxin has been shown to occur in clusters in cell membranes (Lang et al, 2001; Sieber et al, 2007; Rickman et al, 2010), clusters that disperse upon cholesterol depletion (Lang et al, 2001). In cells, spatially and functionally distinct clusters, containing predominantly one of two heterodimer forms, are influenced by the underlying lipid microenvironment (Rickman et al, 2010). Thus, single munc18-1 molecules could accumulate in functionally and spatially heterogeneous distinct membrane domains

through a tight interaction with syntaxin. These experiments also demonstrated that most munc18-1 molecules do not reside within interaction-distance of a membrane-proximal vesicle, suggesting that these 'munc18-1 depots' are distinct from the sites of exocytosis. In fact, these 'in-between' areas of high molecular densities may be acting as an important functional entity, providing a concentrated pool of munc18-1 to facilitate and enhance bilayer fusion. Molecules were found to move between these depots, suggesting that there is an element of recycling of munc18-1 between membrane sites. It remains unknown whether these more mobile munc18-1 molecules are associated with syntaxin or not. However, as the interaction with munc18-1 and syntaxin in membrane domains may act as a local barrier to diffusion, such inter-molecular interactions may cage a small number of munc18-1 molecules in order to drive the fusion of a secretory vesicle.

Although live-cell imaging with super-resolution microscopy is still in its infancy, it is likely that future research will focus heavily on the cellular dynamics and local environments on the molecular scale. A future study of the characteristics of munc18-1 dynamics in clustered regions could provide insight into whether molecules exhibit reduced mobility or directed motion as a result of interactions with large dense core vesicles or SNARE complexes. Also, it is of particular interest to determine whether molecules exhibit heterogeneities in each of their trajectories, a change in behaviour possibly underlying an interaction between munc18-1 and the SNARE complex.

CHAPTER 6:

THE MOLECULAR DYNAMICS OF LARGE COHORTS OF SINGLE MUNC18-1 MOLECULES IN CENTRAL NERVE TERMINALS

6.1 INTRODUCTION

The sheer complexity of the nervous system relies on the ability of neurons to communicate with each other through the release of neurotransmitters in a highly localised and Ca^{2+} dependent manner (reviewed in Südhof, 2004). Synaptic exocytosis is one of the most highly organised forms of intracellular membrane fusion, achieving such specificity and exquisite regulation through the concerted action of the SNARE proteins (Söllner et al, 1993a,b). SNAREs possess conserved features that underlie the general mechanisms of vesicle cycling whilst exhibiting unique properties evolved to meet the demands of Ca^{2+} dependent synaptic exocytosis. The synchronized action of a number of accessory proteins is also required to oversee the highly ordered and localised nature of SNARE mediated exocytosis (Südhof and Rothman, 2009).

Sec1/Munc18 proteins (SM proteins), identified in the nervous system of *C. elegans* (Hosono et al, 1992; Genyo-Ando et al, 1993), *Drosophila* (Salzberg et al, 1993; Harrison et al, 1994) and mammals (Hata et al, 1993; Garcia et al, 1994; Pevsner et al, 1994b) are a class of accessory factors that are present at all SNARE-catalysed membrane fusion sites (Gerber et al, 2008). SM proteins were first suggested to interact directly with syntaxin by genetic work in yeast (Aalto et al, 1993), an observation later to be confirmed biochemically with mammalian proteins (Hata et al, 1993; Garcia et al, 1994; Pevsner et al, 1994b). The dynamic interactions between munc18-1 and syntaxin homologues, documented to be both location and function dependent, are thought to reflect the multifaceted nature of the vesicle cycle (Gulyas-Kovacs et al, 2007; Gerber et al, 2008).

It was previously shown that rbSecl, a mammalian neuronal protein homologous to the yeast SM Sec1p protein, is widespread in its subcellular localisation (Garcia et al, 1995). This distribution was shown to parallel that of syntaxin and SNAP-25 despite the fact that active zones, sites of spatially restricted synaptic vesicle fusion, only occupy a small percentage of the axonal plasma membrane (Galli et al, 1995; Garcia et al, 1995). Following this observation it was demonstrated, using immunohistochemistry and electron microscopy, that munc18-1 colocalised with cytoskeletal proteins in the rat olfactory bulb (Bhaskar et al, 2004) and that its distribution moved to the cytoplasmic fraction of rat

hippocampal neurons upon intense activation (Zhang et al, 2011). Despite these aforementioned attempts to decipher the spatial arrangement of SM proteins, findings not supported in any other study, it has been repeatedly shown and generally agreed upon that munc18-1 and syntaxin colocalise with each other at synaptic terminals (Bennett et al, 1992; Yoshida et al, 1992; Südhof, 1995; Okamoto et al, 2000). A number of these studies have demonstrated highly punctate munc18-1 immunolabelling throughout the brain, with munc18-1 particularly abundant at active zones and lacking in the postsynaptic density (Bennett et al, 1992; Yoshida et al, 1992; Südhof, 1995; Okamoto et al, 2000). Findings to suggest that both munc18-1 and syntaxin are arranged at synapses are consistent with previously characterised biochemical interactions and functional assays of munc18-1 in synaptic vesicle exocytosis. However, despite intensive study the spatial arrangement of munc18-1 and syntaxin in neuronal cells has never been defined at a molecular level.

It has been widely established that munc18-1 interacts directly with syntaxin (Aalto et al, 1993; Hata et al, 1993; Garcia et al, 1994; Pevsner et al, 1994b) via two distinct mechanisms, closed form and N-terminal binding (Burgoyne and Morgan, 2007; Dulubova et al, 2007; Rickman et al, 2007; Shen et al, 2007). What has never been explored is the 'whens' and 'wheres' of these interactions, i.e. where do these proteins interact for the first time and when do they first enter into a long-, or short-, lived interaction within an intact neuron? In spite of previous biochemical studies demonstrating the high affinity interaction of munc18-1 and syntaxin (Hata et al, 1993; Garcia et al, 1994; Pevsner et al, 1994a), it was shown by Garcia and colleagues that the neuronal SM protein rbSecl and syntaxin are not stably associated *in situ* (Garcia et al, 1995). This study went on to suggest that munc18-1 may well associate with syntaxin in a transient manner in order to allow its interaction with downstream effectors to proceed. This result supported a previous finding which suggested that only a small proportion of rbSecl was able to bind immobilised recombinant syntaxin (Hodel et al, 1994).

Most studies to date have utilised approaches such as protein mutagenesis (Rickman et al, 2007; Deak et al, 2009), GST pulldowns (Pevsner et al, 1994a) and crystallography (Misura et al, 2000; Toonen and Verhage, 2007) to investigate the complex interactions between munc18-1 and syntaxin. These biochemical techniques involve reconstructing

and reconstituting biological systems, thereby providing an initial characterisation of protein-protein interaction dynamics. However, translating these *in vitro* findings to the physiologically relevant behaviours observed *in vivo* ultimately requires methods to probe protein–protein interactions without affecting the physiological functions of the biological system. Therefore, whilst *in vitro* biochemical, electrophysiological and ultra-structural data concerning the interaction status of munc18-1 and syntaxin is highly specific, the sensitivity needed to decipher their precise spatio-temporal arrangement at the molecular level is lacking.

One advanced method available to elucidate biological mechanisms in living cells by monitoring real-time protein-protein interactions is Fluorescence Correlation Spectroscopy (FCS). FCS is a non-invasive experimental technique used to accurately probe the local dynamics, concentration and photo-physics of single molecules that control various physiologic processes (Madge et al, 1972). FCS is based on the analysis of spontaneous intensity fluctuations of a low concentration of fluorescently labelled molecules diffusing through a small, typically femtolitre observation volume (section 2.8.7). The recorded fluctuations in fluorescence, caused by a range of physical parameters, can be quantified in terms of their strength and duration by autocorrelating the intensity signal (Schwille et al, 1997; Haustein and Schwille, 2004; Kim et al, 2007). The autocorrelation function measures the self-similarity of a time series signal giving biophysical readouts concerning molecular diffusion coefficients and concentrations. Performing cross correlation analysis compares the signal between fluorescent channels, thereby measuring the extent of cross-talk between fluorescently tagged molecules. Taken together, FCS delivers quantitative information on molecular number, concentration, rate of diffusion and interaction status on a μsec timescale in biologically intact systems (Bacia et al, 2006).

Performing FCS in a living cell poses a demanding, yet feasible analytical approach to the study of biological molecules in their native environment. Despite FCS requiring a low concentration (<1 nM), adequate brightness and mobility (>0.1 μms^{-1}) of fluorescent molecules (Müetze et al, 2011), it is an ideal tool to study the molecular dynamics in living cells. Since the development of FCS in the 1970s, a vast number of *in vivo* and *in vitro* studies have been conducted, primarily taking advantage of the spatial resolution of

FCS. Initial measurements using FCS focused on the lateral transport of receptor complexes on the plasma membrane (Schlessinger et al, 1976; Elson et al, 1976). More recently FCS has elucidated the mechanisms behind the oscillations of the cyanobacterial circadian clock (Goda et al, 2011), the diffusion of fluorescently labelled tubulin in squid giant axons (Terada et al, 2000) and the precise stages of the SNARE mediated fusion pathway within reconstituted membranes (Cypionka et al, 2009).

Despite intensive study into the multifaceted interaction between munc18-1 and syntaxin, the spatial and temporal pattern of their molecular distribution and interaction in central synapses remains undefined. Therefore, this study employed molecular imaging techniques ground state depletion followed by individual molecule return (GSDIM), photoactivatable localisation microscopy (PALM) and fluorescence correlation spectroscopy (FCS) to define the arrangement of endogenous munc18-1 and syntaxin molecules in central neurons. By imaging large cohorts of single molecules it was possible to quantify their molecular movements preceding, during and immediately after exocytosis.

6.2. THE ACCUMULATION OF ENDOGENOUS MUNC18-1 AND SYNTAXIN MOLECULES AT NERVE TERMINALS.

To date, the precise intracellular localisation of neuronal munc18-1 relative to that of presynaptic t-SNARE syntaxin has never been probed at a single molecule level. To investigate the molecular organisation of munc18-1 and syntaxin on a nanometer scale this study employed both GSDIM (Fölling et al, 2008) and PALM (Betzig et al, 2006). GSDIM involved immunodetecting endogenous munc18-1 and syntaxin with a fluorophore-conjugated antibody (Alexa-647), and driving this into a long-lived (seconds) 'dark-state' using intensity laser illumination in the presence of a reducing buffer (Fölling et al, 2008). Single Alexa-647 molecules spontaneously re-emerge from this dark state, permitting the localisation of individual immunodetected epitopes separated in a time stack, as discussed in Chapter 5. DIV 14 cortical neurons were chemically fixed for 60 – 90 minutes to ensure complete immobilisation (Sieber et al, 2007), munc18-1 or syntaxin

were immunolabelled with Alexa-647 and synapsin, a presynaptic marker, was immunolabelled with Alexa-488.

GSDIM imaging revealed that both endogenous syntaxin (Figure 6.1) and munc18-1 (Figure 6.1B) single molecules are enriched within central nerve terminals, when compared to their molecular distribution in neuronal processes, as shown previously (Bennett et al, 1992; Yoshida et al, 1992; Südhof, 1995; Okamoto et al, 2000). This finding is in contrast with a previous finding demonstrating that rbSec1, a mammalian neuronal SM protein, has a widespread distribution in the axon of a neuron (Garcia et al, 1995). This discrepancy might be explained by the fact that Garcia et al (1995) analysed the localisation of two alternatively spliced isoforms, rbSeclA and B, both differing in subcellular localisation and at their COOH termini (Garcia et al, 1995).

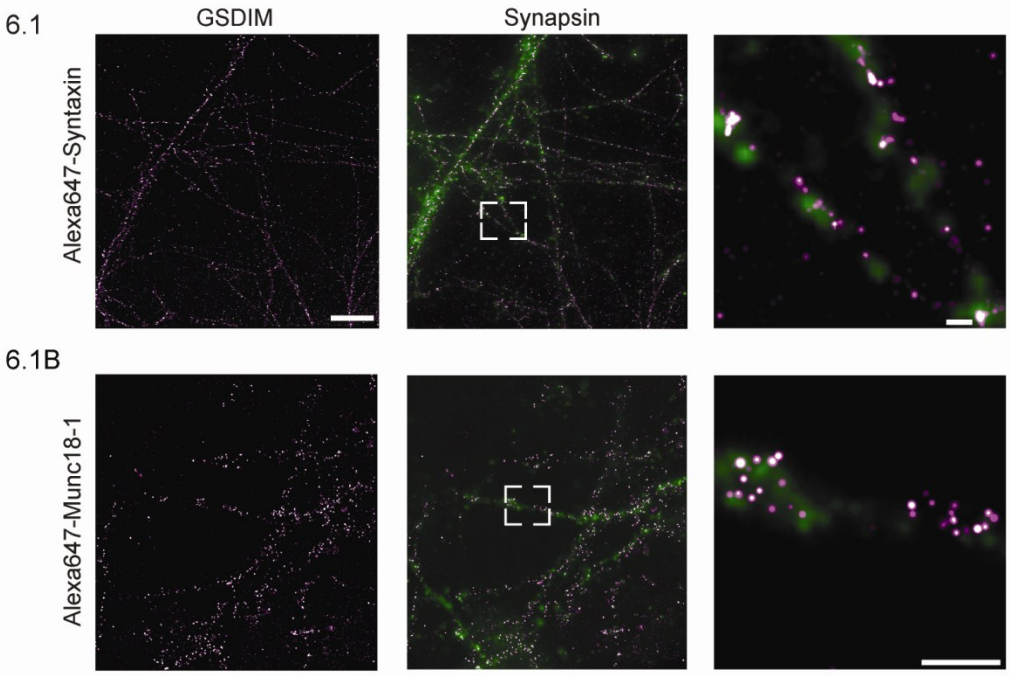

Figure 6.1. *Endogenous munc18-1 and syntaxin cluster at synaptic terminals*. A GSDIM map of immunolabelled Alexa647-munc18-1 or -syntaxin in cortical neurons (*left panels, magenta*). Fixed cells were co-immunostained with Alexa488-synapsin in order to label synapses and the images merged (*middle panel, green*). Scale bar: 5 µm. A merged image of left and middle panels corresponding to the boxed region is shown at a higher zoom (*right panels*). Scale bar 500 nm. Both syntaxin and munc18-1 single molecules are seen to cluster in synapses.

GSDIM data are invaluable for defining, with the highest possible resolution, the spatial distributions of endogenous proteins. However, due to individual molecules moving between states of fluorescence this technique prevents further statistical analysis, as discussed in Chapter 5. To overcome these limitations, this study next used PALM to compare the distribution of heterologous munc18-1 and syntaxin with the spatial pattern of endogenous molecules ascertained using GSDIM.

6.3 Concentration of heterologous munc18-1 and syntaxin in synapses.

PALM optically resolves fluorescent proteins to molecular resolution through the serial photo-activation and -irreversible photo-destruction of subsets of photoactivatable molecules (Betzig et al, 2006). Thus, to achieve the highest possible resolution of single heterologous munc18-1 and syntaxin molecules in primary cortical neurons, PALM imaging was employed. DIV 14 cortical neurons co-expressing either photoactivatable (PA)-mCherry-munc18-1/ EGFP-syntaxin (EGFP provided diffraction-limited resolution data) or conversely, PA-mCherry-syntaxin/ EGFP-munc18-1 were chemically fixed 2 days post transfection and examined. Positional information describing PA-mCherry-syntaxin and PA-mCherry-munc18-1 molecules was subsequently rendered into molecular maps, where exogenous munc18-1 and syntaxin molecules were seen to co-cluster with one another in varicosities (Figure 6.2 and 6.2B).

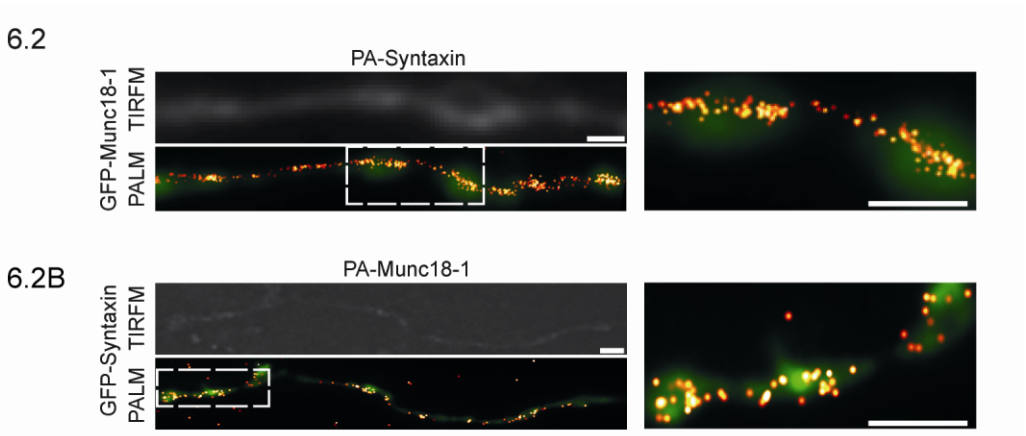

Figure 6.2. *Heterologous munc18-1 and syntaxin colocalise with each other in neuronal varicosities*. All frames containing either munc18-1 or syntaxin signals from single molecules were summed and displayed as an intensity image to approximate a diffraction limited image (*greyscale, top left panels*). PALM localisation maps show single molecules of PA-mCherry-syntaxin (n = 5 cells) or PA-mCherry-munc18-1 (n = 6 cells, 6.2B) clustering with either EGFP-munc18-1 or EGFP-syntaxin respectfully (*bottom left panels*). The boxed regions are displayed at a higher zoom (*right panels*). Scale bars, 500 nm.

In order to determine whether these areas represented nerve terminals, neurons were transfected with PA-mCherry-syntaxin, fixed 48 hours later and co-immunolabelled against synapsin. PALM imaging confirmed that single syntaxin molecules clustered at synapsin positive synapses (Figure 6.3). This molecular distribution, with sparse and largely individual molecules in processes but dense accumulations in synapses, suggests that molecules are trafficked along axons before accumulation and retention in pre-synaptic areas.

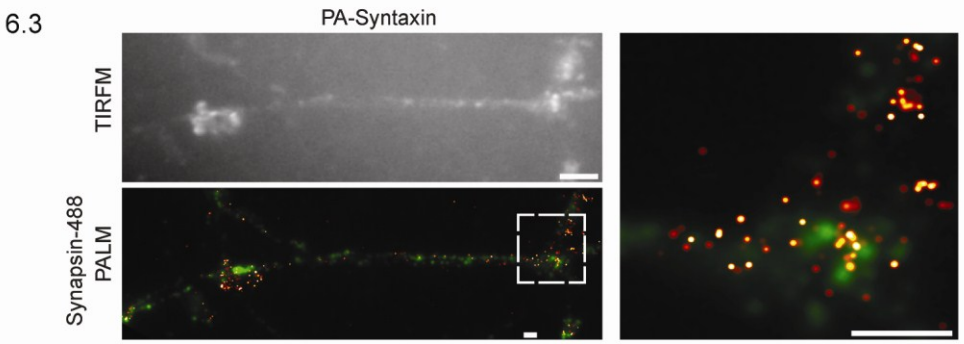

Figure 6.3. *Syntaxin molecules accumulate at synapses*. DIV 14 cortical neurons expressing PA-syntaxin were fixed and immunolabelled with synapsin-488 (*left bottom panel*). All localised PA-syntaxin single molecules were summed to approximate a conventional diffraction limited image (*top left panel*), $n = 4$ cells. Scale bar 5 μm. A rendered map of single molecules at a higher magnification within the boxed region of a neuron (*right panel*) displays the co-clustering of syntaxin molecules with synapsin. Scale bar 500 nm.

Following the confirmation that both munc18-1 and syntaxin proteins were restricted to synaptic terminals it was of interest to next quantify their molecular movements within these regions of a live neuronal cell using sptPALM, a technique introduced in Chapter 5 (Manley et al, 2008).

6.4 SINGLE MUNC18-1 MOLECULES EXHIBIT RESTRICTED KINETICS WITHIN SYNAPTIC TERMINI OF LIVE NEURONAL CELLS.

Single munc18-1 molecules were localised under sptPALM imaging and tracked using Imaris (Bitplane), with single molecule trajectories shown as tracks with colour corresponding to the start (*blue*) and end (*white*) of the acquisition (Figure 6.4, n = 1302 molecules, n = 4 experiments). As hypothesised, munc18-1 molecules in synapses exhibited a caged and restricted motion, as shown by both the speed and displacement of tracks within varicosities of the neuronal cell, typically only moving between 0.046-0.107 μm/s in length (Figure 6.4B). Outside synapses a spatially distinct population of munc18-1 molecules displayed directed movement, travelling in straight tracks and at greater speed between nerve terminals and moving up to 2.6 μm in length between synapses (Figure 6.4B).

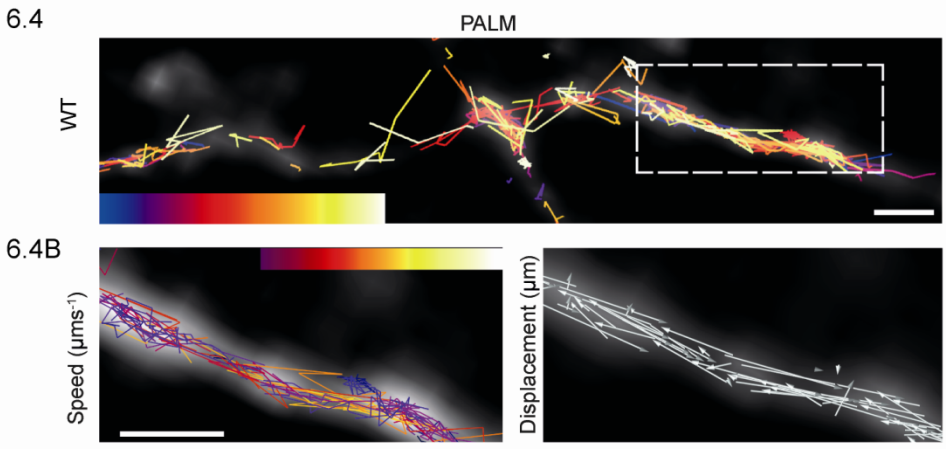

Figure 6.4. *The movement of munc18-1 molecules in synapses is restricted.* Summed images (grey) of cortical neurons co-transfected with PA-mCherry-munc18-1 and EGFP-syntaxin (*top panel*). Munc18-1 single molecule tracks are overlaid. The summed images in grey approximate diffraction limited imaging, and indicate the outline of the neurons. Single molecule trajectories are shown as tracks with colour corresponding to the start (*blue*) and end (*white*) of the acquisition (*top panel*). 6.4B. Munc18-1 molecular tracks from the boxed region in the top panel were colour coded in terms of track speed (purple - slow, white - fast, *bottom left panel*) and the displacements of all munc18-1 single molecule tracks are represented in arrow form (the arrow connects the start and end point of each molecular trajectory, *bottom right panel*). Scale bar 5 µm.

Munc18-1 has been shown to be essential in the trafficking of syntaxins to membrane fusion sites in neuroendocrine cells (Rowe et al, 1999, 2001; Medine et al, 2007). Within their neuronal counterparts current models suggest that the pre-synaptic localisation of munc18-1 is also attributed to its high affinity interaction with syntaxin (Pevsner et al, 1994a; Gerber et al, 2008). In neuronal cells this trafficking function is less well defined, principally because, until recently, imaging approaches lacked sufficient spatial and temporal resolution to determine molecular localisations in neuronal preparations (Kim et al, 2010). Could the distinct and directed kinetics of munc18-1 molecules in axons and dendrites be attributed to its high affinity interaction with syntaxin? In order to address this question the interaction between munc18-1 and syntaxin was abolished by prohibiting syntaxin from adopting its closed conformation ("open"; L165A, E166A; Dulubova et al, 1999) and deleting its N-terminal interaction motif (Δ6; Rickman et al, 2007). It has been previously shown that syntaxin1a^{open}Δ6 has a greatly reduced k_d for munc18-1, eliminating interaction in living cells and acting in a dominant negative manner affecting single vesicle dynamics and exocytosis (Rickman et al, 2007).

sptPALM experiments were performed with DIV 14 neurons transfected with PA-mCherry-munc18-1 and syntaxin1a^{open}Δ6, acquiring PALM data with a 30 frame-per-second rate (Figure 6.5). Single particle tracking revealed that (n = 956 molecules, n = 3 experiments) track speed increased within synapses, as shown by the coloured tracks, but displacement, the distance between the start and the end points of each track, decreased outside synapses, indicating that the molecules had lost directionality and were moving in an unregulated manner (Figure 6.5B). Importantly, the displacements of the kinetically distinct population of munc18-1 molecules within synapses remained apparently unaltered.

This study next compared the 10% fastest molecules between syntaxin and syntaxin (open Δ6) - expressing neurons, following the finding that munc18-1 molecular speed in axons is higher than in synapses (Figure 6.4B and 6.5B). Munc18-1 molecules in the presence of interaction-deficient syntaxin were found to move in an uncoordinated manner in neuronal processes (Figure 6.5C). The slowest decile of all munc18-1 molecules was relatively unaltered (slowest 5% WT = 4.68% molecules, mutant = 4.81%) in the presence of interaction-deficient syntaxin and was localised to synapses. The dramatic effect of

disrupting the inter-molecular interaction with syntaxin on munc18-1 molecular behaviour demonstrates that this interaction is indeed required for the efficient trafficking of munc18-1 along neuronal processes, but surprisingly, not for the accumulation and retention of munc18-1 molecules in synapses.

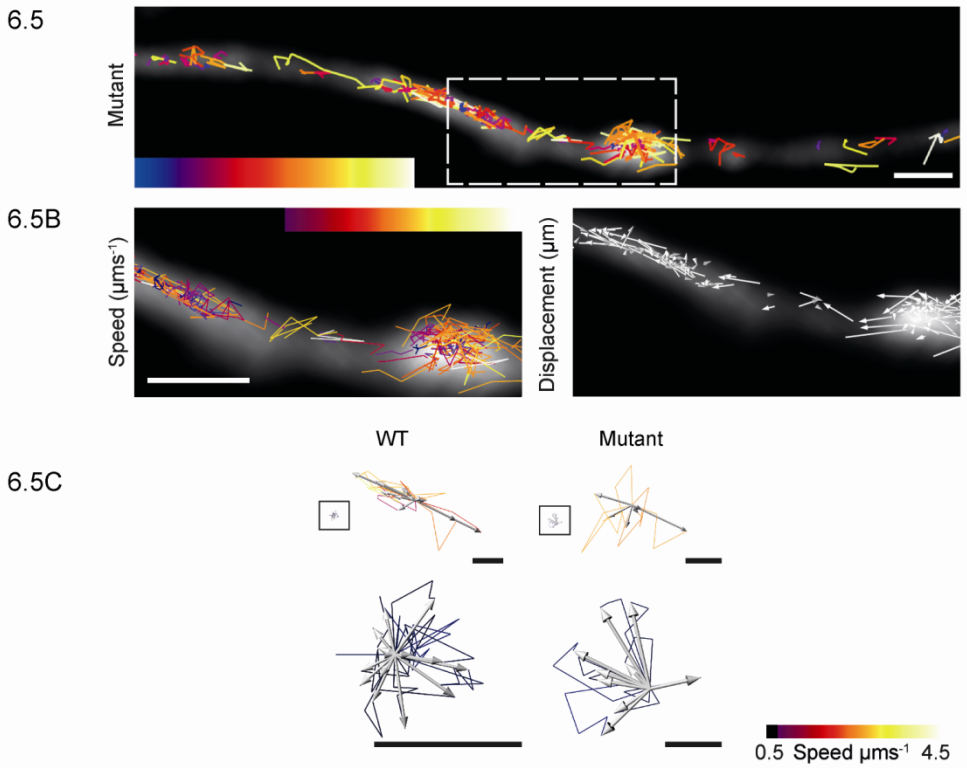

Figure 6.5. *Munc18-1 molecules do not require syntaxin interaction to localise in synapses*. Summed images (grey) of cortical neurons co-transfected with PA-mCherry-munc18-1 and EGFP-syntaxin(openΔ6). Munc18-1 single molecule tracks are overlaid. The summed images in grey approximate diffraction limited imaging, and indicate the outline of the neurons. Single molecule trajectories are shown as tracks with colour corresponding to the start (*blue*) and end (*white*) of the acquisition (*top panel*). Scale bar 5 µm. 6.5B. Munc18-1 molecular tracks from the boxed region in the top panel are colour coded in terms of track speed (purple - slow, white - fast) and the displacements of all munc18-1 single molecule tracks are represented in arrow form (the arrow connects the start and end point of each molecular trajectory). Munc18-1 molecules in the presence of interaction-incapable syntaxin do not exhibit the long, directed motions in the neuronal processes seen in the presence of wild-type syntaxin, but synaptic localisation is maintained. Scale bar 5 µm. 6.5C. Munc18-1 molecular tracks from the boxed regions of the top panels in figure 6.4 and 6.5 were translated so that their start points all originate from the same point, whilst maintaining length and direction. This provides a visualisation tool to compare multiple tracks from different samples. The fastest and slowest moving 10% of munc18-1 molecules were extracted from the distribution of all track speeds and colour coded for speed, with displacement arrows superimposed (upper panels, scale bar 500 nm). This emphasizes the loss of directionality in the presence of interaction-deficient syntaxin compared to wild-type syntaxin. The slowest 10% of tracked munc18 molecules are shown boxed as these have constrained, short trajectories, confined to synapses. The lower panels represent a zoom of the boxed areas, scale bar 100 nm.

Imaris is the most powerful commercially available software for the tracking and analysis of single particles. However, a major problem with this package is its inability to correctly identify all fluorescent molecules in a relatively noisy image (due to low illumination and fast acquisition speeds) to ensure that all particles have a relationship between time points. Due to the immense number of molecules contained within each dataset and to avoid artefacts and inaccuracies in the tracking process this study decided to use particle tracking algorithms written and conducted by Lei Yang, Heriot-Watt University, Edinburgh, as introduced in Chapter 5. These algorithms proved to be more accurate at identifying all fluorescent objects and accurately joining them together as part of a track. Furthermore this more accurate tracking algorithm had the capability to dissect molecular speed and directionality, thus enabling more reliable quantification of molecular movements in such dynamic, noisy images.

6.5 SINGLE MUNC18-1 MOLECULES ARE CAGED WITHIN NEURONAL CELLS.

Using this custom designed tracking algorithm combined with detailed analysis of molecular trajectories it was possible to accurately probe the directionality of single munc18-1 molecules in a living neuron. This analysis revealed no directional preference of munc18-1 molecules in their choice of initial track movements (Figure 6.6; n = 6584 munc18-1 molecules, n = 3 cells), indicating complete freedom of directional motion for munc18-1 molecules regardless of syntaxin interaction (6.6B; n = 9499 munc18-1 molecules tracked in the presence of dominant negative syntaxin1a$^{open}\Delta 6$, n = 3 cells). A significant difference was found, however, in molecular speed; in the presence of interaction-incapable syntaxin munc18-1 molecules had significantly faster velocities (Figure 6.6B), as shown previously with Imaris software (Figure 6.5). This increase in speed might be expected if soluble molecules no longer interacted with a transmembrane protein.

6.6

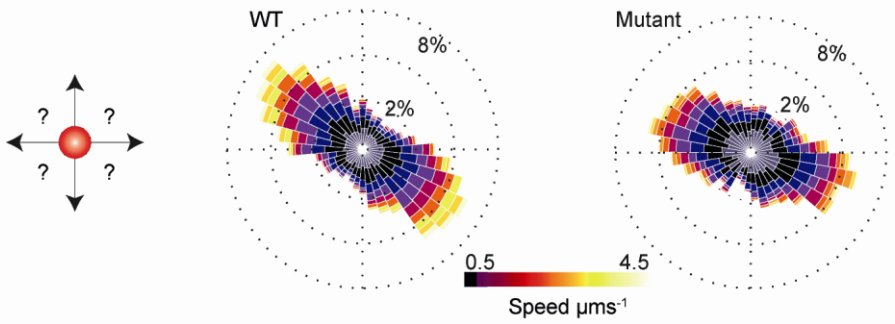

6.6B

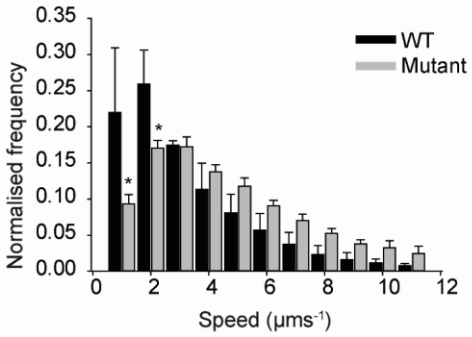

Figure 6.6. *Analysis of the directionality of single munc18-1 molecules within live neuronal cells*. The angle of momentum was calculated for every munc18-1 molecule tracked (1613 tracks in the presence of wild-type EGFP-syntaxin, 3605 tracks with syntaxin1aopenΔ6), assuming no prior knowledge of direction (*cartoon, left*). A circular histogram ('Rose diagram') was generated, accumulating track angles into 36 bins. Amplitude of each bin indicates the number of tracks, colour coding is for speed (blue – slow – yellow – fast). Percentages indicate bin amplitude as a fraction of the total tracks. Molecules show a complete freedom of choice of initial track direction, following the direction of the neuronal processes.6.6B Combined calculated molecular speeds from multiple experiments (wild-type: 6584 tracks, mutant = 9499 tracks, $n = 3$ independent experiments). Munc18-1 molecules move significantly faster when interaction with syntaxin is disrupted (Two way ANOVA, asterisk indicates $p < 0.05$).

This study, as compared with Chapter 5, put forward a more detailed question of the munc18-1 molecular motion data; once moving in a particular direction, where do single molecules go next? (Figure 6.7) Analysing the trajectory angle taken by every molecule at the second position of a trajectory (Figure 6.7B), relative to the previous movement, found that single munc18-1 and mutant molecules were highly likely to reverse their directions once already moving forward (Figure 6.7B).

6.7

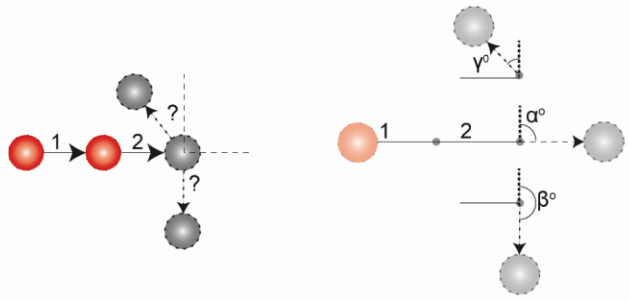

6.7B

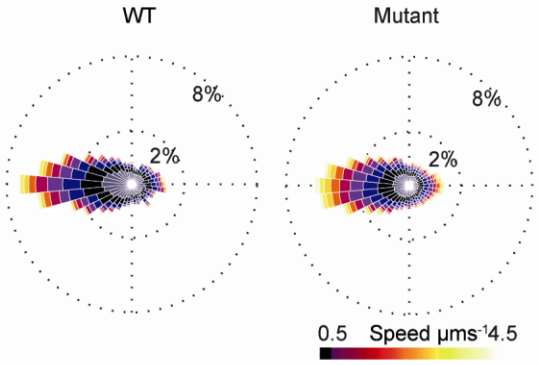

Figure 6.7. *Munc18-1 molecules are likely to reverse in trajectory following their initial movement*. Combined track angles measured between the second and third positions of every munc18-1 molecule trajectory was calculated, using a priori information of direction the angle of momentum. 6.7B. This analysis revealed that molecules are highly likely to reverse after moving forwards for a short distance. Rose diagrams were plotted (wild-type: 6584 tracks, mutant = 9499 tracks) showing this behaviour is unaffected by syntaxin interaction.

As with neuroendocrine cells, the reason for this reversing behaviour could be either due to a 'zig-zag' motion, overlying a general linear directionality, or due to a 'caged' motion, where molecules are able to move only a certain distance from their origin (Figure 6.8). These two possibilities can be distinguished by correlating track length with displacement (Figure 6.8B). This analysis revealed that the majority of munc18-1 molecules had a caged motion, never moving more than 1 μm in a single direction before reversing; furthermore, this behaviour was not dependent on an interaction with syntaxin (Figure 6.8B). It could be reasoned that this 'trapping' of munc18-1 molecules may be responsible for the endogenous and heterologous molecular distribution seen in fixed samples (Figure 6.1), where single munc18-1 molecules accumulate in nerve terminals. To confirm this, 'contour maps', quantifying the density of molecular tracks over every pixel of an image, were plotted (Figure 6.8C). This approach illustrated that munc18-1 molecules accumulate in varicosities across the neuronal cell and that this distribution is not dependent on syntaxin interaction. Despite the fact that this mutant has previously been shown to act in a 'dominant-negative' manner (Rickman et al, 2007), it should be mentioned that endogenous syntaxin might be rescuing the mutant cells to a certain extent.

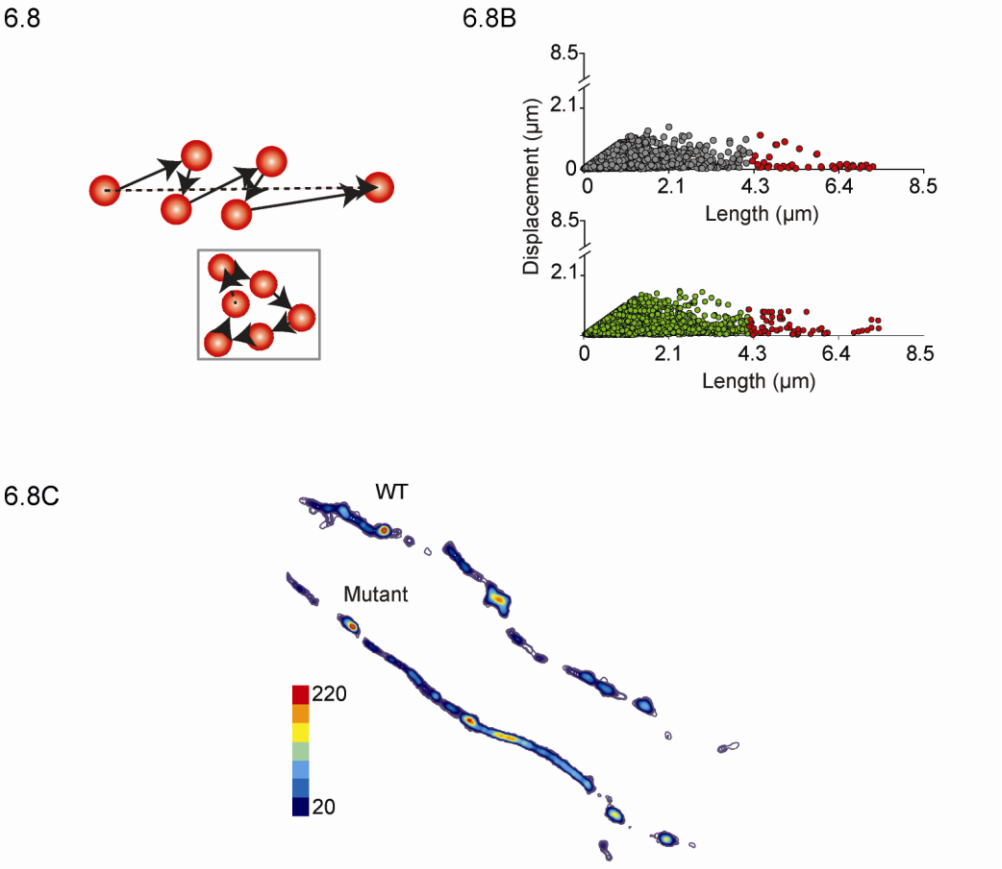

Figure 6.8. *Munc18-1 molecules exhibit caged motion within neuronal processes*. The reversal behaviour seen in the Rose diagrams in figure 6.7 could be due to a 'zig-zag' or a 'caged' motion (*cartoon*). These two possibilities can be dissected by correlating the total track length (shown as a solid arrows) with track displacement (dashed arrow). 6.8B. These plots show that trajectories with long track lengths but short displacements (red points) are maintained both with wild-type syntaxin (*upper graph*, grey points) and when interaction is abolished (*lower graph*, green points). 6.8C. A density plot showing number of molecular tracks crossing each pixel in the image, colour coding is for track number. This figure illustrates that munc18-1 molecules accumulate in varicosities across the neuronal cell and that this distribution is not dependent on syntaxin interaction.

6.6 MUNC18-1 AND SYNTAXIN INTERACT IN A HETEROGENEOUS MANNER ACROSS LIVE NEURONAL NETWORKS.

Munc18-1 has been attributed to a range of essential functions, as a chaperone (Rowe et al, 1999; Medine et al, 2007), as a 'docking factor' (Voets et al, 2001), acting with SNAP-25 and synaptotagmin (de Wit et al, 2009), and as an essential modulator of the very latest stages of synaptic vesicle fusion (de Wit et al, 2009), even shaping fusion pore kinetics (Fisher et al, 2001; Jorgacevski et al, 2011). These distinct functions suggest a molecular interaction pathway between docking and fusion (Gerber et al, 2008), as it is accepted that munc18-1 must regulate vesicle exocytosis via interaction with the N-terminus of syntaxin (as opposed to 'closed' syntaxin interaction) in the ternary SNARE complex (Shen et al, 2007). This hypothesis supports the earlier finding that syntaxin interaction is not required for the synaptic retention of munc18-1 (Figure 6.5), but suggests an activity-dependent interaction switch on the millisecond-timescale immediately preceding exocytosis in nerve terminals.

As an initial test of this hypothesis, fluorescence lifetime imaging microscopy was employed to measure Förster resonance energy transfer (FRET) between proximal (within 5 nm) acceptor (syntaxin) and donor (munc18-1) molecules in living neurons. The donor, mCerulean-syntaxin, in the presence of unfused EYFP, had a single fluorescence lifetime at the plasma membrane (Figure 6.9, *green line*) in agreement with previous findings (Medine et al, 2007; Rickman et al, 2007). However, in the presence of the FRET acceptor EYFP-munc18-1, a second fluorescence lifetime component was reported, indicating a specific protein-protein interaction (Figure 6.9, *red line*). FLIM analysis showed a statistically significant quenching of the mean fluorescence lifetime of donor mCerulean-syntaxin from 2155 ± 90 ps (mean ± S.E., n = 13 experiments), in the absence of a proximal FRET acceptor, to 1295 ± 130 ps (mean ± S.E., n = 10 experiments) in the presence of EYFP-munc18-1 (Figure 6.9B), indicative of FRET. The weighted mean fluorescence lifetime data, containing both interacting and non-interacting values and their respective amplitudes, was bimodal (Figure 6.9) due to two spatially segregated types of munc18-1-syntaxin interactions containing different FRET efficiencies.

6.9

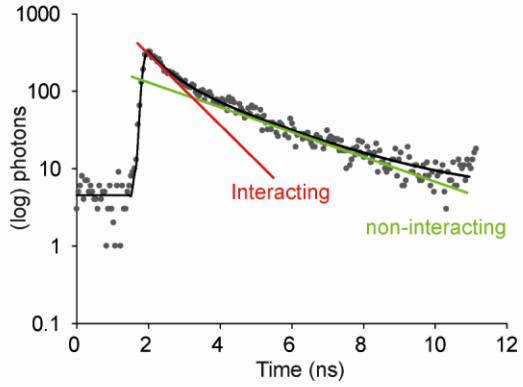

6.9B

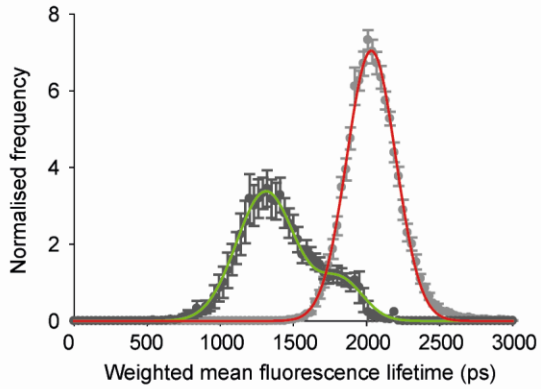

Figure 6.9. *TCSPC-FLIM reports a molecular interaction between munc18-1 and syntaxin within a live neuron*. FLIM was used to quantify the extent of interaction between munc18-1 and syntaxin. Cortical neurons were transfected with mCerulean-syntaxin and EYFP-munc18-1 on DIV 14 and imaged 48 hours post transfection. TCSPC-FLIM analysis confirmed that in the absence of an EYFP acceptor syntaxin followed a single fluorescence decay (dark gray). In the presence of a proximal acceptor (EYFP-munc18-1), this decay was described by a bi-exponential decay (light gray). The time constants of the bi-exponential functions correspond to a short FRET lifetime (red line) and a longer fluorescence lifetime identical to the non-FRET control (green line). 6.9B. The weighted mean fluorescence lifetime values were plotted as a frequency distribution histogram with a mean fluorescence lifetime of 2155 ± 90 ps (mean ± S.E., n = 13 cells) in the absence of an EYFP acceptor. Expression of EYFP-munc18-1 resulted in a quenching of the fluorescence lifetime to 1295 ± 130 ps (mean ± S.E., n = 10 cells), a fluorescence decay better fit by a double-Gaussian distribution. This indicates interaction heterogeneity across neuronal networks.

In order to determine where munc18-1 and syntaxin were interacting across a neuronal network every pixel in the image was assigned a colour corresponding to non-interacting and interacting FLIM values (*red - non-interacting, green - interacting*). Plotting this figure revealed that munc18-1 and syntaxin interactions were distributed across the neuronal cell in a heterogeneous manner and importantly, interactions in varicosities were detected only some of the time (Figure 6.10).

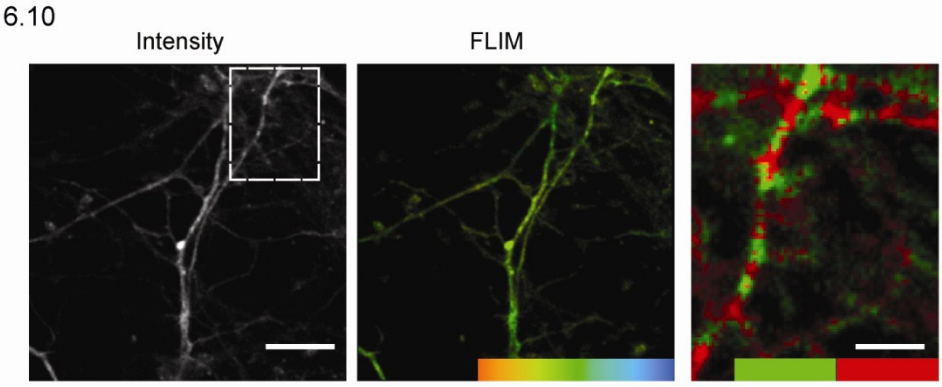

Figure 6.10. *Munc18-1 and syntaxin interact heterogeneously across a network of neurons*. Intensity (gray scale) and fluorescence lifetime images on a colour scale from 1250 to 2250 ps (red – 1250 ps – blue – 2250 ps) are shown, for neuronal networks co-expressing mCerulean-syntaxin and EYFP-munc18-1. The boxed area in the intensity image is zoomed and the binary colour scale selected according to the double-Gaussian fit shown in Figure 6.11. Green values – 500-1600 ps (FRET), red values 1600-2500 ps (non-interacting). Both the FRET and non-FRET components are present in varying proportions and in a heterogeneous manner across live neuronal networks. Scale bars: 5 μm.

After demonstrating a spatially restricted interaction between munc18-1 and syntaxin this study next probed whether this heterogeneous interaction was regulated by neuronal activity. Sixty second FLIM recordings were taken of EYFP-munc18-1 and mCerulean-syntaxin expressing live DIV 14 cortical neurons before and after increasing the intracellular level of Ca^{2+} by the addition of 5 μM ionomycin (Liu and Hermann, 1978). Plotting every pixel in the image but assigning donor fluorescence lifetime value a colour revealed that areas on the plasma membrane contained significantly less energy transfer, confirming that the munc18-1-syntaxin interaction was spatially regulated (Figure 6.11). Perhaps surprisingly, cellular stimulation did not result in a change in the level of molecular interaction, with the proportion of interacting and non-interacting molecules remaining unaltered (Figure 6.11B). This may reflect the fact that the munc18-1-syntaxin interaction is not just dependent on Ca^{2+} and may involve a cascade or pathway downstream of depolarisation.

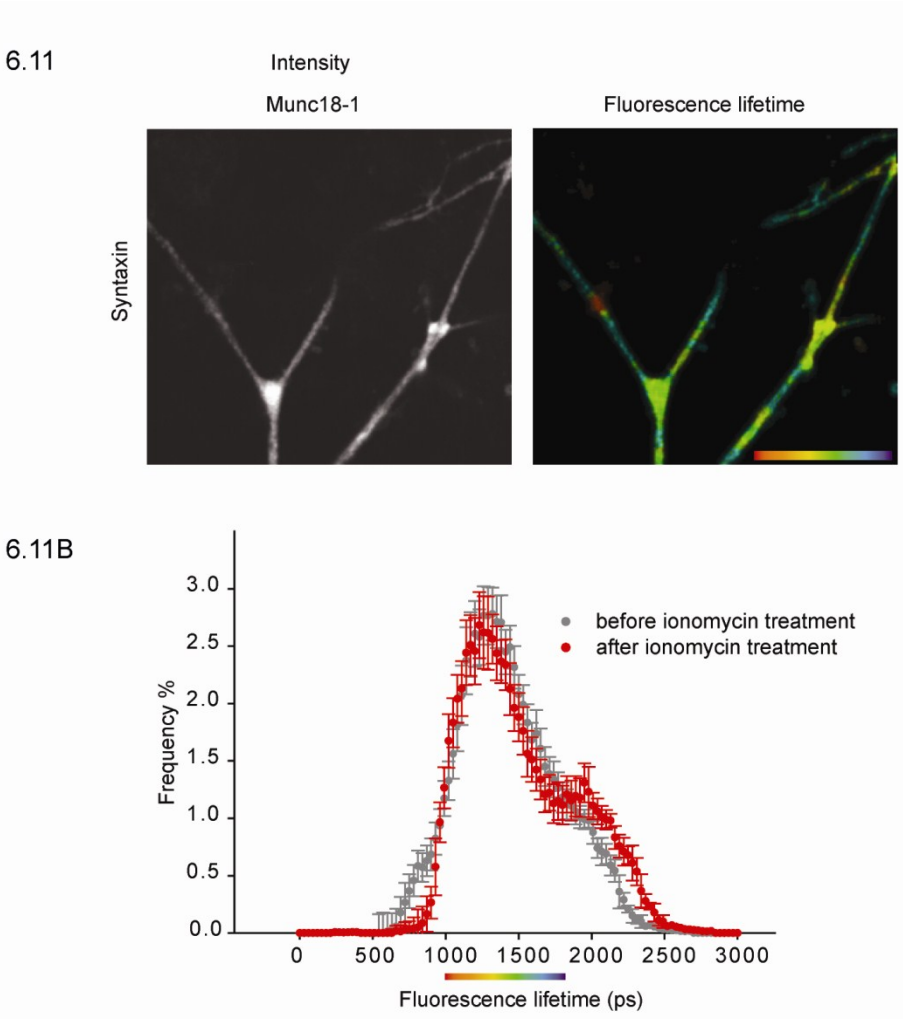

Figure 6.11. *The interaction between munc18-1 and syntaxin recorded by TCSPC-FLIM is not altered upon evoked neuronal activity.* Intensity (gray scale) and fluorescence lifetime images on a colour scale from 1250 to 2250 ps (red – 1250 ps – blue – 2250 ps) are shown for DIV 14 neurons co-expressing mCerulean-syntaxin and EYFP-munc18-1. 6.13B. Weighted residuals of syntaxin and munc18-1 before (grey lines, n = 6) and after (red lines, n = 8) the addition of 5 µM ionomycin were plotted as a frequency distribution histogram. There was no difference in the proportion of interaction between munc18-1 and syntaxin upon cellular depolarisation.

FLIM represents a state-of-the-art technique for delivering information describing both molecular lifetimes and the proportion of molecules participating in energy transfer (Duncan et al, 2004). Despite its advantages FLIM suffers from slow temporal resolution and diffraction-limited spatial resolution (Duncan et al, 2004). It is therefore possible that FLIM does not possess the adequate sensitivity to report an activity dependent change in interaction status between munc18-1 and syntaxin, an interaction that is likely to occur on a faster time-scale.

All molecular imaging techniques so far used in this thesis, namely GSDIM, PALM and FLIM, lack the required temporal resolution to be able to visualise dynamic protein-protein interactions. Measuring a dynamic molecular event in a synapse would ideally require a non-invasive molecular resolution technique with exquisite temporal resolution. To achieve sufficient resolution and observe highly regulated molecular events specific to a living synapse this study next employed fluorescence correlation spectroscopy (FCS). FCS performs correlation analysis of fluctuations in fluorescence intensities caused by the entry and exit of single fluorescent molecules into and out of a small excitation volume (Figure 6.12; Kim et al, 2007). Analysis of accumulated molecular fluctuations, acquired on a μs timescale, delivers quantitative information on molecular number, concentration, rate of diffusion and interaction status (Kim et al, 2010).

6.12

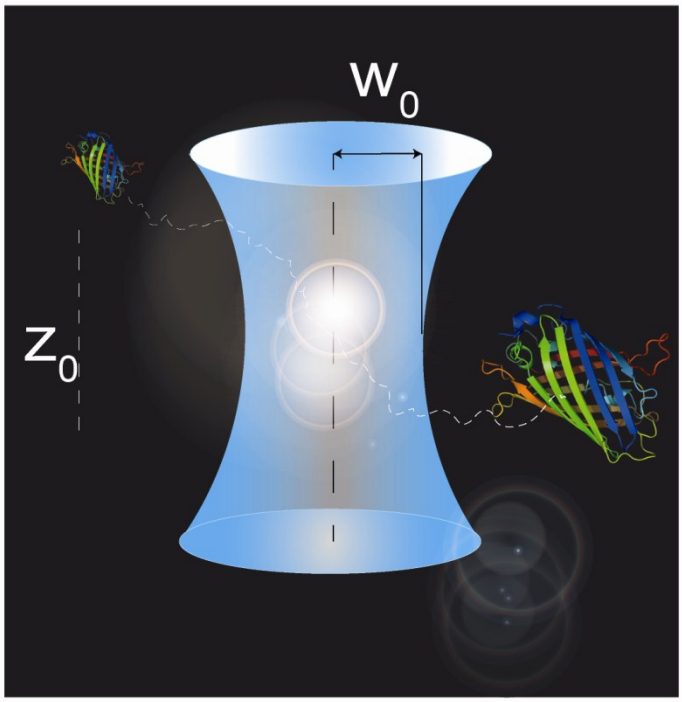

Figure 6.12. *Fluorescence Correlation Spectroscopy (FCS).* Fluorescence Correlation Spectroscopy (FCS) was used to determine the munc18-1-syntaxin interaction status in synapses before and during exocytosis. Single fluorescent molecules emit bursts of photons as they move across a small (<1 femtoliter) excitation volume 'parked' on a synapse. The dimensions of the excitation spot (w0 and z0) are determined experimentally.

6.7 THE ACCURACY OF FLUORESCENCE CORRELATION SPECTROSCOPY IN REPORTING PROTEIN-PROTEIN INTERACTION *IN VITRO*.

The ability of FCS to report molecular interactions and diffusion rates using highly purified fluorescent proteins in solution was initially determined. FCS was performed using defined concentrations (10 nM) of EGFP and mCherry (Chapter 2, section 2.5.2). When mixed in solution, no cross-correlation between the photon fluctuations occurred, indicating that the two proteins did not interact (Figure 6.13). Repeating the experiment using an EGFP-mCherry fusion protein yielded FCS autocorrelation curves for green and red fluorescence with identical decay constants (indicative of similar diffusion rates) and substantial cross-correlation indicating that both fluorescent molecules behaved in an identical spatio-temporal manner in the excitation volume (Figure 6.13B).

The rate of diffusion of EGFP-munc18-1 molecules in a cellular environment was next quantified. For this, HEK-293 cells were chosen, known not to express syntaxin1 or any other munc18-binding proteins (Rowe et al, 1999). Munc18-1 in this cellular expression system was cytosolic, and FCS autocorrelation analysis yielded a diffusion rate of 9.26 ± 1.86 $\mu m^2 s^{-1}$ (mean ± SEM, n = 9 independent experiments). This molecular diffusion was slower than for cytosolic unfused EGFP (D = 19.66 ± 1.06 $\mu m^2 s^{-1}$, also slower than EGFP in solution *in vitro*), because munc18-1-EGFP has a greater molecular mass than EGFP (Figure 6.13C).

6.13

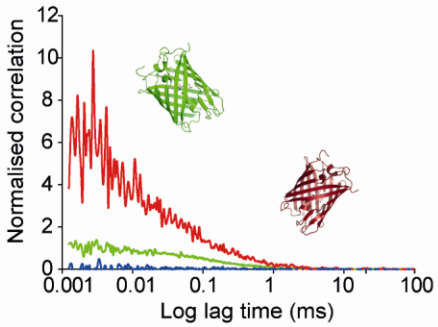

6.13B

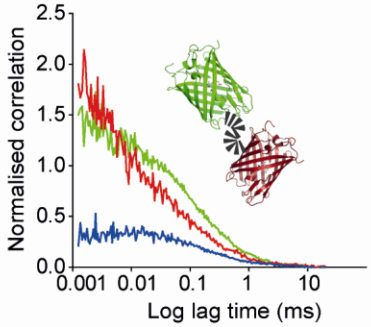

6.13C

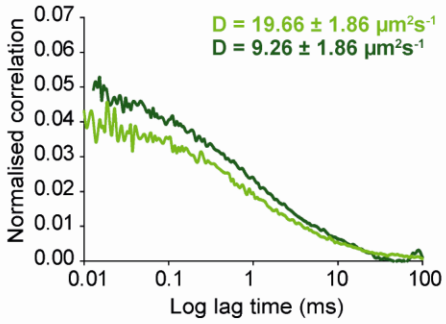

Figure 6.13. *Characterisation of the FCS system using highly purified fluorescent proteins.* 10 nM of each of EGFP and mCherry were mixed and FCS recordings made. Autocorrelation curves are shown for both, showing EGFP (green curve) and mCherry (red curve) to have independent rates of diffusion. Negligible cross-correlation (blue curve) is apparent. 6.13B. 10 nM of purified EGFP-mCherry fusion protein was analysed using FCS in the same way. Both green and red proteins now exhibit similar diffusion rates and concentrations (indicated by autocorrelation amplitude). Cross-correlation of the photon fluctuation signals (blue curve) confirm that both fluorescent proteins behave in the same way in the excitation spot. 6.13C. A representative FCS autocorrelation trace of cytosolic EGFP-munc18-1 (light green line) and EGFP alone (dark green line) was measured in HEK-293 cells. The rates of diffusion were calculated from the derived autocorrelation curves (Inset numbers, mean ± SEM, n = at least 9 independent experiments).

6.8 MUNC18-1 AND SYNTAXIN DIFFUSE AT SIMILAR RATES BUT DO NOT INTERACT IN A RESTING SYNAPSE.

Whilst the SNARE hypothesis model remains compatible with a large body of experimental evidence (Schiavo et al, 1992; Blasi et al, 1993b; Protopopov et al, 1993), the precise sequence of molecular interactions that precede and promote SNARE complex formation and vesicular fusion within an intact nerve cell are still unclear. In order to determine the dynamics of munc18-1 and syntaxin in living neurons this study next focused on acquiring data from synapses containing EGFP-munc18-1 and mCherry-syntaxin (Figure 6.14; Kim et al, 2010). Synapses containing the lowest detectable fluorescence were selected for analysis, and both the EGFP-munc18-1 and mCherry-syntaxin photon count fluctuations were measured with a 2 μsec acquisition rate. Auto-correlation curves for these data accumulated over 5 - 10 seconds were generated, delivering similar diffusion rates for munc18-1 and syntaxin molecules (5.19 ± 0.84 $\mu m^2 s^{-1}$ and 3.26 ± 0.83 $\mu m^2 s^{-1}$, respectively; mean ± S.E.M., $n = 20$ independent experiments; Figure 6.14B).

Accurate measurement of membrane protein diffusion may be hampered by membrane flow and other confounding factors (Weiss et al, 2003); however, the relatively short diffusion time for syntaxin is in agreement with that measured for other trans-membrane proteins in cells (Weiss et al, 2003; Bacia et al, 2004). Within a resting synapse munc18-1 and syntaxin have similar rates of diffusion which are not statistically different from one another (unpaired t-test). The fact that both proteins are moving at the same rate is an indication of a protein-protein interaction. However, little or no cross-correlation was detected between munc18-1 and syntaxin molecular fluctuations in the majority of experiments suggesting the idea that both proteins are not interacting in a resting synapse. Also, the rate of synaptic munc18-1 in synapses appears slower than in the cytosol of HEK293 cells (Figure 6.13C), indicating that it cannot be free in the pre-synaptic cytosol and must therefore be bound via a syntaxin-independent interaction.

6.14

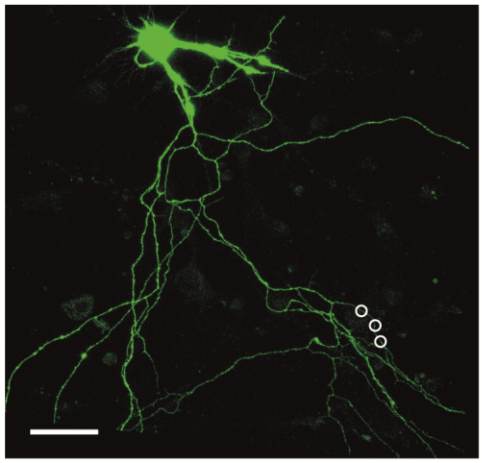

6.14B

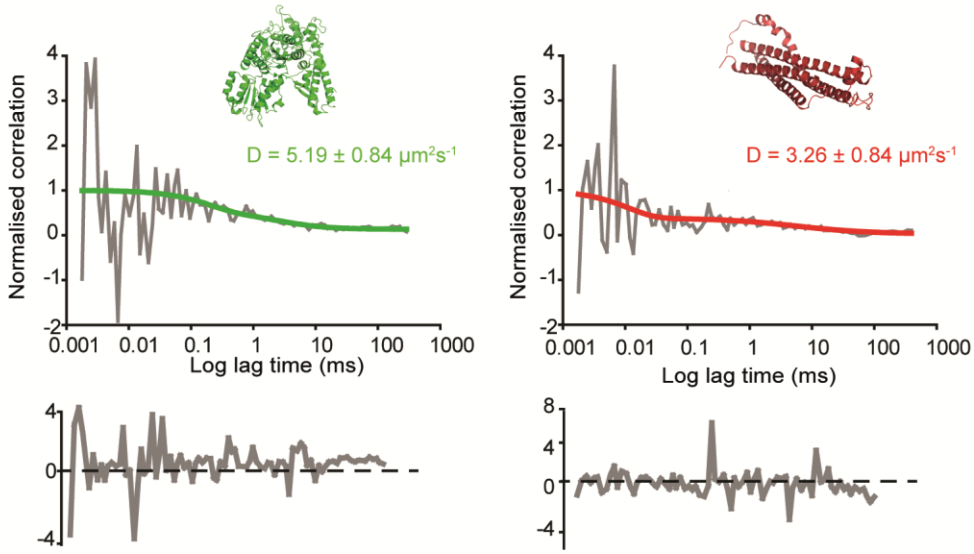

Figure 6.14. *Munc18-1 amd syntaxin display similar diffusion rates in a resting synapse*. A representative DIV 14 cortical neuron transfected with EGFP-munc18-1 and mCherry-syntaxin (not shown) is shown. Circles indicate synapses from where FCS measurements were made. 6.14B. Representative FCS curves acquired from synapses containing both EGFP-munc18-1 (autocorrelation in green) and mCherry-syntaxin (autocorrelation in red). Both proteins have similar rates of diffusion in synapses (n = 20 independent experiments). Plotted residuals of the fit are shown below.

Taken together with the sptPALM and FLIM data, these different measurements confirm that the majority of syntaxin and munc18-1 molecules within varicosities do not interact in resting central synapses before exocytosis. This is consistent with a previous finding showing that despite rbSecl, a SM homologue, and syntaxin1 being localised in the same regions of a nerve cell, the majority of the two proteins are not associated with each other *in situ* (Garcia et al, 1995). Is this finding an indication that non-interacting munc18-1 and syntaxin may serve to inhibit the formation of the synaptic SNARE fusion complex and the catalysis of synaptic vesicle fusion, possibly within and outside active zones? Taking this further, SNARE mediated vesicular fusion may then only be driven through a stable association between munc18-1 and the ternary complex upon neuronal depolarisation.

6.9 Neuronal activity results in a fall in the diffusion rate of syntaxin.

To determine whether neuronal activity could evoke an interaction between munc18-1 and syntaxin, or whether a change in their mobilities could be observed, a 20 Hz train of electrical depolarisations lasting 10 seconds was delivered during FCS recordings. Monitoring of intracellular Ca^{2+} (acquired at a 2 μsec rate, Figure 6.15) confirmed the activity of these nerve terminals. This thesis has previously shown that the same electrical treatment is sufficient to induce synaptic vesicle exocytosis, indicated by FM-dye unloading (Figure 4.9). During stimulation, a decrease in the rate of munc18-1 molecular diffusion from 5.19 ± 0.84 $\mu m^2 s^{-1}$ to 3.17 ± 0.47 $\mu m^2 s^{-1}$ was recorded (Figure 6.15; mean ± S.E.M., n = 15 synapses). Furthermore, the rate of syntaxin molecular diffusion rate significantly decreased upon stimulation, from 3.26 ± 0.84 $\mu m^2 s^{-1}$ to 0.63 ± 0.14 $\mu m^2 s^{-}1$ (mean ± S.E.M., n = 15 synapses, $p < 0.05$, unpaired t-test, Figure 6.15B). This dramatic fall in the diffusion rate of syntaxin might well represent syntaxin entering the ternary SNARE complex to drive synaptic vesicle fusion. It would therefore be of interest to determine whether the diffusion rates of SNAP-25 and synaptobrevin, proteins known to interact with syntaxin, followed a similar trend in mobility upon neuronal activity.

6.15

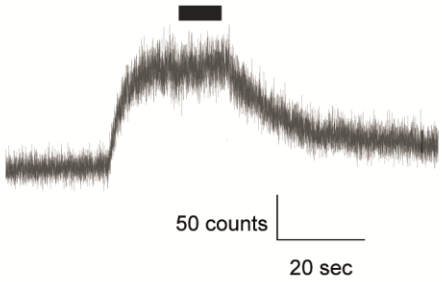

6.15B

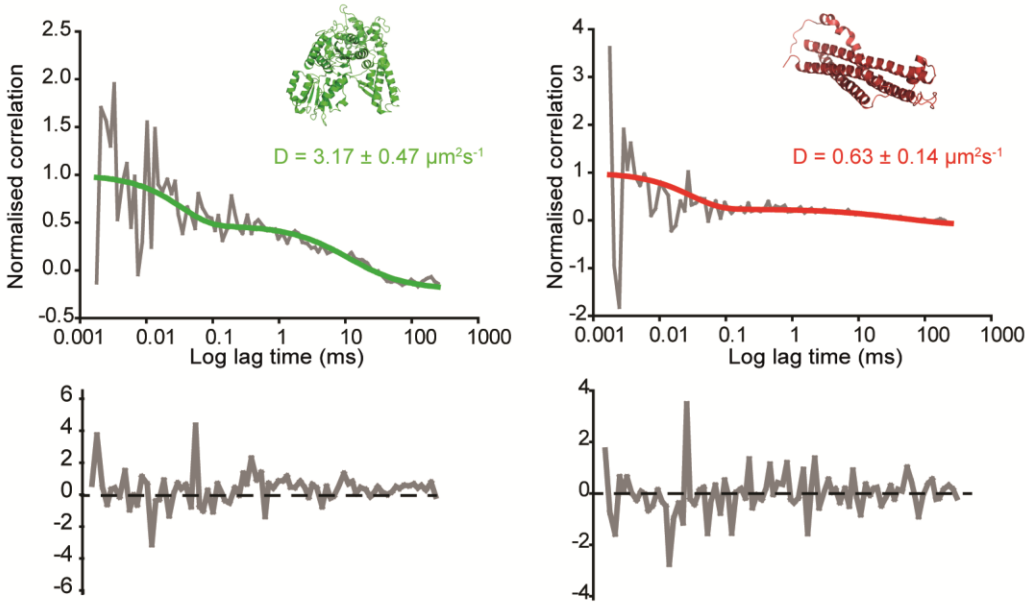

Figure 6.15. *The diffusion rate of syntaxin is reduced upon electrical stimulation*. DIV 14 cortical neurons expressing EGFP-munc18-1 and mCherry-syntaxin were stimulated with 20 Hz action potentials for 20 seconds. Photon fluctuation trace shows response from Fluo-5 indicating Ca^{2+} influx into synapses. Black bar indicates where FCS data were acquired. 6.15B. Representative FCS traces reveal the rate of diffusion of mCherry-syntaxin (red, inset values, mean ± S.E.M., $n = 20$ independent experiments) is significantly reduced ($P < 0.05$, unpaired t-test). Plotted residuals of the fit are shown below.

FCS recordings taken 20 seconds post-stimulation revealed that the diffusion rate of syntaxin (3.21 ± 0.44 $\mu m^2 s^{-1}$, mean ± S.E.M., n = 20 independent experiments, $p < 0.05$, unpaired t-test, Figure 6.16) had recovered to a similar rate recorded immediately prior to stimulation whereas the diffusion rate of munc18-1 had only partially recovered (3.93 ± 0.50 $\mu m^2 s^{-1}$). Furthermore, during and 20 seconds following stimulation, no detectable cross-correlation between munc18-1 and syntaxin molecular fluctuations was observed. Therefore, the finding that both proteins had significantly different diffusion rates with no cross-talk between channels indicated that both proteins were behaving differently within the depolarised synapse – i.e., the molecules were not in a complex (Figure 6.16B). This change in the diffusion rates of munc18-1 and syntaxin may reflect a general mechanism in which they, and possibly other exocytic proteins, modulate neuronal functions. Perhaps the reason it is thought that munc18-1 and syntaxin interact at all times in the literature reflects the lack of available techniques that possess sufficient temporal speed and resolution required to detect such rapid changes in molecular diffusion and interaction status. Furthermore, the fact that variability exists between the level of interaction of munc18-1 and syntaxin during some FCS recordings could be simply attributed to the different regulatory principles imposed on the synapse used in each measurement (de Jong et al, 2012). Earlier this year it was shown that presynaptic sensitivity, vesicular protein expression and vesicular release of a particular synapse were dependent on the distance from the soma (de Jong et al, 2012). Lastly, it is noteworthy to mention that FCS can suffer from limitations, especially when sampling a noisy sample, like a neuron. The fact that no robust protein-protein interaction was detected in the majority of experiments could also be due to the high concentration of proteins positioned at a synapse, hence a low signal to noise ratio. In order to avoid these potential artefacts, neurons expressing low levels of fusion proteins were always selected for experimentation.

6.16

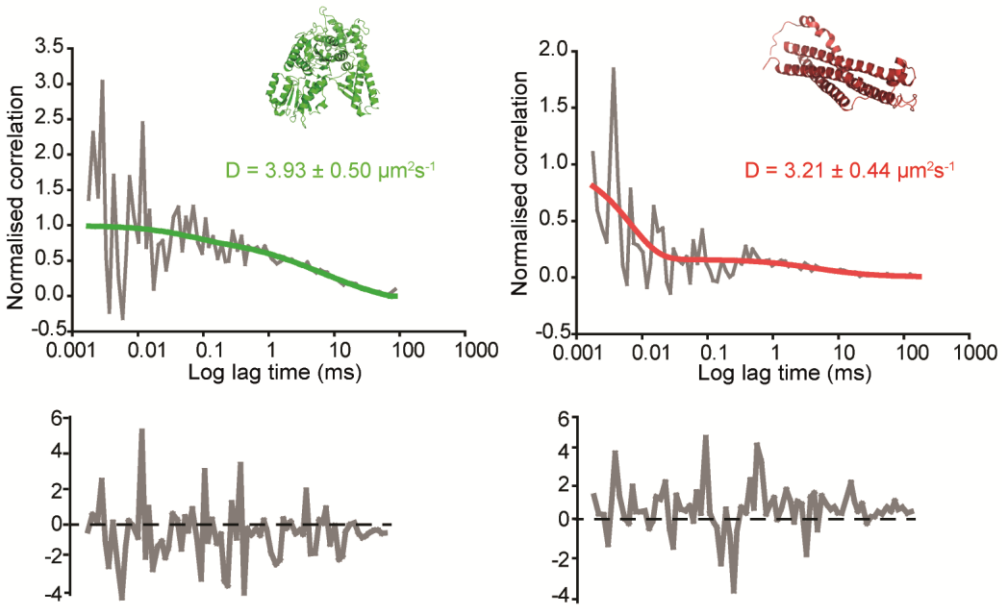

6.16B

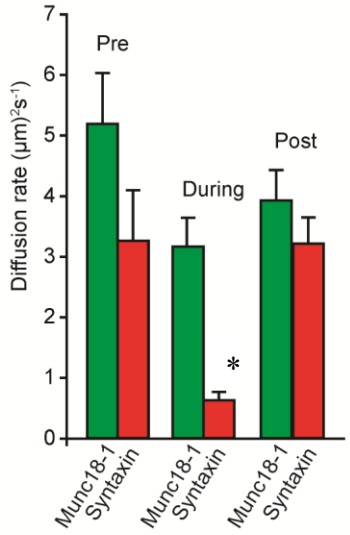

Figure 6.16. *The diffusion rate of syntaxin recovers 20 seconds following stimulation.* DIV 14 cortical neurons expressing EGFP-munc18-1 and mCherry-syntaxin were stimulated with 20 Hz action potentials and FCS recordings were made 20 seconds later. Plotted residuals of the fit are shown below. 6.15B. A graph showing the diffusion rates of both munc18-1 and syntaxin before, during and after electrical stimulation ($P < 0.05$, unpaired t-test between all conditions and syntaxin during stimulation).

6.10 CONCLUSION

SM protein biology has long been controversial; munc18-1 was originally thought to be an inhibitory factor, as it was isolated by virtue of its high affinity interaction with monomeric syntaxin, sequestering it in an inactive form (Pevsner et al, 1994a). Contemporaneous findings that munc18-1 acted at the latest stages of vesicle exocytosis proved controversial (Fisher et al, 2001), but later it emerged that munc18-1 could indeed interact, via a different binding site in syntaxin, with the ternary SNARE complex (Dulubova et al, 2007; Rickman et al, 2007; Shen et al, 2007). Importantly, however, the precise temporal sequence of interactions between the SNAREs and regulators in the run up to synaptic vesicle fusion remains speculative, not least because of a lack of suitable approaches to directly probe molecular localisations, movements and interactions *in situ*.

Over the last few years a number of super resolution techniques have emerged and enabled the investigation of biological structures and mechanisms with a nanosecond spatio-temporal resolution. The advancement of super-resolution techniques have permitted investigation into perhaps one of the most important structures within the nervous system, the synapse, a term coined by Sherrington in 1897 after the Greek word for 'clasp' (Cowan and Kandel, 2001). Using both GSDIM and PALM this study has confirmed that munc18-1 and syntaxin colocalise with each other at synaptic terminals, seen previously on a diffraction-limited level (Bennett et al, 1992; Yoshida et al, 1992; Südhof, 1995; Okamoto et al, 2000). Single molecule imaging PALM has recently been extended to live cells, enabling the non-invasive visualisation of dynamic processes in living cells using genetically encoded fluorescent proteins. Using sptPALM this study also showed that single munc18-1 molecules exhibit two kinetically and spatially distinct populations within a living neuron. A population of restricted, largely immobile munc18-1 molecules are confined to synapses whereas another population exhibits a more directed and faster movement between synapses. This is the first time that divergent munc18-1 behaviours have been observed in a living neuron, a characteristic which could be attributed to the mode of interaction employed in that defined area of the neuron.

It is thought that munc18-1 functions through its direct interaction with syntaxin (Hata et al, 1993; Pevsner et al, 1994a). The universal importance of munc18-1 has been evidenced in a number of organisms, with the genetic manipulation of munc18-1 resulting in deficits in cellular secretion (Novick et al, 1980), syntaxin trafficking (Arunachalam et al, 2008; Medine et al, 2007), large dense core vesicle docking (Voets et al, 2001) and neurotransmission (Gengyo-Ando et al, 1993; Verhage et al, 2000). Despite strong evidence supporting an essential role of munc18-1 in vesicular fusion, it also has to be noted that disrupting the expression of munc18-1 results in a concomitant reduction in syntaxin expression levels (Voets et al, 2001; Arunachalam et al, 2008). Investigating the crucial interaction between munc18-1 and syntaxin on a single molecule level using sptPALM demonstrates that ablating the interaction between munc18-1 and syntaxin severely affects the directionality of munc18-1, resulting in an average decrease in the displacement of munc18-1 molecules. This finding supports the idea that munc18-1 and syntaxin chaperone one another, both requiring a stable interaction in order to facilitate their trafficking and delivery to defined areas of a cell (Rowe et al. 1999, 2001; Medine et al. 2007; Rickman et al. 2007). Importantly, an interaction between munc18-1 and syntaxin is not required to maintain the accumulation of munc18-1 once synaptically localised.

Alongside a change in the displacement of single munc18-1 molecules, a significant difference was found in molecular speed upon the removal of a syntaxin interaction. Munc18-1 molecules had significantly faster velocities (Figure 6.6B), an observation consistent with interrupting an interaction between a soluble and transmembrane protein. Taken together, these observations suggest that munc18-1 molecules not participating in an interaction with syntaxin molecules are not trafficking to the appropriate cellular sites, indicating a stable interaction with syntaxin is essential for the correct localisation of munc18-1, most probably to fusion sites. These finding add another dimension to SM knockout studies conducted in a variety of organisms, perhaps such severe and detrimental phenotypes are a result of munc18-1 unable to reach its final destination and therefore unable to carry out its essential function(s) in the synaptic vesicle lifecycle.

The interaction between munc18-1 and syntaxin is paramount in a wide variety of cellular processes, intimating that both proteins must interact at some stage in the synaptic vesicle

lifecycle. However, despite a large body of evidence detailing the modes of interaction between munc18-1 and syntaxin, nothing is currently known about precisely when these proteins interact in real time. Using the extremely high spatial and temporal resolutions offered by fluorescence correlation spectroscopy (FCS) this study was able to provide information on munc18-1/syntaxin concentrations, mobility coefficients and rate constants of their protein-protein reactions. This study presents several independent lines of evidence to support the hypothesis that munc18-1 and syntaxin molecules interact in neuronal processes to enable efficient molecular trafficking to synapses, but that once in the synapse, these molecules are held apart in a resting and active nerve terminal. Despite both proteins displaying similar diffusion constants prior to stimulation, little cross correlation was observed, indicating that they were not interacting at the point of measurement. This observation now introduces the possibility that munc18-1 and syntaxin are not always in constant communication despite their high affinity interaction, suggesting spatial segregation in the synapse. This result is in accordance with an earlier finding demonstrating that complexes involving syntaxin, SNAP-25, VAMP, αSNAP and NSF were not associated with munc18-1 (Pevsner et al, 1994b).

FCS recordings revealed that the diffusion rate of syntaxin was reduced significantly during depolarisation. This slow and sequestered behaviour might in fact reflect syntaxin entering the SNARE complex in order to drive exocytosis. On the other hand, munc18-1 also slows down in molecular motion upon stimulation, indicating that both proteins might actually bind to a much larger protein, or protein complex which is restricting their movement within synaptic terminals. The active zone is a pre-synaptic structure found beneath the presynaptic plasma membrane, the principal site for Ca^{2+}-dependent neurotransmitter release (Landis et al, 1988). Since the discovery and characterisation of the active zone a number of essential components have been shown to reside in its matrix, including bassoon (tom Dieck et al, 1998), piccolo (Cases-Langhoff et al, 1996), RIM1 (Wang et al, 1997), munc13-1 (Brose et al, 1995) and CAST (Ohtsuka et al, 2002), with the remaining molecular composition remaining unclear. Most active zone proteins are comparatively large in structure and thought to form complex protein-protein interactions resulting in the formation of macromolecular protein complexes (Ohtsuka et al, 2002). The functional interactions between active zone proteins have been shown to mediate synaptic vesicle priming (Betz et al, 2001), vesicle transport (Wang et al, 2002) and the

release of neurotransmitters (Mochida et al, 1996). Combining the finding that munc18-1 and syntaxin have a long and sequestered diffusion time during neuronal depolarisation with previously characterised interactions with a number of active zone proteins (Betz et al, 1997; Gladycheva et al, 2004; Guan et al, 2008), suggests that both proteins may be sequestered into a large, slowly diffusing pre-synaptic-membrane bound molecular complex involved in catalysing synaptic vesicle fusion. Furthermore, immediately following neurotransmitter release the diffusion rates of munc18-1 and syntaxin increase to near pre-stimulation levels. This change may reflect the transient nature of pre-synaptic protein-protein interactions involved in eliciting synaptic vesicle fusion upon the arrival of an action potential.

The extremely short delay between nerve terminal depolarisation and synaptic vesicle exocytosis is primarily attributed to vesicles residing in a metastable state at active zones, poised and ready for fast Ca^{2+}-triggered fusion with the plasma membrane. The arrival of an action potential generates a stimulation-dependent increase in local Ca^{2+} and results in vesicular fusion within 200 μs (reviewed in Lin and Scheller, 2000). Therefore, a rapid change in the interaction status of the protein machinery driving SNARE mediated vesicle fusion would be undetectable using TCSPC-FLIM, a technique which lacks the temporal sensitivity of FCS. Using FCS this study has revealed for the first time that munc18-1 and syntaxin may not in fact interact in a synapse before, during and after evoked synaptic vesicle fusion. It is conceivable to imagine that spatially segregating a number of exocytic proteins could serve as a negative clamp, arresting the stages preceding full fusion. This mechanism would therefore prevent spontaneous and indiscriminate SNARE complex assemblies outside the active zone or until vesicles are required to fuse (Hayashi et al, 1994). Finally, elevations in cytosolic Ca^{2+} triggered by the arrival of an action potential may act to release this clamp allowing SNARE complex formation and the fusion reaction to proceed (Rothman, 1994b), a reaction not necessarily involving a direct munc18-1-syntaxin interaction.

Whereas most intracellular membrane fusion events are constitutive and unregulated, neurotransmission depends on the coupling of neurotransmitter release to Ca^{2+} influx into the nerve terminal (Katz, 1969). This concept introduces another possible explanation to account for why the molecular behaviour of munc18-1 and syntaxin change upon the

arrival of an action potential. Synaptotagmin, the putative Ca^{2+} sensor essential for fast synchronous SNARE-mediated neuronal exocytosis (Geppert et al, 1994; Yoshihara and Littleton, 2002) has been shown to induce the aggregation of cellular membranes in response to Ca^{2+} (Popoli and Mengano, 1988; Popoli et al, 1991; Perin et al, 1990). The short delay period between Ca^{2+} influx and synaptic vesicle fusion suggests that synaptotagmin must be associated with the fusion machinery prior to Ca^{2+} influx into the nerve terminal. In support of this suggestion SNARE complexes were shown to co-purify with synaptotagmin in the absence of Ca^{2+} (Söllner et al, 1993a; McMahon et al, 1995; Li et al, 1995), with native synaptotagmin specifically binding to the t-SNARE heterodimer, formed from syntaxin and SNAP-25 with high affinity (Rickman and Davletov, 2003; Rickman et al, 2004). More recently it was reported that vesicles dock when synaptotagmin-1 binds to syntaxin/SNAP-25 acceptor complexes and, together with munc18-1, constitute the minimal docking machinery (de Wit et al, 2009). Therefore, it is conceivable to imagine that upon neuronal depolarisation membrane bound synaptotagmin, already bound to syntaxin (Kee and Scheller, 1996; Fernandez et al, 1998; Rickman and Davletov, 2003; Rickman et al, 2004), binds to entering Ca^{2+} which triggers its oligomerisation (Damer and Creutz, 1996). Ca^{2+} binding would therefore lead to a conformational change in synaptotagmin, potentially acting as an electrostatic switch in the molecular configuration of syntaxin, tethering it at the active zone and allowing it to enter into the ternary SNARE complex to drive SNARE complex formation and vesicle fusion. It might well be the case that munc18-1-syntaxin protein-protein interactions are required upstream of membrane association and not directly in the catalysis of the final fusion event of vesicles in close apposition to the active zone of a nerve terminal. These results can be summarised by a simplistic model which is based on the interpretation of the functionality of the munc18-1-syntaxin interaction within synaptic terminals (Figure 6.16).

6.17

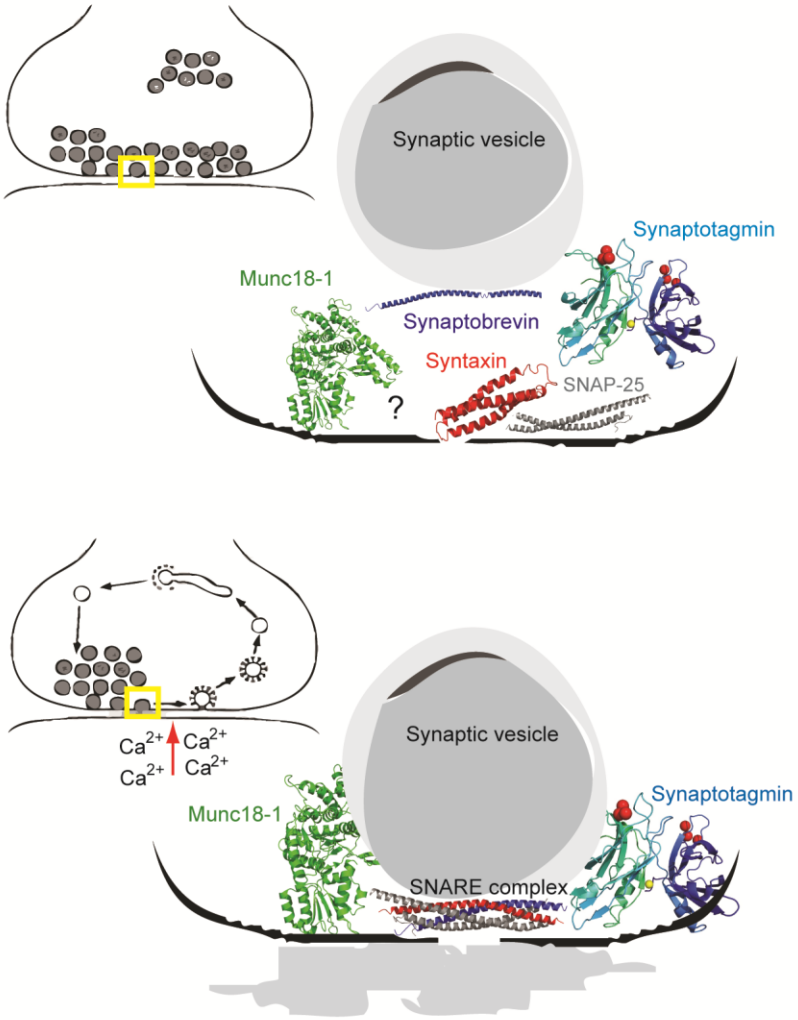

Figure 6.17. *A diagrammatical interpretation of the activity dependent interaction between munc18-1 and syntaxin within central nerve terminals*. This proposed model includes an illustration of both a resting (above) and recycling synaptic terminal (below), as indicated by the presence of Ca^{2+} ions and release of neurotransmitter. The crystal structures of munc18-1 (green), syntaxin (red), synaptotagmin (rainbow; Vrljic et al, 2010)), synaptobrevin (blue) and SNAP-25 (grey) are shown. This schematic diagram illustrates that within a resting synapse the readily releasable pool (RRP) of vesicles is docked at the plasma membrane awaiting nervous input. Munc18-1 is found tethered to the active zone in a complex (represented by a question mark) which is diffusing at a similar rate to syntaxin. Upon neuronal depolarisation RRP vesicles fuse with the plasma membrane and are recycled in order to sustain synaptic transmission during nervous activity. The diffusion of syntaxin is significantly reduced in order to drive SNARE complex assembly and synaptic vesicle exocytosis.

CHAPTER 7:

FINAL CONCLUSIONS

7.1 SUMMARY OF FINDINGS.

Mammalian-regulated secretion is absolutely dependent on four evolutionarily conserved proteins: three SNARE proteins and munc18-1. Dissecting the functional outcomes of the spatially organised protein interactions between these factors has been difficult because of the close interrelationship between different binding modes. This investigation had two main aims; firstly to biochemically characterise the munc18-1-syntaxin-N-terminal interaction to determine its downstream functionality within a living cell. The SNARE protein, syntaxin, is regulated by munc18-1 (Pevsner et al, 1994b). This regulation is central to exocytosis but despite a large amount of biochemical, electrophysiological and ultra-structural data, the spatio-temporal arrangement of munc18-1 and syntaxin at the molecular level remains undefined. Therefore the second aim of this investigation was to resolve the spatial and temporal pattern of their molecular distribution and interaction in both central synapses and neuroendocrine cells.

The findings from this thesis fall into three main areas. Firstly it was found that the munc18-1-syntaxin-N-terminal interaction had a pronounced influence on the behaviour of vesicles at the plasma membrane and their likelihood to undergo fusion. Furthermore N-terminal interaction not only regulates a specific pool of secretory vesicles and imparts a greatly increased fusion probability within neuroendocrine cells but also exists as a catalyst for the fusion of readily releasable synaptic vesicles within central synapses. A second main finding involved defining the molecular architecture of SM/vesicle relationships in fusion competent PC12 cells. Lastly, another finding of this investigation demonstrated that munc18-1 requires syntaxin to traffic efficiently along axons but not for its retention in nerve terminals. Moreover, no interaction between synaptic munc18-1 and syntaxin molecules was detected in nerve terminals, with the rate of syntaxin significantly slowing down upon Ca^{2+}-triggered exocytosis.

7.2 CHARACTERISATION OF THE FUNCTIONALITY OF THE MUNC18-1-SYNTAXIN-N-TERMINAL INTERACTION.

The synchronized action of SNARE mediated exocytosis is reliant on a number of accessory proteins to regulate its highly ordered and localised nature (Südhof and Rothman, 2009). Sec1/Munc18 proteins (SM proteins) are a class of such accessory factors that are present at all SNARE-catalysed membrane fusion sites (Gerber et al, 2008). It is known that munc18-1 and syntaxin interact via at least two distinct modes, one with monomeric 'closed' syntaxin and the other involving its highly conserved N-terminus (Dulubova et al, 2007; Rickman et al, 2007; Shen et al, 2007).

At the inception of this study, and in contrast with the consensus on SNARE protein function, conflicting findings had emerged regarding the precise role of the munc18-1-syntaxin-N-terminal interaction. N-terminal binding had been shown to stimulate secretory vesicle dynamics at the plasma membrane (Rickman and Duncan, 2010), SNARE assembly *in vitro* (Shen et al, 2007; Schollmeier et al, 2011), synaptic fusion in the calyx of Held (Khvotchev et al 2007) and synaptic vesicle priming (Deak et al, 2009). Moreover, the 4-helical SNARE bundle, containing the syntaxin N-peptide region, is the minimal complement required for munc18-1-mediated stimulation of membrane fusion *in vitro* (Shen et al, 2010). However, and in stark contrast, other studies have reported that the N-terminal interaction is indispensable for SNARE mediated membrane fusion (Arunachalam et al, 2007; Han et al, 2009; Malintan et al, 2009; Diao et al, 2010; Meijer et al, 2012). The controversy relating to the functionality of the N-terminal interaction can be partly attributed to the poorly conserved munc18-1 amino acid residues targeted in one recent study (E132 and F115; Malintan et al, 2009). Therefore residues not indicative of essential function (Madabushi et al, 2002) have obscured the functionality of the N-terminal interaction and demanded further work to clarify its precise role in the membrane fusion process.

Structural information available on SM-SNARE protein configurations and binding modes enabled this study to both identify and characterise important residues regulating N-terminal binding, paving the way for a more detailed understanding of its role in mediating

downstream cellular events. Biochemical separation of binding modes between munc18-1 and syntaxin revealed the extent of N-terminal binding occurring in an *in vitro* setting and highlighted those munc18-1 residues important in facilitating the N-terminal interaction, namely residue I127 (Figures 3.1 and 3.2). Using various GST-syntaxin constructs in combination with selected munc18-1 mutants demonstrated the extent of disruption of N-terminal binding *in vitro*, with munc18-1[I127A] resulting in the largest reduction in binding to syntaxin. These *in vitro* binding assays also demonstrated that N-terminal binding involves a number of ionic interactions, in contrast with closed form binding (Figure 3.1).

Following preliminary *in vitro* identification of munc18-1 residues essential in mediating N-terminal interaction this study further characterised where N-terminal binding predominated within a cellular environment. Protein co-localisation and FLIM studies revealed that the N-terminal interaction was primarily utilised at the plasma membrane and key for the efficient targeting of syntaxin to sites of vesicular fusion, as reported previously (Figures 3.5 and 3.6; Rowe et al, 2001; Medine et al, 2007; Rickman et al, 2007; Arunachalam et al, 2008). It is noteworthy to mention that N-terminal binding is not the sole interaction mode responsible for the trafficking of syntaxin given that both munc18-1 and syntaxin molecules still reach the plasma membrane upon N-terminal ablation, as revealed by PALM (Figures 5.9B and 5.10B) and co-localisation studies (Rickman et al, 2007). It is therefore reasonable to assume that those molecules not reaching the plasma membrane as efficiently (Figure 3.5) or not engaging in N-terminal interactions once there (Figure 4.4) are responsible for the downstream cellular effects seen throughout this investigation.

In this study mutating the hydrophobic pocket of munc18-1 to quantifiably disrupt N-terminal interaction with syntaxin also resulted in significant changes in vesicle dynamics and fusion efficiency (Figures 4.1 and 4.3). This investigation identified two distinct pools of vesicles, based on their relative mobilities, in live neuroendocrine cells (Figure 4.5). Analysis of these kinetically distinct pools revealed that the majority of fusion events arise from a minority pool of relatively mobile membrane proximal vesicles, which in turn relies on N-terminal interactions. Demonstrating that the majority of fusion events arise from a more mobile subset pool of vesicles supports the theory suggesting that

secretory vesicles undergo molecular-scale movements immediately prior to membrane fusion (Degtyar et al, 2007). Therefore interaction with the syntaxin N-peptide can confer differential release probabilities to secretory vesicles and may contribute to the delineation of secretory vesicle pools. This observation fits well with the finding that disrupting the casein kinase II phosphorylation site at the N-terminus of syntaxin, a key mediator of the munc18-1-syntaxin-N-terminal interaction, also results in a significantly reduced percentage of fusing vesicles specifically residing in the readily releasable pool of synaptic vesicles in a central nerve terminal (Figures 4.9 and 4.10).

Specialised secretory cells, e.g. neuronal and neuroendocrine cells, share a number of characteristics, namely both are filled with membrane bound vesicles containing chemical compounds used in the transmission of a signal. Vesicles reside in distinct pools with only a small fraction of the morphologically docked and primed vesicles available for immediate release upon the arrival of a physiological stimulus (Burgess and Kelly, 1987; Greengard et al, 1993; Pieribone et al, 2005; Brodin et al, 1997; Kuromi and Kidokoro, 1998; Rizzoli and Betz, 2004). The remainder of vesicles are thought to constitute a large reserve pool awaiting recruitment into the readily releasable pool (RRP) for further rounds of exocytosis. For example, fluorescence microscopy studies on chromaffin cells demonstrated that approximately 450–1000 large dense core vesicles are morphologically docked at the plasma membrane (Burgoyne, 1991; Parsons et al, 1995; Steyer et al, 1997), with only a fraction of these vesicles rapidly released upon stimulation (Neher and Zucker, 1993; Parsons et al, 1995). It has been shown that distinct populations of vesicles within neuronal and neurosecretory cells are segregated functionally (Rosenmund and Stevens, 1996; Von Gersdorff and Matthews, 1997; Kuromi and Kidokoro, 1998) and, specifically within chromaffin cells spatially, according to age (Duncan et al, 2003). By disrupting the N-terminal interaction in both neurons (syntaxin[S14E], Figures 4.9C and 4.10) and neuroendocrine cells (munc18-1[I127A], Figures 4.3 and 4.5) the proportion of fusion events from a specific postdocking pool of vesicles, most likely to reside in the RRP, is reduced. Both results suggest that fusion competent vesicles ready for immediate Ca^{2+} triggered fusion within the RRP of both neuronal and neuroendocrine cells rely on N-terminal interactions for events immediately postdocking and preceding exocytosis. However, the fact that munc18-1[I127A] resulted in no difference in the extent of RRP fusion in neuronal cells despite playing a significant role in driving large dense core

vesicle exocytosis may simply point towards the fact that endogenous proteins can over-ride the effects of transfected mutant proteins or that differences may exist in the regulation of exocytosis between both cellular models. For example, the rate of synaptic vesicle exocytosis measured in cerebellar synapses is reported to be 0.1 ms (Sabanti and Regehr, 1996). In contrast, LDCV exocytosis in chromaffin cells occurs at a speed of 7–27 ms (Chow et al, 1992; Voets, 2000). Therefore, the fastest modes of Ca^{2+}-triggered LDCV exocytosis are more than 10-fold slower than fast synaptic vesicle exocytosis and proceed at approximately 100 fold slower following stimulation. Perhaps the great difference in release kinetics subjects the molecular machinery governing fast neurotransmission, namely the SNAREs, munc18-1 and synaptotagmin, to stricter regulatory mechanisms. In that case the N-terminal hydrophobic pocket of munc18-1, specifically residue I127, may play more of a redundant role in synaptic vesicle exocytosis due to the differences that exist within the interplay between components of the SNARE complex and their positive and negative regulatory effectors.

Approximately twenty years following Katz's seminal finding, showing that neurotransmission depends on the coupling of synaptic vesicle release to Ca^{2+} influx into the nerve terminal (Katz and Miledi, 1967), the discovery of synaptotagmin-1, the putative Ca^{2+}-sensor for synaptic exocytosis, was made (Perin et al, 1990). Later it was shown that synaptotagmin and syntaxin interact *in vitro* (Li et al, 1995; Kee and Scheller, 1996; Rickman and Davletov, 2003; Rickman et al, 2004) through a highly acidic region of the extreme N-terminal peptide of syntaxin and the C2A domain of synaptotagmin I in a Ca^{2+}-dependent manner (Fernandez et al, 1998). Combining the concept of vesicular pools and the actions of synaptotagmin suggests that preventing the munc18-1-syntaxin-N-terminal interaction (using syntaxin[S14E]) alters the fusion capabilities of readily releasable synaptic vesicles by disrupting an interaction between the N-terminal peptide of syntaxin and synaptotagmin. With synaptotagmin, syntaxin-1, SNAP-25 and munc18-1 constituting the minimal docking machinery (de Wit et al, 2009), a disruption between this acceptor complex could also prove to destabilise the initial association of those readily releasable vesicles with the plasma membrane. These stable protein-protein interactions are therefore required downstream of membrane association and may be serving as an electrostatic switch in the immediate fusion of vesicles primed and ready for Ca^{2+} triggered release.

All of the above results, in combination with the finding that N-terminal interaction is specific to the plasma membrane of a neuroendocrine cell (Figure 4.4), indicate that this mode of binding is only engaged with a subset of vesicles poised for membrane fusion. Assuming this is correct, it is therefore unsurprising that perturbing the N-terminal interaction only affects those membrane proximal vesicles that give rise to the majority of fusion events in neuroendocrine cells and the readily releasable pool of synaptic vesicles within central synapses.

7.3 THE INTERACTIONS, MOBILITIES AND DISTRIBUTIONS OF SINGLE MOLECULES.

Despite a large effort focused on the roles of munc18-1 in the exocytotic pathway its intracellular localisation on a molecular level and how it may act upon single vesicles prior to the final fusion event remains unknown. SM proteins are essential factors in all intracellular trafficking routes (Novick and Schekman, 1979; Novick et al, 1980; Novick et al, 1981), synaptic transmission (Brenner, 1974; Salzberg et al, 1993; Harrison et al, 1994; Verhage et al, 2000) and promoting the docking of vesicles in neuroendocrine cells (Voets et al, 2001; Toonen et al, 2006; Verhage and Sørensen, 2008). It is clear that munc18-1 is required in the process of both vesicle docking and postdocking events but a coherent explanation of how SM proteins are structurally organised on the molecular level in order to carry out their precise functions has been hampered by the lack of available techniques.

This investigation employed super-resolution techniques Ground state depletion-individual molecule return (GSDIM) microscopy and Photoactivation Localisation Microscopy (PALM) to show that single munc18-1 molecules exist in a non-random spatial distribution, resulting in areas of low and high molecular density. Interestingly, areas of lower molecular densities corresponded to areas that were specifically targeted by secretory vesicles. This finding is similar to the spatial organisation of syntaxin which has been shown to reside in dense clusters (Sieber et al, 2007; Rickman et al, 2010) which do not coincide with secretory vesicles (Barg et al, 2010). In addition, resolving the

heterogeneous distribution of munc18-1 supports the data generated using sptPALM (Figures 5.14 and 5.15, Manley et al, 2008). Single munc18-1 molecule tracking data shows that munc18-1 moves freely across the plasma membrane of a neuroendocrine cell but displays confined, caged kinetics in sites enriched with other munc18-1 molecules (Figures 5.15). Therefore, tracking large cohorts of single munc18-1 molecules demonstrated that the heterogeneities of single molecular motions were responsible for their spatial distribution across the membrane of neurosecretory cells.

This finding is consistent with sptPALM data gathered from the behaviours of single munc18-1 molecules within live neuronal networks. These experiments revealed two kinetically and spatially distinct populations of munc18-1; one population consisted of restricted, largely immobile molecules confined to synapses whereas another population displayed a more directed, faster movement between synapses. Similarly the dynamics of single munc18-1 molecules also accounted for the distribution of endogenous syntaxin (Figure 6.1) and munc18-1 (Figure 6.1B), both enriched within central nerve terminals when compared to their molecular distribution in neuronal processes. Furthermore, ablating the interaction between munc18-1 and syntaxin severely affected the directionality and molecular speed of munc18-1, supporting the idea that munc18-1 and syntaxin require a stable interaction in order to facilitate their trafficking and delivery to defined areas of a cell (Rowe et al, 2001; Medine et al. 2007; Rickman et al. 2007).

Further analysis of the molecular kinetics of munc18-1 in live neuroendocrine cells revealed that domains of the planar bilayer were preferred by munc18-1 molecules (Figure 5.18B). The restricted kinetics of munc18-1 molecules in these membrane hot-spots are likely to reflect the recruitment of munc18-1 molecules to membrane-inserted transmembrane syntaxin as this is the principal mechanism for munc18-1-membrane association (Hata et al, 1993; Rowe et al, 1999, 2001; Medine et al, 2007; Arunachalam et al, 2008). Moreover, perturbing the N-terminal interaction between munc18-1 and syntaxin had no effect on the molecular speed of munc18-1, indicating that the syntaxin-N-peptide is perhaps not critical in the recruitment of munc18-1 to the plasma membrane, as previously suggested (Rathore et al, 2010). The spatio-temporal organisation of relatively immobile munc18-1 molecules into hot-spots, distinct from vesicle docking sites but interspersed with more mobile molecules, is suggestive of munc18-1 recycling

between molecular depots. Indeed, this study demonstrated that munc18-1 molecular populations moved in a directed manner across the membrane, appearing to recycle between molecular storage depots where munc18-1 was enriched.

It is intuitive to think that for munc18-1 to act at the final stage of fusion its presence must be associated with syntaxin (and probably the other SNAREs) and an adjacent vesicle for exocytosis to proceed. Munc18-1 molecules were primarily localised in areas of the plasma membrane that were largely devoid of membrane proximal vesicles (Figures 5.4 and 5.5). This observation supports a previous study which showed that yeast SM proteins Sso and Sec9 are localised along the entire plasmalemma and not only at the tips of the bud, where the bulk of exocytosis occurs (Brennwald et al, 1994). Furthermore, the low number of munc18-1 molecules close to the secretory vesicle is likely to be sufficient for the catalysis of membrane fusion and falls within the range observed for the SNAREs in a variety of biophysical experiments (Hua and Scheller, 2001; Han et al, 2004; Karatekin et al, 2010; Mohrmann et al, 2010; van den Bogaart et al, 2010; Sinha et al, 2011). This analysis demonstrated that vesicles only have a 20% probability of being physically associated with one or two munc18-1 molecules. Moreover approximately 80% of vesicles were found to have no adjacent munc18-1 molecule associated and these vesicles cannot move sufficient distances at the plasma membrane to reach their nearest neighbour munc18-1 molecule. In this case it is probable that secretory vesicles residing in a region of the plasma membrane with insufficient numbers of munc18-1 molecules would be unable to fuse and may help to explain why the majority of membrane proximal vesicles are left unused. Therefore, either only a few molecules are required for exocytosis to proceed or this finding may reflect other functions of this molecule, in addition to its participation in the formation of SNARE fusion complexes.

This comparatively low number of munc18-1 molecules found residing underneath a secretory vesicle differs hugely from current estimates of approximately 70 synaptobrevin copies expressed on a single synaptic vesicle (Takamori et al, 2006). Interestingly, and only under certain culture conditions, it has been reported that syntaxin is in approximately 20-fold excess over munc18-1 in PC12 cells (Schutz et al., 2005). However, the molar ratio in the purified syntaxin/munc18-1 complex has been shown to be 1:1 (Rickman and Davletov, 2005), in agreement with the crystal structure (Misura et

al, 2000) and indicative of a tight association (Dulubova et al, 1999). It is therefore possible that a large proportion of syntaxin remains free from munc18-1 in solution and a limited number of munc18-1 molecules recycle between SNARE complexes in order to drive the formation of the SNARE complex and the fusion of a single secretory vesicle.

It remains to be seen whether multiple munc18-1-syntaxin complexes can act cooperatively to further enhance the likelihood of fusion. It is also unknown whether the number of SNARE complexes or munc18-1 molecules required to fuse a vesicle differ depending on the type of vesicle, which functional pool that vesicle resides in or even what type of fusion event is occurring. Together, these findings provide a working model where a small number of munc18-1 molecules recycle between molecular storage depots with membrane locations distinct from vesicle docking sites to directly affect downstream vesicle dynamics and exocytosis. Therefore, these findings place munc18-1 as a key regulator of SNARE function, acting at multiple locations throughout the SNARE life cycle. A number of conclusions regarding the functionality and molecular architecture of munc18-1-syntaxin interaction in neuroendocrine cells can be summarised in a simplistic model (Figure 7.1).

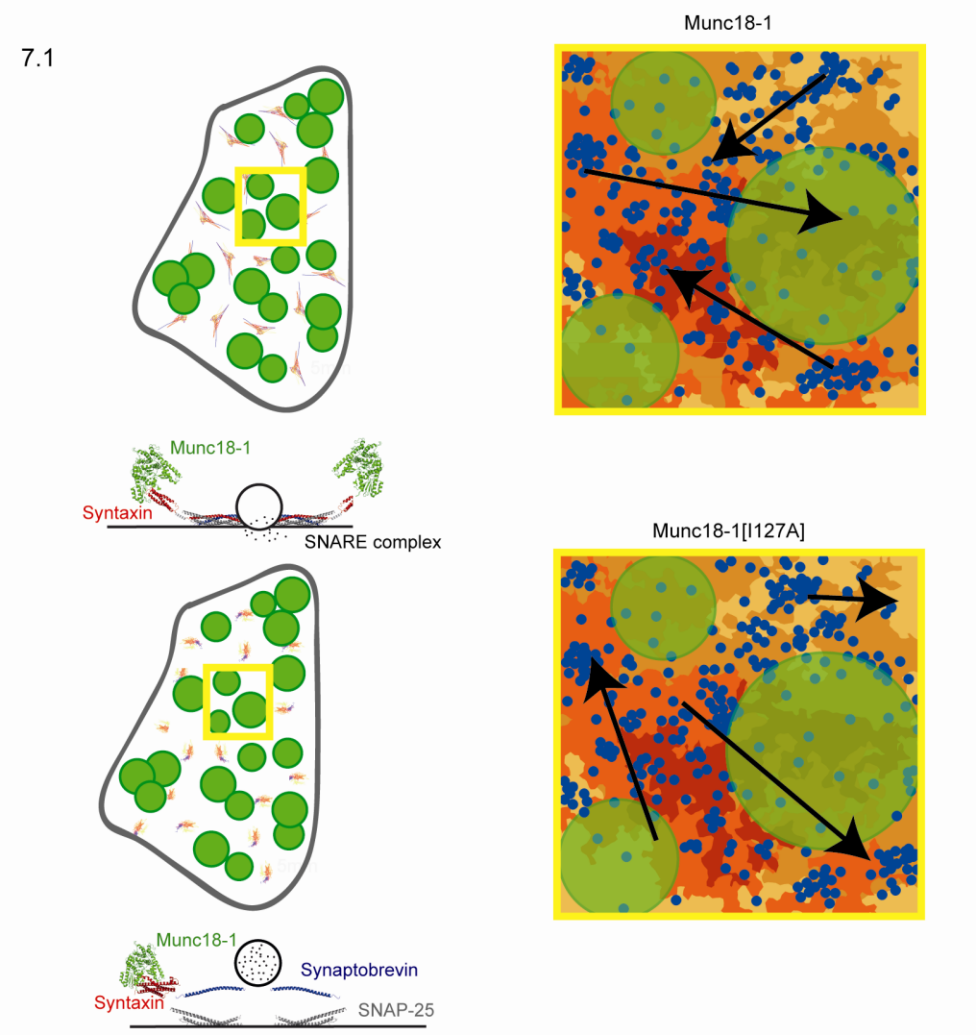

Figure 7.1. *Schematic model of the downstream cellular effects of the syntaxin N-terminal peptide and spatial organisation of munc18-1 molecules in neuroendocrine cells*. This proposed model depicts the base of a neuroendocrine cell containing secretory vesicles (*green*) and single munc18-1 molecules (*blue*) imaged by Total Internal Reflection Fluorescence Microscopy (TIRFM). Individual vesicle trajectories are shown as tracks with colour corresponding to time during acquisition (blue – start to red – end). Perturbation of the N-terminal interaction between munc18-1 and syntaxin (munc18-1[I127A]) results in a reduction in vesicle kinetics and fusion efficiency at the plasma membrane. This model also illustrates that a small number of munc18-1 molecules are located directly underneath a vesicle, with the majority of munc18-1 molecules localised to areas of the plasma membrane not targeted by secretory vesicles. Furthermore, munc18-1 molecules move between areas of high and low molecular densities, as shown by the arrows. Therefore this model suggests that N-terminal binding is crucial in mediating the kinetics and fusion probabilities of vesicles, processes which are not reliant on the spatial distribution of munc18-1, syntaxin and vesicles.

7.4 THE INTERACTION STATUS BETWEEN MUNC18-1 AND SYNTAXIN IN NEURONAL CELLS.

The great complexity of the functions performed by the nervous system relies on the ability of neurons to communicate with each other in defined and precisely timed patterns. Data concerning both the spatial and temporal control of the munc18-1-syntaxin molecular interactions and how they affect prefusion synaptic vesicle dynamics is largely unknown. One reason for this involves the difficulty associated with reconstituting the regulation of the munc18-1-syntaxin complex seen *in vitro* into a physiologically accurate account of the importance of these putative binding partners *in vivo*.

SNAREs and SNARE regulatory proteins are phosphorylated *in vitro* (Gerst, 1999; Lin and Scheller, 2000) but what remains to be resolved is when this phosphorylation occurs, the prevailing regulatory mechanism(s) and the downstream functional significance. This thesis has demonstrated that phosphorylated syntaxin, specifically on serine-14 of the N-terminal peptide, resides in specific domains separate from active zones, in agreement with a previous observation (Figure 4.7; Fölleti et al, 2000). This result indicates that phosphorylated syntaxin may provide a regulatory mechanism to differentiate between functional and non-functional synapses in order to prevent indiscriminate fusion outside pre-defined areas. Therefore, by disrupting the phosphorylation status of the N-terminal peptide of syntaxin the architecture of fusion sites on the plasma membrane are disturbed, resulting in a loss and mis-regulation of exocytotic events. This hypothesis fits well with the findings that phosphomimetic disruption of serine^{14} of syntaxin results in a reduction in the proportion of fusing synaptic vesicles residing in the readily releasable pool of central nerve terminals (Figure 4.9C) and the arrest of vesicle fusion in neuroendocrine cells (Rickman and Duncan, 2010).

This investigation provided evidence to suggest that the phosphorylation status of serine^{14} on the N-terminal peptide of syntaxin is not regulated by neuronal activity (Figure 4.8) but is somehow important in catalysing the fusion of vesicles in close apposition with the active zone. This incongruity therefore led to the idea that another Ca^{2+} dependent syntaxin molecular mechanism was in place to control rapid synaptic fusion. The

interaction between munc18-1 and syntaxin is paramount to a wide variety of cellular processes, intimating that both proteins must interact at some stage in the synaptic vesicle lifecycle. The precise temporal sequence of this interaction in the run up to synaptic vesicle fusion remains speculative, not least because of a lack of suitable approaches to directly probe molecular localisations, movements and interactions *in situ*. Conflicting reports have suggested that munc18-1 and syntaxin are never stably associated (Garcia et al, 1995), that munc18-1 dissociates from syntaxin upon SNARE complex formation (Zilly et al, 2006) and that munc18-1 remains bound to syntaxin via its N-terminus throughout SNARE complex formation and subsequent membrane fusion (Dulubova et al, 2007).

In this thesis Fluorescence Correlation Spectroscopy (FCS) was employed to define and quantify the molecular movements of munc18-1 and syntaxin preceding, during and immediately after exocytosis. Analysis revealed that synaptic munc18-1 molecules are not directly interacting with syntaxin in resting nerve terminals. Further investigation revealed that the rate of syntaxin diffusion was significantly reduced during stimulation, reflecting the formation of the ternary SNARE complex, or implying that syntaxin (and munc18-1) binds to a much larger complex, restricting its movement and tethering it to synaptic terminals in order to drive synaptic vesicle fusion (Figure 6.15B). This result further supports the hypothesis that the molecular dynamics of single proteins are responsible for their spatial arrangement. It would be of interest in the future to determine if this activity dependent switch in diffusion rates was observed in all types of neuronal specific Ca^{2+} triggered exocytosis and whether neurosecretory cells also possess this regulatory mechanism. It would also be of great interest to determine what protein(s) or macro-molecular complexes are involved in reducing the mobility of munc18-1 and syntaxin during neuronal depolarisation.

The extremely accurate and rapid timing seen in Ca^{2+}-regulated synaptic exocytosis is mediated by specific interactions between SNARE proteins, their accessory molecules, Ca^{2+} and the phospholipid bilayer. A number of effectors have been proposed to regulate munc18-1 binding and syntaxin activation, including members of the munc13 (Betz et al, 1997) and Doc2 protein families (Verhage et al, 1997) and through the catalytic activity of protein kinase C (Barclay et al, 2003). In addition to SNARE and SM protein interactions,

syntaxin has also been reported to interact with voltage-gated Ca^{2+} channels in mammalian neurons, an association proposed to colocalise Ca^{2+} channels and presynaptic release sites to support the efficient initiation of neurotransmitter release (Catterall, 2000). The short delay period between Ca^{2+} influx and synaptic vesicle fusion unequivocally suggests that synaptotagmin, the Ca^{2+} sensor essential for fast synchronous SNARE-mediated neuronal exocytosis (Geppert et al, 1994; Yoshihara and Littleton, 2002), must be associated with the fusion machinery prior to Ca^{2+} influx into the nerve terminal. In support of this suggestion SNARE complexes were shown to co-purify with synaptotagmin in the absence of Ca^{2+} (Söllner et al, 1993a; McMahon et al, 1995; Li et al, 1995). Neuronal depolarisation induces membrane associated synaptotagmin, already bound to syntaxin as previously shown (Kee and Scheller, 1996; Fernandez et al, 1998; Rickman and Davletov, 2003; Rickman et al, 2004), to bind free Ca^{2+} and oligomerise (Damer and Creutz, 1996). Ca^{2+} binding would therefore lead to a conformational change in synaptotagmin, potentially acting as an electrostatic switch in the molecular configuration of syntaxin, forcing it to become locked in position at the plasma membrane in order to drive SNARE complex formation and vesicle fusion. This mechanism fits well with the model previously proposed by Rizo and colleagues suggesting that a change in the synaptotagmin-syntaxin interaction is central in the regulation of Ca^{2+}-triggered synaptic vesicle exocytosis (Shao et al, 1997). Therefore, the activity dependent switch reported in this thesis may reflect a rapid change in the structural arrangement of the fusion machinery, particularly between munc18-1, syntaxin and synaptotagmin, recently claimed to constitute the minimal docking machinery (de Wit et al, 2009). The fact that this is the first report showing that munc18-1 and syntaxin are not directly interacting in a nerve terminal during exocytosis may simply be due to the lack of available techniques that offer the adequate temporal resolution required.

A number of findings from this thesis point towards a key interaction between munc18-1, syntaxin and synaptotagmin. Perturbing the munc18-1-syntaxin molecular interaction in both neurons and neuroendocrine cells resulted in the partial trapping of both proteins in intracellular compartments, with munc18-1 unable to be efficiently delivered to sites of membrane fusion (Figures 3.5 and 6.5). The ultimate downstream effect resulting from these disruptions, now presumably affecting the actions and binding of synaptotagmin and syntaxin, resulted in a reduction in the proportion of readily releasable vesicles fusing with

the plasma membrane and a fall in the level of neuroendocrine exocytosis. The findings from this thesis therefore introduce another dimension to the regulation of vesicle exocytosis, with the membrane associated fusion competent vesicles requiring an activity dependent switch in molecular behaviours (in the case of neurons at least) and a stable interaction between the N-terminus of syntaxin, munc18-1 and synaptotagmin. Regulated exocytosis is an exquisitely coordinated form of intracellular membrane fusion and understanding the complexity of this process requires further characterisation of a) the mechanisms of membrane fusion and b) how fusion is temporally and spatially controlled at the molecular level.

7.5 CONCLUDING REMARKS.

The dynamic interactions seen between SM and syntaxin homologues are thought to reflect the multifaceted nature of the vesicle cycle and to meet the demands of regulated exocytosis (Gerber et al, 2008). The findings presented here contribute to a greater understanding of the functionality of the munc18-1-syntaxin interaction in regulating SNARE mediated vesicular fusion, providing important insights into the spatially and temporally regulated molecular mechanisms mediating the final fusion event. Additionally, this investigation highlights the importance of combining *in vitro* biochemical data with quantitative super-resolution imaging approaches to resolve protein-protein interactions and molecular dynamics within living cells. Together, this integrated approach will prove to be fundamental in unravelling the molecular mechanisms which mediate the dynamic shift in the munc18-1-syntaxin interaction during the vesicle lifecycle. These protein-protein interactions are required downstream of membrane association and are essential in catalysing the final fusion event of vesicles in close apposition to the plasma membrane. Therefore, the understanding of molecular conformations adopted by proteins and their spatial organisation within cells will lead to a more complete appreciation of the molecular machinery of SNARE driven membrane fusion. Further development of current imaging techniques, particularly 3D PALM, and cellular models, for example transgenic animals with the munc18-1 gene replaced with a photoactivatable alternative, will ultimately lead to the ability to quantify protein-protein dynamics immediately before, during and after membrane exocytosis.

PUBLICATIONS AND CONFERENCES

Refereed Publications:

Smyth, A.M., Rickman, C. and Duncan, R.R. (2010) Vesicle fusion probability is determined by the specific interactions of munc18. *J Biol Chem* **285**: 38141-8.

Smyth, A.M., Duncan, R.R. and Rickman, C. (2010) Munc18-1 and syntaxin1: unravelling the interactions between the dynamic duo. *Cell Mol Neurobiol* **30**: 1309-13.

Abstracts from International Conferences *(*denotes presentation)**:***

Smyth, A.M*., Cousin, M.A., Rickman, C. and Duncan, R.R. Quantifying single molecular dynamics at the plasma membrane. *16th International Symposium on Chromaffin Cell Biology,* Beijing, China, July 11-15, 2011.

Smyth, A.M., Cousin, M.A., Rickman, C. and Duncan, R.R**.** Probing the munc18-1-syntaxin1a interaction at the molecular level in living cells. *8th Molecular Mechanisms of Exocytosis and Endocytosis*, Edinburgh, UK, April 3-5, 2011.

Smyth, A.M., Rickman, C., Hockridge, J.G., Cousin, M.A. and Duncan, R.R. The functional significance of the munc18-1-syntaxin interaction. *15th International Symposium on Chromaffin Cell Biology,* Merida, Mexico, November 12-16, 2009.

Smyth, A.M*., Cousin, M.A., Rickman, C. and Duncan, R.R. Visualising SNARE protein dynamics using PALM. *Scottish Microscopy Group Meeting*, University of Glasgow, UK, November 11, 2009.

Smyth, A.M., Rickman, C., Hockridge, J.G., Cousin, M.A. and Duncan, R.R. The functional significance of the munc18-1-syntaxin interaction. *7th Molecular Mechanisms of Exocytosis and Endocytosis*, Edinburgh, UK, April 5-7, 2009.

APPENDIX

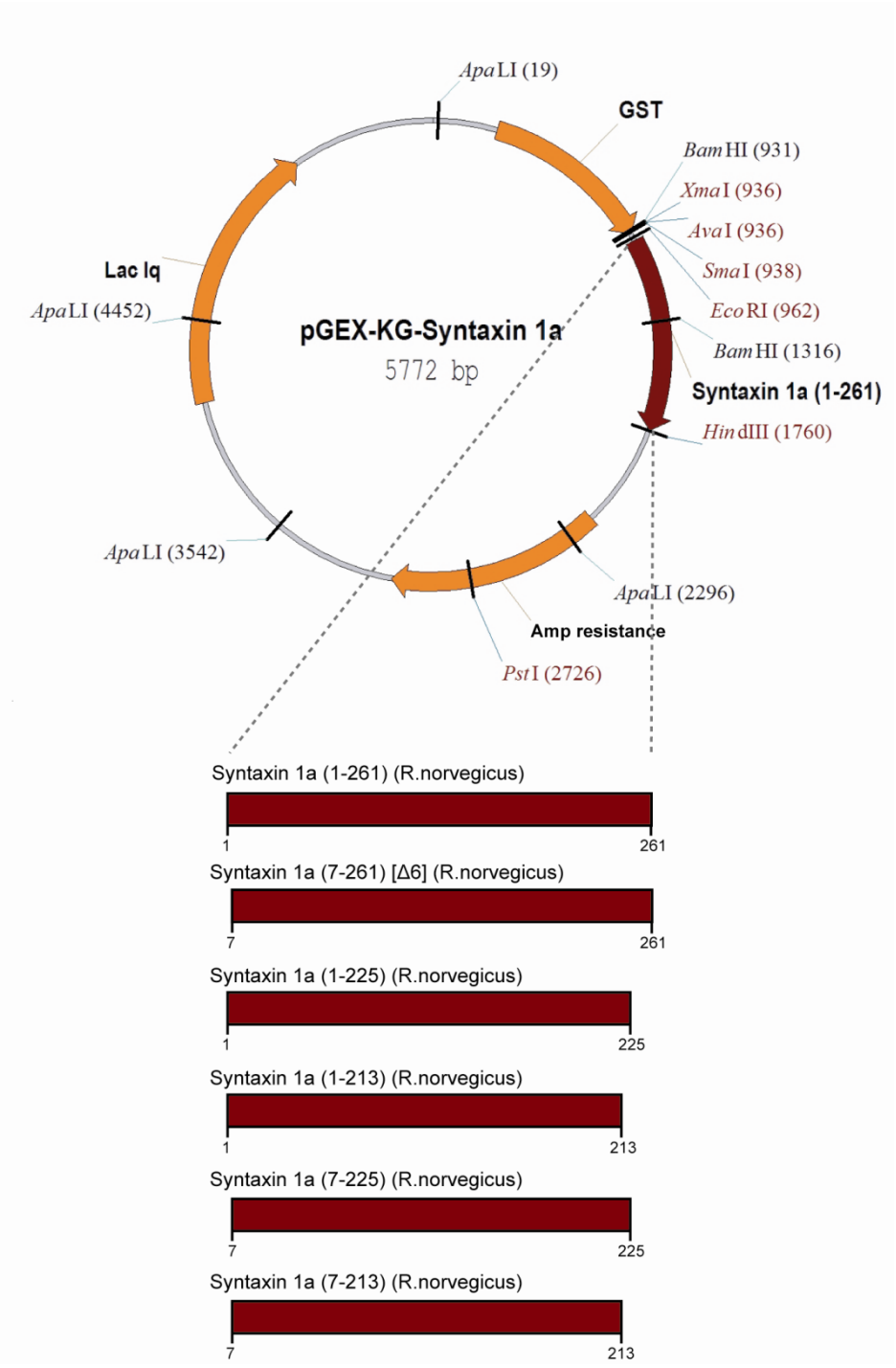
ApaLI (19)
GST
BamHI (931)
XmaI (936)
AvaI (936)
SmaI (938)
EcoRI (962)
BamHI (1316)
Syntaxin 1a (1-261)
HindIII (1760)
ApaLI (2296)
Amp resistance
PstI (2726)
ApaLI (3542)
Lac Iq
ApaLI (4452)
pGEX-KG-Syntaxin 1a
5772 bp
Syntaxin 1a (1-261) (R.norvegicus)
1
261
Syntaxin 1a (7-261) [Δ6] (R.norvegicus)
7
261
Syntaxin 1a (1-225) (R.norvegicus)
1
225
Syntaxin 1a (1-213) (R.norvegicus)
1
213
Syntaxin 1a (7-225) (R.norvegicus)
7
225
Syntaxin 1a (7-213) (R.norvegicus)
7
213

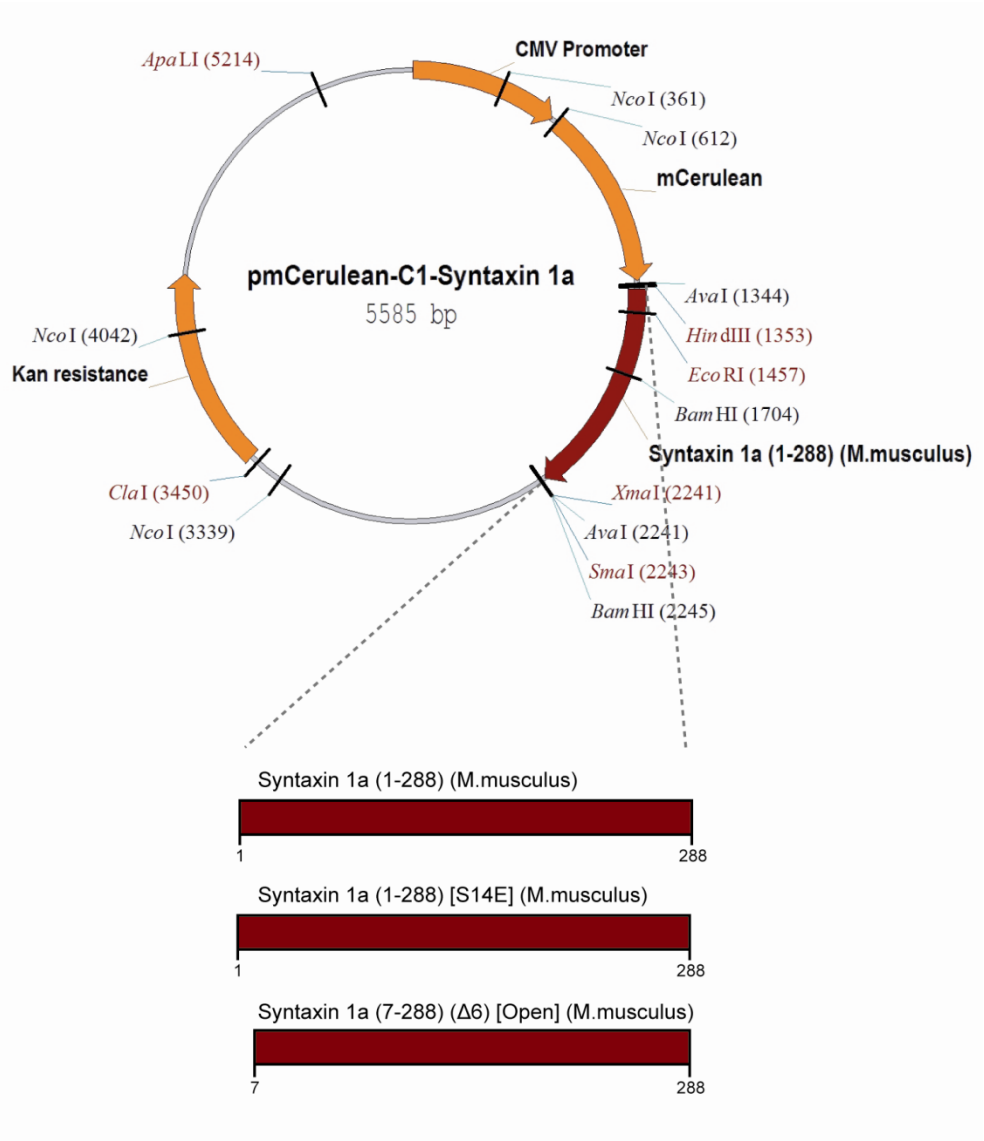
ApaLI (5214)
CMV Promoter
NcoI (361)
NcoI (612)
mCerulean
pmCerulean-C1-Syntaxin 1a
5585 bp
AvaI (1344)
HindIII (1353)
EcoRI (1457)
BamHI (1704)
Syntaxin 1a (1-288) (M.musculus)
NcoI (4042)
Kan resistance
ClaI (3450)
NcoI (3339)
XmaI (2241)
AvaI (2241)
SmaI (2243)
BamHI (2245)
Syntaxin 1a (1-288) (M.musculus)
1
288
Syntaxin 1a (1-288) [S14E] (M.musculus)
1
288
Syntaxin 1a (7-288) (Δ6) [Open] (M.musculus)
7
288

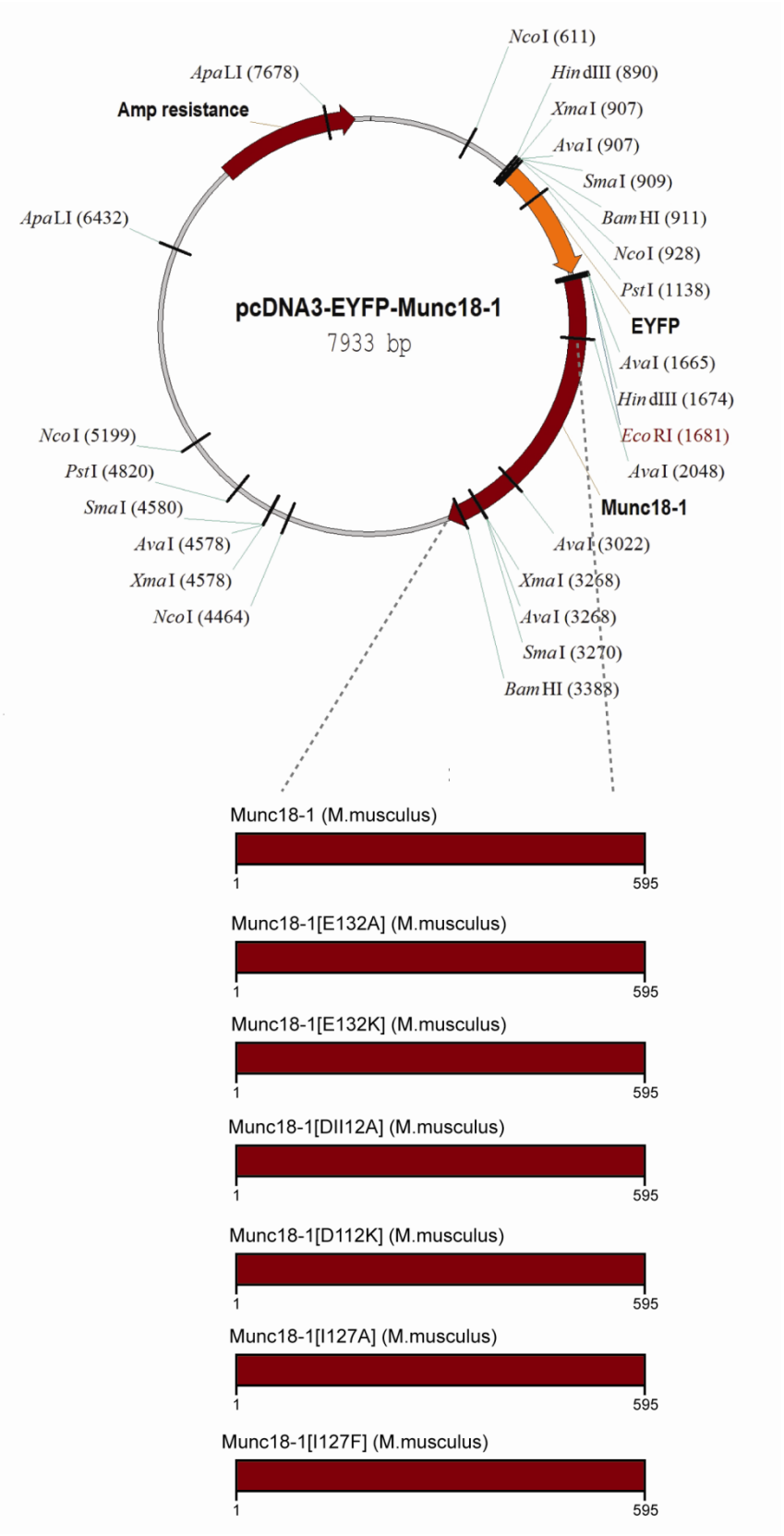
NcoI (611)
HindIII (890)
XmaI (907)
AvaI (907)
SmaI (909)
BamHI (911)
NcoI (928)
PstI (1138)
EYFP
AvaI (1665)
HindIII (1674)
EcoRI (1681)
AvaI (2048)
Munc18-1
AvaI (3022)
XmaI (3268)
AvaI (3268)
SmaI (3270)
BamHI (3388)
ApaLI (7678)
Amp resistance
ApaLI (6432)
pcDNA3-EYFP-Munc18-1
7933 bp
NcoI (5199)
PstI (4820)
SmaI (4580)
AvaI (4578)
XmaI (4578)
NcoI (4464)
Munc18-1 (M.musculus)
1
595
Munc18-1[E132A] (M.musculus)
1
595
Munc18-1[E132K] (M.musculus)
1
595
Munc18-1[DII12A] (M.musculus)
1
595
Munc18-1[D112K] (M.musculus)
1
595
Munc18-1[I127A] (M.musculus)
1
595
Munc18-1[I127F] (M.musculus)
1
595

BIBLIOGRAPHY

Aalto, M.K., Ronne, H. and Keränen, S. (1993) Yeast syntaxins Sso1p and Sso2p belong to a family of related membrane proteins that function in vesicular transport. *EMBO J* **12**(11): 4095-104.

Abbe, E (1873) *Arch Mikroskop Anat* **9**: 413-420.

Abderrahmani, A., Niederhauser, G., Plaisance, V., Roehrich, M.E., Lenain, V., Coppola, T., Regazzi, R., Waeber, G. (2004) Complexin I regulates glucose-induced secretion in pancreatic beta-cells. *J Cell Sci* **117**(11): 2239-47.

Allersma, M.W., Bittner, M.A., Axelrod, D. and Holz, R.W. (2006) Motion matters: Secretory granule motion adjacent to the plasma membrane and exocytosis. *Mol Biol Cell* **17**(5): 2424-38.

Arunachalam, L., Han, L., Tassew, N. G., He, Y., Wang, L., Xie, L., Fujita, Y., Kwan, E., Davletov, B., Monnier, P. P., Gaisano, H. Y. and Sugita, S. (2008) Munc18-1 Is Critical for Plasma Membrane Localisation of Syntaxin1 but Not of SNAP-25 in PC12 Cells. *Mol Biol Cell* **19**(2): 722-34.

Axelrod, D. (2001) Total internal reflection fluorescence microscopy in cell biology. *Traffic* **2**(11): 764-74.

Bacia, K., Schuette, C.G., Kahya, N., Jahn, R. and Schwille, P. (2004) SNAREs prefer liquid-disordered over "raft" (liquid-ordered) domains when reconstituted into giant unilamellar vesicles. *J Biol Chem* **279**(36): 37951-5.

Bacia, K., Kim, S.A., Schwille, P. (2006) Fluorescence cross-correlation spectroscopy in living cells. *Nat Methods* **3**(2): 83-89.

Bajohrs, M., Darios, F., Peak-Chew, S. Y. and Davletov, B. (2005) Promiscuous interaction of SNAP-25 with all plasma membrane syntaxins in a neuroendocrine cell. *Biochem J* **392**(Pt 2): 283-9.

Balch, W. E., Dunphy, W. G., Braell, W. A. and Rothman, J. E. (1984) Reconstitution of the transport of protein between successive compartments of the Golgi measured by the coupled incorporation of N-acetylglucosamine. *Cell* **39**(2 Pt 1): 405-16.

Barclay, J. W., Craig, T. J., Fisher, R. J., Ciufo, L. F., Evans, G. J., Morgan, A. and Burgoyne, R. D. (2003) Phosphorylation of Munc18 by protein kinase C regulates the kinetics of exocytosis. *J Biol Chem* **278**(12): 10538-45.

Barg, S., Knowles, M.K., Chen, X., Midorikawa, M. and Almers, W. (2010) Syntaxin clusters assemble reversibly at sites of secretory granules in live cells. *Proc Natl Acad Sci USA* **107**(48): 20804-9.

Barnstable, C. J., Hofstein, R. and Akagawa, K. (1985) A marker of early amacrine cell development in rat retina. *Brain Res* **352**(2): 286-90.

Barrett, E. F. and Stevens, C. F. (1972) The kinetics of transmitter release at the frog neuromuscular junction. *J Physiol* **227**(3): 691-708.

Bastiaens, P.I. and Squire, A. (1999) Fluorescence lifetime imaging microscopy: spatial resolution of biochemical processes in the cell. *Trends Cell Biol* **9**(2): 48-52.

Baumert, M., Maycox, P. R., Navone, F., De Camilli, P. and Jahn, R. (1989) Synaptobrevin: an integral membrane protein of 18,000 daltons present in small synaptic vesicles of rat brain. *EMBO J* **8**(2): 379-84.

Becherer, U., Pasche, M., Nofal, S., Hof, D., Matti, U. and Rettig, J. (2007) Quantifying exocytosis by combination of membrane capacitance measurements and total internal reflection fluorescence microscopy in chromaffin cells. *PLoS ONE* **2**(6): 505.

Bellen, H. (1999) Neurotransmitter Release. Oxford, Oxford University Press.

Bennett, M.K., Calako, N. and Scheller, R.H. (1992) Syntaxin: a synaptic protein implicated in docking of synaptic vesicles at presynaptic active zones. *Science* **257**(5067): 255-9.

Bennett, M. K. and Scheller, R. H. (1993a) The molecular machinery for secretion is conserved from yeast to neurons. *Proc Natl Acad Sci U S A* **90**(7): 2559-63.

Bennett, M. K., Miller, K. G. and Scheller, R. H. (1993b) Casein kinase II phosphorylates the synaptic vesicle protein p65. *J Neurosci* **13**(4): 1701-7.

Betz, W.J., Mao, F. and Bewick, G.S. (1992) Activity-dependent fluorescent staining and destaining of living vertebrate motor nerve terminals. *J Neurosci* **12**(2): 363-75.

Betz, W. J. and Bewick, G. S. (1993) Optical monitoring of transmitter release and synaptic vesicle recycling at the frog neuromuscular junction. *J Physiol* **460**: 287-309.

Betz, W.J., Mao, F. and Smith, C.B. (1996) Imaging exocytosis and endocytosis. *Curr Opin Neurobiol* **6**(3): 365-71.

Betz, A., Okamoto, M., Benseler, F. and Brose, N. (1997) Direct interaction of the rat unc-13 homologue Munc13-1 with the N terminus of syntaxin. *J Biol Chem* **272**(4): 2520-6.

Betz, A., Thakur, P., Junge, H. J., Ashery, U., Rhee, J. S., Scheuss, V., Rosenmund, C., Rettig, J. and Brose, N. (2001) Functional interaction of the active zone proteins Munc13-1 and RIM1 in synaptic vesicle priming. *Neuron* **30**(1): 183-96.

Betzig, E., Patterson, G.H., Sougrat, R., Lindwasser, O.W., Olenych, S., Bonifacino, J.S., Davidson, M.W., Lippincott-Schwartz, J., Hess, H.F. (2006) Imaging intracellular fluorescent proteins at nanometer resolution. *Science* **313**(5793): 1642-5.

Bhaskar, K., Shareef, M.M., Sharma, V.M., Shetty, A.P., Ramamohan, Y., Pant, H.C., Raju, T.R. and Shetty, K.T. (2004) Co-purification and localisation of Munc18-1 (p67) and Cdk5 with neuronal cytoskeletal proteins. *Neurochem Int* **44**(1): 35-44.

Bittner, M.A. and Holz, R.W. (1992) Kinetic analysis of secretion from permeabilized adrenal chromaffin cells reveals distinct components. *J Biol Chem* **267**(23): 16219-25.

Blasi, J., Chapman, E. R., Yamasaki, S., Binz, T., Niemann, H. and Jahn, R. (1993a) Botulinum neurotoxin C1 blocks neurotransmitter release by means of cleaving HPC-1/syntaxin. *EMBO J* **12**(12): 4821-8.

Blasi, J., Chapman, E.R., Link, E., Binz, T., Yamasaki, S., De Camilli, P., Südhof, T.C., Niemann, H. and Jahn, R. (1993b) Botulinum neurotoxin A selectively cleaves the synaptic protein SNAP-25. *Nature* **365**(6442): 160-3.

Bowen, M. E., Weninger, K., Brunger, A. T. and Chu, S. (2004) Single molecule observation of liposome-bilayer fusion thermally induced by soluble N-ethylmaleimide sensitive-factor attachment protein receptors (SNAREs). *Biophys J* **87**(5): 3569-84.

Bracher, A. and Weissenhorn, W. (2002) Structural basis for the Golgi membrane recruitment of Sly1p by Sed5p. *EMBO J* **21**(22): 6114-24.

Braun, M., Ramracheya, R., Johnson, P. R. and Rorsman, P. (2009) Exocytotic properties of human pancreatic beta-cells. *Ann N Y Acad Sci* **1152**: 187-93.

Brenner, S. (1974) The genetics of *Caenorhabditis elegans*. *Genetics* **77**(1): 71-94.

Brennwald, P., Kearns, B., Champion, K., Keranen, S., Bankaitis, V. and Novick, P. (1994) Sec9 is a SNAP-25-1ike component of a yeast SNARE complex that may be the effector of See4 function in exocytosis. *Cell* **79**(2): 245-58.

Brodin, L., Low, P., Gad, H., Gustafsson, J., Pieribone, V. A. and Shupliakov, O. (1997) Sustained neurotransmitter release: new molecular clues. *Eur J Neurosci* **9**(12): 2503-11.

Brose, N., Hofmann, K., Hata, Y. and Südhof, T.C. (1995) Mammalian homologues of Caenorhabditis elegans unc-13 gene define novel family of C2-domain proteins. *J Biol Chem* **270**(42): 25273-80.

Bryant, N. J. and James, D. E. (2001) Vps45p stabilizes the syntaxin homologue Tlg2p and positively regulates SNARE complex formation. *EMBO J* **20**(13): 3380-8.

Burgess, T. L. and Kelly, R. B. (1987) Constitutive and regulated secretion of proteins. *Annu Rev Cell Biol* **3**: 243-93.

Burgoyne, R.D. (1991) Control of exocytosis in adrenal chromaffin cells. *Biochim Biophys Acta* **1071**(2): 174-202.

Burgoyne, R. D. and Morgan, A. (2003) Secretory granule exocytosis. *Physiol Rev* **83**(2): 581-632.

Burgoyne, R. D. and Morgan, A. (2007) Membrane trafficking: three steps to fusion. *Curr Biol* **17**(7): 255-8.

Burgoyne, R.D., Barclay, J.W., Ciufo, L.F., Graham, M.E., Handley, M.T. and Morgan, A. (2009) The functions of Munc18-1 in regulated exocytosis. *Ann N Y Acad Sci* **1152**: 76–86.

Burkhardt, P., Hattendorf, D. A., Weis, W. I. and Fasshauer, D. (2008) Munc18a controls SNARE assembly through its interaction with the syntaxin N-peptide. *EMBO J* **27**(7): 923-33.

Burkhardt, P., Stegmann, C. M., Cooper, B., Kloepper, T. H., Imig, C., Varoqueaux, F., Wahl, M. C. and Fasshauer, D. (2011) Primordial neurosecretory apparatus identified in the choanoflagellate Monosiga brevicollis. *Proc Natl Acad Sci USA* **108**(37): 15264-9.

Calakos N, Bennett MK, Peterson KE, Scheller RH (1994) Protein-protein interactions contributing to the specificity of intracellular vesicular trafficking. *Science* **263**(5150)**:** 1146-9.

Caro, L. G. and Palade, G. E. (1964) Protein Synthesis, Storage, and Discharge in the Pancreatic Exocrine Cell. An Autoradiographic Study. *J Cell Biol* **20**: 473-95.

Carpp, L.N., Ciufo, L.F., Shanks, S.G., Boyd, A. and Bryant, N.J. (2006) The Sec1p/Munc18 protein Vps45p binds its cognate SNARE proteins via two distinct modes. *J Cell Biol* **173**(6): 927–36.

Carr, C. M., Grote, E., Munson, M., Hughson, F. M. and Novick, P. J. (1999) Sec1p binds to SNARE complexes and concentrates at sites of secretion. *J Cell Biol* **146**(2): 333-44.

Carr, C.M. and Rizo, J. (2010) At the junction of SNARE and SM protein function. *Curr Opin Cell Biol* **22**(4): 488–95.

Cases-Langhoff, C., Voss, B., Garner, A. M., Appeltauer, U., Takei, K., Kindler, S., Veh, R. W., De Camilli, P., Gundelfinger, E. D. and Garner, C. C. (1996) Piccolo, a novel 420 kDa protein associated with the presynaptic cytomatrix. *Eur J Cell Biol* **69**(3): 214-23.

Catterall, W.A. (2000) Structure and regulation of voltage-gated Ca^{2+} channels. *Annu Rev Cell Dev Biol* **16**: 521-55.

Ceccarelli, B. and Hurlbut, W. P. (1980) Ca^{2+}-dependent recycling of synaptic vesicles at the frog neuromuscular junction. *J Cell Biol* **87**(1): 297-303.

Chamberlain, L.H., Burgoyne, R.D. and Gould, G.W. (2001) SNARE proteins are highly enriched in lipid rafts in PC12 cells: Implications for the spatial control of exocytosis. *Proc Natl Acad Sci USA*. **98**(10): 5619–24.

Chamberlain, L.H. and Gould, G.W. (2002) The vesicle- and target-SNARE proteins that mediate Glut4 vesicle fusion are localised in detergent-insoluble lipid rafts present on distinct intracellular membranes. *J Biol Chem* **277**(51): 49750–4.

Chapman, E. R., An, S., Barton, N. and Jahn, R. (1994) SNAP-25, a t-SNARE which binds to both syntaxin and synaptobrevin via domains that may form coiled coils. *J Biol Chem* **269**(44): 27427-32.

Chapman, E.R. (2002) Synaptotagmin: a $Ca^{(2+)}$ sensor that triggers exocytosis? *Nat Rev Mol Cell Biol* **3**(7): 498–508.

Chen, Y. A., Scales, S. J., Jagath, J. R. and Scheller, R. H. (2001) A discontinuous SNAP-25 C-terminal coil supports exocytosis. *J Biol Chem* **276**(30): 28503-8.

Chen, Y. A. and Scheller, R. H. (2001) SNARE-mediated membrane fusion. *Nat Rev Mol Cell Biol* **2**(2): 98-106.

Chen, X., Lu, J., Dulubova, I. and Rizo, J. (2008) NMR analysis of the closed conformation of syntaxin-1. *J Biomol NMR* **41**(1): 43-54.

Childs, G. V., Unabia, G., Tibolt, R. and Lloyd, J. M. (1987) Cytological factors that support nonparallel secretion of luteinizing hormone and follicle-stimulating hormone during the estrous cycle. *Endocrinology* **121**(5): 1801-13.

Chow, R.H., von Ruden, L. and Neher, E. (1992) Delay in vesicle fusion revealed by electrochemical monitoring of single secretory events in adrenal chromaffin cells. *Nature* **356**(6364): 60– 3.

Ciufo, L. F., Barclay, J. W., Burgoyne, R. D. and Morgan, A. (2005) Munc18-1 regulates early and late stages of exocytosis via syntaxin-independent protein interactions. *Mol Biol Cell* **16**(2): 470-82.

Clary, D. O., Griff, I. C. and Rothman, J. E. (1990a) SNAPs, a family of NSF attachment proteins involved in intracellular membrane fusion in animals and yeast. *Cell* **61**(4): 709-21.

Clary, D. O. and Rothman, J. E. (1990b) Purification of three related peripheral membrane proteins needed for vesicular transport. *J Biol Chem* **265**(17): 10109-17.

Connell, E., Darios, F., Broersen, K., Gatsby, N., Peak-Chew, S. Y., Rickman, C. and Davletov, B. (2007) Mechanism of arachidonic acid action on syntaxin-Munc18. *EMBO Rep* **8**(4): 414-9.

Coppola, T., Frantz, C., Perret-Menoud, V., Gattesco, S., Hirling, H. and Regazzi, R. (2002) Pancreatic beta-cell protein granuphilin binds Rab3 and Munc-18 and controls exocytosis. *Mol Biol Cell* **13**(6): 1906-15.

Cowan, W. M. and Kandel, E. R. (2000) Brief History of Neurotransmission. Synapses. W. M. Cowan, T. C. Südhof and C. F. Stevens. Baltimore. The John Hopkins University Press.

Craig, T. J., Evans, G. J. and Morgan, A. (2003) Physiological regulation of Munc18/nSec1 phosphorylation on serine-313. *J Neurochem* **86**(6): 1450-7.

Cypionka, A., Stein, A., Hernandez, J.M., Hippchen, H., Jahn, R. and Walla, P.J. (2009) Discrimination between docking and fusion of liposomes reconstituted with neuronal SNARE-proteins using FCS. *Proc Natl Acad Sci USA* **106**(44): 18575-80.

Damer, C.K. and Creutz, C.E. (1996) Calcium-dependent self-association of synaptotagmin I. *J Neurochem* **67**(4): 1661–8.

Dascher, C., Ossig, R., Gallwitz, D. and Schmitt, H. D. (1991) Identification and structure of four yeast genes (SLY) that are able to suppress the functional loss of YPT1, a member of the RAS superfamily. *Mol Cell Biol* **11**(2): 872-85.

Degtyar, V.E., Allersma, M.W., Axelrod, D. and Holz, R.W. (2007) Increased motion and travel, rather than stable docking, characterize the last moments before secretory granule fusion. *Proc Natl Acad Sci USA* **104**(40): 15929-34.

de Jong, A.P.H., Schmitz, S.K., Toonen, R.F.G. and Verhage, M. (2012) Dendritic position is a major determinant of presynaptic strength. *J Cell Biol* **197**(2): 327-37.

De Robertis, E. and Bennett, H. S. (1955) Some features of the submicroscopic morphology of synapses in frog and earthworm. *J Biophys Biochem Cytol* **1**(1): 47-58.

de Vries, K. J., Geijtenbeek, A., Brian, E. C., de Graan, P. N., Ghijsen, W. E. and Verhage, M. (2000) Dynamics of munc18-1 phosphorylation/dephosphorylation in rat brain nerve terminals. *Eur J Neurosci* **12**(1): 385-90.

de Wit, H., Cornelisse, L. N., Toonen, R. F. and Verhage, M. (2006) Docking of secretory vesicles is syntaxin dependent. *PLoS ONE* **1**: 126.

de Wit, H., Walter, A. M., Milosevic, I., Gulyas-Kovacs, A., Riedel, D., Sørensen, J. B. and Verhage, M. (2009) Synaptotagmin-1 docks secretory vesicles to syntaxin-1/SNAP-25 acceptor complexes. *Cell* **138**(5): 935-46.

de Wit, H. (2010) Morphological docking of secretory vesicles. *Histochem Cell Biol* **134**(2): 103-13.

Deak, F., Xu, Y., Chang, W. P., Dulubova, I., Khvotchev, M., Liu, X., Südhof, T. C. and Rizo, J. (2009) Munc18-1 binding to the neuronal SNARE complex controls synaptic vesicle priming. *J Cell Biol* **184**(5): 751-64.

Del Castillo, J. and Katz, B. (1954) Quantal components of the end-plate potential. *J Physiol* **124**(3): 560-73.

Diao, J., Su, Z., Lu, X., Yoon, T. Y., Shin, Y. K. and Ha, T. (2010) Single-Vesicle Fusion Assay Reveals Munc18-1 Binding to the SNARE Core Is Sufficient for Stimulating Membrane Fusion. *ACS Chem Neurosci* **1**(3): 168-174.

Dietrich, C., Yang, B., Fujiwara, T., Kusumi, A. and Jacobson, K. (2002) Relationship of lipid rafts to transient confinement zones detected by single particle tracking. *Biophys J* **82**(1): 274–84.

Diggle, P. J. (2003) Statistical Analysis of Spatial Point Patterns. New York: Oxford University Press Inc.

Dodge, F. A., Jr. and Rahamimoff, R. (1967) Co-operative action a calcium ions in transmitter release at the neuromuscular junction. *J Physiol* **193**(2): 419-32.

Donnert, G., Keller, J., Medda, R., Andrei, M.A., Rizzoli, S.O., Lührmann, R., Jahn, R., Eggeling, C. and Hell, S.W. (2006) Macromolecular-scale resolution in biological fluorescence microscopy. *Proc Natl Acad Sci USA* **103**(31): 11440-5.

Douglass, A.D. and Vale, R.D. (2005) Single-Molecule Microscopy Reveals Plasma Membrane Microdomains Created by Protein-Protein Networks that Exclude or Trap Signaling Molecules in T Cells. *Cell* **121**(6): 937-50.

Doussau, F. and Augustine, G. J. (2000) The actin cytoskeleton and neurotransmitter release: an overview. *Biochimie* **82**(4): 353-63.

Dresbach, T., Burns, M. E., O'Connor, V., DeBello, W. M., Betz, H. and Augustine, G. J. (1998) A neuronal Sec1 homolog regulates neurotransmitter release at the squid giant synapse. *J Neurosci* **18**(8): 2923-32.

Dulubova, I., Sugita, S., Hill, S., Hosaka, M., Fernandez, I., Südhof, T. C. and Rizo, J. (1999) A conformational switch in syntaxin during exocytosis: role of munc18. *EMBO J* **18**(16): 4372-82.

Dulubova, I., Yamaguchi, T., Wang, Y., Südhof, T.C. and Rizo, J. (2001) Vam3p structure reveals conserved and divergent properties of syntaxins. *Nat Struct Biol* **8**(3): 258-64.

Dulubova, I., Yamaguchi, T., Gao, Y., Min, S.W., Hurveva, I., Südhof, T.C. and Rizo, J. (2002) How Tlg2p/syntaxin 16 'snares' Vps45. *EMBO J* **21**(14): 3620-31.

Dulubova, I., Yamaguchi, T., Arac, D., Li, H., Huryeva, I., Min, S.W., Rizo, J. and Südhof, T.C. (2003) Convergence and divergence in the mechanism of SNARE binding by Sec1/Munc18-like proteins. *Proc Natl Acad Sci USA* **100**(1): 32–37.

Dulubova, I., Khvotchev, M., Liu, S., Huryeva, I., Südhof, T. C. and Rizo, J. (2007) Munc18-1 binds directly to the neuronal SNARE complex. *Proc Natl Acad Sci USA* **104**(8): 2697-702.

Dumas, M., Schwab, M.E., Baumann, R. and Thoenen, H. (1979) Retrograde transport of tetanus toxin through a chain of two neurons. *Brain Res* **165**: 354-7.

Duncan, R.R., Greaves, J., Wiegand, U.K., Matskevich, I., Bodammer, G., Apps, D.K., Shipston, M.J. and Chow, R.H. (2003) Functional and spatial segregation of secretory vesicle pools according to vesicle age. *Nature* **422**(6928): 176-80.

Duncan, R.R., Bergmann, A., Cousin, M.A., Apps, D.K. and Shipston, M.J. (2004) Multi-dimensional time-correlated single photon counting (TCSPC) fluorescence lifetime imaging microscopy (FLIM) to detect FRET in cells. *J Microsc* **215**(1): 1-12.

Ellena, J.F., Liang, B., Wiktor, M., Stein, A., Cafiso, D.S., Jahn, R. and Tamm, L.K. (2009) Dynamic structure of lipid-bound synaptobrevin suggests a nucleation-propagation mechanism for trans-SNARE complex formation. *Proc Natl Acad Sci USA* **106**(48): 20306-11.

Elmqvist, D. and Quastel, D.M. (1965) A quantitative study of end-plate potentials in isolated human muscle. *J Physiol* **178**(3): 505-29.

Elson, E.L., Schlessinger, J., Koppel, D.E., Axelrod, D. and Webb, W.W. (1976) Measurement of lateral transport on cell surfaces. *Prog Clin Biol Res* **9**: 137-47.

Ewers, H., Smith, A.E., Sbalzarini, I.F., Lilie, H., Koumoutsakos, P. and Helenius, A. (2005) Single-particle tracking of murine polyoma virus-like particles on live cells and artificial membranes. *Proc Natl Acad Sci USA* **102**(42): 15110-5.

Fasshauer, D., Antonin, W., Margittai, M., Pabst, S. and Jahn, R. (1999) Mixed and non-cognate SNARE complexes. Characterization of assembly and biophysical properties. *J Biol Chem* **274**(22): 15440-6.

Fasshauer, D. (2003) Structural insights into the SNARE mechanism. *Biochim Biophys Acta* **1641**(2-3): 87-97.

Fasshauer, D. and Margittai, M. (2004) A transient interaction of SNAP-25 and syntaxin nucleates SNARE assembly. *J Biol Chem* **279**(9): 7613-21.

Feder, T.J., Brust-Mascher, I., Slattery, J.P., Baird, B. and Webb, W.W. (1996) Constrained diffusion or immobile fraction on cell surfaces: a new interpretation. *Biophys J* **70**(6): 2767-73.

Fernandez, I., Ubach, J., Dulubova, I., Zhang, X., Südhof, T.C. and Rizo, J. (1998) Three-dimensional structure of an evolutionarily conserved N-terminal domain of syntaxin1A. *Cell* **94**(6): 841-9.

Ferro-Novick, S. and Jahn, R. (1994) Vesicle fusion from yeast to man. *Nature* **370**(6486): 191-3.

Fischer von Mollard, G.F. and Stevens, T.H. (1999) The *Saccharomyces cerevisiae* v-SNARE Vti1p is required for multiple membrane transport pathways to the vacuole. *Mol Biol Cell* **10**(6): 1719–32.

Fisher, R. J., Pevsner, J. and Burgoyne, R. D. (2001) Control of fusion pore dynamics during exocytosis by Munc18. *Science* **291**(5505): 875-8.

Fletcher, A. I., Shuang, R., Giovannucci, D. R., Zhang, L., Bittner, M. A. and Stuenkel, E. L. (1999) Regulation of exocytosis by cyclin-dependent kinase 5 via phosphorylation of Munc18. *J Biol Chem* **274**(7): 4027-35.

Foletti, D. L., Lin, R., Finley, M. A. and Scheller, R. H. (2000) Phosphorylated syntaxin 1 is localised to discrete domains along a subset of axons. *J Neurosci* **20**(12): 4535-44.

Fölling, J., Bossi, M., Bock, H., Medda, R., Wurm, C.A., Hein, B., Jakobs, S., Eggeling, C., Hell, S.W. (2008) Fluorescence nanoscopy by ground-state depletion and single-molecule return. *Nat Methods* **5**(11): 943-5.

Foran, P., Lawrence, G. W., Shone, C. C., Foster, K. A. and Dolly, J. O. (1996) Botulinum neurotoxin C1 cleaves both syntaxin and SNAP-25 in intact and permeabilized chromaffin cells: correlation with its blockade of catecholamine release. *Biochemistry* **35**(8): 2630-6.

Foster, L.J., De Hoog, C.L. and Mann, M. (2003) Unbiased quantitative proteomics of lipid rafts reveals high specificity for signaling factors. *Proc Natl Acad Sci USA* **100**(10): 5813–8.

Fries, E. and Rothman, J. E. (1980) Transport of vesicular stomatitis virus glycoprotein in a cell-free extract. *Proc Natl Acad Sci USA* **77**(7): 3870-4.

Fujita, Y., Sasaki, T., Fukui, K., Kotani, H., Kimura, T., Hata, Y., Südhof, T. C., Scheller, R. H. and Takai, Y. (1996) Phosphorylation of Munc-18/n-Sec1/rbSec1 by protein kinase C: its implication in regulating the interaction of Munc-18/n-Sec1/rbSec1 with syntaxin. *J Biol Chem* **271**(13): 7265-8.

Fukuda, M., Kanno, E., Saegusa, C., Ogata, Y. and Kuroda, T. S. (2002) Slp4-a/granuphilin-a regulates dense-core vesicle exocytosis in PC12 cells. *J Biol Chem* **277**(42): 39673-8.

Furgason, M.L., MacDonald, C., Shanks, S.G., Ryder, S.P., Bryant, N.J. and Munson, M. (2009) The N-terminal peptide of the syntaxin Tlg2p modulates binding of its closed conformation to Vps45p. *Proc Natl Acad Sci USA* **106**(34): 14303–8.

Galli, T., Garcia, P.E., Mundigl, O., Chilcote, T.J. and De Camilli, P. (1995) v- and t-SNAREs in neuronal exocytosis: a need for additional components to define sites of release. *Neuropharmacology* **34**(11): 1351-60.

Garcia, E. P., Gatti, E., Butler, M., Burton, J. and De Camilli, P. (1994) A rat brain Sec1 homologue related to Rop and UNC18 interacts with syntaxin. *Proc Natl Acad Sci USA* **91**(6): 2003-7.

Garcia, P.E., McPherson, P.S., Chilcote, T.J., Takei, K. and De Camilli, P. (1995) rbSec1A and B colocalise with syntaxin 1 and SNAP-25 throughout the axon, but are not in a stable complex with syntaxin. *J Cell Biol* **129**(1): 105-120.

Gengyo-Ando, K., Kamiya, Y., Yamakawa, A., Kodaira, K., Nishiwaki, K., Miwa, J., Hori, I. and Hosono, R. (1993) The C. elegans unc-18 gene encodes a protein expressed in motor neurons. *Neuron* **11**(4): 703-11.

Gengyo-Ando, K., Kitavama, H., Mukaida, M. and Ikawa, Y. (1996) A murine neural-specific homolog corrects cholinergic defects in Caenorhabditis elegans unc-18 mutants. *J Neurosci* **16**(21): 6695-702.

Geppert, M., Goda, Y., Hammer, R.E., Li, C., Rosahl, T.W., Stevens, C.F. and Südhof, T.C. (1994) Synaptotagmin 1: A major Ca^{2+} sensor for transmitter release at a central synapse. *Cell* **79**(4): 717-27.

Gerber, S. H., Rah, J. C., Min, S. W., Liu, X., de Wit, H., Dulubova, I., Meyer, A. C., Rizo, J., Arancillo, M., Hammer, R. E., Verhage, M., Rosenmund, C. and Südhof, T. C. (2008) Conformational switch of syntaxin-1 controls synaptic vesicle fusion. *Science* **321**(5895): 1507-10.

Gerst, J. E. (1999) SNAREs and SNARE regulators in membrane fusion and exocytosis. *Cell Mol Life Sci* **55**(5): 707-34.

Gladycheva, S.E., Ho, C.S., Lee, Y.Y. and Stuenkel, E.L. (2004) Regulation of syntaxin1A-munc18 complex for SNARE pairing in HEK293 cells. *J Physiol* **558**(Pt 3): 857-71.

Glick, B. S. and Rothman, J. E. (1987) Possible role for fatty acyl-coenzyme A in intracellular protein transport. *Nature* **326**(6110): 309-12.

Goda, K., Ito, H., Kondo, T. and Oyama, T. (2012) Fluorescence correlation spectroscopy to monitor Kai protein-based circadian osciallltions in real time. *J Biol Chem* **287**(5): 3241-8.

Goldstein, J. L., Anderson, R. G. and Brown, M. S. (1979) Coated pits, coated vesicles, and receptor-mediated endocytosis. *Nature* **279**(5715): 679-85.

Gonzalo, S., Greentree, W. K. and Linder, M. E. (1999) SNAP-25 is targeted to the plasma membrane through a novel membrane-binding domain. *J Biol Chem* **274**(30): 21313-8.

Graham, M.E., Sudlow, A.W. and Burgoyne, R.D. (1997) Evidence against an acute inhibitory role of nSec-1 (munc-18) in late steps of regulated exocytosis in chromaffin and PC12 cells. *J Neurochem* ***69****(6):*2369-77.

Graham, M.E., Handley, M.T., Barclay, J.W., Ciufo, L.F., Barrow, S.L., Morgan, A. and Burgoyne, R.D. (2008) A gain-of-function mutant of Munc18-1 stimulates secretory granule recruitment and exocytosis and reveals a direct interaction of Munc18-1 with Rab3. *J Biochem* **409**(2): 407-16.

Greengard, P., Valtorta, F., Czernik, A. J. and Benfenati, F. (1993) Synaptic vesicle phosphoproteins and regulation of synaptic function. *Science* **259**(5096): 780-5.

Grosshans, B.L., Ortiz, D. and Novick, P. (2006) Rabs and their effectors: achieving specificity in membrane traffic. *Proc Natl Acad Sci USA* **103**(32): 11821–7.

Grote, E., Carr, C. M. and Novick, P. J. (2000) Ordering the final events in yeast exocytosis. *J Cell Biol* **151**(2): 439-52.

Guan, R., Dai, H. and Rizo, J. (2008) Binding of the Munc13-1 MUN domain to membrane-anchored SNARE complexes. *Biochemistry* **47**(6): 1474-81.

Gulyas-Kovacs, A., de Wit, H., Milosevic, I., Kochubey, O., Toonen, R., Klingauf, J., Verhage, M. and Sørensen, J.B. (2007) Munc18-1: sequential interactions with the fusion machinery stimulate vesicle docking and priming, *J Neurosci* **27**(32): 8676-86.

Hamilton, R.S., Parton, R.M., Oliveira, R.A., Vendra, G., Ball, G., Nasmyth, K. & Davis, I. (2010) ParticleStats: open source software for the analysis of particle motility and cytoskeletal polarity. *Nucl Acids Res* **38**: 641-6.

Han, X., Wang, C. T., Bai, J., Chapman, E. R. and Jackson, M. B. (2004) Transmembrane segments of syntaxin line the fusion pore of Ca^{2+}-triggered exocytosis. *Science* **304**(5668): 289-92.

Han, L., Jiang, T., Han, G. A., Malintan, N. T., Xie, L., Wang, L., Tse, F. W., Gaisano, H. Y., Collins, B. M., Meunier, F. A. and Sugita, S. (2009) Rescue of Munc18-1 and -2 double knockdown reveals the essential functions of interaction between Munc18 and closed syntaxin in PC12 cells. *Mol Biol Cell* **20**(23): 4962-75.

Han, G. A., Malintan, N. T., Saw, N. M., Li, L., Han, L., Meunier, F. A., Collins, B. M. and Sugita, S. (2011) Munc18-1 domain-1 controls vesicle docking and secretion by interacting with syntaxin-1 and chaperoning it to the plasma membrane. *Mol Biol Cell* **22**(21): 4134-49.

Hanson, P. I. and Whiteheart, S. W. (2005) AAA+ proteins: have engine, will work. *Nat Rev Mol Cell Biol* **6**(7): 519-29.

Harata, N., Pyle, J. L., Aravanis, A. M., Mozhayeva, M., Kavalali, E. T. and Tsien, R. W. (2001) Limited numbers of recycling vesicles in small CNS nerve terminals: implications for neural signaling and vesicular cycling. *Trends Neurosci* **24**(11): 637-43.

Harrison, S. D., Broadie, K., van de Goor, J. and Rubin, G. M. (1994) Mutations in the Drosophila Rop gene suggest a function in general secretion and synaptic transmission. *Neuron* **13**(3): 555-66.

Hata, Y., Slaughter, C. A. and Südhof, T. C. (1993) Synaptic vesicle fusion complex contains unc-18 homologue bound to syntaxin. *Nature* **366**(6453): 347-51.

Hata, Y. and Südhof, T. C. (1995) A novel ubiquitous form of Munc-18 interacts with multiple syntaxins. Use of the yeast two-hybrid system to study interactions between proteins involved in membrane traffic. *J Biol Chem* **270**(22): 13022-8.

Haustein, E. and Schwille, P. (2004) Single-molecule spectroscopic methods. *Curr Opin Struct Biol* **14**(5): 531-40.

Hayashi, T., McMahon, H., Yamasaki, S., Binz, T., Hata, Y., Südhof, T. C. and Niemann, H. (1994) Synaptic vesicle membrane fusion complex: action of clostridial neurotoxins on assembly. *EMBO J* **13**(21): 5051-61.

Hayashi, T., Yamasaki, S., Nauenburg, S., Binz, T. and Niemann, H. (1995) Disassembly of the reconstituted synaptic vesicle membrane fusion complex *in vitro*. *EMBO J* **14**(10): 2317-25.

Hell, S.W. and Wichmann, J. (1994) Breaking the diffraction resolution limit by stimulated emission: stimulated-emission-depletion fluorescence microscopy. *Opt Lett* **19**(11): 780-2.

Hell, S.W., Jakobs, S. and Kastrup, L. (2003) Imaging and writing at the nanoscale with focused visible light through saturable optical transitions. *Appl Phys A* **77**: 859-60.

Hell, S.W. (2009) Microscopy and its focal switch. *Nat Methods* **6**(1):24-32.

Hess, D. T., Slater, T. M., Wilson, M. C. and Skene, J. H. (1992) The 25 kDa synaptosomal-associated protein SNAP-25 is the major methionine-rich polypeptide in rapid axonal transport and a major substrate for palmitoylation in adult CNS. *J Neurosci* **12**(12): 4634-41.

Hess, S.T., Girirajan, T.P., Mason, M.D. (2006) Ultra-high resolution imaging by fluorescence photoactivation localisation microscopy. *Biophys J* **91**(11): 4258-72.

Hess, S.T., Gould, T.J., Gudheti, M.V., Maas, S.A., Mills, K.D. and Zimmerberg, J. (2007) Dynamic clustered distribution of hemagglutinin resolved at 40 nm in living cell membranes discriminates between raft theories. *Proc Natl Acad Sci USA* **104**(44): 17370-5.

Hess, S.W. (2007) Far-field optical nanoscopy. *Science* **316**(5828): 1153-8.

Hessler, N.A., Shirke, A.M. and Malinow, R. (1993) The probability of transmitter release at a mammalian central synapse. *Nature* **366**(6455): 569-72.

Hirling, H. and Scheller, R.H. (1996) Phosphorylation of synaptic vesicle proteins: modulation of the α-SNAP interaction with the core complex. *Proc Natl Acad Sci USA* **93**(21): 11945-9.

Ho, A., Morishita, W., Hammer, R. E., Malenka, R. C. and Südhof, T. C. (2003) A role for Mints in transmitter release: Mint 1 knockout mice exhibit impaired GABAergic synaptic transmission. *Proc Natl Acad Sci USA* **100**(3): 1409-14.

Hodel, A., Schäfer, T., Gerosa, D. and Burger, M.M (1994) In chromaffin cells, the mammalian Sec1p homologue is a syntaxin 1A-binding protein associated with chromaffin granules. *J Biol Chem* **269**(12): 8623-6.

Hosono, R., Hekimi, S., Kamiya, Y., Sassa, T., Murakami, S., Nishiwaki, K., Miwa, J., Taketo, A. and Kodaira, K. I. (1992) The unc-18 gene encodes a novel protein affecting the kinetics of acetylcholine metabolism in the nematode Caenorhabditis elegans. *J Neurochem* **58**(4): 1517-25.

Hu, K., Carroll, J., Fedorovich, S., Rickman, C., Sukhodub, A. and Davletov, B. (2002) Vesicular restriction of synaptobrevin suggests a role for calcium in membrane fusion. *Nature* **415**(6872): 646-50.

Hu, S. H., Latham, C. F., Gee, C. L., James, D. E. and Martin, J. L. (2007) Structure of the Munc18c/Syntaxin4 N-peptide complex defines universal features of the N-peptide binding mode of Sec1/Munc18 proteins. *Proc Natl Acad Sci USA* **104**(21): 8773-8.

Hua, Y. and Scheller, R. H. (2001) Three SNARE complexes cooperate to mediate membrane fusion. *Proc Natl Acad Sci USA* **98**(14): 8065-70.

Huang, C. C., Yang, D. M., Lin, C. C. and Kao, L. S. (2011) Involvement of Rab3A in Vesicle Priming During Exocytosis: Interaction with Munc13-1 and Munc18-1. *Traffic* **12**(10): 1356-70.

Hui, E., Johnson, C. P., Yao, J., Dunning, F. M. and Chapman, E. R. (2009) Synaptotagmin-mediated bending of the target membrane is a critical step in Ca(2+)-regulated fusion. *Cell* **138**(4): 709-21.

Hunt, J.M., Bommert, K., Charlton, M.P., Kistner, A., Habermann, E., Augustine, G.J. and Betz, H. (1994) A post-docking role for synaptobrevin in synaptic vesicle fusion. *Neuron* **12**(6): 1269-79.

Inoue, A., Obata, K. and Akagawa, K. (1992) Cloning and sequence analysis of cDNA for a neuronal cell membrane antigen, HPC-1. *J Biol Chem* **267**(15): 10613-9.

Jahn, R. and Südhof, T. C. (1999) Membrane fusion and exocytosis. *Annu Rev Biochem* **68**: 863-911.

Jahn, R. (2000) Sec1/Munc18 proteins: mediators of membrane fusion moving to center stage. *Neuron* **27**(2): 201-4.

Jahn, R., Lang, T. and Südhof, T. C. (2003) Membrane fusion. *Cell* **112**(4): 519-33.

Jahn, R. (2004) Principles of exocytosis and membrane fusion. *Ann N Y Acad Sci* **1014**: 170-8.

Jamieson, J. D. and Palade, G. E. (1967) Intracellular transport of secretory proteins in the pancreatic exocrine cell. I. Role of the peripheral elements of the Golgi complex. *J Cell Biol* **34**(2): 577-96.

Johnson, J. R., Ferdek, P., Lian, L. Y., Barclay, J. W., Burgoyne, R. D. and Morgan, A. (2009) Binding of UNC-18 to the N-terminus of syntaxin is essential for neurotransmission in Caenorhabditis elegans. *Biochem J* **418**(1): 73-80.

Jorgacevski, J., Potokar, M., Grilc, S., Kreft, M., Liu, W., Barclay, J. W., Buckers, J., Medda, R., Hell, S. W., Parpura, V., Burgoyne, R. D. and Zorec, R. (2011) Munc18-1 tuning of vesicle merger and fusion pore properties. *J Neurosci* **31**(24): 9055-66.

Kai, M., Sakane, F., Jia, Y. J., Imai, S., Yasuda, S. and Kanoh, H. (2006) Lipid phosphate phosphatases 1 and 3 are localised in distinct lipid rafts. *J Biochem* **140**(5): 677-86.

Karatekin, E., Di Giovanni, J., Iborra, C., Coleman, J., O'Shaughnessy, B., Seagar, M. & Rothman, J. E. (2010) A fast, single-vesicle fusion assay mimics physiological SNARE requirements *Proc Natl Acad Sci USA* **107**(8): 3517-21.

Katagiri, H., Terasaki, J., Murata, T., Ishihara, H., Ogihara, T., Inukai, K., Fukushima, Y., Anai, M., Kikuchi, M., Miyazaki, J. and et al. (1995) A novel isoform of syntaxin-binding protein homologous to yeast Sec1 expressed ubiquitously in mammalian cells. *J Biol Chem* **270**(10): 4963-6.

Katz, B. and Miledi, R. (1967) The timing of calcium action during neuromuscular transmission. *J Physiol* **189**(3): 535-44.

Katz, B. (1969) The release of neural transmitter substances. Liverpool University Press, Liverpool, UK.

Kee, Y. and Scheller, R.H. (1996) Localisation of synaptotagmin-binding domains on syntaxin. *J Neurosci.* **16**(6): 1975–81.

Kelly, R. B. (1993) Storage and release of neurotransmitters. *Cell* **72** Suppl: 43-53.

Khvotchev, M., Dulubova, I., Sun, J., Dai, H., Rizo, J. and Südhof, T. C. (2007) Dual modes of Munc18-1/SNARE interactions are coupled by functionally critical binding to syntaxin-1 N terminus. *J Neurosci* **27**(45): 12147-55.

Kim, S.A., Heinze, K.G. and Schwille, P. (2007) Fluorescence correlation spectroscopy in living cells. *Nat Methods* **4**(11): 963-73.

Kim, S.A., Sanabria, H., Digman, M.A., Gratton, E., Schwille, P., Zipfel, W.R. and Waxham, M.N. (2010) Quantifying translational mobility in neurons: comparison between current optical techniques. *J Neurosci* **30**(49): 16409-16.

Kuromi, H. and Kidokoro, Y. (1998) Two distinct pools of synaptic vesicles in single presynaptic boutons in a temperature-sensitive Drosophila mutant, shibire. *Neuron* **20**(5): 917-25.

Kusumi, A., Sako, Y. and Yamamoto, M. (1993) Confined lateral diffusion of membrane receptors as studied by single particle tracking (nanovid microscopy). Effects of calcium-induced differentiation in cultured epithelial cells. *Biophys J* **65**(5): 2021-40.

Lakowicz, J.R., Szmacinski, H., Nowaczyk, K., Lederer, W.J., Kirby, M.S., Johnson, M.L. (1994) Fluorescence lifetime imaging of intracellular calcium in COS cells using Quin-2. *Cell Calcium* **15**(1): 7-27.

Landis, D. M., Hall, A. K., Weinstein, L. A. and Reese, T. S. (1988) The organization of cytoplasm at the presynaptic active zone of a central nervous system synapse. *Neuron* **1**(3): 201-9.

Lang, T., Bruns, D., Wenzel, D., Riedel, D., Holyroyd, P., Thiele, C. and Jahn, R. (2001) SNAREs are concentrated in cholesterol-dependent clusters that define docking and fusion sites for exocytosis. *EMBO J* **20**(9): 2202-13.

Li, C., Ullrich, B., Zhang, J.Z., Anderson, G.W., Brose, N. and Südhof, T.C. (1995) Ca^{2+}-dependent and -independent activities of neural and non-neural synaptotagmins. *Nature* **375**(6532): 594–599.

Lin, R.C. and Scheller, R.H. (2000) Mechanisms of synaptic vesicle exocytosis. *Annu Rev Cell Dev Biol* **16**: 19-49.

Liu, C. and Hermann, T.E. (1978) Characterization of ionomycin as a calcium ionophore. *J Biol Chem* **253**(17): 5892-4.

Lippincott-Schwartz, J. and Patterson, G.H. (2003) Development and use of fluorescent protein markers in living cells. *Science* **300**(5616): 87-91.

Loranger, S. S. and Linder, M. E. (2002) SNAP-25 traffics to the plasma membrane by a syntaxin-independent mechanism. *J Biol Chem* **277**(37): 34303-9.

Low, S.H., Vasanji, A., Nanduri, J., He, M., Sharma, N., Koo, M., Drazba, J. and Weimbs, T. (2006) Syntaxins 3 and 4 are concentrated in separate clusters on the plasma membrane before the establishment of cell polarity. *Mol Biol Cell* **17**(2): 977–89.

Ma, C., Li, W., Xu, Y. and Rizo, J. (2011) Munc13 mediates the transition from the closed syntaxin-Munc18 complex to the SNARE complex. *Nat Struct Mol Biol* **18**(5): 542-9.

Madabushi, S., Yao, H., Marsh, M., Kristensen, D.M., Philippi, A., Sowa, M.E. and Lichtarge, O. (2002) Structural clusters of evolutionary trace residues are statistically significant and common in proteins. *J Mol Biol* **316**(1): 139-54.

Magde, D., Elson, E. and Webb, W.W. (1972) Thermodynamic Fluctuations in a Reacting System - Measurement by Fluorescence Correlation Spectroscopy. *Phys Rev Lett*. **29**(11): 705-8.

Maksymowych, A.B. and Simpson, L.L. (1998) Binding and transcytosis of botulinum neurotoxin by polarized human colon carcinoma cells. *J Biol Chem* **273**(34): 21950-7.

Maksymowych, A.B., Reinhard, M., Malizio, C.J., Goodnough, M.C., Johnson, E.A. and Simpson, L.L. (1999) Pure botulinum neurotoxin is absorbed from the stomach and small intestine and produces peripheral neuromuscular blockade. *Infect Immun* **67**(9): 4708-12.

Malacombe, M., Bader, M. F. and Gasman, S. (2006) Exocytosis in neuroendocrine cells: new tasks for actin. *Biochim Biophys Acta* **1763**(11): 1175-83.

Malhotra, V., Orci, L., Glick, B. S., Block, M. R. and Rothman, J. E. (1988) Role of an N-ethylmaleimide-sensitive transport component in promoting fusion of transport vesicles with cisternae of the Golgi stack. *Cell* **54**(2): 221-7.

Malintan, N. T., Nguyen, T. H., Han, L., Latham, C. F., Osborne, S. L., Wen, P. J., Lim, S. J., Sugita, S., Collins, B. M. and Meunier, F. A. (2009) Abrogating Munc18-1-SNARE complex interaction has limited impact on exocytosis in PC12 cells. *J Biol Chem* **284**(32): 21637-46.

Manley, S., Gillette, J.M., Patterson, G.H., Shroff, H., Hess, H.F., Betzig, E. and Lippincott-Schwartz, J. (2008) High-density mapping of single-molecule trajectories with photoactivated localisation microscopy. *Nat Methods* **5**(2): 155-157.

Manley, S., Gillette, J.M. and Lippincott-Schwartz, J. (2010) Single-particle tracking photoactivated localisation microscopy for mapping single-molecule dynamics. *Methods Enzymol* **475**: 109-120.

Martens, S., Kozlov, M. M. and McMahon, H. T. (2007) How synaptotagmin promotes membrane fusion. *Science* **316**(5828): 1205-8.

Martinez-Arca, S., Proux-Giillardeaux, V., Alberts, P., Louvard, D. and Galli, T. (2003) Ectopic expression of syntaxin1 in the ER redirects TI-VAMP- and cellubrevin-containing vesicles. *J Cell Sci* **116**(13): 2805-16.

Mayer, A., Wickner, W. and Haas, A. (1996) Sec18p (NSF)-driven release of Sec17p (alpha-SNAP) can precede docking and fusion of yeast vacuoles. *Cell* **85**(1): 83-94.

McEwen, J. M. and Kaplan, J. M. (2008) UNC-18 promotes both the anterograde trafficking and synaptic function of syntaxin. *Mol Biol Cell* **19**(9): 3836-46.

McEvoy, A.L., Greenfield, D., Bates, M. and Liphardt, J. (2010) Q&A: Single-molecule localisation microscopy for biological imaging. *BMC Biol* **8**: 106.

McMahon, H.T., Missler, M., Li, C. and Südhof, T.C. (1995) Complexins: Cytosolic proteins that regulate SNAP receptor function. *Cell* **83**(1): 111-19.

McNeilly, A. S., Crawford, J. L., Taragnat, C., Nicol, L. and McNeilly, J. R. (2003) The differential secretion of FSH and LH: regulation through genes, feedback and packaging. *Reprod Suppl* **61**: 463-76.

Medine, C. N., Rickman, C., Chamberlain, L. H. and Duncan, R. R. (2007) Munc18-1 prevents the formation of ectopic SNARE complexes in living cells. *J Cell Sci* **120**(Pt 24): 4407-15.

Meijer, M., Burkhardt, P., de Wit, H., Toonen, R.F., Fasshauer, D. and Verhage, M. (2012) Munc18-1 mutations that strongly impair SNARE-complex binding support normal synaptic transmission. *EMBO J* [Epub ahead of print]

Minton, N. P. (1995) Molecular genetics of clostridial neurotoxins. *Curr Top Microbiol Immunol* **195**: 161-94.

Misura, K. M., Scheller, R. H. and Weis, W. I. (2000) Three-dimensional structure of the neuronal-Sec1-syntaxin 1a complex. *Nature* **404**(6776): 355-62.

Mochida, S., Sheng, Z. H., Baker, C., Kobayashi, H. and Catterall, W. A. (1996) Inhibition of neurotransmission by peptides containing the synaptic protein interaction site of N-type Ca^{2+} channels. *Neuron* **17**(4): 781-8.

Moerner, W.E. and Kador, L. (1989) Optical detection and spectroscopy of single molecules in a solid. *Phys Rev Lett* **62**(21): 2535-8.

Mohrmann, R., de Wit, H., Verhage, M., Neher, E. and Sorensen, J. B. (2010) Fast vesicle fusion in living cells requires at least three SNARE complexes. *Science* **330**(6003): 502-5.

Montecucco, C. and Schiavo, G. (1994) Mechanism of action of tetanus and botulinum neurotoxins. *Mol Microbiol* **13**(1): 1-8.

Müetze, J., Ohrt, T. and Schwille, P. (2011) Fluorescence correlation spectroscopy in vivo. *Las Photo Rev* **5**(1): 52-67.

Murthy, V.N., Sejnowski, T.J. and Stevens, C.F. (1997) Heterogeneous release properties of visualized individual hippocampal synapses. *Neuron* **18**(4): 599-612.

Nakata, T. and Hirokawa, N. (1992) Organization of cortical cytoskeleton of cultured chromaffin cells and involvement in secretion as revealed by quick-freeze, deep-etching, and double-label immunoelectron microscopy. *J Neurosci* **12**(6): 2186-97.

Nakada, C., Ritchie, K., Oba, Y., Nakamura, M., Hotta, Y., Iino, R., Kasai, R.S., Yamaguchi, K., Fujiwara, T. and Kusumi, A. (2003) Accumulation of anchored proteins forms membrane diffusion barriers during neuronal polarization. *Nat Cell Biol* **5**(7): 626–32.

Neher, E. and Zucker, R.S. (1993) Multiple calcium-dependent processes related to secretion in bovine chromaffin cells. *Neuron* **10**(1): 21-30.

Nichols, B. J., Ungermann, C., Pelham, H. R., Wickner, W. T. and Haas, A. (1997) Homotypic vacuolar fusion mediated by t- and v-SNAREs. *Nature* **387**(6629): 199-202.

Nili, U., de Wit, H., Gulyas-Kovacs, A., Toonen, R. F., Sorensen, J. B., Verhage, M. and Ashery, U. (2006) Munc18-1 phosphorylation by protein kinase C potentiates vesicle pool replenishment in bovine chromaffin cells. *Neuroscience* **143**(2): 487-500.

Novick, P. and Schekman, R. (1979) Secretion and cell-surface growth are blocked in a temperature-sensitive mutant of Saccharomyces cerevisiae. *Proc Natl Acad Sci USA* **76**(4): 1858-62.

Novick, P., Field, C. and Schekman, R. (1980) Identification of 23 complementation groups required for post-translational events in the yeast secretory pathway. *Cell* **21**(1): 205-15.

Novick, P., Ferro, S. and Schekman, R. (1981) Order of events in the yeast secretory pathway. *Cell* **25**(2): 461-9.

O'Connor, V., Heuss, C., De Bello, W.M., Dresbach, T., Charlton, M.P., Hunt, J.H., Pellegrini, L.L., Hodel, A., Burger, M.M., Betz, H., Augustine, G.J. and Schafer, T. (1997) Disruption of syntaxin-mediated protein interactions blocks neurotransmitter secretion. *Proc Natl Acad Sci USA* **94**(22): 12186-91.

Ohara-Imaizumi, M., Nishiwaki, C., Kikuta, T., Kumakura, K., Nakamichi, Y. and Nagamatsu, S. (2004) Site of docking and fusion of insulin secretory granules in live MIN6 beta cells analyzed by TAT-conjugated anti-syntaxin 1 antibody and total internal reflection fluorescence microscopy. *J Biol Chem* **279**(9): 8403–8.

Ohtsuka, T., Takao-Rikitsu, E., Inoue, E., Inoue, M., Takeuchi, M., Matsubara, K., Deguchi-Tawarada, M., Satoh, K., Morimoto, K., Nakanishi, H. and Takai, Y. (2002) Cast: a novel protein of the cytomatrix at the active zone of synapses that forms a ternary complex with RIM1 and munc13-1. *J Cell Biol* **158**(3): 577-90.

Okamoto, M. and Südhof, T. C. (1997) Mints, Munc18-interacting proteins in synaptic vesicle exocytosis. *J Biol Chem* **272**(50): 31459-64.

Okamoto, M., Matsuyama, T. and Sugita, M. (2000) Ultrastructural localisation of mint1 at synapses in mouse hippocampus. *Eur J Neurosci* **12**(8): 3067-72.

O'Kane, C.J., Schiavo, G. and Sweeney, S.T. (1999) Toxins that affect neurotransmitter release. Neurotransmitter release, Bellen, H. (ed). Oxford University Press, Oxford.

Orita, S., Sasaki, T., Komuro, R., Sakaguchi, G., Maeda, M., Igarashi, H. and Takai, Y. (1996) Doc2 enhances Ca^{2+}-dependent exocytosis from PC12 cells. *J Biol Chem* **271**(13): 7257-60.

Orrit, M. and Bernard, J. (1990) Single pentacene molecules detected by fluorescence excitation in a p-terphenyl crystal. *Phys Rev Lett* **65** (21): 2716-9.

Osen Sand, A., Staple, J. K., Naldi, E., Schiavo, G., Rossetto, O., Petitpierre, S., Malgaroli, A., Montecucco, C. and Catsicas, S. (1996) Common and distinct fusion proteins in axonal growth and transmitter release. *J Comp Neurol* **367**(2): 222-34.

Ossig, R., Dascher, C., Trepte, H. H., Schmitt, H. D. and Gallwitz, D. (1991) The yeast SLY gene products, suppressors of defects in the essential GTP-binding Ypt1 protein, may act in endoplasmic reticulum-to-Golgi transport. *Mol Cell Biol* **11**(6): 2980-93.

Oyler, G. A., Higgins, G. A., Hart, R. A., Battenberg, E., Billingsley, M., Bloom, F. E. and Wilson, M. C. (1989) The identification of a novel synaptosomal-associated protein, SNAP-25, differentially expressed by neuronal subpopulations. *J Cell Biol* **109**(6 Pt 1): 3039-52.

Pabst, S., Margittai, M., Vainius, D., Langen, R., Jahn, R. and Fasshauer, D. (2002) Rapid and selective binding to the synaptic SNARE complex suggests a modulatory role of complexins in neuroexocytosis. *J Biol Chem* **277**(10): 7838-48.

Palade, G. (1975) Intracellular aspects of the process of protein synthesis. *Science* **189**(4206): 867.

Pawley, J.B. (1995) Handbook of Biological Confocal Microscopy. *Plenum, New York.*

Parlati, F., Weber, T., McNew, J. A., Westermann, B., Söllner, T. H. and Rothman, J. E. (1999) Rapid and efficient fusion of phospholipid vesicles by the alpha-helical core of a SNARE complex in the absence of an N-terminal regulatory domain. *Proc Natl Acad Sci USA* **96**(22): 12565-70.

Parsons, T.D., Coorssen, J.R., Horstmann, H. and Almers, W. (1995) Docked granules, the exocytic burst, and the need for ATP hydrolysis in endocrine cells. *Neuron* **15**(5): 1085-96.

Parton, R.M., Hamilton, R.S., Ball, G., Yang, L., Cullen, C.F., Lu, W., Ohkura, H. and Davis, I. (2011) A PAR-1-dependent orientation gradient of dynamic microtubules directs posterior cargo transport in the Drosophila oocyte. *J Cell Biol* **194**(1): 121-35.

Pellegrini, L.L., O'Connor, V. and Betz, H. (1994) Fusion complex formation protects synaptobrevin against proteolysis by tetanus toxin light chain. *FEBS Lett* **353**(3): 319-23.

Peng, R. and Gallwitz, D. (2004) Multiple SNARE interactions of an SM protein: Sed5p/Sly1p binding is dispensable for transport. *EMBO J* **23**(20): 3939–49.

Perin, M.S., Fried, V.A., Mignery, G.A., Jahn, R. and Südhof, T.C. (1990) Phospholipid binding by a synaptic vesicle protein homologous to the regulatory region of protein kinase C. *Nature* **345**(6272): 260-3.

Pevsner, J., Hsu, S. C., Braun, J. E., Calakos, N., Ting, A. E., Bennett, M. K. and Scheller, R. H. (1994a) Specificity and regulation of a synaptic vesicle docking complex. *Neuron* **13**(2): 353-61.

Pevsner, J., Hsu, S. C. and Scheller, R. H. (1994b) n-Sec1: a neural-specific syntaxin-binding protein. *Proc Natl Acad Sci USA* **91**(4): 1445-9.

Pieren, M. Schmidt, A. and Mayer, A. (2010) The SM protein Vps33 and the t-SNARE H(abc) domain promote fusion pore opening. *Nat Struct Mol Biol* **17**(6): 710–7.

Pieribone, V. A., Shupliakov, O., Brodin, L., Hilfiker-Rothenfluh, S., Czernik, A. J. and Greengard, P. (1995) Distinct pools of synaptic vesicles in neurotransmitter release. *Nature* **375**(6531): 493-7.

Poirier, M. A., Hao, J. C., Malkus, P. N., Chan, C., Moore, M. F., King, D. S. and Bennett, M. K. (1998a) Protease resistance of syntaxin.SNAP-25.VAMP complexes. Implications for assembly and structure. *J Biol Chem* **273**(18): 11370-7.

Poirier, M. A., Xiao, W., Macosko, J. C., Chan, C., Shin, Y. K. and Bennett, M. K. (1998b) The synaptic SNARE complex is a parallel four-stranded helical bundle. *Nat Struct Biol* **5**(9): 765-9.

Popoli, M. and Mengano, A. (1988) A hemagglutinin specific for sialic acids in a rat brain synaptic vesicle-enriched fraction. *Neurochem Res* **13**(1): 63–7.

Popoli, M., Paterno, R. and Campanella, G. (1991) Identification and partial purification of a GM1-binding protein from presynaptic vesicles. *Acta Neurol (Napoli)* ***13(3):*** 213–9.

Protopopov, V., Govindan, B., Novick, P. and Gerst, J.E. (1993) Homologs of the synaptobrevin/VAMP family of synaptic vesicle proteins function on the late secretory pathway in S. cerevisiae. *Cell* **74**(5): 855-61.

Rathore, S. S., Bend, E. G., Yu, H., Hammarlund, M., Jorgensen, E. M. and Shen, J. (2010) Syntaxin N-terminal peptide motif is an initiation factor for the assembly of the SNARE-Sec1/Munc18 membrane fusion complex. *Proc Natl Acad Sci USA* **107**(52): 22399-406.

Rickman, C. and Davletov, B. (2003) Mechanism of calcium-independent synaptotagmin binding to target SNAREs. *J Biol Chem* **278**(8): 5501-4.

Rickman, C., Archer, D. A., Meunier, F. A., Craxton, M., Fukuda, M., Burgoyne, R. D. and Davletov, B. (2004) Synaptotagmin interaction with the syntaxin/SNAP-25 dimer is

mediated by an evolutionarily conserved motif and is sensitive to inositol hexakisphosphate. *J Biol Chem* **279**(13): 12574-12579.

Rickman, C. and Davletov, B. (2005) Arachidonic acid allows SNARE complex formation in the presence of Munc18. *Chem Biol* **12**(5): 545-53.

Rickman, C., Medine, C. N., Bergmann, A. and Duncan, R. R. (2007) Functionally and spatially distinct modes of munc18-syntaxin 1 interaction. *J Biol Chem* **282**(16): 12097-103.

Rickman, C. and Duncan, R. R. (2010). Munc18/Syntaxin interaction kinetics control secretory vesicle dynamics. *J Biol Chem* **285**(6): 3965-72.

Rickman, C., Medine, C. N., Dun, A. R., Moulton, D. J., Halemani, N. D., Riszzoli, S. O., Chamberlain, L. H. & Duncan, R. R. (2010) tSNARE protein conformations patterned by the lipid microenvironment *J Biol Chem* **285**(18): 13535-41.

Richards, D.A., Guatimosim, C., Rizzoli, S.O. and Betz, W.J. (2003) Synaptic vesicle pools at the frog neuromuscular junction. *Neuron* **39**(3): 529-41.

Richards, D.A., Bai, J. and Chapman, E.R. (2005) Two modes of exocytosis at hippocampal synapses revealed by rate of FM1-43 efflux from individual vesicles. *J Cell Biol* **168**(6): 929-39.

Ripley, B.D. (1977) Modelling spatial patterns. *J Royal Stat Soc* **39**: 172-212.

Ripley, B. D. (1987) Statistical Inferences for Spatial Processes. Cambridge: Cambridge University Press.

Risinger, C. and Bennett, M. K. (1999) Differential phosphorylation of syntaxin and synaptosome-associated protein of 25 kDa (SNAP-25) isoforms. *J Neurochem* **72**(2): 614-24.

Rizzoli, S. O. and Betz, W. J. (2004) The structural organization of the readily releasable pool of synaptic vesicles. *Science* **303**(5666): 2037-9.

Rizzoli, S.O. and Betz, W.J. (2005) Synaptic vesicle pools. *Nat Rev Neurosci* **6**(1): 57-69.

Rorsman, P. and Renstrom, E. (2003) Insulin granule dynamics in pancreatic beta cells. *Diabetologia* **46**(8): 1029-45.

Rosenmund, C., Clements, J.D. and Westbrook, G.L. (1993) Non-uniform probability of glutamate release at a hippocampal synapse. *Science* **262**(5134): 754-7.

Rosenmund, C. and Stevens, C. F. (1996) Definition of the readily releasable pool of vesicles at hippocampal synapses. *Neuron* **16**(6): 1197-207.

Rothman, J. E. (1994a) Intracellular membrane fusion. *Adv Second Messenger Phosphoprotein Res* **29**: 81-96.

Rothman, J. E. (1994b) Mechanisms of intracellular protein transport. *Nature* **372**(6501): 55-63.

Rothman, J. E. and Fries, E. (1981) Transport of newly synthesized vesicular stomatitis viral glycoprotein to purified Golgi membranes. *J Cell Biol* **89**(1): 162-8.

Rowe, J., Corradi, N., Malosio, M. L., Taverna, E., Halban, P., Meldolesi, J. and Rosa, P. (1999) Blockade of membrane transport and disassembly of the Golgi complex by expression of syntaxin 1A in neurosecretion-incompetent cells: prevention by rbSEC1. *J Cell Sci* **112** (Pt 12): 1865-77.

Rowe, J., Calegari, F., Taverna, E., Longhi, R. and Rosa, P. (2001) Syntaxin 1A is delivered to the apical and basolateral domains of epithelial cells: the role of munc-18 proteins. *J Cell Sci* **114**(Pt 18): 3323-32.

Rust, M.J., Bates, M. and Zhuang, X. (2006) Sub-diffraction-limit imaging by stochastic optical reconstruction microscopy (STORM). *Nat Methods* **3**(10): 793-5.

Ryan, T.A., Reuter, H., Wendland, B., Schweizer, F.E., Tsien, R.W. and Smith, S.J. (1993) The kinetics of synaptic vesicle recycling measured at single presynaptic boutons. *Neuron* **11**(4): 713-24.

Sabatini, B.L. and Regehr, W.G. (1996) Timing of neurotransmission at fast synapses in the mammalian brain. *Nature* **384**(6605): 170– 172.

Sako, Y., Minoghchi, S. and Yanagida, T. (2000) Single-molecule imaging of EGFR signalling on the surface of living cells. *Nat Cell Biol* **2**(3): 168-72.

Salzberg, A., Cohen, N., Halachmi, N., Kimchie, Z. and Lev, Z. (1993) The Drosophila Ras2 and Rop gene pair: a dual homology with a yeast Ras-like gene and a suppressor of its loss-of-function phenotype. *Development* **117**(4): 1309-19.

Sankaranarayanan, S. and Ryan, T.A (2000) Real-time measurements of vesicle-SNARE recycling in synapses of the central nervous system. *Nat Cell Biol* **2**(4): 197-204.

Sassa, T., Harada, S., Ogawa, H., Rand, J. B., Maruyama, I. N. and Hosono, R. (1999) Regulation of the UNC-18-Caenorhabditis elegans syntaxin complex by UNC-13. *J Neurosci* **19**(12): 4772-7.

Schermelleh, L., Carlton, P.M., Haase, S., Shao, L., Winoto, L., Kner, P., Burke, B., Cardoso, M.C., Agard, D.A., Gustafsson, M.G., Leonhardt, H. and Sedat, J.W. (2008) Subdiffraction multicolour imaging of the nuclear periphery with 3D structured illumination microscopy. *Science* **320**(5881): 1332-6.

Schiavo, G., Benfenati, F., Poulain, B., Rossetto, O., Polverino de Laureto, P., DasGupta, B. R. and Montecucco, C. (1992) Tetanus and botulinum B neurotoxins block neurotransmitter release by proteolytic cleavage of synaptobrevin. *Nature* **359**(6398): 832-5.

Schiavo, G., Rossetto, O., Catsicas, S., Polverino de Laureto, P., DasGupta, B. R., Benfenati, F. and Montecucco, C. (1993a) Identification of the nerve terminal targets of botulinum neurotoxin serotypes A, D, and E. *J Biol Chem* **268**(32): 23784-7.

Schiavo, G., Santucci, A., Dasgupta, B. R., Mehta, P. P., Jontes, J., Benfenati, F., Wilson, M. C. and Montecucco, C. (1993b) Botulinum neurotoxins serotypes A and E cleave SNAP-25 at distinct COOH-terminal peptide bonds. *FEBS Lett* **335**(1): 99-103.

Schiavo, G., Shone, C. C., Rossetto, O., Alexander, F. C. and Montecucco, C. (1993c) Botulinum neurotoxin serotype F is a zinc endopeptidase specific for VAMP/synaptobrevin. *J Biol Chem* **268**(16): 11516-9.

Schiavo, G., Malizio, C., Trimble, W. S., Polverino de Laureto, P., Milan, G., Sugiyama, H., Johnson, E. A. and Montecucco, C. (1994) Botulinum G neurotoxin cleaves VAMP/synaptobrevin at a single Ala-Ala peptide bond. *J Biol Chem* **269**(32): 20213-6.

Schiavo, G., Shone, C. C., Bennett, M. K., Scheller, R. H. and Montecucco, C. (1995) Botulinum neurotoxin type C cleaves a single Lys-Ala bond within the carboxyl-terminal region of syntaxins. *J Biol Chem* **270**(18): 10566-70.

Schiavo, G. and Montecucco, M. (1997) Clostridial neurotoxins. In: Bacterial Toxins. Tools in Cell Biology and Pharmacology, ed. K. Aktories. London: Chapman & Hall.

Schlessinger, J., Koppel, D.E., Axelrod, D., Jacobson, K., Webb, W.W. and Elson, E.L. (1976) Lateral transport on cell membranes: mobility of concanavalin A receptors on myoblasts. *Proc Natl Acad Sci USA* **73**(7): 2409-13.

Schoch, S., Castillo, P. E., Jo, T., Mukherjee, K., Geppert, M., Wang, Y., Schmitz, F., Malenka, R. C. and Südhof, T. C. (2002) RIM1alpha forms a protein scaffold for regulating neurotransmitter release at the active zone. *Nature* **415**(6869): 321-6.

Schollmeier, Y., Krause, J. M., Kreye, S., Malsam, J. and Söllner, T. H. (2011) Resolving the function of distinct Munc18-1/SNARE protein interaction modes in a reconstituted membrane fusion assay. *J Biol Chem* **286**(35): 30582-90.

Schulze, K. L., Littleton, J. T., Salzberg, A., Halachmi, N., Stern, M., Lev, Z. and Bellen, H. J. (1994) rop, a Drosophila homolog of yeast Sec1 and vertebrate n-Sec1/Munc-18 proteins, is a negative regulator of neurotransmitter release in vivo. *Neuron* **13**(5): 1099-108.

Schütz, G.J., Schindler, H. and Schmidt, T. (1997) Single-molecule microscopy on model membranes reveals anomalous diffusion. *Biophys J* **73**(2): 1073–80.

Schütz, D., Zilly, F., Lang, T., Jahn, R. and Bruns, D. (2005) A dual function for munc-18 in exocytosis of PC12 cells. *Eur J Neurosci* **21**(9): 2419-32.

Schwab, M.E. and Thoenen, H. (1976) Electron microscopic evidence for a transsynaptic migration of tetanus toxin in spinal cord motoneurons: an autoradiographic and morphometric study. *Brain Res* **105**(2): 213-227.

Schwab, M.E. and Thoenen, H. (1978) Selective binding, uptake, and retrograde transport of tetanus toxin by nerve terminals in the rat iris. An electron microscope study using colloidal gold as a tracer. *J Cell Biol* **77**(1): 1-13.

Schwab, M.E., Suda, K. and Thoenen, H. (1979) Selective retrograde transsynaptic transfer of a protein, tetanus toxin, subsequent to its retrograde axonal transport. *J Cell Biol* **82**(3): 798-810.

Schwille, P., Meyer-Almes, F-J. and Rigler, R. (1997) Dual-color fluorescence cross-correlation spectroscopy for multicomponent diffusional analysis in solution. *Biophys J* **72**(4): 1878-86.

Shao, X., Li, C., Fernandez, I., Zhang, X., Südhof, T. C. and Rizo, J. (1997) Synaptotagmin-syntaxin interaction: the C2 domain as a Ca^{2+}-dependent electrostatic switch. *Neuron* **18**(1): 133-42.

Shen, J., Tareste, D. C., Paumet, F., Rothman, J. E. and Melia, T. J. (2007) Selective activation of cognate SNAREpins by Sec1/Munc18 proteins. *Cell* **128**(1): 183-95.

Shen, J., Rathore, S.S., Khandan, L. and Rothman, J.E. (2010) SNARE bundle and syntaxin N-peptide constitute a minimal complement for munc18-1 activation of membrane fusion. *J Chem Biol* **190**(1): 55-63.

Sieber, J.J., Willig, K.I., Heintzmann, R., Hell, S.W. and Lang, T. (2006) The SNARE motif is essential for the formation of syntaxin clusters in the plasma membrane. *Biophys J* **90**(8): 2843–51.

Sieber, J. J., Willig, K. I., Kutzner, C., Gerding-Reimers, C., Harke, B., Donnert, G., Rammner, B., Eggeling, C., Hell, S. W., Grubmuller, H. and Lang, T. (2007) Anatomy and dynamics of a supramolecular membrane protein cluster. *Science* **317**(5841): 1072-6.

Simons, K. and Ikonen, E. (1997) Functional rafts in cell membranes. *Nature* **387**(6633): 569–72.

Sinha, R., Ahmed, S., Jahn, R. and Klingauf, J. (2011) Two synaptobrevin molecules are sufficient for vesicle fusion in central nervous system synapses. *Proc Natl Acad Sci USA* **108**(34): 14318-23.

Söllner, T., Bennett, M. K., Whiteheart, S. W., Scheller, R. H. and Rothman, J. E. (1993a) A protein assembly-disassembly pathway in vitro that may correspond to sequential steps of synaptic vesicle docking, activation, and fusion. *Cell* **75**(3): 409-18.

Söllner, T., Whiteheart, S. W., Brunner, M., Erdjument-Bromage, H., Geromanos, S., Tempst, P. and Rothman, J. E. (1993b) SNAP receptors implicated in vesicle targeting and fusion. *Nature* **362**(6418): 318-24.

Sørensen, J.B., Nagy, G., Varoqueaux, F., Nehring, R.B., Brose, N., Wilson, M.C. and Neher, E. (2003) Differential Control of the Releasable Vesicle Pools by SNAP-25 Splice Variants and SNAP-23. *Cell* **114**(1): 75-86.

Stein, A., Weber, G., Wahl, M.C. and Jahn, R. (2009) Helical extension of the neuronal SNARE complex into the membrane. *Nature* **460**(7254): 525-8.

Stephens, D.J. and Allan, V.J. (2003) Light microscopy techniques for live cell imaging. *Science* **300**(5616): 82-6.

Steyer, J.A., Horstmann, H. and Almers, W. (1997) Transport, docking and exocytosis of single secretory granules in live chromaffin cells. *Nature* **388**(6641): 474-8.

Südhof, T. C., Baumert, M., Perin, M. S. and Jahn, R. (1989) A synaptic vesicle membrane protein is conserved from mammals to Drosophila. *Neuron* **2**(5): 1475-81.

Südhof, T.C., De Camilli, P., Niemann, H. and Jahn, R. (1993) Membrane fusion machinery: insights from synaptic proteins. *Cell* **75**(1): 1-4.

Südhof, T.C. (1995) The synaptic vesicle cycle: a cascade of protein-protein interactions. *Nature* **375**(6533): 645-53.

Südhof, T.C. (2000) The synaptic vesicle cycle revisited. *Neuron* **28**(2): 317-20.

Südhof, T. C. (2004) The synaptic vesicle cycle. *Annu Rev Neurosci* **27**: 509-47.

Südhof, T.C. and Rothman, J.E. (2009) Membrane fusion: grappling with SNARE and SM proteins. *Science* **323**(5913): 474-7.

Sutton, R. B., Fasshauer, D., Jahn, R. and Brunger, A. T. (1998) Crystal structure of a SNARE complex involved in synaptic exocytosis at 2.4 A resolution. *Nature* **395**(6700): 347-53.

Tadokoro, S., Nakanishi, M. and Hirashima, N. (2005) Complexin II facilitates exocytotic release in mast cells by enhancing Ca^{2+} sensitivity of the fusion process. *J Cell Sci* **118**(10): 2239-46.

Takamori, S., Holt, M., Stenius, K., Lemke, E. A., Gronborg, M., Riedel, D., Urlaub, H., Schenck, S., Brugger, B., Ringler, P., Muller, S. A., Rammner, B., Grater, F., Hub, J. S.,

De Groot, B. L., Mieskes, G., Moriyama, Y., Klingauf, J., Grubmuller, H., Heuser, J., Wieland, F. and Jahn, R. (2006). Molecular anatomy of a trafficking organelle. *Cell* **127**(4): 831-46.

Tellam, J. T., McIntosh, S. and James, D. E. (1995) Molecular identification of two novel Munc-18 isoforms expressed in non-neuronal tissues. *J Biol Chem* **270**(11): 5857-63.

Tellam, J. T., Macaulay, S. L., McIntosh, S., Hewish, D. R., Ward, C. W. and James, D. E. (1997) Characterization of Munc-18c and syntaxin-4 in 3T3-L1 adipocytes. Putative role in insulin-dependent movement of GLUT-4. *J Biol Chem* **272**(10): 6179-86.

Terada, S., Kinjo, M. and Hirokawa, N. (2000) Oligomeric tubulin in large transporting complex is transported via kinesin in squid giant axons. *Cell* **103**(1): 141-55.

Teramura, Y., Ichinose, J., Takagi, H., Nishida, K., Yanagida, T. and Sako, Y. (2006) Single-molecule analysis of epidermal growth factor binding on the surface of living cells. *EMBO J* **25**(18): 4215-22.

The Yeast Genome Directory (1997) *Nature* **387**(6632): 5.

Tian, J. H., Das, S. and Sheng, Z. H. (2003) Ca2+-dependent phosphorylation of syntaxin-1A by DAP-kinase regulates its interaction with Munc-18. *J Biol Chem* **278**(28): 26265-74.

Togneri, J., Cheng, Y.S., Munson, M., Hughson, F.M. and Carr, C.M. (2006) Specific SNARE complex binding mode of the Sec1/Munc-18 protein, Sec1p. *Proc Natl Acad Sci USA* **103**(47): 17730-5.

tom Dieck, S., Sanmarti-Vila, L., Langnaese, K., Richter, K., Kindler, S., Soyke, A., Wex, H., Smalla, K. H., Kampf, U., Franzer, J. T., Stumm, M., Garner, C. C. and Gundelfinger, E. D. (1998) Bassoon, a novel zinc-finger CAG/glutamine-repeat protein selectively localised at the active zone of presynaptic nerve terminals. *J Cell Biol* **142**(2): 499-509.

Toonen, R.F. and Verhage, M. (2003) Vesicle trafficking: pleasure and pain from SM genes. *Trends Cell Biol* **13**(4): 177-86.

Toonen, R.F., de Vries, K.J., Zalm, R., Südhof, T.C. and Verhage, M. (2005) Munc18-1 stabilizes syntaxin1, but is not essential for syntaxin1 targeting and SNARE complex formation. *J Neurochem* **93**(6): 1393-400.

Toonen, R.F., Kochubey, O., de Wit, H., Gulyas-Kovacs, A., Konijnenburg, B., Sørensen, J.B., Klingauf, J. and Verhage, M. (2006) Dissecting docking and tethering of secretory vesicles at the target membrane. *EMBO J* **25**(16): 3725-37.

Toonen, R. F. and Verhage, M. (2007) Munc18-1 in secretion: lonely Munc joins SNARE team and takes control. *Trends Neurosci* **30**(11): 564-72.

Trimble, W. S., Cowan, D. M. and Scheller, R. H. (1988) VAMP-1: a synaptic vesicle-associated integral membrane protein. *Proc Natl Acad Sci USA* **85**(12): 4538-42.

Tsuboi, T. and Fukuda, M. (2006) The Slp4-a linker domain controls exocytosis through interaction with munc18-1-syntaxin-1a complex. *Mol Biol Cell* **17**(5): 2101-12.

Uhles, S., Moede, T., Leibiger, B., Berggren, P. O. and Leibiger, I. B. (2003) Isoform-specific insulin receptor signaling involves different plasma membrane domains. *J Cell Biol* **163**(6): 1327-37.

Ungermann, C., Nichols, B. J., Pelham, H. R. and Wickner, W. (1998) A vacuolar v-t-SNARE complex, the predominant form in vivo and on isolated vacuoles, is disassembled and activated for docking and fusion. *J Cell Biol* **140**(1): 61-9.

van den Bogaart, G., Holt, M. G., Bunt, G., Riedel, D., Wouters, F. S. and Jahn, R. (2010) One SNARE complex is sufficient for membrane fusion. *Nat Struct Mol Biol* **17**(3): 358-64.

Veit, M., Söllner, T. H. and Rothman, J. E. (1996) Multiple palmitoylation of synaptotagmin and the t-SNARE SNAP-25. *FEBS Lett* **385**(1-2): 119-23.

Verhage, M., de Vries, K. J., Roshol, H., Burbach, J. P., Gispen, W. H. and Südhof, T. C. (1997) DOC2 proteins in rat brain: complementary distribution and proposed function as vesicular adapter proteins in early stages of secretion. *Neuron* **18**(3): 453-61.

Verhage, M., Maia, A. S., Plomp, J. J., Brussaard, A. B., Heeroma, J. H., Vermeer, H., Toonen, R. F., Hammer, R. E., van den Berg, T. K., Missler, M., Geuze, H. J. and Südhof, T. C. (2000) Synaptic assembly of the brain in the absence of neurotransmitter secretion. *Science* **287**(5454): 864-9.

Verhage, M. and Sorensen, J. B. (2008) Vesicle docking in regulated exocytosis. *Traffic* **9**(9): 1414-24.

Voets, T., Neher, E. and Moser, T. (1999) Mechanisms underlying phasic and sustained secretion in chromaffin cells from mouse adrenal slices. *Neuron* **23**(3): 607-15.

Voets, T. (2000) Dissection of three Ca2+-dependent steps leading to secretion in chromaffin cells from mouse adrenal slices. *Neuron* **28**(2): 537– 45.

Voets, T., Toonen, R. F., Brian, E. C., de Wit, H., Moser, T., Rettig, J., Südhof, T. C., Neher, E. and Verhage, M. (2001) Munc18-1 promotes large dense-core vesicle docking. *Neuron* **31**(4): 581-91.

Von Gersdorff, H. and Matthews, G. (1997) Depletion and replenishment of vesicle pools at ribbon-type synaptic terminal. *J Neurosci* **17**(6): 1919-27.

Vrljic, M., Nishimura, S.Y., Brasselet, S., Moerner, W.E. and McConnell, H.M. (2002) Translational diffusion of individual class II MHC membrane proteins in cells. *Biophys J* **83**(5): 2681-92.

Vrljic, M., Strop, P., Ernst, J.A., Sutton, R.B., Chu, S. and Brunger, A.T. (2010) Molecular mechanism of the synaptotagmin-SNARE interaction in Ca^{2+}-triggered vesicle fusion. *Nat Struct Mol Biol* **17**(3): 325-31.

Wada, Y., Kitamoto, K., Kanbe, T., Tanaka, K. and Anraku, Y. (1990) The SLP1 gene of Saccharomyces cerevisiae is essential for vacuolar morphogenesis and function. *Mol Cell Biol* **10**(5): 2214-23.

Wang, Y., Okamoto, M., Schmitz, F., Hofmann, K. and Südhof, T. C. (1997) Rim is a putative Rab3 effector in regulating synaptic-vesicle fusion. *Nature* **388**(6642): 593-8.

Wang, Y., Liu, X., Biederer, T. and Südhof, T. C. (2002) A family of RIM-binding proteins regulated by alternative splicing: Implications for the genesis of synaptic active zones. *Proc Natl Acad Sci USA* **99**(22): 14464-9.

Wasser, C.R., Ertunc, M., Liu, X. And Kavalali, E.T. (2007) Cholesterol-dependent balance between evoked and spontaneous synaptic vesicle recycling. *J Physiol* **579**(Pt 2): 413-29.

Weber, T., Zemelman, B. V., McNew, J. A., Westermann, B., Gmachl, M., Parlati, F., Söllner, T. H. and Rothman, J. E. (1998) SNAREpins: minimal machinery for membrane fusion. *Cell* **92**(6): 759-72.

Weimer, R. M., Richmond, J. E., Davis, W. S., Hadwiger, G., Nonet, M. L. and Jorgensen, E. M. (2003) Defects in synaptic vesicle docking in unc-18 mutants. *Nat Neurosci* **6**(10): 1023-30.

Weiss, M., Hashimoto, H. and Nilsson, T. (2003) Anomalous protein diffusion in living cells as seen by fluorescence correlation spectroscopy. *Biophys J* **84**(6): 4043-52.

Weninger, K., Bowen, M. E., Choi, U. B., Chu, S. and Brunger, A. T. (2008) Accessory proteins stabilize the acceptor complex for synaptobrevin, the 1:1 syntaxin/SNAP-25 complex. *Structure* **16**(2): 308-20.

Westphal, V., Rizzoli, S.O., Lauterbach, M.A., Kamin, D., Jahn, R. and Hell, S.W. (2008) Video-rate far-field optical nanoscopy dissects synaptic vesicle movement. *Science* **320**(5873): 246-9.

Wickner, W. (2010) Membrane fusion: Five lipids, four SNAREs, three chaperones, two nucleotides, and a Rab, all dancing in a ring on yeast vacuoles. *Annu Rev Cell Dev Biol* **26**: 115–36.

Wienisch, M. and Klingauf, J. (2006) Vesicular proteins exocytosed and subsequently retrieved by compensatory endocytosis are nonidentical. *Nat Neurosci* **9**(8): 1019-27.

Wieser, S., Moertelmaier, M., Fuertbauer, E., Stockinger, H. and Schütz, G.J. (2007) (Un)Confined Diffusion of CD59 in the Plasma Membrane Determined by High-Resolution Single Molecule Microscopy. *Biophys J* **92**(10): 3719-28.

Williams, A.L., Ehm, S., Jacobson, N.C., Xu, D. and Hay, J.C. (2004) rsly1 binding to syntaxin 5 is required for endoplasmic reticulum-to-Golgi transport but does not promote SNARE motif accessibility. *Mol Biol Cell* **15**(1): 162–175.

Williamson, L. C., Halpern, J. L., Montecucco, C., Brown, J. E. and Neale, E. A. (1996) Clostridial neurotoxins and substrate proteolysis in intact neurons: botulinum neurotoxin C acts on synaptosomal-associated protein of 25 kDa. *J Biol Chem* **271**(13): 7694-9.

Willig, K. I., Rizzoli, S. O., Westphal, V., Jahn, R. and Hell, S. W. (2006) STED microscopy reveals that synaptotagmin remains clustered after synaptic vesicle exocytosis. *Nature* **440**(7086): 935-9.

Wilson, D. W., Wilcox, C. A., Flynn, G. C., Chen, E., Kuang, W. J., Henzel, W. J., Block, M. R., Ullrich, A. and Rothman, J. E. (1989) A fusion protein required for vesicle-mediated transport in both mammalian cells and yeast. *Nature* **339**(6223): 355-9.

Wu, M. N., Littleton, J. T., Bhat, M. A., Prokop, A. and Bellen, H. J. (1998) ROP, the Drosophila Sec1 homolog, interacts with syntaxin and regulates neurotransmitter release in a dosage-dependent manner. *EMBO J* **17**(1): 127-39.

Xu, T., Binz, T., Niemann, H. and Neher, E. (1998) Multiple kinetic components of exocytosis distinguished by neurotoxin sensitivity. *Nat Neurosci* **1**(3): 192-200.

Xu, T., Rammner, B., Margittai, M., Artaleio, A.R., Neher, E. and Jahn, R. (1999) Inhibition of SNARE complex assembly differentially affects kinetic components of exocytosis. *Cell* **99**(7): 713-22.

Yamaguchi, T., Dulubova, I., Min, S.W., Rizo, J. and Südhof, T.C. (2002) Sly1 binds to golgi and ER syntaxins via a conserved N-terminal peptide motif. *Dev Cell* **2**(3): 295-305.

Yamasaki, S., Baumeister, A., Binz, T., Blasi, J., Link, E., Cornille, F., Roques, B., Fykse, E. M., Südhof, T. C., Jahn, R. et al. (1994a) Cleavage of members of the synaptobrevin/VAMP family by types D and F botulinal neurotoxins and tetanus toxin. *J Biol Chem* **269**(17): 12764-72.

Yamasaki, S., Binz, T., Hayashi, T., Szabo, E., Yamasaki, N., Eklund, M., Jahn, R. and Niemann, H. (1994b) Botulinum neurotoxin type G proteolyses the Ala81-Ala82 bond of rat synaptobrevin 2. *Biochem Biophys Res Commun* **200**(2): 829-35.

Yamasaki, S., Hu, Y., Binz, T., Kalkuhl, A., Kurazono, H., Tamura, T., Jahn, R., Kandel, E. and Niemann, H. (1994c) Synaptobrevin/vesicle associated membrane protein (VAMP) of *Aplysia californica*: structure and proteolysis by tetanus toxin and botulinal neurotoxins type D and F. *Proc Nat Acad Sci USA* **91**(11): 4688-92.

Yang, B., Gonzalez, L., Jr., Prekeris, R., Steegmaier, M., Advani, R. J. and Scheller, R. H. (1999) SNARE interactions are not selective. Implications for membrane fusion specificity. *J Biol Chem* **274**(9): 5649-53.

Yang, B., Steegmaier, M., Gonzalez, L. C., Jr. and Scheller, R. H. (2000) nSec1 binds a closed conformation of syntaxin1A. *J Cell Biol* **148**(2): 247-52.

Yang, L., Parton, R., Ball, G., Qiu, Z., Greenaway, A.H., Davis, I. and Lu, W. (2010) An adaptive non-local means filter for denoising live-cell images and improving particle detection. *J Struct. Biol* **172**(3): 233–43.

Yildiz, A., Forkey, J.N., McKinney, S.A., Ha, T., Goldman, Y.E. and Selvin, P.R. (2003) Myosin V walks hand-over-hand: single fluorophore imaging with 1.5-nm localisation. *Science* **300**(5628): 2061-5.

Yoshida, A., Oho, C., Omori, A., Kuwahara, R., Ito, T. and Takahashi, M. (1992) HPC-1 is associated with synaptotagmin and omega-conotoxin receptor. *J Biol Chem* **267**(35): 24925-8.

Yoshihara, M. and Littleton, J.T. (2002) Synaptotagmin 1 functions as a calcium sensor to synchronize neurotransmitter release. *Neuron* **36**(5): 897-908.

Zhang, W., Efanov, A., Yang, S. N., Fried, G., Kolare, S., Brown, H., Zaitsev, S., Berggren, P. O. and Meister, B. (2000) Munc-18 associates with syntaxin and serves as a negative regulator of exocytosis in the pancreatic beta -cell. *J Biol Chem* **275**(52): 41521-7.

Zhang, Y.P., Wan, P., Wang, H.Q., Zhao, H., Xu, Y.X., Yang, R. and Zhu, C.Q. (2011) Effect of neuronal excitotoxicity on Munc18-1 distribution in nuclei of rat hippocampal neuron and primary cultured neuron. *Neurosci Bull* **27**(3): 163-72.

Zilly, F. E., Sorensen, J. B., Jahn, R. and Lang, T. (2006) Munc18-Bound Syntaxin Readily Forms SNARE Complexes with Synaptobrevin in Native Plasma Membranes. *PLoS Biol* **4**(10): 330.

Zilly, F.E., Halemani, N.D., Walrafen, D., Spitta, L., Schreiber, A., Jahn, R. and Lang, T. (2011) Ca^{2+} induces clustering of membrane proteins in the plasma membrane via electrostatic interactions. *EMBO J* **30**(7):1209-20.